

Structure-property relationships of homogeneous cellulose blends and their application potential in thermoplastic processing

Kerstin Ulrike Müller

Vollständiger Abdruck der vom TUM Campus Straubing für Biotechnologie und Nachhaltigkeit der Technischen Universität München zur Erlangung einer

Doktorin der Naturwissenschaften (Dr. rer. nat.)

genehmigten Dissertation.

Vorsitz: Prof. Dr. Rubén Dario Costa Riquelme

Prüfer*innen der Dissertation:

1. Prof. Dr. Cordt Zollfrank
2. Prof. Dr.-Ing. Iman Taha
3. Prof. Dr. Johannes Ganster

Die Dissertation wurde am 14.11.2022 bei der Technischen Universität München eingereicht und durch den TUM Campus Straubing für Biotechnologie und Nachhaltigkeit am 27.06.2023 angenommen.

Danksagung

Die vorliegende Dissertation entstand während meiner Tätigkeit als wissenschaftliche Mitarbeiterin am Fraunhofer-Institut für Verfahrenstechnik und Verpackung in Freising. Mit diesen Zeilen möchte ich mich bei all denjenigen bedanken, die zum Gelingen dieser Arbeit beigetragen haben.

Mein besonderer Dank gilt meinem Doktorvater Prof. Dr. Cordt Zollfrank für die wissenschaftliche Betreuung meiner Arbeit, seine Unterstützung und den stets hilfreichen und fachlichen Austausch in den verschiedenen Phasen der Doktorarbeit.

Prof. Dr.-Ing. Iman Taha sowie Prof. Dr. Johannes Ganster danke ich für das Interesse an meiner Arbeit und der Übernahme der Prüfung. Prof. Dr. Rubén Costa möchte ich für die Übernahme des Prüfungsvorsitzes und die Organisation der Prüfung in Straubing danken.

Einen herzlichen Dank möchte ich meinem Mentor Prof. Dr. Markus Schmid aussprechen, der mir das wissenschaftliche Arbeiten bereits als Studentin nähergebracht hat und mir immer wieder helfen konnte, Ordnung in mein Gedankenchaos zu bringen.

Bei Dr. Andreas Mäurer möchte ich mich für die Möglichkeit zu dieser Arbeit, das entgegengebrachte Vertrauen bei der Bearbeitung und die Diskussionen auf Augenhöhe bedanken.

Ein großer Dank geht an meine Kolleginnen und Kollegen der Abteilungen VR und ME, die mich über die Jahre mit Rat und Tat unterstützt haben. Allen voran meine Mitstreiterinnen Katharina und Tanja, die mir fachlich, aber noch viel mehr menschlich, zur Seite standen. Das Kollegium hat es mir durch die familiäre Atmosphäre insgesamt leichtgemacht, die kleinen und großen Krisen einer solchen Arbeit zu überstehen. Allen voran möchte ich Norbert Rodler dafür danken, immer ein offenes Ohr für jegliche Belange zu haben und stets mit Optimismus in den Tag zu starten.

Mein Dank gilt auch den Studierenden Anna Kotlyar, Anna Tichy, Tina Friedenauer und Kathryn Jerwann, die durch ihre vielen Stunden im Labor und Technikum wesentlich zu dieser Arbeit beigetragen haben.

Abseits des Instituts danke ich meinen Mitbewohnerinnen und Mitbewohnern, die Freising zu meinem Zuhause gemacht haben und mir immer wieder zeigen, wie man respektvoll mit den Eigenarten eines jeden umgehen kann. Auch meinen Eltern und Teresa danke ich für ihr bedingungsloses Vertrauen und ihre entspannte Offenheit und Motivation. Danke an Markus, dass du alle Launen in dieser spannenden Zeit mit Rücksicht und Geduld ertragen hast und wir weiter unseren gemeinsamen Weg gehen.

Scientific Publications

Publications in direct relation to this work

Müller, K., Fürtauer, S., Schmid, M., Zollfrank, C. (2022), *Cellulose blends from gel extrusion and compounding with polylactic acid*, Journal of Applied Polymer Science 2022, 139(37), e52794. <https://doi.org/10.1002/app.52794>

Müller, K., Van Opdenbosch, D., Zollfrank, C. (2022), *Cellulose blends with polylactic acid or polyamide 6 from solution blending: Microstructure and polymer interactions*, Materials Today Communications 30, 103074. <https://doi.org/10.1016/j.mtcomm.2021.103074>

Müller, K., Zollfrank, C. (2020) *Ionic liquid aided solution-precipitation method to prepare polymer blends from cellulose with polyesters or polyamide*, European Polymer Journal, 133, 109743. <https://doi.org/10.1016/j.eurpolymj.2020.109743>

Müller, K., Zollfrank, C., Schmid, M. (2019) *Natural Polymers from Biomass Resources as Feedstocks for Thermoplastic Materials*, Macromolecular Materials & Engineering 2019, 304, 1800760. <https://doi.org/10.1002/mame.201800760>

Further publications

Schmid, M., Müller, K. (2019) *Whey Protein Films and Coatings*. In Deeth, H. *Whey Proteins: From Milk to Medicine*. Amsterdam: Elsevier. <https://doi.org/10.1016/B978-0-12-812124-5.00012-6>

Detzel, A., Bodrogi, F., Kauertz, B., Bick, C., Welle, F., Schmid, M., Schmitz, K., Müller, K., Kaeb, H. (2018) *Biobasierte Kunststoffe als Verpackung von Lebensmitteln*. Beauftragte Studie des Bundesministeriums für Ernährung und Landwirtschaft / Fachagentur Nachwachsende Rohstoffe.

Schmid, M., Merzbacher, S., Müller, K. (2018) *Time-dependent crosslinking of whey protein-based films during storage*. Materials Letters, 215, 8-10. <https://doi.org/10.1016/j.matlet.2017.12.047>

Schmid, M., Merzbacher, S., Brzoska, N., Müller, K., Jesdinszki, M. (2017) *Improvement of Food Packaging-Related Properties of Whey Protein Isolate-Based Nanocomposite Films and Coatings by Addition of Montmorillonite Nanoplatelets*. Frontiers in Materials, 4, 35. <https://doi.org/10.3389/fmats.2017.00035>

Schmid, M., Prinz, T.K., Müller, K. & Haas, A. (2017) *UV Radiation Induced Cross-Linking of Whey Protein Isolate-Based Films*. International Journal of Polymer Science, vol. 2017, 6 pages. <https://doi.org/10.1155/2017/1846031>

Müller, K., Jesdinszki, M., Schmid, M. (2017) *Modification of functional properties of whey protein isolate nanocomposite films and coatings with nanoclays*. Journal of Nanomaterials, 2017, 10. <https://doi.org/10.1155/2017/6039192>

Müller, K., Bugnicourt, E., Latorre, M., Jorda, M., Echegoyen Sanz, Y., Lagaron, J., Miesbauer, O., Bianchin, A., Hankin, S., Bölz, U., Pérez, G., Jesdinszki, M., Lindner, M., Scheuerer, Z., Castelló, S. & Schmid, M. (2017) *Review on the Processing and Properties of Polymer Nanocomposites and Nanocoatings and Their Applications in the Packaging, Automotive and Solar Energy Fields*. Nanomaterials, 7, 47. <https://doi.org/10.3390/nano7040074>

Schmid, M., Herbst, C., Müller, K., Stäbler, A., Schlemmer, D., Coltelli, M.-B. & Lazzeri, A. (2016) *Effect of Potato Pulp Filler on the Mechanical Properties and Water Vapour Transmission Rate of Thermoplastic WPI/PBS Blends*. Polymer-Plastics Technology and Engineering, 55, 510-517. <https://doi.org/10.1080/03602559.2015.1098690>

Coltelli, M.-B., Wild, F., Bugnicourt, E., Cinelli, P., Lindner, M., Schmid, M., Weckel, V., Müller, K., Rodriguez, P., Stäbler, A., Rodríguez-Turienzo, L. & Lazzeri, A. (2015) *State of the Art in the Development and Properties of Protein-Based Films and Coatings and Their Applicability to Cellulose Based Products: An Extensive Review*. Coatings, 6, 1-59. <https://doi.org/10.3390/coatings6010001>

Schmid, M., Müller, K., Sänglerlaub, S., Stäbler, A., Starck, V., Ecker, F. & Noller, K. (2014) *Mechanical and barrier properties of thermoplastic whey protein isolate/ethylene vinyl acetate blends*. Journal of Applied Polymer Science, 131, 41172. <https://doi.org/10.1002/app.41172>

Presentations and posters

Müller, K. (2022) *PLA in current Research Projects: Material Development - Packaging Applications - Recycling*, PLA World Congress, München, Mai 2022

Goderbauer, P., Müller, K. (2022) *Papier als alternativer Packstoff - funktional, recyclingfähig, siegelbar*, Kooperation Fraunhofer IVV/IVLV: Neue Verpackungen - zirkulär, nachhaltig, digital, Online-Konferenz, April 2022

Müller, K. (2021) *Neue Ansätze zur Nutzung nativer Cellulose in thermoplastischen Anwendungen*, BIO-raffiniert XI, Oberhausen/Online, Februar 2021

Müller, K. (2020) *Thermoplastische Celluloseblends: ein lösungsmittel-basierter Ansatz zur stofflichen Nutzung nativer Cellulose*, Straubinger Campus Colloquium, Straubing/Online, November 2020

Kaiser, K., Müller, K. (2019) *Recycling von Post-Consumer Verpackungen*, 44. Münchner Klebstoff- und Veredelungs-Symposium, München, Oktober 2019

Müller, K. (2018) *Biobasierte Kunststoffe als Verpackung für Lebensmittel*, VDMA Forum Packmittel, Fernwald, Oktober 2018

Müller, K. (2018) *Technofunktionalität von biobasierten Kunststoffen/ Chancen und Herausforderungen biobasierter Kunststoffe anhand von Fallbeispielen*, BMEL Expertenworkshop „Biobasierte Kunststoffe als Verpackung von Lebensmitteln“, Berlin, März 2018

Müller, K. (2018) *Barriereverbesserung durch anorganische Nanopartikel*, VVD-Workshop meets Freisinger Tage: Flexible Packstoffe im Verpackungsprozess – Materialien, Prozesse, Qualitätskontrolle. Freising, Januar/Februar 2018

Müller, K., Schmid, M. (2017) *Barrier properties of whey protein isolate-based nanocomposite films and coatings*. Poster at the 2nd Innovations in Food Packaging, Shelf Life and Food Safety Conference, 3.-6. Oktober 2017, Stadthalle Erding, München.

Müller, K., Schmid, M. (2017) *Mechanical properties of whey-protein isolate based nanocomposites*. Poster at the 2nd Innovations in Food Packaging, Shelf Life and Food Safety Conference, 3.-6. Oktober 2017, Stadthalle Erding, München.

Content

Danksagung	I
Scientific Publications.....	II
Content.....	V
Zusammenfassung	VII
Summary.....	IX
1 General Introduction.....	1
1.1 Bioeconomy: Need for materials from renewable resources and bio-based products	1
1.2 Scientific questions and research approach	2
2 Theoretical Background: Polymer solutions and blends.....	5
2.1 Polymer types and interactions.....	5
2.1.1 Thermoplasticity	6
2.2 Polymer solutions	7
2.2.1 Dissolution of cellulose	10
2.3 Polymer composites and blends	12
2.3.1 Thermodynamics	12
2.3.2 Morphology of polymer blends	14
2.3.3 Characterization techniques of polymer blends	15
2.3.4 Cellulose blends with synthetic polymers	16
3 Technical Background: Biogenic polymers and their technical use.....	18
3.1 Bio-based polymers/natural polymers	18
3.2 Conversion of thermoplastic polymers.....	18
3.2.1 Extruder types and advantages of co-rotating twin screw extruders.....	19
3.3 Review: Natural Polymers from Biomass Resources as Feedstocks for Thermoplastic Materials	22
4 Ionic liquid aided solution-precipitation method to prepare polymer blends from cellulose with polyesters or polyamide.....	41
5 Cellulose blends with polylactic acid or polyamide 6 from solution blending: microstructure and polymer interactions	57
6 Cellulose blends from gel extrusion and compounding with polylactic acid.....	78

7	Discussion, conclusion and outlook.....	96
7.1	Compatibility of synthetic polymers with cellulose	97
7.2	Influence of formulation and process parameters on blend structure and properties	98
7.3	Blend preparation: solution and extrusion blending with ionic liquids.....	101
7.4	Conclusion.....	102
7.5	Outlook	103
	Bibliography	XI

Zusammenfassung

Im Bereich der thermoplastischen Kunststoffe gibt es seit vielen Jahren Bestrebungen, synthetische Polymere entweder durch die Substitution der Rohstoffquelle oder durch die Entwicklung neuer, biobasierter Materialien zu ersetzen. Die direkte stoffliche Nutzung von nachwachsenden Rohstoffen nutzt nicht nur die vorhandenen Synthesekapazitäten der Natur intelligent, sondern spart auch energie- und ressourcenintensive Prozessschritte. Neben dem Einsatz von Cellulose als Füllstoff ist es bisher nicht gelungen, native Cellulose thermoplastisch zu verarbeiten. Aufgrund des starken Netzwerks aus Wasserstoffbrückenbindungen in der Cellulose ist der Energieaufwand, der zum Schmelzen des Polymers erforderlich wäre, so hoch, dass bereits vorher ein Abbau des Polymers stattfindet. Lediglich Cellulosederivate, bei denen die Hydroxylgruppen der Cellulose substituiert wurden, zeigen thermoplastische Eigenschaften.

In diesem Kontext untersucht die vorliegende Arbeit einen rein physikalischen Modifikationsansatz, bei dem polymere Abstandhalter zwischen die Celluloseketten eingebracht werden, um deren intermolekulare Wasserstoffbrückenbindungen zu schwächen.

Durch Mischen in Lösung mit anschließender Fällung wurden Kombinationen aus Cellulose mit verschiedenen Biopolyestern oder Polyamid 6 hergestellt und mittels mikroskopischer, thermischer, und struktureller Analysemethoden systematisch auf ihre Kompatibilität untersucht. Hierbei zeigte Polymilchsäure die stärksten Wechselwirkungen, was in einem einphasigen Blend resultierte. Während mit Polyamid 6 noch kristalline und amorphe Domänen beider Blendpartner identifiziert werden konnten, zeigte die Kombination mit Polymilchsäure eine rein amorphe Morphologie, bei der weder optisch noch analytisch zwischen Domänen der kombinierten Polymere differenziert werden kann.

Trotz theoretischer, thermodynamischer Unmischbarkeit der Blendpartner ist es damit möglich, im entwickelten Löse-Fäll-Prozess polymere Abstandhalter auf molekularer Ebene in das Cellulosenetzwerk einzubringen. Daraus resultiert ein Material, welches sich hinsichtlich seiner Eigenschaften von bekannten, mehrphasigen Systemen signifikant unterscheidet. Die entwickelten Celluloseblends sind biobasiert, biologisch abbaubar und optisch transparent.

Die vorliegende Arbeit zeigt auch, dass der Herstellungsprozess solcher Blends von einem Mischen verdünnter Cellulose- und Polymilchsäure-Lösungen auf einen kontinuierlichen Extrusionsprozess konzentrierter Cellulosegele mit einer Polymerschmelze rein technisch übertragbar ist. Es konnten Cellulosegele mit bis zu

45 Gew.% Celluloseanteil mittels Extrusion hergestellt werden. Im folgenden Compoundierungsschritt zeigten sich allerdings Abbauprozesse durch die zur Lösung der Cellulose verwendeten ionische Flüssigkeit, die zu Verfärbungen und verringerten Zugfestigkeit und Flexibilität des Materials führten. Die absolute Zugfestigkeit und die Dehnungswerte der extrudierten Cellulose/Polymilchsäure Blends (1:1) betragen ~40 MPa bzw. 1,3 %. Diese Werte sind vergleichbar mit einem mehrphasigen Verbundwerkstoff derselben Zusammensetzung, der das doppelte Molekulargewicht von Polymilchsäure enthielt. Die Blends sind unter Druck und Temperatur formbar und haben das Potenzial, in gängigen thermoplastischen Verfahren eingesetzt zu werden.

Diese Arbeit leistet damit einen wesentlichen Beitrag zur Erweiterung der technischen Nutzung des am häufigsten und ubiquitär vorkommenden natürlichen Polymers Cellulose. Die entwickelten Blends zeigen ein hohes Substitutionspotential der bislang dominierenden fossil-basierten Kunststoffe, was einen weiteren Schritt beim Übergang einer linearen Wirtschaft in Richtung einer kreislauforientierten Bioökonomie ermöglicht.

Summary

In the field of thermoplastics, there have been efforts for many years to replace synthetic polymers either by substituting the raw material source or by developing new, bio-based materials. The direct material use of renewable raw materials not only makes intelligent use of nature's existing synthesis capacities, but also saves energy- and resource-intensive process steps. Besides the use of cellulose as a filler, it has not yet been possible to thermoplastically process native cellulose. Due to the strong hydrogen bond network in cellulose, the energy input that would be required to melt the polymer is so high that degradation of the polymer already occurs beforehand. Therefore, so far only cellulose derivatives in which the hydroxyl groups of cellulose have been substituted display thermoplastic properties.

In this context, this work investigates a solely physical modification approach by introducing polymeric spacers between the cellulose chains to weaken their intermolecular hydrogen bonding.

Combinations with different biopolyesters or polyamide 6 were prepared by solution blending with subsequent precipitation and systematically investigated for their compatibility with cellulose using microscopic, thermal, and structural analysis methods. Polylactic acid showed the strongest interactions, resulting in a single-phase blend. While crystalline and amorphous domains of both blend partners could still be identified with polyamide 6, the combination with polylactic acid showed a purely amorphous morphology in which neither optical nor analytical differentiation between domains of the combined polymers was possible.

Despite theoretical thermodynamic immiscibility of the blend partners, it is thus possible to introduce polymeric spacers at the molecular level into the cellulose network in the developed dissolution-precipitation process. This results in a material that differs significantly from known multiphase systems in terms of its properties. The cellulose blends developed are bio-based, biodegradable and optically transparent.

The present work also shows that the manufacturing process of such blends is technically transferable from a solution blending of dilute cellulose and polylactic acid solutions to a continuous extrusion process of a concentrated cellulose gel with a polymer melt. Cellulose gels with up to 45 wt% cellulose content could be prepared via extrusion. However, in the subsequent compounding step, degradation processes occurred due to the ionic liquid used to dissolve the cellulose, which led to discoloration and reduced tensile strength and flexibility of the final blend material. The absolute tensile strength and elongation values of the extruded cellulose/polylactic acid blends (1:1) were ~40 MPa and 1.3%, respectively. These values were comparable to a multiphase composite of the

same composition containing twice the molecular weight of polylactic acid. The blends were moldable under the input of pressure and temperature and show potential to be applied in common thermoplastic processes.

This work thus makes a considerable contribution to expanding the technical use of cellulose, the most abundant and ubiquitous natural polymer. The developed blends could potentially substitute the so far dominating fossil-based plastics, which enables a further step in the transition of a linear economy towards a circular bioeconomy.

1 General Introduction

1.1 Bioeconomy: Need for materials from renewable resources and bio-based products

In a bioeconomy, fossil raw materials and their derivatives as well as power generation are gradually being replaced by materials and energy based on renewable raw materials. Both energy security by reducing the dependence on fossil fuels and action on climate change by reducing greenhouse gases remain the so-called ‘grand challenges’ facing society.¹ On a global level, the United Nations Member States defined 17 sustainable development goals, including a responsible consumption and production, climate action, the establishment of a resilient infrastructure and promotion of inclusive and sustainable industrialization and innovation.² In Europe, political support is given by the bioeconomy strategy, contributing to the European Green Deal.³ Plans for a bioeconomy envision a bio-based industry sector in which some fossil-derived plastics and chemicals are replaced by new or equivalent products derived at least in part from biomass.⁴ Some of these bio-based products already exist, such as bio-based polymers.

Polymers themselves have become an integral part of our everyday lives in countless applications. Particularly in recent years, it has become clear how important polymers are, e.g. in protecting food, ensuring safe medical care or increasing fuel efficiency in the mobility sector. To promote, support and enable a sustainable society, we need polymers. However, we also have become aware that polymers can cause serious environmental problems.⁵ World-wide plastics production reached 367 million tons in 2020⁶, of which most originate from fossil resources and, as packaging makes up 42% of the quantity, are disposed after a very short period of use.⁷ Although an increasing fraction of plastics is either recycled whenever an infrastructure for collection and sorting is available or incinerated for energy recovery, the largest part still ends up in landfills or in the oceans.⁷ Those problems are currently being addressed with the development of new recycling strategies⁸ or the use and further development of biodegradable polymers.⁹ At the same time, switching raw materials from fossil to renewable resources can also solve some environmental problems associated with fossil fuel extraction and make plastic production sustainable.⁵ In this context, there is a growing interest in the production of composites from biologically produced materials, recycled materials, waste materials and combinations thereof.¹⁰

Recycled plastics can be reused to produce blends and composites, reducing dependence on virgin fossil-based materials. Also hybrid composites of fossil-based polymers and bio-resourced fillers, such as natural fibers, have attracted attention, and even fully bio-

based composites are emerging.¹⁰ In both cases, compatibility of the materials used is the major scientific challenge to improve processability and mechanical performance.¹⁰ Research in this area of polymer blends and composites has the potential to achieve the important global sustainability goal of responsible consumption and production by lowering the current material footprint.

1.2 Scientific questions and research approach

When developing new bio-based materials, the raw material source and process design must also be considered. If the naturally existing polymer structure is to be used for technical applications, two main problems quickly become apparent: (1) many proteins and α -polysaccharides compete for use as food or feed and (2) the structures of natural polymers do not allow thermoplasticity due to crosslinking or strong secondary intra- and intermolecular interactions.

The first problem can be solved by using biomass residues (lignocellulosics). Other β -polysaccharides are also ubiquitously available and do not compete with food or feed, for example, chitin. The components of lignocellulosic biomass are cellulose, hemicelluloses, and lignin. Due to its polymer structure, cellulose is an interesting candidate for thermoplastic processing:

- cellulose is a linear, unbranched, semi-crystalline homopolymer
- celluloses show a broad and sufficiently high molecular weight range

Attempts to overcome the second-named problem and use cellulose as a thermoplastic material have been made before. One modification strategy that has also been implemented on an industrial scale is chemically modified celluloses. With the chemical modification of the structure, properties of natural polymers such as biocompatibility or biodegradability, are lost at the same time. This is not the case with physical modifications that do not interfere with the natural polymer structure. Therefore, this work provides insight into **how and to what extent physical modifications influence the structure-property relationships of moldable blends based on native cellulose.**

To achieve this goal, polymeric spacers are inserted between the cellulose chains to mask the intermolecular interactions within the cellulose and allow thermomechanical deformation. The cellulose chains are made available by dissolving them in an ionic liquid and a co-solvent.

In the first step, various polymers that can interact via hydrogen bonds are mixed with the cellulose in dilute solutions and the polymer mixtures are precipitated. The solvent is recovered from the mixture to obtain a binary mixing system. Compatibility is characterized by structural, thermal and optical analyses.

In a second step, the two systems most compatible with cellulose are prepared in a wide range of cellulose/polymer ratios to find out if there are any mixing gaps and how the miscibility changes with different compositions.

In a third step, the production process of the most favorable blends is scaled up with the goal of using less solvent and characterizing the mechanical properties of the blend. For this purpose, an extrusion process is developed in which a cellulose ionogel is mixed with a polymer melt. In this step, the suitability of the newly developed materials in a thermoplastic forming process is demonstrated.

The following scientific questions that have to be answered arise from this research approach:

1. Which synthetic polymers can be used as spacers based on compatibility with cellulose?

In the case of cellulose, intermolecular interactions between the polysaccharide chains are dominated by hydrogen bonding. Therefore, the ability to strongly interact with the hydroxyl group of the cellulose and form hydrogen bonds is a major requirement when searching for compatible synthetic polymers. In chapter 4, different polyesters as well as polyamide 6 are investigated for their ability to form thermoplastic, compatible, or possibly miscible blends with cellulose.

2. How does the polymer ratio influence the blend structure of compatible systems?

Composition and temperature are the main factors determining the phase behavior of polymer blends. Two selected compatible systems, cellulose/polyamide 6 and cellulose/polylactic acid, are investigated for their structural-property relations depending on polymer ratio. The study is described in chapter 5. From this, recommendations for the design of the formulation of cellulose blends can be derived.

3. Can the manufacturing process of such blends be transferred from solution to extrusion?

The use of solvents such as ionic liquids is viewed critically for both ecological and economic reasons. For the production of cellulose blends, therefore, the aim is to use a process with as little solvent as possible. Therefore, chapter 6 investigates whether the manufacturing process of homogeneous cellulose/PLA blends can be transferred from solution to extrusion. Recommendations for the preparation and application potentials of cellulose/PLA blends are derived from this study.

4. How do process parameters influence blend properties?

The production process of native cellulose blends includes different processes, such as dissolution, mixing, precipitation, and extraction. At each step, process parameters, such as temperature, time or formulation concentrations have an impact on the final blends. The influence of the solvents and anti-solvents used are discussed in chapters 4-6. Rapid precipitation and residual solvent in the blends are discussed in chapter 5, while chapter 6 investigates the influence of extrusion and extraction parameters with a focus on polymer degradation.

The approach to using low molecular weight spacers, such as plasticizers or oligomers, although discussed in chapter 3.3, is experimentally excluded from this work for limitations in the preparation and stability of such material combinations due to easier extractability and migration issues.

2 Theoretical Background: Polymer solutions and blends

2.1 Polymer types and interactions

Polymers are macromolecules with repeating monomer units. Polymers derived from only one monomer type are called homopolymers, while two or more monomers result in co-polymers.

There are different classifications for polymers, while the most popular ones are based on synthesis itself, such as addition or condensation polymers, or the resulting material properties such as thermal or mechanical behavior.

The length of a polymer chain clearly influences the material properties and performance. Since polymers consist of many macromolecules, the molecular weight of a polymer always shows a distribution between shorter and longer polymer chains.¹¹ Usually, characteristic key values are given, such as the number average molecular weight M_n , the weight average molecular weight M_w or their quotient displaying the polydispersity PD.

Solid polymers can be divided by different structural levels (Figure 1), from the atomic structure or constitution to its configuration based on primary bonds, followed by its conformation (spatial arrangement of the entire chain) and, especially in the case of semi-crystalline polymers, morphology or supramolecular structure.¹²

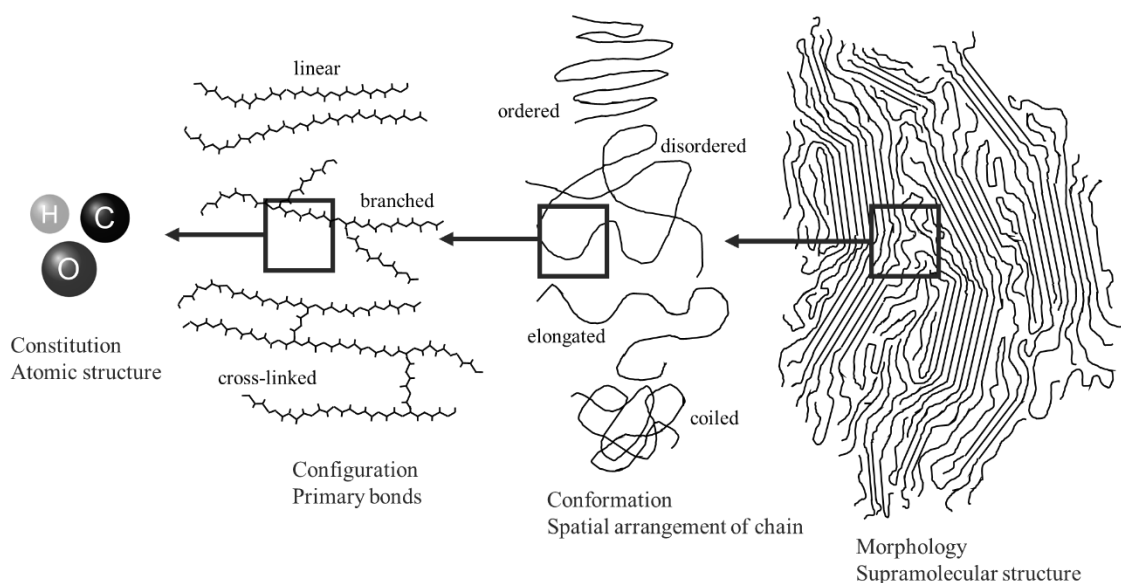


Figure 1. Schematic structural levels in polymers

The constitution of a polymer also includes branching or cross-linking of the polymer chains. Changes in conformation influence the supramolecular structure and the final properties, such as thermal and mechanical behavior. Based on those properties, three main groups of polymers are typically classified, namely thermoplastics, elastomers, and thermosets.¹¹ The network structure of elastomers is wide-meshed and allows stretching under mechanical load. Depending on the degree of cross-linking, elastomers might still be fusible, also referred to as thermoplastic elastomers. The strongly cross-linked structure of a thermoset is hardly stretchable and also no longer fusible.¹¹ Thermoplastics display linear or branched chains that are typically not cross-linked. Their main characteristic is the reversible ability to melt and solidify during thermal processing.

2.1.1 Thermoplasticity

In analogy to the theories of isothermal elasticity, thermoelasticity deals with the reversible mechanical behavior of materials, however, considering sensitivity to temperature variations.¹³ Similarly, Prager extended the theory of thermoplasticity based on considerations on isothermal plasticity.^{14, 15}

This property is owed to the chemistry and structure of the molecules, with long-chain macromolecules being the most important structural feature of this class of materials.¹⁶ A second characteristic feature is the large number of internal degrees of freedom within the polymer chain back-bone, resulting in coil conformation.¹⁷ The accompanying entropy-controlled behavior complicates the relationships between various structural parameters and the physical properties of polymer solids.¹⁶

Although monomers are usually quite small molecules, the main chain constitution defines the mechanical properties as well as crystallization behavior¹⁸ to a large extent.¹⁶ The constitution and configuration of the main chain also determine the local behavior of a polymer chain, such as inter- and intramolecular interactions and chemical reactivity.¹⁶ In thermoplastic polymers, only weak intermolecular interactions such as van der Waals, dipole-dipole forces or hydrogen bonds exist between the polymer chains.¹⁷ They can be broken more or less easily upon the input of energy, which allows a large relative motion of the polymer chains. In other words: at a sufficiently high temperature, thermoplastics start to flow, forming viscoelastic melts.¹⁶ When cooled down again, the melt solidifies by either vitrification or, in the case of semicrystalline polymers, crystallization.¹⁶

The morphology or supramolecular structure of semicrystalline polymers, defines their final performance such as mechanical response, environmental stability or optical properties¹⁹. Crystallizable polymers are mainly accompanied by stereoregularity of the chain, absence of branching and stronger inter-chain interactions.¹⁶ Crystalline domains melt upon heating. Based on different crystallite types and sizes, the melting occurs in a

temperature range possibly up to 30 Kelvin rather than a certain melting temperature or melting point.¹¹

In amorphous thermoplastics, there is generally no supramolecular structure.¹⁶ Practically, however, amorphous domains undergo softening upon heating and are transformed from being a brittle solid to becoming a ductile or rubbery solid. At and above this glass transition temperature T_g , the molecular structure exhibits macromolecular mobility and consequently the free volume, being the gap between the molecular chains, increases.^{20, 21}

Semicrystalline polymers both undergo glass transition in the amorphous domains and crystallite melting upon heating. In general, properties of semicrystalline polymers are less sensitive to temperature variations and often have superior chemical resistance and mechanical properties by means of stiffness and strength compared to the majority of glassy polymers.^{16, 22}

2.2 Polymer solutions

In polymer science and engineering, the dissolution of polymers is an important area of interest.²³ Besides coatings or adhesives, polymer solutions have been used in various applications such as polymer recycling,^{24, 25} in the medical field for tissue engineering²⁶ or implants,²⁷ or, especially by using natural polymers, to produce fibers.²⁸⁻³¹

Compared to non-polymeric materials, which dissolve instantaneously, the dissolution process of polymers can be divided in two different steps, namely solvent diffusion and chain disentanglement. When the polymer comes into contact with a thermodynamically compatible solvent, the solvent diffuses into the polymer.²³ At this first stage, the penetration distance of the solvent molecules depends primarily on the free volume, which in turn varies with the flexibility of the chains, backbone, and side groups, as well as the thermal history of the polymer.³² These solvent molecules act as a plasticizer, resulting in a gel-like swollen layer between the polymer and the solvent. This boundary or surface layer was further divided by Ueberreiter³³ into an infiltration layer, a solid swollen layer, a gel layer and a liquid layer, Figure 2. Initially, the solvent begins to push the swollen polymer substance into the solvent. As time progresses, a more dilute upper layer is pushed toward the solvent stream. As solvent continues to penetrate the solid polymer, the swollen surface layer increases. At the end of the swelling time, a quasi-stationary state is reached where the transport of the macromolecules from the surface into the solution prevents a further increase of the layer. After an induction time, the polymer gel completely disintegrates into solution.^{23, 33}

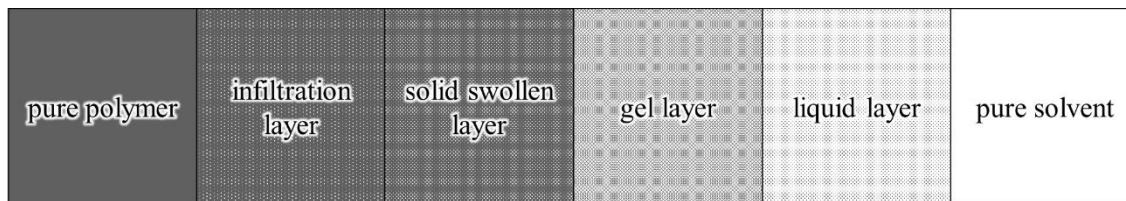


Figure 2. Schematic of the surface layer between polymer and solvent according to Ueberreiter and Asmussen³³

Depending on temperature, not all layers are present. When dissolving an amorphous polymer at approximately its glass transition temperature, the infiltration layer and the solid swollen layer disappear, and the surface layer consists only of the gel and liquid layers. The entire surface layer becomes completely uniform at the flow temperature, which is the limit at which the polymer itself begins to flow.³³

Various factors affect the solubility of a polymer. First of all, the dissolution rate of a polymer decreases with increased molecular weight. Depending on the polymer-solvent system, different relations between the molecular weight and the dissolution rates or the thickness of the surface layer have been observed.^{32, 34, 35} The dissolution depends on the ability of the polymer to disentangle and consequently dissolve in the solvent. As this is a function of molecular weight, larger molecular weights require a higher degree of disentanglement and thus a higher degree of swelling prior to dissolution.³⁶

Entanglement of polymer chains is defined by the structural level of conformation. Going back to the lower structural levels, configuration as well as constitution define the suitability of a polymer to interact with the solvent molecules. Differences in free volume and segment stiffness are also responsible for the different behavior from polymer to polymer.²³

Solvent-polymer interactions are frequently described by the Flory-Huggins interaction parameter. The solution theory which was investigated independently by Flory³⁷ and Huggins³⁸ describes a lattice model of the thermodynamics of polymer solutions that takes into account the large diversity of molecular volumes in fitting the usual expression for the entropy of mixing. The thermodynamic equation for the change of the Gibbs energy ΔG_m is composed of the mixing enthalpy (ΔH_m) and mixing entropy (ΔS_m):

$$\Delta G_m = \Delta H_m - T * \Delta S_m \quad (1)$$

If there were no interactions between the two substances, there would be no enthalpy of mixing and the entropy of mixing would be ideal and thus positive, making ΔG negative at any mixing ratio. There would be complete miscibility. It follows that mixing gaps must be explained by interactions between components.

The resulting expression for the change in Gibbs energy is based on a term for the ideal mixture entropy adapted for polymers and an interaction parameter describing the sum of all interactions:^{39, 40}

$$\Delta G_m = RT \left[\phi_1 \phi_2 \chi_{12} + \frac{\phi_1}{X_1} \ln \phi_1 + \frac{\phi_2}{X_2} \ln \phi_2 \right] \quad (2)$$

with X_1 and ϕ_1 being the number of monomeric units and volume fraction of the solvent ($X_1=1$) and X_2 and ϕ_2 being the number of monomeric units and volume fraction of the polymer, R and T being the gas constant and absolute temperature and χ_{12} being the interaction parameter for the components. This dimensionless parameter determines interactions between polymer chains and the solvent, which is related to the interactions on the monomer length scale and the chain length.⁴¹ The traditionally called Flory-Huggins interaction parameter χ is an important factor for the miscibility of polymer mixtures and solutions:

If $\chi < 0.5$, the solvent is typified as a good solvent for the polymer, with the polymer chains being present as extended coils resulting in expanded conformation. An interaction parameter $\chi > 0.5$ indicates a poor solvent, associated with chain aggregation, in the worst case, phase separation. In the case of a polymer blend, the parameter χ can still be defined, and miscibility generally occurs when $\chi < 0$ because the high molar volume of both components reduces combinatorial entropy.⁴² Possible combinations can be easily understood using the lattice model, Figure 3.

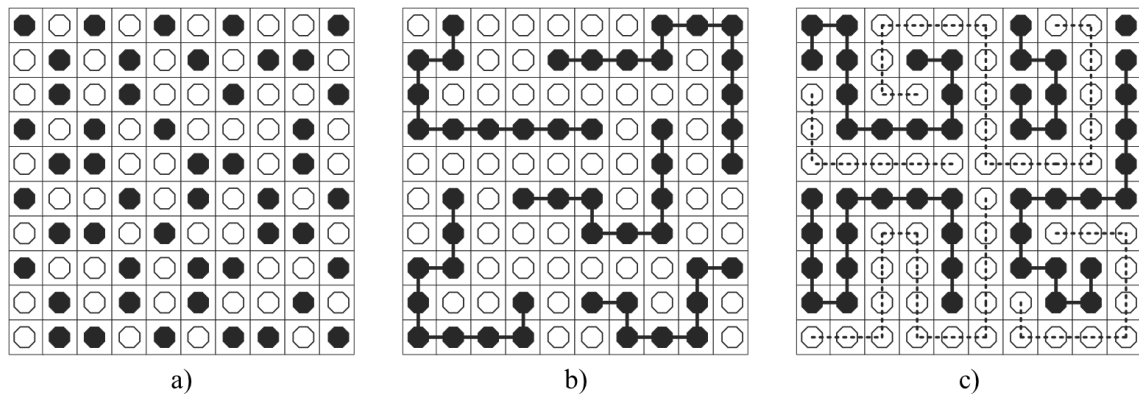


Figure 3. a) Lattice with random mixing of two spheres (10^{30} combinations), b) Lattice with random mixing of polymer and solvent (10^{16} combinations), c) Lattice with random mixing of two types of polymer chains (10^3 combinations). Adapted from Thomas et al.⁴³

However, simple theoretic models tend to make unrealistic assumptions. For example, most solubility theories only refer to amorphous polymers in favorable, ‘good’ solvents. Therefore, the behavior for e.g. semi-crystalline polymers can differ greatly, and has to be factored.⁴⁴ Also, the concentration regimes are assumed to be diluted, giving the possibility of the polymer chains to primarily interact with the solvent molecules. In this regime the polymer chains interact only weakly via direct as well

as indirect (hydrodynamic) interactions.⁴⁵ Therefore, they show an almost ideal viscous flow behavior and the viscosity value is directly proportional to the concentration.⁴⁶ In semidilute solutions, the polymer chains start to overlap and intermolecular hydrodynamic and topological interactions such as chain entanglements or restricted rotational and translational degrees of freedom become important.^{45,47} Depending on the polymer structure and molecular weight, this happens already at very low concentrations. Above a critical concentration c^* , chains are overlapped and strongly entangled. Their mobility in this concentrated regime is greatly reduced compared to dilute solutions.

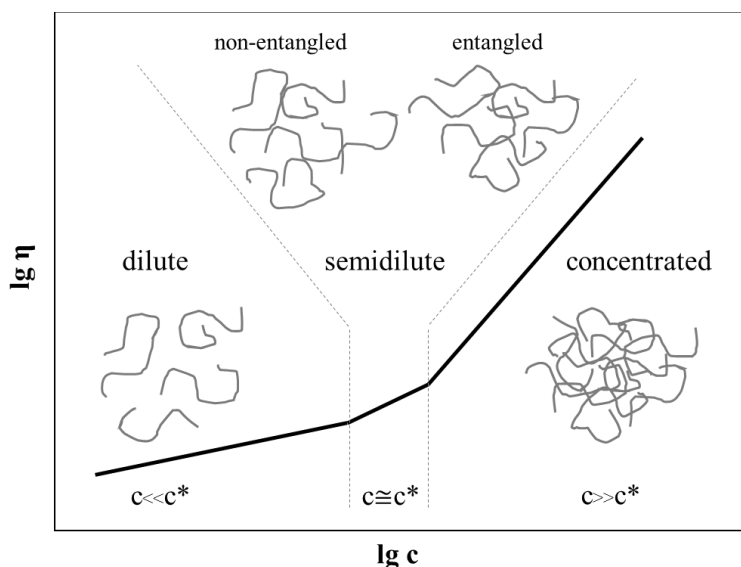


Figure 4. Dependence of the low-shear viscosity on the concentration in polymer solutions. Concentration regimes can be divided in dilute, semidilute and concentrated solutions. Adapted from Mezger⁴⁶

As concentration and entanglement increase, there is a greater increase in the low-shear viscosity values, as indicated by the larger slope of the $\eta(c)$ function in the concentrated regime (Figure 4).⁴⁶ The change from non-entangled to entangled state demands a minimum molecular weight that is independent of concentration but dependent on polymer structure.⁴⁵

2.2.1 Dissolution of cellulose

Found in cell walls of plants, such as cotton and wood, native cellulose is rather difficult to process. It is a homopolysaccharide made up of repeated β -D-anhydroglucose units linked by β -1,4 glycosidic bonds. Native cellulose is considered a semi-crystalline polymer and contains regions of highly ordered chains held together by a network of intra- and intermolecular hydrogen bonds between hydroxyl units and ether oxygen.⁴⁸ Besides extremely stable crystalline domains, hydrogen bonding as well as hydrophobic interactions are responsible for cellulose solubility (Figure 5).⁴⁹ Therefore, cellulose is generally considered insoluble in common solvents. Nevertheless, methods for converting and utilizing cellulose have been established for decades. Cellulose materials

are currently available in native, regenerated or derivatized forms. However, all processes require physical or chemical modification to bring them out of their natural state. Viscose and lyocell processes, two of the most commonly used processes for cellulose regeneration, use harsh solvents such as carbon disulfide, *N*-methylmorpholine *N*-oxide (NMMO) or a number of strong acids and bases.

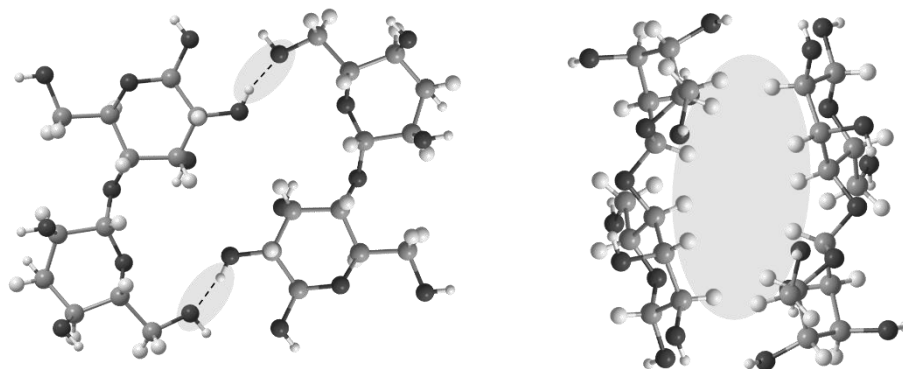


Figure 5. Hydrophilic and hydrophobic parts of the cellulose molecule: left, top view of the glucopyranose ring plane highlighting hypothetical hydrogen bonding between the hydroxyl groups located on the equatorial positions of the intermediate ring; right, side view of the glucopyranose ring plane showing the hydrogen atoms of C–H bonds on the axial positions of the ring. Adapted from Medronho and Lindman⁴⁹

Other common cellulose solvents are for example aqueous inorganic complexes (e.g. cupriethylenediamine hydroxide), concentrated salt solutions (e.g. zinc chloride, ammonium, calcium and sodium thiocyanate solutions), salts dissolved in organic solvents (e.g. lithium chloride/*N,N*-dimethylacetamide, ammonia/ammonium salt, tetrabutylammonium fluoride/dimethyl sulfoxide) or aqueous alkali (lithium hydroxide or sodium hydroxide solutions).⁵⁰ More recent approaches focus on ionic liquids⁵¹ and deep eutectic solvents⁵² that have been found to be efficient solvents for native cellulose. Therefore, ionic liquids have been frequently used not only for dissolution, but also as reaction media for cellulose derivatization.^{53, 54} Ionic liquids are salts with melting temperatures below 100°C, emerging as potentially environmentally friendly and economic alternatives to classical solvents. Properties of ionic liquids rely heavily on the anion and cation they are made of, however, they are generally viscous in nature.⁵⁵ Co-solvents are often used in association with ionic liquids to decrease the aggregation of ions in solution, thus decreasing the viscosity and enhancing the cellulose dissolution, while anti-solvents, such as water can diminish the solubilizing power.^{56, 57} Unlike many common solvents, ionic liquids are known for their negligible vapor pressure and good thermal stability. Hence, they can be recovered with low degradation, offering the possibility for recycling and multiple usages making them an interesting candidate for more environmentally friendly processing.⁵⁸

As for the dissolution mechanism, it is generally accepted that the dissolution of cellulose is mainly due to the ability of the solvent to eliminate inter- and intramolecular hydrogen

bonds between the polymer molecules. On the other hand, cellulose can be considered an amphiphilic molecule, so that the elimination of hydrophobic interactions should also be taken into account with regard to the dissolution mechanism.⁴⁹ This is an particularly interesting aspect when referring to ionic liquids, since the often amphiphilic cation, typically not involved in hydrogen bond interactions with the cellulose hydroxyl groups, could facilitate dissolution.⁴⁹ Therefore, not only the anion but also the cation influence the dissolution capacity of cellulose and must be considered when using ionic liquids⁵⁹.

Although often promoted as environmentally friendly and non-derivatizing for cellulose, in particular the most commonly used imidazolium-based ionic liquids interact with cellulose.^{60, 61} Their persistence and toxicity in the environment remain under investigation.^{62, 63} Additional challenges for large-scale applications of ionic liquids are their high production costs, high viscosities, sensitivity to moisture and insufficiently developed suitable purification processes.^{49, 64, 65}

2.3 Polymer composites and blends

The combination of different materials may have many advantages. Material properties can be combined and easily adjusted. Polymer composites are defined as multiphase materials in which reinforcing fillers are integrated into a polymer matrix. The resulting mechanical properties cannot be achieved with any of the components alone.⁶⁶ The main focus is on materials which are stiffer and stronger than the known thermoplastics alone, but keep their easy processability and light weight. Miscible polymer blends are technologically relevant because they offer the potential for new materials without the cost and time of new synthesis. Such polymer blends benefit from synergistic effects that distinguish them from a simple linear combination of properties.⁶⁷

Polymer blends can be prepared by various methods. The main pathways include mechanical mixing, e.g. of polymer melts or fine powders, or mixing of polymer solutions. Mixing two or more polymers in solution is always accompanied by a step to remove the solvent from the blend during the forming process like film casting, coating, freeze or spray drying. For economic reasons, mechanical melt blending prevails.⁶⁸

2.3.1 Thermodynamics

Miscibility itself is rather a thermodynamic term, describing homogeneity down to the molecular level. In practice, miscibility is a mixture whose domain size is comparable to the dimension of the macromolecular statistical segment.⁶⁹ Miscibility is determined by the polymeric structure of the individual components. Being able to interact via specific interactions such as hydrogen bonding, van der Waals forces or ionic forces, miscibility can be specifically favored in the direction of a polymer. Besides the ability to interact, the molecular weight of the components is a crucial factor in polymer miscibility. In low

molecular weight substances, the combinatorial entropy contribution is very high compared to high molecular weight polymers.⁷⁰ Therefore, solvent mixtures show a much wider range of miscibility, followed by polymer solutions and polymer blends, where the range of miscible combinations is much smaller (also see Figure 3). As a result, most polymer blends are actually immiscible.⁷¹

The thermodynamic requirement for miscibility is associated with the negative value of the free energy of mixing (see equation 1). For polymer blends, an additional requirement with respect to concentrations has to be considered as well,

$$G_m < 0 \text{ and } \left(\frac{\partial^2 \Delta G_m}{\partial \phi_i^2} \right)_{T,P} > 0 \quad (1', 3)$$

where ϕ_i is the volume fraction of polymer i in the blend, and T and P represent temperature and pressure. The Gibbs free energy as a function of volume fraction in a binary system generates a phase diagram showing a concave curve. Negative values of equation 3, even though $G_m < 0$, result in areas of the phase diagram in which the mixture is divided into a phase rich in component 1 and a phase rich in component 2. Those blends are referred to as partially miscible.⁷⁰ For such systems, temperature is a crucial factor. For most high molecular weight components, an increase in temperature leads to phase separation of otherwise homogeneous systems, i.e. the existence of the lower critical solution temperature (LCST). The upper critical solution temperature (UCST) predominates systems containing solvent rather than polymer blends.^{68, 70} Both are frequently used to generate phase diagrams for different polymer combinations, Figure 6.

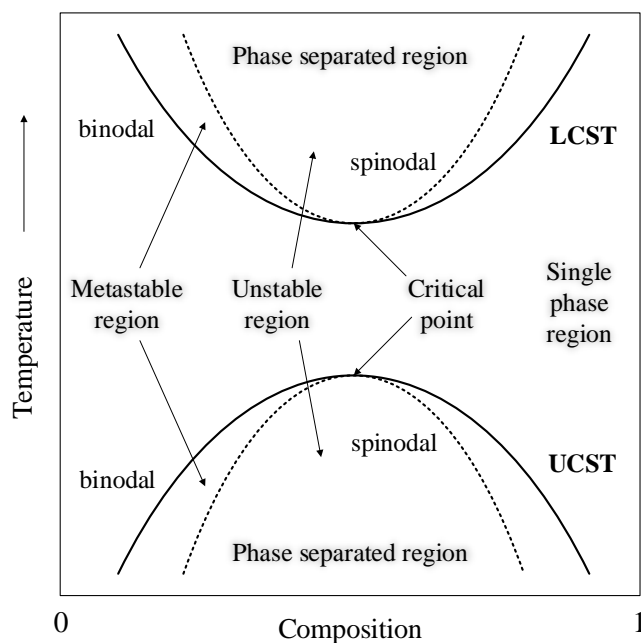


Figure 6. Phase diagram showing lower critical solution temperature (LCST) and upper critical solution temperature (UCST) behavior for polymer blends. Adapted from Robeson⁷⁰

In theory, the thermodynamics (e.g. interactions of polymer-solvent and polymer-polymer) are the main factor whether or not a homogeneous, compatible or even miscible blend can be formed by solution or melt blending. In practice, the efficiency of mixing, certainly plays a decisive role. In general, higher viscosities of a polymer solution (or melt) demand higher shear to achieve an efficient degree of mixing. This also means, that practically, by the input high shear or mixing energy, polymers can be forced to a certain degree of mixing independent from their thermodynamic compatibility. Therefore, a suitable blend preparation process can be able to form homogeneous blends even if not miscible or compatible in theory. This can be caused in particular by rapid precipitation of a polymer blend. If the time for precipitation is significantly shorter than the time for phase separation by polymer diffusion, a homogeneous, compatible blend of polymers is obtained by freezing the metastable blend structures.^{72, 73}

2.3.2 Morphology of polymer blends

Polymers blends combine at least two different polymers. Their phase sizes, shape and distribution mainly determine their properties. Although the term morphology typically refers to the supramolecular structure of a polymer, in connection with polymer blends it is used to describe the size, shape and spatial distribution of one blend phase with respect to the other.⁷⁴

Immiscible blends display a heterogeneous phase with limited interaction between the polymer components. Most immiscible blends consist of a continuous phase of one

component in which the second is dispersed. Depending on polymer types, ratios and processing conditions, co-continuous phase morphologies are also possible.⁷⁵ Their morphology will not only depend on the material parameters such as blend composition, viscosity ratio, elasticity ratio or interfacial tension, but also on the processing conditions, for example temperature, time and intensity of mixing or the nature of the flow.⁷⁴ Example morphologies are given in Figure 7.

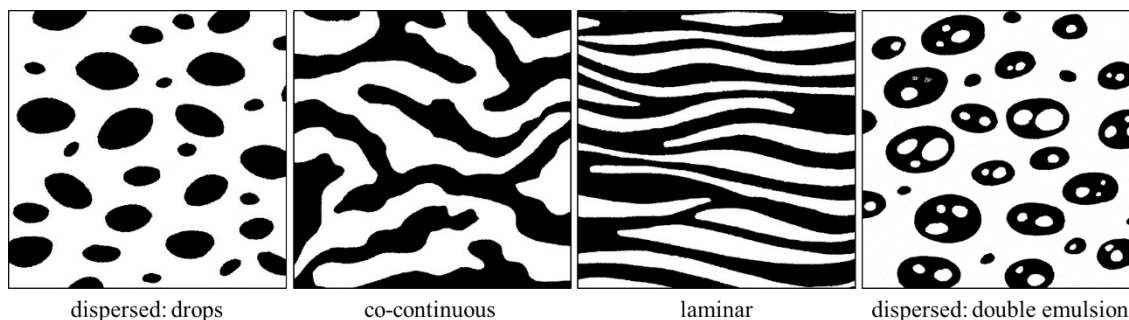


Figure 7. Schematic of possible morphologies which can be produced from melt blending. Note that for dispersed morphologies various shapes are possible. Adapted from Macosko⁷⁶

The interface of the blend system is characterized by polymer-polymer interaction such as hydrogen bonding or other physical forces. The stronger the interactions, the lower the interfacial tension, which determines phase separation, interdiffusion or even miscibility.⁴³ Interfacial tension can be reduced by adding so called compatibilizers, enhancing phase stability and often increased mechanical properties due to better load transfer at the interfaces.⁷⁷ Interdiffusion or compatibilization in immiscible polymer blends result in the formation of interphases,⁶⁹ referring to partial miscibility. Since compatibilizers are commonly introduced to the polymer chains via chemical reactions, the approach of using compatibilizers in cellulose blends was not followed. An overview about chemical modifications including compatibilization of natural and synthetic polymer blends are included in chapter 3.3.

2.3.3 Characterization techniques of polymer blends

Various methods are used to determine the miscibility or, more generally, the thermodynamic properties of polymer mixtures. Besides thermodynamic investigations, which are not directly related to miscibility, the determination of interaction parameters (for example Flory-Huggins, equation 2), investigations of phase equilibria or indirect methods for the determination of miscibility are available.⁶⁹

Regarding indirect methods, the determination of the glass transition temperatures remains the most popular approach. In simplified terms, it is as follows: Immiscibility results in two separate glass transitions, while miscibility is characterized by the presence of a unique transition that lies between the glass transition temperatures of the single

polymers. Different equations have been established to predict the glass transition temperatures of polymer blends and random co-polymers, with the Fox equation⁷⁸ probably being the most widely used one. Since it does not consider intermolecular interactions, however, other approaches by Gordon and Taylor⁷⁹, Couchman and Karasz⁸⁰ or Kwei⁸¹ are available.

As pointed out in the thermodynamics section before, specific interactions between the polymer components play a decisive role in determining their miscibility. Hydrogen bonding, dipole-dipole and ionic interactions are the most common ones in polymer blends. Characterization techniques to investigate such interactions are mainly Fourier-transform infrared (FTIR) spectroscopy, neutron or X-ray scattering, ellipsometry, neutron reflectivity and nuclear magnetic resonance (NMR) spectroscopy.⁴³ Regarding FTIR, hydrogen bonding has been extensively studied by Coleman and Painter⁸²⁻⁸⁴. The chemical composition and interactions between the functional groups in a polymer blend can be determined directly using FTIR.⁸⁵

To investigate phase behavior of polymer blends, mainly the LCST is determined. Phase separation is experimentally observed using light scattering, neutron scattering, ellipsometry or rheology.⁴³

To determine whether a blend is single or multi-phased, microscopy techniques such as polarized light microscopy, atomic force microscopy (AFM), scanning electron microscopy (SEM) and transmission electron microscopy (TEM) are direct means to visualize the morphology of the phases. The generated morphology can furthermore be visualized using infrared or Raman imaging.⁴³ For SEM and TEM, staining or etching techniques are described to enhance contrast in multi-component systems.⁸⁶

In multi-phased blends, the compatibility of the components decides upon their morphology, and is therefore directly related to most material properties. The evaluation of physical properties, such as thermal and mechanical properties, is thus part of the indirect determination methods for miscibility or compatibility. Common experimental techniques are thermogravimetric analysis, differential scanning calorimetry, dynamic mechanical thermal analysis or universal testing machines.⁴³

In both solution and melt processing, the rheological behavior of solutions or viscoelastic melts determines process design, and monitoring viscosities is important to achieve effective mixing in polymer blends. Polymer solutions, gels and melts are frequently characterized using capillary viscosimetry or rotary rheometers.

2.3.4 Cellulose blends with synthetic polymers

Due to the infusibility of cellulose, blends with synthetic polymers were generally prepared by solution blending in low-concentration polymer solutions. Early studies were performed by Nishio, Manley, and Masson using N,N-dimethylacetamide/lithium

chloride to prepare blends with poly(acrylonitrile), poly(vinyl alcohol), polyamide 6 and poly(ϵ -caprolactone).⁸⁷⁻⁹² Although intermolecular interactions in the amorphous phase were concluded, crystalline phases of each polymer were still present.⁸⁸⁻⁹⁰ Manley and Masson also investigated cellulose blends with poly(vinyl pyrrolidone) and poly(4-vinyl pyridine) using dimethyl sulfoxide-paraformaldehyde as solvent. For both blend systems, miscibility on a scale of 2.7 and 2.5 nm, respectively, was concluded.^{91, 92} The studies mainly focused on general compatibility of the blend systems, but did not address any applications or processability at larger scale. In this context, although suitable for blend preparation in lab scale, it should be noted that both selected solvent systems are harmful to human health and, in the case of paraformaldehyde, potentially carcinogenic.⁹³

When targeting more ecologic and economic blend preparation techniques, the reduction of solvent amount is a crucial factor. Regarding cellulose blends, this can be achieved by combining cellulose solutions of high cellulose concentrations and polymer melts. Therefore, the solvent system must meet three main criteria: thermal stability at polymer melting temperatures, high dissolution capacity for cellulose, and minimum ecotoxicity. If one compares common solvents for cellulose in this context (see chapter 2.2.1), ionic liquids are the most suitable solvents. However, only a few studies are known on this so far. Ionic liquids have been used to prepare cellulose blend fibers with polyamides and polyacrylonitrile. While *m*-aramide and PA 6 exhibited good miscibility with unmodified cellulose, solutions blended with aliphatic polyamides and polyacrylonitrile revealed rapid phase separation.⁹⁴ Hameed et al. prepared blends of epoxy and cellulose in an ionic liquid, resulting in flexible, thermoset materials with good compatibility especially at low cellulose contents.⁹⁵ Recently, homogeneous blends of cellulose and PLA were produced using ionic liquids. Blend films showed high transparency and enhanced biodegradability.^{96, 97} Although some of those studies have already indicated applications for the blend materials, none has investigated the application potential of such blends in thermoplastic processes so far.

3 Technical Background: Biogenic polymers and their technical use

3.1 Bio-based polymers/natural polymers

A major goal in the bioeconomy regarding bio-based materials is the abandonment of fossil-based plastics. Alternative materials from bio-based resources are widely available. The frequently used term ‘biopolymers’ covers diverse polymers with multiple properties. They are either derived from bio-based raw materials and/or are biodegradable. Technically used bio-based plastics mainly use bio-derived monomers and are subsequently polymerized. Well-known representatives are drop-in solutions such as bio-polyethylene or bio-polyamide or biopolyesters such as polylactic acid or polybutylene succinate. Although bio-based plastics have been regarded as a promising solution for the replacement of fossil sources, overall environmental impact is questioned since the agricultural input required to produce raw materials often outweighs the environmental benefits.⁹⁸ Newer approaches that use waste or by-products from the biomass sector as feedstocks are more promising.⁹⁹

Another possibility is the direct use of natural synthesized polymers. Technically relevant polymers are derived from biomass, such as cellulose and lignin, or from microbial, such as polyhydroxyalkanoates.¹⁰⁰ Biomass residues are of particular interest due to their frequent and ubiquitous occurrence. To be able to substitute fossil-based plastics however, there is one main drawback: their lack of thermoplasticity. Figure 8 illustrates different synthesis routes for bio-based polymers.

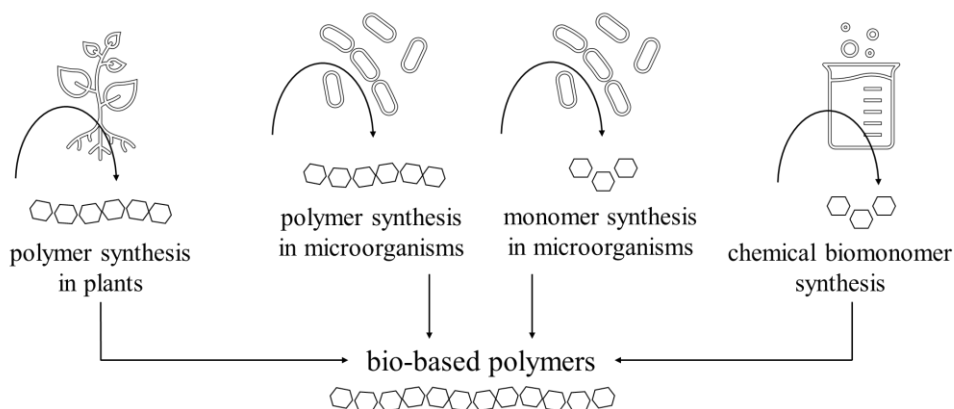


Figure 8. Synthesis routes of bio-based polymers. Adapted from Bonten¹¹.

3.2 Conversion of thermoplastic polymers

Thermoplasticity is a property of polymers that mainly enables reversible, easy and cost-effective forming, which is a key advantage over other materials in industrial production. As described before, these polymers can be processed when heated above a critical

temperature, but return to their rigid solid state when cooled. This enables forming operations to convert the polymers into nearly any imaginable shape. Also, reforming is possible – enabling recycling of thermoplastic materials. Compared to other methods such as solvent-based processes, the melting process is the most widely used and convenient method for producing thermoplastic materials because it is simple, industrially cheap and cost-effective.¹⁰¹ Environmental concerns about solvents are also to be considered,¹⁰² adding a further advantage to melt processing.

Forming processes are divided into primary and secondary operations, resulting in finished or semi-finished products such as films, fibers, filaments, 3D-printed or injection-molded parts. Figure 9 summarizes shaping operations applied for thermoplastic polymers.

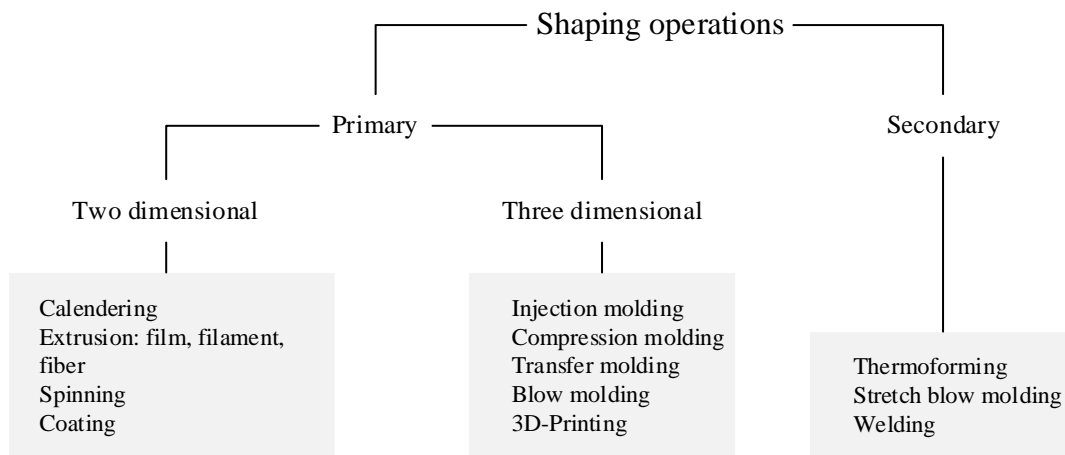


Figure 9. Shaping operations of thermoplastic polymers. Adapted from Shenoy and Saini¹⁰³

The suitability of a polymer for a processing method depends largely on its flow and deformation properties.¹⁰³ The first processing of commodity plastics after their synthesis typically takes place in (twin screw) extruders¹¹ to produce granules or pellets, which are the general intermediate forms for further processing steps shown in Figure 9.

3.2.1 Extruder types and advantages of co-rotating twin screw extruders

Extruders are economically dominant for the continuous melting of thermoplastics. Enabling a continuous process in large quantities, extruders made economic limitations disappear and contributed significantly to the success of plastics.¹⁰⁴ Types of extruders can be classified by their number of screws (Figure 10).

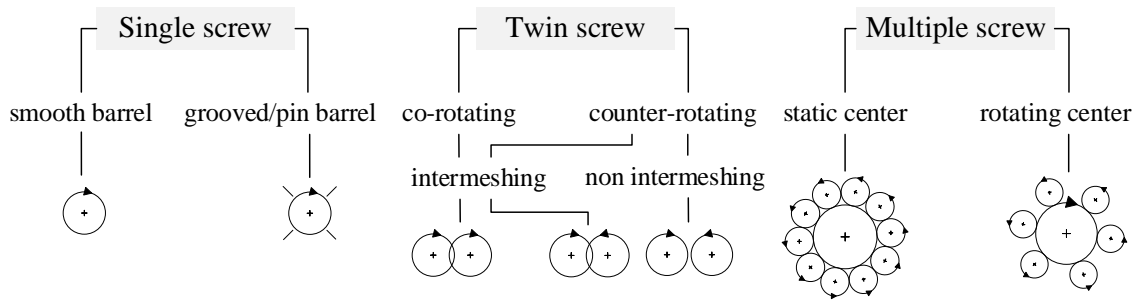


Figure 10. Classification of extruders by the number of screws. Adapted from Kohlgrüber¹⁰⁴

Single screw extruders are mainly used for melting and pressure build-up. Based on the limited mixing ability of single-screw extruders, co-rotating twin screw extruders are often used for compounding tasks.^{104, 105} Multiple screw extruders are for example ring extruders or planetary rollers.

Co-rotating twin-screw extruders have a modular design and can therefore be easily adapted to different processing requirements and product properties.¹⁰⁴ In particular, applications such as the modification of polymers during the process, require safe conveying of materials with different viscosities, the possibility of flexible additive addition, rapid mixing and homogenization of components, and efficient degassing.¹⁰⁶

Closely intermeshing, co-rotating twin screws are characterized by an identical geometry of adjacent elements. They are arranged symmetrically and are driven at the same screw speed.¹⁰⁵ An advantage of this design is the close interlocking of the screw flights, which enables forced conveying of the material and self-cleaning.¹⁰⁷ Twin screw extruders with co-rotating screws do not form closed conveying chambers. The polymer melt is moved around the screws in eight-shaped directions due to drag forces. In this process, high shear forces can be achieved in the space between the screws due to the constant displacement of the melt, resulting in better mixing of the melt components.¹⁰⁶

Besides the historical division in feeding, kneading and metering zone the processing zones of an extruder are nowadays further understood, leading to an extended zone classification according to the respective function. Kohlgrüber and Bierdel name seven zones of a twin screw extruder, namely solid feed, plasticization, additive feed, dispersion, homogenization, degassing, and discharge zone.¹⁰⁵ In the first zone, the solid polymer in the form of powders or resins is metered via a hopper and conveyed and compacted by the screw. In the following, the polymer is further compacted by a reduced flight depth of the screw. The compression and the heat input via the barrel and the internal friction cause the polymer to melt and plasticize. In the third zone, additives, especially fillers, can be added to the polymer melt. The next zones ensure distributive or dispersive mixing of the added material with the melt, so that a homogeneous mass is formed. In the subsequent degassing step, water, residual monomers or other solvents can be removed if required. The discharge zone has the task of building up pressure just before

the nozzle. After the polymer melt has been discharged, the extrudate cools down and solidifies again.¹⁰⁵

Different screw tasks, such as material conveying, compaction, plasticizing, mixing or homogenizing, require different screw designs. Beside some special elements, mainly conveying and kneading elements in different designs are common. Depending on the pitch or width of the kneading disks, they can act as conveying or return elements. The widths of the kneading discs and their offset also influence the degree of mixing. The larger the offset angle, the higher the mixing effect and the lower the conveying efficiency. Offset angles $> 90^\circ$ have a backward conveying effect. The wider the kneading elements, the lower the distributive mixing effect, while the dispersive mixing effect increases due to the higher energy input. Return conveying elements ensure complete filling of the cylinder required for plasticizing. If wide conveying elements are installed downstream of these elements, the pressure can be lowered and thus the proportion of volatile components increased. This effect is mainly used in degassing zones to achieve good removal of the volatile components.^{105, 108}

3.3 Review: Natural Polymers from Biomass Resources as Feedstocks for Thermoplastic Materials

by Kerstin Müller, Cordt Zollfrank and Markus Schmid¹⁰⁹

Macromol. Mater. Eng. **2019**, *304*, 1800760. <https://doi.org/10.1002/mame.201800760>

This review sums up current attempts to induce thermoplasticity in natural polymers via chemical and physical modification at the examples of chitin, cellulose and lignin.

In order to use natural polymers as base materials in existing processing or even recycling processes, they must have thermoplastic properties. Based on their structure, natural polymers such as chitin/chitosan, cellulose or lignin show strong intermolecular interactions, and in particular a large number of hydrogen bonds often accompanied by high crystallinity. To overcome those interactions, a high amount of energy is needed, basically accompanied by polymer degradation, before any softening or melting of the material occurs. However, chemical and physical modification processes are capable of providing those natural polymers with thermoplasticity. Despite their differences in chemical structure, the modifications made to achieve thermoplastic processing properties of chitin/chitosan, cellulose and lignin are basically the same: the masking of the hydroxyl groups to reduce intermolecular interactions and thus improve chain mobility, which in turn allows softening at a given temperature (or energy input), making the materials formable. Modifications can be divided by chemical and physical modifications.

Chemical derivatization mainly targets substitution or grafting of the hydroxyl groups present on the polymer backbone. Longer alkyl radicals can prevent hydrogen bonding and enhance processing properties. Chemical grafting also improves the compatibility in polymer blends, opening up new material combinations. However, those structural changes also affect the initial properties of the native polymers, such as biodegradability. Physical modifications do not alter the chemical structure and therefore remain those initial properties. Physical modification of natural polymers can be achieved by external plasticization or, including larger molecules, polymer blending. External plasticizers interpose between polymer chains and are bound only via intermolecular forces such as van-der-Waals forces and hydrogen bonding. Frequently used plasticizers include polyols, citrates, or medium chain length polyethers such as polyethyleneglycol. Since they are able to interact with the polymers, solvents such as ionic liquids or deep eutectic solvents are also gaining importance in the plasticization of natural polymers. As for blends, the focus of this review is on polymer blends that exhibit good miscibility as determined by thermal or optical analysis. Intermolecular interactions remain the crucial factor for compatibility. According to relevant literature, only few miscible blends are available without further compatibilization.

Author contributions: Kerstin Müller developed the concept for the manuscript and wrote the manuscript. Markus Schmid helped to structure the content and contributed to the manuscript. Cordt Zollfrank revised the manuscript.

REVIEW

Thermoplastic Biopolymers

Macromolecular
Materials and Engineering
www.mme-journal.de

Natural Polymers from Biomass Resources as Feedstocks for Thermoplastic Materials

Kerstin Müller, Cordt Zollfrank, and Markus Schmid*

With the objective of a more sustainable circular economy, one long-term goal is the utilization of renewable resources as feedstock for the production of polymer-based materials. In order to successfully process such materials using existing industrial-scale technologies or even recycling processes, the natural polymers must have thermoplastic properties. With only a few exceptions, natural polymers are not thermoplastic. However, chemical and physical modification techniques are able to induce thermoplasticity in natural polymers from biomass resources such as cellulose, lignin, and chitin. Modification techniques focus on masking the hydroxyl groups to disrupt dense hydrogen bonding and so enable polymer chain mobility upon heating. The introduction of long alkyl chains into the polymer backbone effectively improves the thermoplastic processing of natural polymers. With regard to polymer blending, chemical grafting and graft copolymerization are powerful tools for enhancing compatibility. For both chemical and physical modification, solvents such as ionic liquids and deep eutectic solvents are currently being explored for biomass and fiber processing and show promise for the future development of thermoplastic biopolymers. This review describes possible modifications, potential processing difficulties, and gives a summary of relevant studies described in the scientific literature.

achieved either by substitution of the raw material source or by modification of natural polymers to generate new, bio-based materials. There is a growing demand for using renewable raw materials and material recycling in order to have more sustainable utilization of resources and reduce negative environmental impacts. Most conventional synthetic polymers are non-biodegradable and remain in the environment for a long time, resulting in intense environmental debate about marine pollution and the contamination of aquatic and terrestrial systems by microplastics. Natural polymers are generally biodegradable and play an essential role in nature because of their beneficial material properties and functionalities. Due to their abundance, biomass containing such polymers is often inexpensive and can be found all over the world. The usage of natural polymers is gaining importance. However, some applications were already established a long time ago, such as the use of casein as a binder and textiles from wool, silk, and leather. More recent applications can be found in

1. Introduction

The shortage of fossil raw materials and energy sources and the additional challenge of population growth mean that there is intense focus on the use of biological resources in a wide range of industries. In the field of thermoplastic materials, efforts are also being made to replace synthetic polymers. This is being


diverse areas including wastewater treatment, medical implants, and enhanced oil recovery.^[1] However, the variety of engineering applications, and especially the recyclability of such materials, is still restricted due to limited processing technologies.

In conventional forming processes, such as injection molding, extrusion and drawing, and molding processes the polymeric materials have to be able to soften or melt at a certain temperature and have to harden upon cooling.^[2] Thermoplastics are composed of long-chain macromolecules. Above a certain temperature, the chains of those linear or branched polymers are able to slide past each other due to the thermal energy input, enabling them to overcome intermolecular attraction.^[3] Depending on their state of order, thermoplastics can be further divided into two types. They can occur in amorphous or in semi-crystalline, partially ordered structures.^[4] Amorphous polymers or polymer regions soften above their glass transition temperature (T_g) and can be formed by thermal or thermomechanical means. Crystalline regions have distinctive melting temperature ranges. In these regions the crystalline structures become corrupted and this is accompanied by release of the enthalpy of fusion. During melting, the rheological behavior of the polymer changes, facilitating melt processing. Recrystallization occurs upon cooling and is decisive for the resulting material properties.

K. Müller
Process Development for Polymer Recycling
Fraunhofer Institute for Process Engineering and Packaging IVV
Giggenhauser Str. 35, 85354 Freising, Germany
E-mail: kerstin.mueller@ivv.fraunhofer.de

K. Müller, Prof. C. Zollfrank
Chair for Biogenic Polymers
TUM Campus Straubing for Biotechnology and Sustainability
Technical University of Munich
Schulgasse 16, 94315 Straubing, Germany

Prof. M. Schmid
Faculty of Life Sciences
Albstadt-Sigmaringen University
Anton-Guenther-Str. 51, 72488 Sigmaringen, Germany

 The ORCID identification number(s) for the author(s) of this article can be found under <https://doi.org/10.1002/mame.201800760>.

DOI: 10.1002/mame.201800760



Thermoplastic behavior naturally occurs in non-crosslinked synthetic polymers in which the intermolecular interactions between the polymer chains are defined by van der Waals interactions rather than hydrogen bonding. Thus less energy is necessary to induce chain mobility and enable thermoplasticity. Intermolecular interactions, and in particular a large number of hydrogen bonds, often accompanied by high crystallinity mean that natural polymers, with the exception of polyhydroxyalkanoates (PHAs), do not usually possess thermoplastic behavior. Hence one major challenge for replacing conventional plastic materials in technical applications is the thermoplastic processing of natural polymers. In addition to chemically synthesized biopolymers based on monomers derived from natural raw materials such as poly(lactic acid) (PLA) or so-called drop-in solutions such as biobased polyethylene (PE) or biopolymers produced via microbial fermentation such as PHAs,^[5] the utilization of natural polymeric structures from proteins and polysaccharides could be an important step toward the goal of sustainable plastic materials.^[6] Moreover, natural building blocks and especially those derived from agricultural industry waste are inexpensive biomaterials^[7] and are therefore not only of ecological but also of economic interest.

2. Potential Approaches for Producing Thermoplastic Natural Polymers

Different techniques have been applied to introduce thermoplastic processing properties to naturally non-thermoplastic polymers. Plasticization techniques can generally be divided into internal and external plasticization. Internal plasticization means the incorporation of covalently bonded groups to the polymer backbone, also referred to as chemical modification. In recent decades graft polymerization techniques and click chemistry have also gained importance in the field of thermoplastic materials.^[8,9] Internal plasticizers can be incorporated during the polymerization process or extrusion process and are non-extractable. External plasticizers interpose between polymer chains and are bound via intermolecular forces such as van der Waals forces and hydrogen bonding, leading to improved chain mobility and free volume.^[2,10] This plasticization method is therefore classified as physical modification.

In the case of hydrophilic natural polymers small polar molecules can be readily incorporated into the polymer matrix; hence water and polyols are widely used as external plasticizers for the extrusion of proteins and polysaccharides. The influence of water molecules on the processing properties of natural polymers is decisive and is evident in everyday situations such as ironing wool or cotton and when blow-drying hair. Their small size and hydrophilic properties allow each molecule to interact with polar residues of the polymer chain, usually polar groups, and they are generally more efficient than other plasticizers.^[10] The compatibility and efficiency of a plasticizer is determined by the ability to form intermolecular interactions. As mentioned previously, those interactions are primarily determined by hydrogen bonding in natural polymers. Hence, the plasticizing efficiency of a molecule can be described by its ability to form hydrogen bonds or by a hydrogen bond breaking mechanism.^[11] Despite this, the main disadvantage



Kerstin Müller is a doctoral research student at the Technical University Munich (TUM) and currently works at the Fraunhofer Institute for Process Engineering and Packaging IVV in Freising in the Process Development for Polymer Recycling department. She holds a master's degree in food technology and biotechnology. Her

research focuses on the material use of polymers from natural resources, biopolymers for technical applications, and polymer recycling. Of special interest to her is the field of thermoplastic processing of proteins and polysaccharides.



Cordt Zollfrank holds a diploma in chemistry from Technical University Munich (TUM). He also obtained his doctorate from TUM in forest sciences and later habilitated in the field of materials science at the University of Erlangen-Nuremberg. As professor in the field of biogenic polymers at TUM Campus Straubing, he develops novel

structural and functional materials using bioinspired synthesis methods. One particular focus of his work is the generation of biogenic (polymer) structures and their conversion into composite materials for technical and biomedical applications.



Markus Schmid holds a diploma in food technology and a master's degree in food processing from the University of Applied Sciences Fulda. He took his doctorate at Technical University Munich (TUM). As professor at Albstadt-Sigmaringen University, his major research and teaching areas are in the field of process

technology and process design in life sciences with emphasis on food preservation and sustainable food packaging technology. He was the lead scientist of the research group for Biopolymers in Paper and Film Applications at the Fraunhofer Institute for Process Engineering and Packaging IVV in Freising.



of low-molecular-weight plasticizers is migration and evaporation (e.g., during processing and storage) leading to a loss of mechanical and barrier properties. For this reason plasticizers of higher molecular weight have been used, from oligomers to blends with other polymers.

Physical blending, or simple mixing of polymers, is widely applied in the processing of thermoplastics. A so-called polymer blend is defined as a “macroscopically homogeneous mixture of two or more different species of polymers,”^[12] where the ingredient content must be above 2 wt%.^[13] Many of those blends are produced for financial reasons to fill the gap between low-cost standard polymers and rather expensive polymers for technical applications. However, polymer blends have special properties that cannot be ascribed to those of the individual blend constituents.^[4] Physical modification by polymer blending can also lead to improved processing properties, plant flexibility, and quick formulation changes.^[13] When two different polymers are mixed, the miscibility of the two components is a key question. Miscible polymer blends are expected to behave similar to a single-phase system whereas immiscible polymer blends have two or multiple phases. Yet still homogeneity depends on the scale on which it is considered. When the dimensions of homogeneity decrease, the properties of each phase differ obviously.^[13,14] Melt-mixing of immiscible polymers, for example during extrusion, usually results in a variety of phase morphologies.^[13] This plays a significant role in determining the properties of such two-phase systems. Incompatibility can be overcome by using compatibilizers, targeting a miscible single-phase system. However, compatibilizers only act at the interfaces of the blend partners, increasing interfacial adhesion and at best resulting in well-dispersed or even co-continuous blend morphology. Non-reactive compatibilization methods use amphiphilic compounds, ranging from low-molecular-weight structures to block-copolymers. As natural polymers often possess a number of reactive groups, reactive compatibilization methods are widely applied. These focus on reactive polymer grafting with several anhydrides or ring-opening polymerization of cyclic esters.^[15]

While the miscibility of blends is a thermodynamic term most frequently described by the Flory–Huggins model in the literature^[16,17] and initially used to predict polymer-solvent miscibility, compatibility is a technical term used to describe whether the final material properties such as processing and mechanical properties are appropriate for a specific application.^[15,18] The compatibility can therefore be modified via the aforesaid physical and chemical modification techniques. Although miscibility has been effectively described using polymer interaction parameters,^[15] literature studies are usually based on thermal analysis, for example by depicting only one T_g and showing a T_g shift with blend ratio variation, or by characterizing blend morphologies using microscopic techniques such as scanning electron microscopy (SEM) and atomic force microscopy (AFM).

With respect to blends, the focus of this review lies on polymer blends that have good miscibility as determined by thermal or optical analysis. Immiscible blends or filled compounds can, however, possess greater or poorer compatibility in terms of thermoplastic processing based on interfacial interactions. In polymer/polysaccharide blends, immiscibility mainly

occurs due to repulsion of polar functionalities and hydrophobic polymer matrices of commonly used synthetic thermoplastics such as polyolefins. Therefore polar biopolymers such as polyesters and polyamides may have promise as thermoplastic blend partners for natural polymers.

This review provides a comprehensive summary of the thermoplastic processing of natural polymers. It focuses on the most abundant natural polymers such as cellulose, lignin, and chitin which can be obtained from natural resources or from waste biomass.

3. Lignocellulosic Biomass

3.1. Cellulose

3.1.1. Structure and Isolation

Cellulose is the most abundant natural polymer and is an essential structural component of the cell walls of higher plants. It is a homopolymer consisting of glucose units connected by β -1,4-glycosidic bonds. The chains are mainly parallel to one another, allowing the formation of highly crystalline regions.^[1] Just like other structural polysaccharides, strong intermolecular and intramolecular hydrogen bonding prevent the thermal processing of unmodified cellulose molecules. This is due to the resulting glass transition higher than their thermal decomposition occurring at 329 °C before melting.^[19]

Cellulose is widely used in various industrial branches such as the paper, textile, packaging, food, and pharmaceutical industries. The most common sources are wood and cotton, with the latter having a much higher cellulose content. As wood is more abundant, pulp and paper processing developed at an early stage and today the main isolation techniques for cellulose from biomass have been developed for wood. Cellulose from wood materials must be separated from lignin and hemicelluloses via physical, chemical, or biochemical processes. Well-known chemical treatments are the sulfate or Kraft process, sulfite process, and soda process. Solvent-based processes using milder conditions and focusing on the lignin removal are *inter alia* the organosolv and organocell process. Another possibility for cellulose dissolution directly from biomass could be the use of ionic liquids (IL), having been widely used for cellulose dissolution in recent years.^[20–28] In particular, ILs with strong hydrogen-bond acceptors with anions such as chloride or acetate have shown the ability to dissolve cellulose under relatively mild conditions.^[29]

3.1.2. Approaches for Thermoplastic Processing

Chemical modification: The development of cellulose with thermoplastic properties derived from chemical modification started back in the nineteenth century.^[30] Thermoplastic cellulose derivatives can be obtained by chemical modifications, primarily focusing on substitution reactions or grafting of the hydroxyl groups present on the polysaccharide backbone.^[31] The molecular structure of cellulose and possible reaction sites are shown in **Figure 1**. Although cellulose nitrates belong to

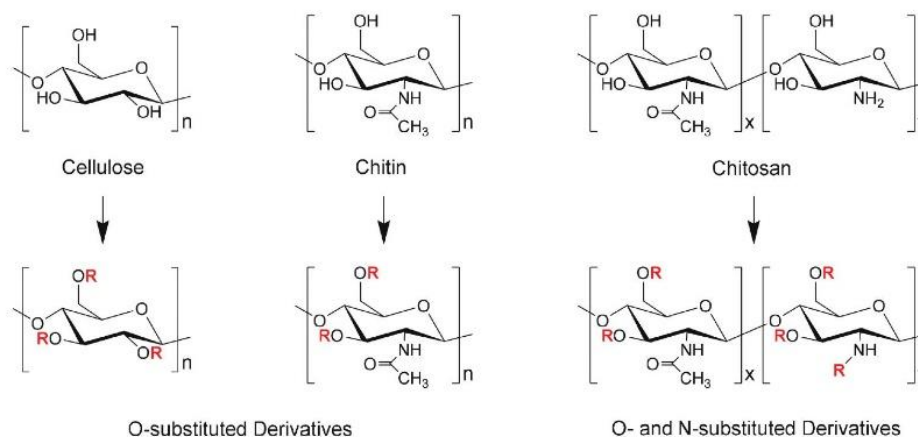


Figure 1. Molecular structures of cellulose, chitin, and chitosan and their potential reaction sites for chemical modification. Adapted with permission.^[33] Copyright 1998, Elsevier.

the thermoplastic cellulose derivatives, their use has become obsolete in most technical applications because it is highly flammable and explosive. They are therefore not further described here. Commercially available derivatives include cellulose esters such as cellulose acetate (CA) and mixed esters such as cellulose acetate propionate (CAP) and cellulose acetate butyrate (CAB). An example application of CA is shown in **Figure 2**. Cellulose can be both esterified and etherified at three hydroxyl groups, therefore monoesters, diesters, or triesters can be formed. Mixed ester or ether derivatives with multiple substituents are also possible and have been shown to improve thermal processing.^[32] The induced thermoplasticity is therefore not only a function of the type of substituents but also depends on the degree of substitution (DS) as well as the number of esters or ethers per cellulose unit. Transparent, amorphous materials can be processed by extrusion and injection molding techniques, most often with the addition of external, mainly monomeric plasticizers due to the narrow processing window between softening or melting and decomposition.

Esterification using long chain fatty acids such as lauric or stearic acid to promote hydrophobicity also leads to thermoplastic cellulose derivatives. Even at low degrees of hydroxyl group substitution, thermoplastic behavior was observed. However, the cellulose backbone stays rigid; therefore higher

degrees of substitution are needed if the material is to be suitable for industrial use without further plasticization.^[37] Mixed cellulose acetate oleate esters have recently been synthesized and films have been prepared via solvent casting. When compared to CA films, the added oleic acid acted as a self-plasticizer for CA leading to lower T_g and melting point, ductile material properties, and even reducing both the oxygen and water vapor permeability.^[38] It should additionally be noted that ILs can also be effectively used in the field of derivatization, serving as reaction media for cellulose modification.^[39–46] Recently, homogeneous esterification was performed in an ionic liquid. Hydroxyl groups were esterified both with bulky and small substituents, resulting in a relatively low T_g from 80 to 160 °C. The resulting materials can be used for common thermoplastic processing without external plasticization.^[47]

Besides esterification, cellulose ethers can also display thermoplastic properties. Via hydroxyl group substitution with alcohols, several derivatives such as methyl cellulose, carboxymethyl cellulose, and hydroxypropyl methylcellulose have been produced and commercialized. They are mainly used in food, cosmetic, and pharmaceutical applications as well as for viscosity control in several engineering applications. Ethyl cellulose possesses thermoplastic properties, with polymer grades such as Ethocel (T_g 129–133 °C, T_m 165–173 °C^[48]) being commercially available. Nevertheless, cellulose ethers can still be



Figure 2. Examples of processed thermoplastic biopolymers from cellulose, chitosan, and lignin. From left to right: a) Computer keyboard and mouse injection molded from cellulose acetate. Reproduced with permission.^[34] Copyright 2018, FKUR Kunststoff GmbH; b) injection molded tension rods made of chitosan. Reproduced with permission.^[35] Copyright 2010, Fraunhofer IFAM; and c) injection molded soap dish using lignin-based ARBOFORM. Reproduced with permission.^[36] Copyright 2019, Original Unverpackt GmbH.

considered to be rigid polymers that require additional plasticization.^[49] For further information on derivatives and their chemical structures, good summaries are given by Teramoto^[31] and Majewicz et al.^[48]

In contrast, graft polymerization is often presented as an effective modification for inducing thermoplasticity without further additives and related undesirable side effects of plasticizer migration^[50] and has therefore been widely used for cellulose modification.^[51] Chemical grafting onto the cellulose backbone has been performed with different monomer and polymer chains such as poly(methyl methacrylate) (PMMA),^[52,53] PLA,^[50,54–57] polystyrene (PS), poly(vinyl acetate) (PVAc),^[51] PHA,^[58] and poly(ϵ -caprolactone) (PCL).^[55] For example, when grafting ϵ -caprolactone and lactic acid onto cellulose diacetate, transparent polymer sheets were obtained from hot-pressing at circa 200 °C without the use of any additional plasticizer.^[55] Other cited studies mainly focused on reaction mechanisms and did not evaluate the thermoplastic properties of the final materials. Interestingly, a number of those graft polymerizations have been performed in ionic liquids within the last decade.^[54–57,59] Via “one-pot” modification in 1-allyl-3-imidazolium chloride ([Amim]Cl) native cellulose was successfully transformed into a series of CP-graft-PLA (CP-g-PLA) copolymers. When the PLA content exceeded 28%, the copolymers showed thermoplastic behavior and were suitable for melt processing.^[54] Biodegradable cellulose-based fibers could be directly formed via melt processing. PLA was grafted onto cellulose, also using [Amim]Cl as a reaction medium in a co-rotating twin screw extruder. Induced thermoplasticity was concluded from mechanical performance and thermal analysis.^[60] Moreover, cellulose derivatives can be further modified by chemical grafting. For example, thermoplastic carboxymethyl cellulose was synthesized by graft copolymerization with methyl acrylate and further blended with polyethylene oxide (PEO) to produce nanofibers.

However, neither thermal analysis nor thermal processing were performed in the study.^[61]

Use of plasticizers: For cellulose, a wide group of industrial plasticizers have been used. For example, citrates, glycol ethers and their esters, and phthalates have been highly recommended as efficient plasticizers for cellulose. For derivatives, and especially cellulose esters, several adipates, azelates, glycol ethers and their esters, glutarates, isobutyrate, phosphates, and phthalates are among the recommended plasticizers, all being able to interact with the polymer chains.^[62] Plasticizer screening for cellulose acetate started in the 1940s, focusing on compatibility in terms of solubility or plasticizer retention under certain conditions.^[63] **Table 1** shows examples of commonly used plasticizers and more recent processing strategies for thermoplastic cellulose.

Ghiya et al.^[64] also showed that citrates such as triethyl citrate and acetyl triethyl citrate display miscibility and also lowered the T_g of cellulose acetate (T_g 190 °C) down to 112 °C with 50% plasticizer addition. Furthermore, the biodegradability of the resulting materials was increased. Regarding the processing, Phuong and Lazzeri^[76] used triacetin in extrusion processing of cellulose diacetate. Extrusion was only possible when using a minimum of 20 wt% triacetin, as below this concentration the melt processing temperature exceeded the decomposition temperature. However, when the plasticizer content was higher 40 wt% the mechanical performance became unacceptably low.

Polyethylene glycol (PEG), another popular plasticizer in biopolymer processing, was also added to cellulose acetate during melt processing. The plasticizer efficiency of PEG 200 was compared to triethyl citrate, with higher melt viscosity reduction during processing and higher tensile strength and elongation at break values in the final materials.^[65]

Cellulose diacetate was further plasticized with diethyl phthalate, showing partial miscibility. It was reported that

Table 1. Examples of physical modifications for thermoplastic cellulose.

Type of cellulose	Modification	Modifier	Mass ratio cell/modifier	Processing	T_g [°C] ^{a)}	Ref.
CA (DS = 2.5)	Plasticization	Triethyl citrate	70/30	Melt extrusion	121/190/—	[64]
CA (DS = 2.5)		Acetyl triethyl citrate	70/30	Melt extrusion	120/190/—	[64]
CA (DS = 2.5)		PEG 200	75/25	Melt extrusion	99/202/—	[65]
CA (DS = 2.5)		Diethyl phthalate	75/25	Solution casting	101/190/—	[66]
MC ^{b)} (DS = 1.6–1.9)		Malic acid	70/30	Solution casting	—/—/—	[67]
MC ^{b)} (DS = 1.6–1.9)		Sorbitol	70/30	Solution casting	—/—/—	[67]
Cellulose		Choline chloride/urea	70/30	Gel formation, plasticizer soaking	—/—/—	[68]
CA (DS = 2.4)		[Bmim]BF ₄	75/25	Paste mixing, film compression	120/225/—	[69]
CAB	Polymer blending	PHB (M_w = 800 000)	75/25	Melt blending @ 190–235 °C	87/114/4.5	[70]
HECA ^{c)}		PHB (M_w = 23 000)	60/40	Solution blending	8/—/10	[71]
CAB		PBS	80/20	Melt blending @ 200 °C	—/—/—	[72]
CA (DS = 1.0)		PA6	80/20	Solution blending, fiber spinning	—/—/—	[73]
CB ^{d)} (DS = 2.4)		PCL (M_w = 32 000)	70/30	Solution blending, solvent evaporation	65 ^{a)} /115 ^{a)} /—	[74]
CB ^{d)} (DS = 2.0)		P(VP-co-MMA) ^{f)} (M_w = 189 000)	80/20	Solution blending, solvent evaporation	115 ^{a)} /139/100	[75]

^{a)}Glass transition temperatures of physically modified cellulose/unmodified cellulose/blend polymer; ^{b)}methyl cellulose; ^{c)}hydroxyethyl cellulose acetate; ^{d)}cellulose butyrate; ^{e)}from DSC thermogram; ^{f)}poly(*N*-vinyl pyrrolidone-co-methyl methacrylate).



phase separation occurred above 25 wt% plasticizer, as evidenced by a change from a single glass transition to two different T_g regions.^[66] They also reported that the Fox equation,^[77] an easy empirical model used to predict T_g of a polymer/plasticizer system, showed large deviations, concluding that the model does not consider interactions such as hydrogen bonding which are dominant in most natural polymer systems. Another approach for cellulose acetate was therefore suggested by Fridman and Sorokina, using the difference between glass and brittle transition temperatures as a criterion for plasticizer efficiency.^[78]

Methyl cellulose films were plasticized with malic acid and sorbitol. The compatibility was deduced from mechanical performance, such as enhanced flexibility, and homogeneous morphology based on SEM micrographs. Based on percentage elongation values, sorbitol showed the highest plasticizing efficiency, however this was mainly due to a higher equilibrium moisture content during storage.^[67] The comparison of plasticizer efficiency with respect to the induced thermoplasticity is still difficult as no investigations of thermal properties have been carried out. However, plasticizers such as citrates or PEG both showed good compatibility with cellulose esters and are advantageous in terms of plasticizer migration compared to conventional low-molecular weight polyols.

As deep eutectic solvents (DES) and ILs have been reported to be good solvents for cellulose,^[79,80] they have also been tested for their plasticizing efficiency in cellulose films. A typical DES, choline chloride and urea, has been suggested to function as an effective plasticizer, showing no phase separation and leading to transparent, soft materials having enhanced elongation. The plasticizer ratios employed varied from ≈ 30 –60%.^[68] Ionic liquid 1-butyl-3-methylimidazolium tetrafluoroborate ([Bmim] BF₄) was used as a plasticizer for cellulose diacetate. A smooth homogenous phase structure, reduced crystallinity, and T_g depression from 225 to 95 °C resulted when incorporating up to 35 wt% [BMIM]BF₄. Such high T_g depression indicates strong intermolecular interactions and reduced hydrogen bonding between the polymer chains. Although no thermoplastic forming process was performed, studies on the melt viscosity at 170–190 °C indicate a greatly reduced working temperature compared to non-plasticized samples.^[69] If one compares the plasticizers described for cellulose esters, [BMIM]BF₄ seems to be one of the most efficient plasticizers when using equal mass concentrations.

Cellulose blends: The method of using higher molecular weight structures can offer several advantages such as reduced or almost no migration, synergistic effects regarding for example mechanical performance and, in cases where thermoplastic polymers are used, the possibility for thermal processing. Attempts to blend cellulose with thermoplastic polymers have been performed extensively. However, with regard to structural compatibility, it is mainly biodegradable polyesters that have been tested. Table 1 shows some examples of compatible blends that have been studied.

PHA/cellulose ester blends are common.^[81] Miscible blend systems have been reported for poly(3-hydroxybutyrate) (PHB) with CAB and CAP. Extruded blends were transparent and

amorphous, although the crystallinity increased with PHB content. Ethyl cellulose, however, though having a T_g similar to CAP, formed immiscible blends with PHB.^[82]

The biodegradable, thermoplastic polymers poly(butylene succinate) (PBS) and PCL were blended with different cellulose. The incorporation of PBS lowered the melt apparent shear viscosity with increasing PBS ratio up to 20 wt%, indicating that PBS acts as a plasticizer for CAB. This is also evident from mechanical testing, where increasing PBS ratios lowered Young's modulus and enhanced elongation. Including additional observations, it was stated that CAB and PBS are miscible in the molten state, however phase separation occurred during cooling mainly due to crystallization of PBS.^[72] Yakub et al. blended polycaprolactam (PA6) and PCL with cellulose monoacetate for fiber formation. Electrospun, nanoscale fibers were bead-free and uniform, indicating good compatibility between those polymers.^[73] Compatibility with PCL was already observed by Tighe et al. who melt blended CAB with PCL with and without several plasticizers.^[83] However, the miscibility changes with ester group and DS, with a high DS required for increased interactions.^[74]

Cellulose diacetate was also blended with modified starch. The polymers were plasticized with triacetin and epoxidized soy bean oil, respectively. Although both polymers share similar structural characteristics, an "island and sea" morphology was obtained even at equal material proportions.^[84] Another study also observed the immiscibility of cellulose acetate/starch blends.^[85] Keeping in mind that there are only a few polymers that are really miscible, structural modifications such as the esterification of cellulose are obviously sufficient to favor interactions between the polymer chains of one polymer rather than inter-polymer interactions, even when both polysaccharides have structural similarities. CA was also combined with lignin. The study only observed one T_g in a cellulose acetate/native lignin blend, whereas acetosolv lignin showed immiscibility. This therefore indicates that the modification during the acetosolv processing of lignin is followed by decreased molecular interaction between both blend partners.^[86] The miscibility behavior of cellulose esters with different vinyl copolymers was also determined as a function of the degree of ester substitution in cellulose esters and the *N*-vinyl pyrrolidone units in vinyl copolymers, showing that cellulose propionate gives the greatest miscibility window compared to acetate or butyrate.^[75] When blending CA with vinyl polymers including PVAc and PVP, thermal analysis indicated immiscibility with PVAc independent of the DS. On the other hand, miscibility between PVP and CA was observed with a DS of less than 2.8, forming homogeneous blends.^[87] Such studies may be used as examples for the assessment of general tolerability behavior. When designing a polymer blend, however, various factors influence the final film properties besides the chemical structures. First of all, the type of mixture (e.g., the mixing of polymer melts or polymer solutions) can be decisive at the thermodynamic level. Chain interactions also depend on the polymer chain lengths and volumes. It is therefore difficult to compare different studies without adequate information about the polymers and processes that have been used.

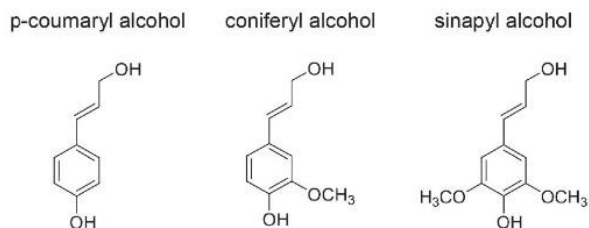


Figure 3. Monomeric phenylpropane units in lignin.

3.2. Lignin

3.2.1. Structure and isolation

Lignin is the matrix polymer in the biogenic composite material that we call wood. Together with cellulose and hemicelluloses it forms the essential components of vascular plants. It is a complex phenolic heteropolymer and mainly occurs in association with polyoses in the plant cell wall which are linked to the cellulose elementary fibrils. Therefore wood is often termed lignocellulose. As a consequence, lignin is a by-product of the paper and pulp industry and its chemical structure alterations also derive from industrial pulp processes such as the Kraft, sulfite, soda, and organosolv processes. The main monolignols (phenylpropane units) that occur in lignin are p-coumaryl alcohol, coniferyl alcohol, and sinapyl alcohol (Figure 3), varying in composition and content. Native lignins are highly cross-linked networks having an amorphous structure due to their complexity and heterogeneity.^[88] Therefore, different T_g values have been observed ranging from 90–150 °C^[89,90] and degradation takes place slowly at temperatures from 250–500 °C,^[91,92] mainly depending on the type of lignin, isolation process, molecular weight, and water content. During isolation processes the degree of polymerization decreases, also leading to decreased molecular weight and thermal stability.^[91,92]

3.2.2. Approaches for Thermoplastic Processing

Unlike unmodified cellulose or chitin, lignin undergoes softening above a certain temperature. Thermoplastic processing of lignin is however limited. It is prevented by strong interactions between hydroxyl groups^[11] and additionally radical-induced self-condensation between functional groups at higher temperatures.^[93] Lignin-based thermoplastic materials are already commercially available; examples are ARBOFORM and Xylomer. ARBOFORM is a composite comprising chemically modified lignin, natural fibers, and various additives that can be used for injection molding.^[94] An example application is shown in Figure 2. Xylomer is a modified lignin-based blend used in various thermoplastic processing methods such as film extrusion and injection molding. For both materials different techniques for plasticization were combined.

Chemical modification: As for cellulose, chemical modification is a common technique for producing thermoplastic lignin. The complex structure of lignin results in various possible reaction sites; primarily hydroxyl groups but also carbonyl

and aldehyde groups. A proposed structure for beech wood lignin is shown in Figure 4. Despite the large number and variety of functional reaction sites in lignin, most modifications have focused on the functionalization of the hydroxyl groups.^[90] Derivatives masking the reactive hydroxyl groups result in lower T_g owing to reduced intermolecular and intramolecular interactions and this facilitates the thermoplastic processing.^[95] The most common modifications for thermoplasticity are etherification, esterification, polymer grafting, and copolymerization. For further information on derivative structures and mechanisms, good overviews are given by Wang et al.^[95] and Laurichesse and Avérous.^[90]

Acetylation reactions are also used to enhance lignin solubility. Standard esterification reactions are performed using acid anhydrides or acyl chlorides and either acid or base catalysts. Here, the length of the alkanate chain and the degree of esterification in the resulting lignin esters determine the changes in T_g and melt behavior. A linear correlation between T_g depression and the chain length of the acyl substitutes was found.^[95,96] Consequently the T_g varies from around 100 °C in lignin acetates, circa 80 °C in lignin propionate, and around 50 °C in lignin butyrate^[97,98] down to 2 °C in lignin laurate.^[97] Another interesting modification strategy for thermoplasticity in this context was presented by Luo et al.^[99] who added carboxylic acid derivatives and organic solvent during lignin extraction from black liquor. However, thermoplastic films could only be processed with the use of additives, again showing that the occurrence of a T_g alone does not necessarily lead to thermoplastic processing properties. Soda lignin was functionalized using *tert*-butyldimethylsilyl chloride and silylation was compared to acetylation with regard to the derivative properties. Silylation enhanced the thermal stability and lowered T_g and additionally improved the solubility in organic solvents. Although pure lignin derivatives were not processed alone, thermoplastic blends with PE were prepared. Material characterization revealed higher compatibility of silylated lignin compared to neat and acetylated samples.^[100]

With regard to etherification, both hydroxyalkylation and methylation, focusing on a reaction with the phenolic hydroxy groups, have been performed.^[95] Hydroxyalkyl derivatives can be obtained by treatment with an alkylene oxide such as ethylene, butylene or propylene oxide in solution. The resulting derivatives have T_g values between 50 and 80 °C.^[102] Methylated lignin shows a minor T_g depression compared to unmodified lignin,^[93] with values decreasing from ≈ 126 –10 °C.^[103] Although no thermoplastic processing was performed, one can deduce that longer alkyl chains should enable chain mobility at lower temperatures, which could enlarge possible processing temperature ranges. This is especially important with respect to any thermosetting behavior caused by radical-induced self-condensation at higher temperatures.

Chemical grafting is an effective technique for overcoming incompatibilities between polymers and is mainly based on radical polymerization. Depending on the polymer combination, the thermal processing properties of the resulting co-polymers can be adjusted. Examples of lignin co-polymers derived from chemical grafting include lignin graft PCL copolymers,^[104] lignin graft PS copolymers,^[105–109] lignin graft PMMA,^[109] and lignin graft poly(*n*-butyl acrylate).^[108]

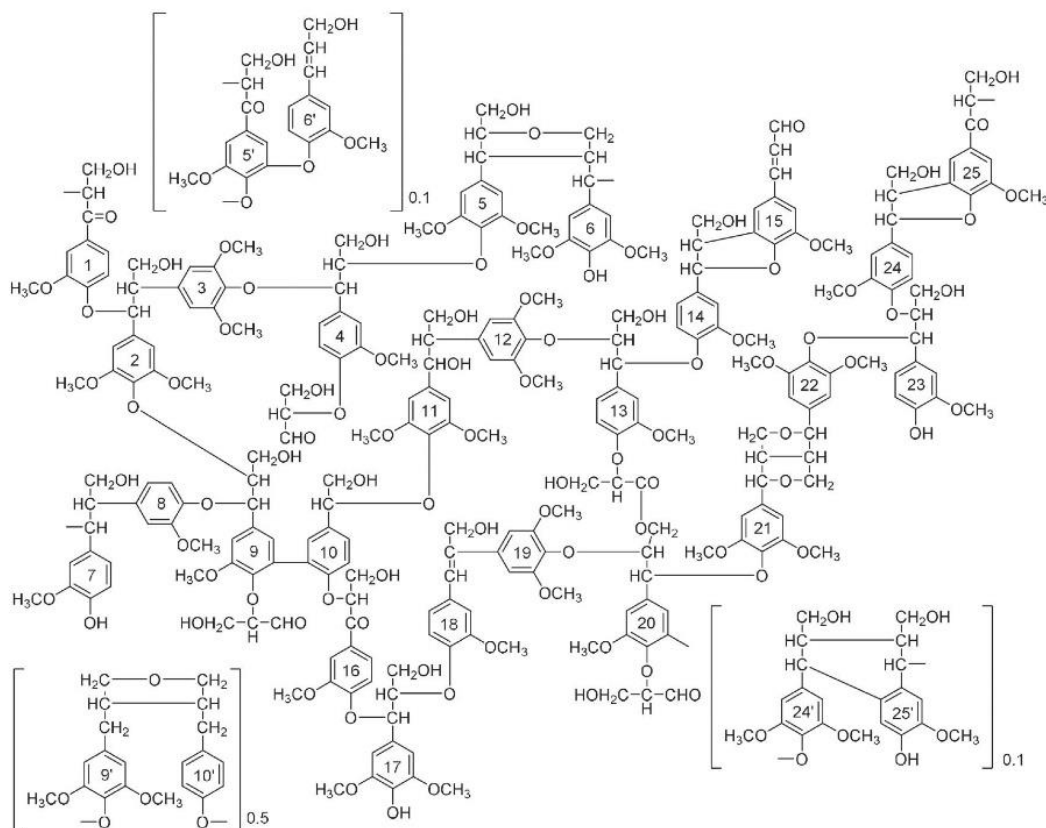


Figure 4. Proposed structure of beech wood lignin. The C_9 phenylpropane units are ascribed consecutive numbers. Units 5/6 (4-O-5 type), 9/10 (β,β -tetrahydrofuran type), and 24/25 (β -5-benzofuran type) can to some extent be replaced by dilignol units shown in brackets. Adapted with permission.^[101] Copyright 1974, Wiley-VCH.

PMMA and PS were grafted onto Kraft lignin using atom transfer radical polymerization (ATRP). This resulted in maximum lignin weight fractions of $\approx 20\%$. PMMA-g-lignin samples had almost twice the elongation of PS-g-lignin samples. Glass transitions increased with lignin content and were detected at 77 and 79 °C at the highest mass fractions respectively.^[109] Another study on PS-g-lignin produced sheets by compression at 150 °C. Differential scanning calorimetry showed endothermic peaks at around 100 °C on all the grafted samples. Furthermore, the grafted polymers possessed biodegradability which is not present in pure PS.^[110]

Kraft lignin and styrene were modified using γ -irradiation. Increased hydrophobicity, mobility in the liquid state, and thermal stability were detected for radiation grafted lignin. At 19 wt% styrene content and for γ -irradiation of 50 kilogray, the T_g decreased to 126 °C.^[107]

Soda lignin-g-PCL was synthesized by ring-opening polymerization. The monomer ratios used varied from 5 to 100 mol per hydroxyl group of the lignin and sheets were compression molded from the resulting materials at 80–100 °C and 150 bar. The T_g of the starting lignin was determined to be 143 °C, while transitions in the grafted samples were only clearly detectable at a molar ratio of 5 (monomer/OH-group) at temperatures of -40 to -30 °C. It was also stated that two categories of materials can be obtained, depending on the applied molar ratio. With

short PCL residual chains, amorphous structures are generated and flexible polymers are produced. Higher molar ratios lead to PCL/lignin phase segregation with crystalline PCL regions, so the brittleness is increased. Modified lignins have been proposed building blocks for polymerization reactions, for example to be carried out on residual OH groups.^[104]

In order to produce alkaline lignin/PLA blends, lignin was grafted with PLA-copolymer via ring-opening polymerization. Relatively high mass fractions of circa 68% were achieved, resulting in a slightly reduced T_g and enhanced mechanical performance based on tensile strain and strength, with the latter only observed at low lignin ratios in final blends.^[111] As graft polymerization is mainly used for incompatible polymers, the resulting materials still show two different phases and thermoplasticity only derives from the intrinsically thermoplastic polymers. When high ratios of the thermoplastic polymer are used, comparison of the induced thermoplastic properties is therefore not sensible.

Use of plasticizers: The easiest way to enable thermoplastic processing is the addition of a plasticizer. Bouajila et al. studied a set of plasticizers such as PEG, aromatic compounds similar to monolignols, and organic acids under dry and wet conditions.^[11] PEG was described as a very good plasticizer for lignin^[112] and different molecular weights can be used to adjust the properties. With regard to lignin plasticization, a



scaled plasticizer efficiency value normalized to that of water was proposed. This is related to the hydrogen bond breaking mechanism, resulting in different calculated functionalities. With this approach, PEG molecules gave a plasticizer efficiency proportional to the number of oxygen atoms and showed the highest calculated functionality. This was followed by smaller ethylene glycols and lignin-like aromatic compounds. The efficiency of a plasticizer refers to the respective T_g of the polymer/plasticizer mixture.^[111] As in an earlier study on different synthetic plasticizers for lignin, the relationships between solubility parameters and plasticizer efficiency were investigated. When comparing a broad variety of phthalic, phosphoric, and aliphatic acid esters, it was observed that softening temperatures were lowered when solubility parameters converged.^[113] However, plasticizers were compared using the same mass ratios without respect to molar ratios. A selection of well-studied plasticizers and recent processing strategies is given in Table 2.

Polyvinyl chloride (PVC) plasticizers such as diethylene glycol dibenzoate (Benzoflex), tricresyl phosphate (Lindol), and alkyl sulfonic phenyl ester (Mesamoll) were reported to have good compatibility with lignin. Three lignins were used, differing in their molecular weight, solubility parameter, and initial T_g . When comparing the same plasticizer loadings, the highest T_g depression was observed using diethylene glycol dibenzoate with a reduction of $\Delta T_g = 65\text{--}86\text{ }^\circ\text{C}$, followed by tricresyl phosphate. In general, higher depression was obtained in dry lignin powder.^[115]

Park and others patented a route to thermoplastic lignin by adding polyols such as ethylene glycol and propylene glycol and melting point reducers such as waxes and oils that are all miscible in the melted state, processed via hot blending. The described examples using tall oil or paraffin wax in PEG 200 plasticized lignin showed melting point reductions from initially $162\text{ }^\circ\text{C}$ to ≈ 50 and $70\text{ }^\circ\text{C}$.^[116]

Following the previously described approach for cellulosics and also being a solvent for lignin, DES^[123] and ILs^[124,125] could additionally serve as potential external plasticizers. Sulfonamides, another group of plasticizers mainly used in hot-melt adhesives, could also benefit miscibility and favor plasticization based on structural similarities to lignin.

By way of supplementary information, it should be noted that due to its bulky structure and various functional groups several attempts to use lignin as a plasticizer have been reported recently. Detailed information can be found elsewhere.^[126–128]

Lignin blends: Using higher molecular weight plasticizers with a polymeric structure, polymer blends are obtained whose properties mainly depend on the miscibility. Compatibility can mainly be ascribed to the degree of intermolecular interactions between two or more of the blend partners. The different types of functional groups in lignin generally favor intermolecular interactions with thermoplastics that are able to form hydrogen bonds such as polyesters and polyamides. However, some steric obstacles are caused by the bulky cross-linked molecules.

Polymers reported to be miscible with lignins include PEG,^[129] PEO, polyethylene terephthalate (PET),^[117] poly(hydroxybutyrate) (PHB),^[130] and PVP.^[119] Poly(vinyl alcohol) (PVA) and polypropylene (PP) appeared to be immiscible.^[117] The miscibility with PEO and PET could be detected

by single T_g depression, with PEO giving greater decreases with increasing PEO fraction compared to PET. Good miscibility with PEO was explained as being due to intense interaction of lignin hydroxyl groups with hydrogen accepting sites of PEO. This aspect was also investigated via Fourier transform infrared (FT-IR). The compatibility of PHB blended with different ratios of soda lignin in a twin screw extruder was investigated. A single T_g was detected up to a lignin ratio of 40 wt%. The compatibility was ascribed to hydrogen bonding between reactive functional groups of lignin and carbonyl groups of PHB. Soda lignin furthermore improved the thermal stability of PHB by means of thermal degradation.

Even if macroscopic or microscopic immiscibility between two polymers is present, intermolecular actions can still be sufficient to form a compatible blend. For example, immiscible blends obtained from PVA/Kraft lignin mixtures via thermal extrusion still formed strong intermolecular interactions. Not only was the PVA crystallinity reduced, but also the melting point depression suggests strong interactions between the two polymers.^[131] Similar blends of PVA/thermoplastic starch (TPS)/lignin were used to adjust the biodegradability of thermoplastic biopolymer films.^[132] Selected compatible blends and processing methods are summarized in Table 2.

Blends with PLA showed immiscibility unless a compatibilizer such as maleic-grafted PLA was used.^[133] However, strong intermolecular interactions were detected using differential scanning calorimetry (DSC) and FT-IR spectroscopy,^[134] concluding that hydrogen bonds between the phenolic hydroxyl groups of lignin and the carbonyl groups of PLA were formed.^[135] The compatibility of such blends could be enhanced via reactive grafting of either PLA copolymers^[111,136] or acrylic monomers^[137] onto lignin.

Various processing techniques can also be combined. Several studies have blended lignin derivatives with other thermoplastic polymers. Different lignin alkyl esters were blended with thermoplastic CAB,^[97] PCL, PVAc, and PVP,^[119,120] mainly resulting in multiphase systems. However, thermal analysis showed good miscibility with PVP and PCL, naturally differing with derivative type. Although hydroxypropyl lignin showed immiscibility with polyethylene-co-vinyl acetate (EVA), it was observed that compatibility increases with increasing vinyl acetate content^[138] due to increased intermolecular interactions such as hydrogen bonding. Recently, highly loaded lignin/EVA composites were fabricated with up to 75 wt% lignin. At these mass fractions the lignin exhibits shear-induced self-plasticization. A pronounced relaxation endotherm superimposes the T_g for composites with close-packed lignin particles, which was ascribed to molecular confinement of the EVA matrix due to internal stresses.^[139]

The thermoplasticity and mechanical performance of initially brittle ethylated and methylated Kraft lignins were improved when miscible blends with around 30 wt% aliphatic polyesters such as poly(butylene adipate) and poly(trimethylene succinate) were produced and characterized. In the case of poly(trimethylene succinate), T_g was lowered from ≈ 150 to $23\text{ }^\circ\text{C}$.^[122] However, polymer mixing was performed in solution and thermoplastic processing properties were not verified. Also, no information about the molecular weights of the polyesters was found.

Table 2. Examples of physical modifications and recent processing strategies for thermoplastic lignin.

Type of lignin	Modification	Modifier	Mass ratio lignin/modifier	Processing	T_g [°C] ^{a)}	Ref.
Kraft	Plasticization	PEG dimethyl ether	80/20	Solution blending	90/160/—	[11]
Kraft		Lactic acid	80/20	Solution blending	60/160/—	[11]
Kraft		Vanillin	80/20	Solution blending	100/160/—	[11]
Organosolv (hardwood)		Diethylene glycol dibenzoate	77/23	Dry mixing, heating @ 145 °C extrusion blending	35/97/—	[114]
Organosolv (hardwood)		Butylbenzyl phthalate	77/23	Dry mixing, heating @ 145 °C extrusion blending	38/97/—	[114]
Organosolv		Glycol dibenzoate	74/26	Dry mixing, extrusion	32/97/—	[115]
Kraft (softwood)		Glycerol	75/25	Hot blending, extrusion	132/—/—	[116]
Kraft (softwood)		PEG 200	75/25	Hot blending, extrusion	162/—/—	[116]
Kraft (softwood)		PEG 200, paraffin wax	68/32 (23 + 9)	Hot blending, extrusion	54/—/—	[116]
Kraft (softwood)		Polypropylene glycol	75/25	Hot blending, extrusion	119/—/—	[116]
Kraft (softwood)		1,3-propanediol	75/25	Hot blending, extrusion	48/—/—	[116]
Kraft (hardwood)	Polymer blending	PEO ($M_w = 100\,000$)	75/25	Mechanical mixing, extrusion spinning	10 ^{b)} /108/—55 ^{b)}	[117]
Kraft (hardwood)		PET ($M_w = 27\,000$)	75/25	Mechanical mixing, extrusion spinning	90 ^{b)} /108/80 ^{b)}	[117]
Soda		PHB	70/30	Extrusion blending	21/134/3	[118]
Organosolv ^{c)}		PVP ($M_w = 24\,500$)	60/40	Solution blending, solvent evaporation	155 ^{b)} /110 ^{b)} /175 ^{b)}	[119]
Organosolv ^{d)}		PCL ($M_w = 40\,000$)	75/25	Solution blending, solvent evaporation	5 ^{b)} /40/—65	[120]
Kraft (softwood) ^{e)}		PLA ($M_w = 80\,000$)	60/40	Melt blending @ 150 °C	56/—/65	[121]
Organosolv ^{f)}		CAB ($M_w = 127\,600$)	70/30	Solvent casting, melt extrusion	95 ^{b)} /120 ^{b)} /87 ^{b)}	[97]
Kraft (softwood) ^{g)}		Poly(trimethylene succinate)	70/30	Solvent casting	23/155/—37	[122]
Kraft (softwood) ^{h)}		PEG ($M_w = 10\,000$)	80/20	Solvent casting	—15/150/—33	[122]

^{a)}Glass transition temperatures of physically modified lignin/unmodified lignin/blend polymer; ^{b)}from DSC-thermogram; ^{c)}esterified (lignin acetate, 60% acylated); ^{d)}esterified (lignin valerate); ^{e)}alkyl-chain modified lignin (42 wt% polylactic acid-modified lignin); ^{f)}esterified (lignin acetate); ^{g)}methylated lignin.

Kim et al. also used alkyl-chain modified lignin in blends with PLA. Good compatibility was achieved by using alkyl chains with solubility parameters similar to the matrix polymer.^[121] By using compatibilization methods, thermoplastic polymers having poor interactions with lignin, such as hydrophobic polyolefins, can also be used as a thermoplastic matrix. Several studies, as well as commercially available materials, involve blending lignin with PE or PP.^[140–142] However, without compatibilization, for example via copolymerization with suitable polymeric structures, phase separation occurs and the lignin only acts as a reinforcing filler.

4. Chitin Biomass

4.1. Chitin and Chitosan

4.1.1. Structure and Isolation

Chitin is a polysaccharide. It occurs naturally in the exoskeleton of several invertebrates, especially marine animals and insects, as well as in the cell walls of fungi, yeasts, and algae. Chitin is considered to be the second most abundant natural polymer. Every year more than 1.5 million tons of chitin are

available as residues from the fishing industry (shell waste), biotechnology (fermentation residues), mushroom cultivation (mycelia), and protein production (insect exoskeletons). It is estimated that so far only 10 000 tons per year are used worldwide, with the main uses being membrane, drug, food, cosmetic, and biomedical applications.^[143] The structure of chitin is similar to cellulose; however, the hydroxyl group at the C2 positions is replaced by an acetyl amino group. One widely used derivative of chitin is chitosan. The term chitosan refers to deacetylated chitin. It represents different structures varying in their degree of *N*-acetylation (DA) or put the other way around in their degree of deacetylation (DD), which highly influences their solubility properties. Due to the amino groups, chitin/chitosan materials possess biocompatibility and antibacterial activity, giving rise to possible applications in the medical, pharmaceutical, textile, and food packaging industries. However, chitin processing is impeded by its extremely poor solubility and thermal degradation prior to or simultaneous to melting in the range of 350 to 410 °C depending on type of crystallinity and heating rate.^[144] Hence, chitosan is favored for further processing due to its solubility in common organic solvents as well as in water and aqueous acidic solutions. The solubility depends on the degree of deacetylation.



A variety of isolation techniques have been used up until now, depending on the source and corresponding chitin ratio. The source and origin mainly determine the crystallinity, purity, and polymer chain arrangement.^[145–147] Up until now, waste crustacean biomass has been the preferred source for chitin isolation; however, techniques to extract chitin from other sources such as sponges,^[148] corals,^[149] mushrooms,^[150–153] insects,^[154–156] and worms^[157] are emerging. Prior to isolation from crustacean waste, contaminants such as proteins, enzymes, minerals, and natural pigments have to be removed. This may demand harsh chemical treatment involving strong bases or acids. For protein removal, enzymatic treatments have been suggested to be a more environmentally friendly alternative.^[158]

Furthermore, ILs have been reported as an alternative for direct extraction of chitin.^[159] Having shown great potential for cellulose dissolution, different ILs have been tested for chitin^[159–164] and chitosan.^[22,163–166] However, differing results have been obtained regarding the solubility behavior. The latter mainly depends on the structural properties of chitin such as its polymorphic form, source, molecular weight, and degree of acetylation.^[145,167]

4.1.2. Approaches for Thermoplastic Processing

Chemical modification: Chemical modifications of chitin have mainly followed the approaches used for cellulose due to structural analogies. However, additional reaction sites are available due to the amino groups in chitosan and acetamido groups in chitin. Chitin and chitosan structures and possible reaction sites are shown in Figure 1. Regio-selective reactions can therefore be significant for the DS distribution, influencing the final properties. The main modifications targeting improved solubility in water and organic solvents have been acylation or alkylation, possibly at both *N*- and *O*- sites of the polysaccharide. Due to its poor solubility, the chemical modification of chitin has often been performed under heterogeneous conditions. Based on their dissolution properties, ILs have been used to promote homogeneous reaction media.^[163,168] Acetylation, alkylation, and grafting reactions have been performed on both chitin and chitosan.^[163] Unfortunately, to the authors' knowledge, only a few studies have dealt with chemical modifications aimed at improving the thermoplastic processing properties.^[169,170] Nevertheless, structural modifications similar to those performed for thermoplastic cellulose could bring new routes for producing thermoplastic materials and are therefore included in this section.

The alkylation of chitins can produce amphiphilic polymers with new interaction sites. Once again, modifications are often aimed at improving the affinity for organic solvents. However, as longer hydrophobic alkyl groups in particular are able to disrupt hydrogen bonding and reduce the initial crystallinity,^[171] such modification could bring about thermoplastic behavior. Alkylation is preferably performed at functional *N*-sites with aldehydes or alkyl halides but conjugate addition reactions such as Michael type reactions are also performed.^[172]

N-benzyl chitosan (DD = 60%) was synthesized with benzaldehyde in the presence of a reducing agent. Modification along the polymer chain decreased the chitosan crystallinity and

changed the degradation behavior. Thermal analysis showed no distinct glass transition in the final materials.^[173] High degrees of substitution of 1.33 for *N*-benzyl chitosan (DA = 20%) were also obtained by reaction with benzyl bromide. The study successfully carried out *N*-alkylation of chitosans with different alkyl halides.^[174] Ethyl, butyl, and octyl chitosan (DD = 85%) films were produced via solution casting. The mechanical properties showed improved strength for the ethyl and butyl chitosans, while the elongation decreased. With a focus on biomedical applications, no hint is given of the thermoplasticity of the films.^[175] Using different aldehydes, partially deacetylated chitin (DD = 92–98%) was *N*-alkylated to final DS from ≈ 0.2 – 0.4 . Improved solubility in methanol was observed and attributed to hydrophobic side chains that are able to disrupt the hydrogen bonding of the chitosan polymer chains.^[176]

As observed for modified cellulose, the introduction of fatty acyl or aromatic acyl residues can break intermolecular hydrogen bonds and change the crystalline structure of chitin or chitosan. This therefore could not only improve the solubility in organic solvents^[177] but could also benefit the thermoplastic properties of such derivatives. Acylation reactions are mostly performed using anhydrides or acyl chlorides. Thermoplastic chitosan oligosaccharides were obtained from acylation with lauroyl chloride in methane sulfonic acid. At the highest molar ratio of 5 (lauroyl chloride:chitosan oligosaccharide), thermal analysis showed endothermic peaks at 64 and 110 °C. Also, changed crystallization behavior of lauroyl side chains and decreased chitosan crystallinity due to weakened intermolecular hydrogen bonds were observed using X-ray diffraction. Thermal behavior was additionally investigated using polarized optical microscopy, showing melting of the lauroyl side chains in a temperature range that can be correlated to the endothermic peak at 64 °C. The second endothermic peak was said to be related to melting of the crystalline regions of chitosan. However, further investigations should be performed to verify this hypothesis. *O*-acylation of chitosan nanofibers (DD = 80%) with short-chain and long-chain fatty acids was carried out by Zhang et al.^[178] to improve the stability in moist environments. Although no investigations on thermoplastic or mechanical behavior were performed, reduced crystallinity and a more amorphous structure were detected for modified chitosan, which could favor chain mobility during thermal processing. Depending on the chain length of the substituents, hydrophobic or hydrophilic properties were observed in water contact measurements. Therefore, the chain length can also play a decisive role with respect to compatibility with plasticizers and blended polymers.

N-acylation of chitosan (DA = 78%) with maleic anhydride was performed with a resulting DS of ≈ 1.2 – 1.6 . Derivatives showed higher thermal stability with regard to the degradation of the polysaccharide structure as well as a change in the initial crystalline structure of chitosan.^[179] Although the study targeted improved antibacterial activity for biomedical applications, maleinization also resulted in improved compatibility of chitosan-PE systems. The chitosan produced had a DA of 8–10% and the maleic anhydride to chitosan molar ratio was 0.4. Solid state acylation was performed via reactive extrusion.^[180] For further information on derivatives and their chemical structures, good overviews are given by Sashiwa and Shigemasa,^[181] Kurita et al.,^[171] and just recently by Khattak et al.^[182]



Many studies have been published over the last decade on chemical grafting. Some of them even focus on the thermoplastic processing properties of chitin and chitosan. Various acrylate monomers were grafted onto crab shell chitin to obtain biodegradable, thermoplastic films. Even so, glycerol was used as an external plasticizer for film formation via hot press. Shell chitin-*g*-PMMA with a grafting ratio of 30% showed thermoplasticity with a broad melting range around 130 °C. It also exhibited the highest tensile strength and water resistance.^[169] Oligo (lactic acid) was successfully grafted onto chitosan (DD = 90%). Although the thermoplastic properties were not determined, the use of blends with chitosan-*g*-PLA and PLA as biomaterials was suggested.^[50] Grafting techniques were also used for electrospun chitosan-graft-poly(lactic-*co*-glycolic acid) (chitosan-*g*-PLGA) composite nanofibers. Chitosan was grafted onto the PLGA surface up to a ratio of almost 40%. The resulting fibers had a smooth and uniform morphology and retained mechanical properties.^[183]

Chitin films regenerated from [Amim]Br solutions were grafted with poly (μ -lactide-*co*- ϵ -caprolactone) by ring-opening copolymerization in different composition ratios. The resulting materials had higher elasticity than pure chitin films.^[184] Chitin whiskers were also grafted with PCL to obtain thermoformable chitin-*g*-PCL bionanocomposites. The plasticization of chitin enabled the production of sheets by injection molding. The melting points and glass transitions of the produced materials were in the range of those of PCL. The highest chitin:PCL weight ratio used was 1:70.^[185]

Chitin was also grafted with PS via free radical polymerization with a chitin:monomer weight ratio of 1:3. A T_g was detected in the range of 106–109 °C, due to the PS polymer. The copolymer also showed higher thermal stability than chitin itself.^[186] Chitin-*g*-PS was also synthesized via ATRP using the IL 1-allyl-3-methylimidazolium bromide ([Amim]Br) for chitin dissolution. This approach was also suggested for other monomers in order to create chitin-based thermoplastic materials.^[187]

Use of plasticizers: Polyols are common plasticizers used for natural polymers, with glycerol being the one that has been used most. Various studies have used chitosan with a high degree of deacetylation, an aqueous acetic acid solution, and glycerol for plasticization and processed the mixture by mechanical kneading followed by a hot press.^[188–191] Also, other polyols such as sorbitol and xylitol have been tested using the same processing method. The added polyols reduced the crystallinity and layered microstructure of chitosan, with glycerol samples showing the lowest degree of crystallinity and sorbitol samples the highest.^[190] Another approach is given in a patent from 2010, where films are casted from aqueous chitosan solutions, mechanically shredded, and then used for extrusion. Depending on the solvents, plasticizers, and cross-linking agents used, derivatization of the chitosan can also occur.^[192] Injection molded tension rods based on patented formulations are shown in Figure 2. Another patent using polysaccharides and thereby also chitosan as a thermoplastic material stated that the incorporation of clay minerals stabilizes the extrusion process and additionally prevents water and plasticizer migration.^[193] Examples are summarized in Table 3.

Elastic films from chitin/chitosan nanowhiskers were produced; plasticized with di-, tri- and tetra-glycerol as well as PEG 600 with a 70/30 ratio (w/w). The plasticizer efficiency was compared by mechanical testing the final film materials. PEG 600 was observed to be less effective than glycerol oligomers, showing the lowest elongation and highest modulus values. T_g values decreased for all the samples but strongly varied with the water content and thermal history, as observed with repeated heating runs. A water content of ≈ 10 wt% in all samples should however be taken into account.^[194] Injectable scaffolds for biomedical applications were obtained from chitosan/PEG 400 and chitosan/PEG 4000 blends containing up to about 25 wt% chitosan (DD = 85%). There was miscibility at all the concentrations studied,^[195] showing PEG to be a suitable plasticizer for chitosan due to their compatibility.

Due to their hydrophobic structure, fats and fatty acids have been used for the plasticization of natural polymers by weakening hydrophilic intermolecular interactions such as hydrogen bonding. Olive and corn oil were used to plasticize chitosan (DD > 75%) / clay nanocomposites. Films were produced by solution casting and hot-pressed at 130 °C and 3 MPa for 5 min. When incorporating 20 wt% oil, T_g values of 153 and 132 °C were detected, respectively. However, based on the mechanical data and phase morphology, olive oil provided better plasticization. Additional incorporation of organoclay minimized phase separation and thus plasticizer migration.^[196] The same manufacturing process was used to compare the plasticizing efficiency of glycerol and oleic acid. When plasticizing efficiency was measured by means of mechanical performance and transition temperature, glycerol provided both higher elongation at break and a lower T_g of 68 °C compared to 127 °C for 20 wt% plasticizer.^[197] Castor oil was also used to plasticize chitosan/starch films produced by solution casting. These films showed higher tensile strength and modulus with increasing chitosan content.^[206] However, to the authors' knowledge, no characterizations concerning thermoplasticity were published.

Due to strong interactions of DES with natural polymers, malonic acid/choline chloride mixtures were also used to efficiently plasticize chitosan. Transparent thin films were produced using the solvent casting method. Glass transitions could be detected from 2 to –2.3 °C with increasing DES ratio from 33–82 wt%. Mechanical testing supported these investigations as the films showed an elastic state at room temperature. The maximum homogeneity of the films was observed between 50 and 75 wt% of added DES.^[198] Another DES, namely choline chloride/citric acid, increased the elongation of chitosan (DD = 76%) films. Homogeneous, hot pressed films could be produced with a chitosan:DES mass ratio of 70:30 at a compression temperature of 110 °C.^[199]

However, there is still a dearth of knowledge about effective plasticizers for processing chitin/chitosan. Comparison of different plasticizers is hindered by the use of chitosans with differing degrees of deacetylation. Also, studies to date have often lacked information about the molecular weights of the chitosans. Furthermore, there are several well-studied biopolymer plasticizers that could be favorable from a chemical structure point of view. These include citrates and low molecular weight substances with amino groups such as urea and ethanolamines.

Table 3. Examples of physical modifications for thermoplastic chitin/chitosan.

Type of chitin	Modification	Modifier	Mass ratio chitin/modifier	Processing	T_g [°C] ^{a)}	Ref.
Chitosan (DD = 96%)	Plasticization	Glycerol	75/25	Mechanical kneading, hot press @ 110 °C	—/—/—	[188]
Chitosan (DD = 90%)		Ethylene glycol	95/5	Solution casting, extrusion @ 90 °C	—/—/—	[192]
Chitosan (DD = 79%)	Polymer blending	Triglycerol	70/30	Solution casting	-40/74/—	[194]
Chitosan (DD = 85%)		PEG 400	23/77	Solution blending, injection	—/—/—	[195]
Chitosan (DD > 75%)		Corn oil	80/20	Solution casting, hot press @ 130 °C	132/173/—	[196]
Chitosan (DD > 75%)		Oleic acid	80/20	Solution casting, hot press @ 130 °C	127/176/—	[197]
Chitosan (DD > 75%)		Glycerol	80/20	Solution casting, hot press @ 130 °C	68/176/—	[197]
Chitosan		Malonic acid/choline chloride	67/33	Solution casting	2/140–150/—	[198]
Chitosan (DD = 76%)		Citric acid/choline chloride	70/30	Paste mixing, hot press @ 110 °C	—/—/—	[199]
Chitosan (DD = 91%)	Spermidine	76/24	Solution casting, heat sealing	—/—/—	[200]	
Chitosan (DD = 85%)	Polymer blending	PA6 ($M_w = 30\,000$)	50/50	Solution blending, solvent evaporation	—/—/—	[201]
Chitosan (DD ≥ 75%)		PVA ($M_w = 31\,000$ – $50\,000$)	20/80	Solution blending, solvent evaporation	23 ^{b)} /150 ^{c)} /—	[202]
Chitosan (DD = 85%)		PVA ($M_w = 10\,000$)	75/25	Solvent casting, hot press, extrusion blending ^{d)}	—/—/—	[203]
Chitosan (DD = 75–85%)	Polymer blending	TPS	10/90	Paste mixing, extrusion	—/—/—	[204]
Chitin ^{e)} (DD = 5%)		PCL ($M_w = 15\,000$)	70/30	Solution blending, solvent evaporation	-35 ^{c)} /107 ^{c)} /-61	[205]

^{a)}Glass transition temperatures of physically modified chitin (chitosan)/unmodified chitin (chitosan)/blend polymer; ^{b)}H₃PO₂ addition; ^{c)}from DSC thermogram; ^{d)}subsequent extrusion blending with 75 wt% PLA; ^{e)}acylated (butyl chitin; DS = 3.08).

Chitin blends: Due to its better solubility in organic solvents and film forming properties, chitosan has been widely blended with polymeric materials such as PMMA, PS, polyaniline, and polycarbonate.^[207] Selected examples are summarized in Table 3. When blending chitosan (DD = 85%) with PA6, electric field-driven phase inversion was used to improve miscibility, diminishing large scale phase separation, and improving the mechanical properties. The application of an electric field was able to modify the orientation of polar groups, which gave rise to increased hydrogen bonding between the polymers.^[201] PVA/chitosan films with 20 wt% chitosan were produced via solvent casting. The miscibility of the amorphous phases was deduced from thermal analysis. Furthermore, hypophosphorous acid (H₃PO₂) acted as a plasticizer as concluded from the T_g depression.^[202] However, blending processes with chitosan are mainly carried out in solution. A thermoplastic route was described by Grande et al.^[203] who first produced thermoplastic chitosan/PVA blends from solution. These were later incorporated into a PLA matrix by extrusion. Special focus in this study was put on drying processes for the chitosan/PVA blends. It was found that spray and freeze drying gave the least residual solvent concentration and most suitable morphology for the subsequent thermoplastic extrusion.

Blends of chitin/chitosan with thermoplastic corn starch (water/glycerol plasticized) were obtained by melt mixing and thermo-compression^[208] as well as by extrusion.^[204] Film fractions showed a uniform surface without any chitosan agglomerates or starch granules. However, the incorporation of chitin showed irregular structures depicting a highly rigid chitin phase.^[208] Similar results were obtained when adding chitin to injection-molded thermoplastic corn starch.^[209] This observation can also be explained by the different solubility

of chitin/chitosan in the aqueous matrix. Chitin chains show extensive hydrogen bonding and crystallinity, preventing them from interacting with solvent or starch molecules.

Greater accessibility of the polymer chains can be promoted by derivatization. Acyl chitin derivatives showed thermodynamic miscibility when blended with poly(ϵ -caprolactone) (PCL).^[205] For example, chitin butyrate/PCL blends showed good miscibility when they were first solution blended, dried, and then hot-pressed into molded films. The results depended inter alia on the degree of substitution of the chitin butyrate.^[210]

Additionally, chitosan can also function as a compatibilizer in blended systems.^[207] In liquid crystalline polycarbonate (LCPC)/PVA blends, the incorporation of chitosan increased the miscibility. The authors suggested that side-chain hydroxyl groups of PVA and amino and hydroxyl groups of chitosan play an important role for intermolecular hydrogen bonding, forming a miscible phase and improving morphology.^[211] The use of chitosan in the reactive extrusion blending of glycerol plasticized starch and maleic anhydride grafted PE caused a reaction between the chitosan amino groups and maleic anhydride, resulting in co-continuous blend morphology.^[212] A similar system led to heterogeneous chitosan/PE blends by reactive compatibilization with maleic anhydride.^[180] Due to the intense research on ILs over recent decades, it is not surprising that they have also been tested as compatibilizers in thermoplastic blend systems. In PP/PA6 blends with a weight ratio of 80:20, 1–10 wt% phosphonium IL improved the thermal and mechanical properties of the final materials.^[213] Being a compatibilizer for a combination of hydrophilic/hydrophobic blends, ILs could also be applied to blend systems combining natural and synthetic polymers such as polyolefins.



5. Conclusions and Outlook

When comparing different approaches for modifying the thermoplastic processing properties of natural polymers, it soon becomes obvious that thermoplasticity is a material property that is very difficult to quantify. Studies focusing on the thermoplasticity of natural polymers mainly consider the T_g as an evaluation criterion. However, they seldom clarify whether thermoplastic processing is possible and do not investigate the thermomechanical properties of the resulting materials. Here it has to be noted that, for example during extrusion, the specific mechanical energy input can be decisive for material forming. This also explains why a T_g measured solely based on heat energy input is neither a condition nor a guarantee for successful thermoplastic processing. Nevertheless, an observed glass transition is still an important indicator for thermoplasticity. With regard to thermal processing, any melting or degradation temperatures should also be investigated in order to ensure there is a viable processing window.

Although the chemical structures of chitin/chitosan, cellulose, and lignin differ from each other, the modifications used to induce thermoplastic processing properties in principle follow the same or similar approaches: masking of hydroxyl groups to diminish intermolecular interactions and so improve chain mobility, allowing softening at a certain temperature (or certain energy input), and enabling formability. Given that added plasticizers or other polymeric molecules often lack compatibility and given that plasticizer migration can occur when low-molecular-weight plasticizers are employed, it would seem that the chemical modification of the natural polymers would offer several benefits. Longer alkyl residues are able to prevent hydrogen bonding and improve the processing properties. Also when used in combination with polymer blending, chemical grafting improves the compatibility and opens up new material combinations. However, formulation changes may be required for thermoplastic processing, for example to adjust the melt viscosity. Therefore, the use of plasticizers or compatibilizers might still be needed in most cases.

Although showing the most promise, chemical modifications do however often suffer from scale-up difficulties and high production costs. This is already apparent in the raw material costs. Apart from cellulose, for which industrial-scale extraction and purification techniques have been established, other common natural polymers are generally not available in consistent quality and quantity. This also leads to high market prices. In addition, their introduction to the marketplace is further complicated by the still disproportionately low price of fossil oil. Nevertheless, future developments should be able to accept additional costs in the material development stage for the goal of a sustainable circular bioeconomy. For both cases, raw materials as well as material processing, recently studied solvents such as ionic liquids and deep eutectic solvents could offer new opportunities for using natural polymers. In particular, several ionic liquids have shown good solubilization of polysaccharides such as chitin and cellulose and have been postulated as innovative and environmentally friendly solvents for biomass valorization. Indeed, existing knowledge about the solubility and miscibility mechanisms should be transferred to this new class of solvents. Following the approaches

for producing thermoplastic starches and proteins, this same knowledge will also be helpful for moving from wet to dry processes, enabling continuous and lower cost processing on an industrial scale. However, for potential future applications such as (food) packaging and automotive or interior components, further obstacles related to plasticizer migration, residual solvents, mechanical and barrier performance, and, especially with respect to lignin, color, and odor, have to be overcome before they represent real alternatives to existing systems. Also, issues such as recyclability and/or biodegradability have not yet been sufficiently addressed and will also be decisive for possible market launches and the potential market success of such biopolymers.

Acknowledgements

This research received no specific grant from any funding agency in the public, commercial, or not-for-profit sectors. K.M. developed the concept for the manuscript and wrote the manuscript. M.S. helped to structure the content and contributed to the manuscript. C.Z. revised the manuscript.

Conflict of Interest

The authors declare no conflict of interest.

Keywords

cellulose, chitin, lignin, plasticizers, thermoplastic biopolymers

Received: December 13, 2018

Revised: January 28, 2019

Published online:

- [1] O. Türk, *Stoffliche Nutzung nachwachsender Rohstoffe: Grundlagen–Werkstoffe–Anwendungen*, Springer Fachmedien, Wiesbaden, Germany **2013**.
- [2] O. G. Piringer, A. L. Baner, *Plastic Packaging: Interactions with Food and Pharmaceuticals*, John Wiley & Sons, Weinheim, Germany **2008**.
- [3] J. A. Brydson, *Plastics Materials*, Butterworths, London **1989**.
- [4] W. Kaiser, *Kunststoffchemie für Ingenieure*, Hanser Fachbuchverlag, Munich, Germany **2007**.
- [5] F. Garavand, M. Rouhi, S. H. Razavi, I. Cacciotti, R. Mohammadi, *Int. J. Biol. Macromol.* **2017**, *104*, 687.
- [6] T. Mekonnen, P. Mussone, H. Khalil, D. Bressler, *J. Mater. Chem. A* **2013**, *1*, 13379.
- [7] P. Morganti, M. B. Coltelli, G. Morganti, *Int. J. Nanotechnol. Nanomed.* **2018**, *3*, 1.
- [8] J. Zhang, D. K. Schneiderman, T. Li, M. A. Hillmyer, F. S. Bates, *Macromolecules* **2016**, *49*, 9108.
- [9] F. Xiong, Y. Han, G. Li, T. Qin, S. Wang, F. Chu, *Sci. Silvae Sin.* **2016**, *52*, 90.
- [10] C. J. R. Verbeek, L. E. Van Den Berg, *Macromol. Mater. Eng.* **2010**, *295*, 10.
- [11] J. Bouajila, P. Dole, C. Joly, A. Limare, *J. Appl. Polym. Sci.* **2006**, *102*, 1445.
- [12] W. Work, K. Horie, M. Hess, R. Stepto, *Pure Appl. Chem.* **2004**, *76*, 1985.



- [13] L. A. Utracki, *Polymer Blends Handbook*, Springer, Dordrecht, The Netherlands **2003**.
- [14] D. Plackett, *Biopolymers: New Materials for Sustainable Films and Coatings*, Wiley, Chichester, UK **2011**.
- [15] B. Imre, B. Pukánszky, *Eur. Polym. J.* **2013**, *49*, 1215.
- [16] P. J. Flory, *J. Chem. Phys.* **1942**, *10*, 51.
- [17] M. L. Huggins, *J. Chem. Phys.* **1941**, *9*, 440.
- [18] C. Koning, M. Van Duin, C. Pagnouille, R. Jerome, *Prog. Polym. Sci.* **1998**, *23*, 707.
- [19] D. Trache, A. Donnot, K. Khimeche, R. Benelmir, N. Brosse, *Carbohydr. Polym.* **2014**, *104*, 223.
- [20] H. Zhang, Y. Xu, Y. Li, Z. Lu, S. Cao, M. Fan, L. Huang, L. Chen, *Polymers* **2017**, *9*, 526.
- [21] M. Gericke, T. Liebert, O. A. E. Seoud, T. Heinze, *Macromol. Mater. Eng.* **2011**, *296*, 483.
- [22] Y. H. Zhou, X. L. Luo, L. L. Huang, S. Lin, L. H. Chen, *J. Biobased Mater. Bioenergy* **2015**, *9*, 389.
- [23] K. Kathirgamanathan, W. J. Grigsby, J. Al-Hakkak, N. R. Edmonds, *Int. J. Polym. Sci.* **2015**, *2015*, 1.
- [24] J. Stanton, Y. Xue, P. Pandher, L. Malek, T. Brown, X. Hu, D. Salas-de la Cruz, *Int. J. Biol. Macromol.* **2018**, *108*, 333.
- [25] S. K. Mahadeva, J. Kim, *Fibers Polym.* **2012**, *13*, 289.
- [26] H. Abushammala, I. Krossing, M.-P. Laborie, *Carbohydr. Polym.* **2015**, *134*, 609.
- [27] R.-L. Wu, X.-L. Wang, F. Li, H.-Z. Li, Y.-Z. Wang, *Bioresour. Technol.* **2009**, *100*, 2569.
- [28] A. Brandt, J. Grasvik, J. P. Hallett, T. Welton, *Green Chem.* **2013**, *15*, 550.
- [29] T. Ueki, M. Watanabe, *Bull. Chem. Soc. Jpn.* **2012**, *85*, 33.
- [30] W. Holger, M. Rolf, S. Joachim, *J. Appl. Polym. Sci.* **1997**, *64*, 231.
- [31] Y. Teramoto, *Molecules* **2015**, *20*, 5487.
- [32] W. G. Glasser, G. Samaranyake, M. Dumay, V. Davé, *J. Polym. Sci., Part B: Polym. Phys.* **1995**, *33*, 2045.
- [33] L. L. Lloyd, J. F. Kennedy, P. Methacanon, M. Paterson, C. J. Knill, *Carbohydr. Polym.* **1998**, *37*, 315.
- [34] FKUR Kunststoff GmbH, *Technische Teile aus Biograde®*, <https://fkur.com/marken/biograde-3/> (accessed: January 2019).
- [35] S. B. Hein, P. Imgrund, *Technical Information, Fraunhofer Institute for Manufacturing Technology and Advanced Materials IFAM* **2012**.
- [36] Original Unverpackt GmbH, *Seifendose aus Fließholz Arboform*, <https://shop.original-unverpackt.de/products/seifendose-aus-fluessholz> (accessed: January 2019).
- [37] I. Krasnou, E. Tarasova, T. Mårtson, A. Krumme, *Int. Polym. Process.* **2015**, *30*, 210.
- [38] G. Tedeschi, S. Guzman-Puyol, U. C. Paul, M. J. Barthel, L. Goldoni, G. Caputo, L. Ceseracciu, A. Athanassiou, J. A. Heredia-Guerrero, *Chem. Eng. J.* **2018**, *348*, 840.
- [39] T. Heinze, K. Schwikal, S. Barthel, *Macromol. Biosci.* **2005**, *5*, 520.
- [40] Y. Cao, H. Li, J. Zhang, *Ind. Eng. Chem. Res.* **2011**, *50*, 7808.
- [41] A. Schenzel, A. Hufendiek, C. Barner-Kowollik, M. A. R. Meier, *Green Chem.* **2014**, *16*, 3266.
- [42] S. Barthel, T. Heinze, *Green Chem.* **2006**, *8*, 301.
- [43] T. Kakko, A. W. T. King, I. Kilpeläinen, *Cellulose* **2017**, *24*, 5341.
- [44] S. Gremos, D. Zarafeta, D. Kekos, F. Kolisis, *Bioresour. Technol.* **2011**, *102*, 1378.
- [45] R. Kakuchi, R. Ito, S. Nomura, H. Abroshan, K. Ninomiya, T. Ikai, K. Maeda, H. J. Kim, K. Takahashi, *RSC Adv.* **2017**, *7*, 9423.
- [46] Y. Zhang, H. Li, X. Li, M. E. Gibril, M. Yu, *Carbohydr. Polym.* **2014**, *99*, 126.
- [47] Z. Chen, J. Zhang, P. Xiao, W. Tian, J. Zhang, *ACS Sustainable Chem. Eng.* **2018**, *6*, 4931.
- [48] T. G. Majewicz, P. E. Erazo-Majewicz, T. J. Podlas (Eds), *Encyclopedia of Polymer Science and Technology*, John Wiley, New York **2002**.
- [49] A. A. Karpukhin, S. E. Panicheva, T. V. Kuznetsova, A. A. Kalinichev, *Fibre Chem.* **2016**, *48*, 212.
- [50] T. Maharana, S. Pattanaik, A. Routaray, N. Nath, A. K. Sutar, *React. Funct. Polym.* **2015**, *93*, 47.
- [51] D. Roy, M. Semsarilar, J. T. Guthrie, S. Perrier, *Chem. Soc. Rev.* **2009**, *38*, 2046.
- [52] R. Y. M. Huang, P. Chandramouli, *J. Polym. Sci., Part A-1: Polym. Chem.* **1969**, *7*, 1393.
- [53] M. Ahmadi, T. Behzad, R. Bagheri, *Iran. Polym. J.* **2017**, *26*, 733.
- [54] Y. H. Luan, J. Wu, M. S. Zhan, J. M. Zhang, J. Zhang, J. S. He, *Chem. J. Chin. Univ.-Chin.* **2012**, *33*, 2135.
- [55] Y. Teramoto, M. Yoshioka, N. Shirashi, Y. Nishio, *J. Appl. Polym. Sci.* **2002**, *84*, 2621.
- [56] C. Yan, J. Zhang, Y. Lv, J. Yu, J. Wu, J. Zhang, J. He, *Biomacromolecules* **2009**, *10*, 2013.
- [57] L. S. Jun, L. H. Sung, J. S. Won, K. Hyun-Chul, L. S. Geun, O. T. Hwan, *J. Appl. Polym. Sci.* **2009**, *112*, 2247.
- [58] T. Yoshikuni, A. Shoko, H. Tomokazu, N. Yoshiyuki, *Macromol. Chem. Phys.* **2004**, *205*, 1904.
- [59] A. Hufendiek, V. Trouillet, M. A. R. Meier, C. Barner-Kowollik, *Biomacromolecules* **2014**, *15*, 2563.
- [60] Y. Zhang, X. Li, Y. Yang, A. Lan, X. He, M. Yu, *RSC Adv.* **2014**, *4*, 34584.
- [61] A. Esmaeili, M. Haseli, *Mater. Sci. Eng., C* **2017**, *77*, 1117.
- [62] G. Wypych, *Handbook of Plasticizers*, ChemTec Pub., Toronto, Canada **2004**.
- [63] C. R. Fordyce, I. W. A. Meyer, *Ind. Eng. Chem.* **1940**, *32*, 1053.
- [64] V. P. Ghiya, V. Dave, R. A. Gross, S. P. McCarthy, *J. Macromol. Sci., Part A* **1996**, *33*, 627.
- [65] B. Wang, J. Chen, H. Peng, J. Gai, J. Kang, Y. Cao, *J. Macromol. Sci., Part B* **2016**, *55*, 894.
- [66] C. Y. Bao, D. R. Long, C. Vergelati, *Carbohydr. Polym.* **2015**, *116*, 95.
- [67] A. Khan, M. B. K. Niazi, S. R. Naqvi, W. Farooq, *J. Polym. Environ.* **2018**, *26*, 291.
- [68] S. Wang, X. Peng, L. Zhong, S. Jing, X. Cao, F. Lu, R. Sun, *Carbohydr. Polym.* **2015**, *117*, 133.
- [69] Z. Li, N. Liu, Y. Yao, S. Chen, H. Wang, H. Wang, *RSC Adv.* **2015**, *5*, 901.
- [70] M. Scandola, G. Ceccorulli, M. Pizzoli, *Macromolecules* **1992**, *25*, 6441.
- [71] L. Zhang, X. Deng, S. Zhao, Z. Huang, *Polymer* **1997**, *38*, 6001.
- [72] X. Wang, S. Huang, Y. Wang, P. Wei, Y. Chen, Y. Xia, Y. Wang, *J. Polym. Res.* **2017**, *24*, 16.
- [73] A. Yakup, S. Tuba, D. Elif, *J. Appl. Polym. Sci.* **2017**, *134*, 45479.
- [74] Y. Nishio, K. Matsuda, Y. Miyashita, N. Kimura, H. Suzuki, *Cellulose* **1997**, *4*, 131.
- [75] K. Sugimura, Y. Teramoto, Y. Nishio, *Cellulose* **2015**, *22*, 2349.
- [76] V. T. Phuong, A. Lazzeri, *Composites, Part A* **2012**, *43*, 2256.
- [77] T. G. Fox, *Bull. Am. Phys. Soc.* **1956**, *1*, 123.
- [78] O. A. Fridman, A. V. Sorokina, *Polym. Sci., Ser. B* **2006**, *48*, 233.
- [79] H. Ren, C. Chen, Q. Wang, D. Zhao, S. Guo, *BioResources* **2016**, *11*, 5435.
- [80] R. P. Swatloski, S. K. Spear, J. D. Holbrey, R. D. Rogers, *J. Am. Chem. Soc.* **2002**, *124*, 4974.
- [81] W. Amass, A. Amass, B. Tighe, *Polym. Int.* **1998**, *47*, 89.
- [82] M. Scandola, *Can. J. Microbiol.* **1995**, *41*, 310.
- [83] B. J. Tighe, A. J. Amass, M. Yasin, *Macromol. Symp.* **1997**, *123*, 133.
- [84] F.-X. Xia, X.-L. Wang, F. Song, Y.-Z. Wang, *J. Polym. Environ.* **2012**, *20*, 1103.
- [85] J. P. Onteniente, L. H. Safa, B. Abbès, *Starch* **2000**, *52*, 267.
- [86] K. Peredo, D. Escobar, J. Vega-Lara, A. Berg, M. Pereira, *Int. J. Biol. Macromol.* **2016**, *83*, 403.
- [87] Y. Miyashita, T. Suzuki, Y. Nishio, *Cellulose* **2002**, *9*, 215.
- [88] E. Sjostrom, *Wood Chemistry: Fundamentals and Applications*, Elsevier Science, San Diego, USA **2013**.
- [89] G. M. Irvine, *Tappi J.* **1984**, *67*, 118.
- [90] S. Laurichesse, L. Avérous, *Prog. Polym. Sci.* **2014**, *39*, 1266.



- [91] S. Wang, K. Wang, Q. Liu, Y. Gu, Z. Luo, K. Cen, T. Fransson, *Bio-technol. Adv.* **2009**, 27, 562.
- [92] G. Jiang, D. J. Nowakowski, A. V. Bridgwater, *Thermochim. Acta* **2010**, 498, 61.
- [93] C. Cui, H. Sadeghifar, S. Sen, D. S. Argyropoulos, *BioResources* **2013**, 8, 864.
- [94] Anonymous (TECNARO Gesellschaft zur industriellen Anwendung nachwachsender Rohstoffe mbH), *DE10151386C2* **2001**.
- [95] C. Wang, S. S. Kelley, R. A. Venditti, *ChemSusChem* **2016**, 9, 770.
- [96] W. G. Glasser, R. K. Jain, *Holzforschung* **1993**, 47, 225.
- [97] I. Ghosh, R. K. Jain, W. G. Glasser, *J. Appl. Polym. Sci.* **1999**, 74, 448.
- [98] S. C. Fox, A. G. McDonald, *BioRes.* **2010**, 5, 990.
- [99] X. G. Luo, X. Y. Lin, F. Liu, *Mater. Sci. Forum* **2009**, 620–622, 241.
- [100] P. Buono, A. Duval, P. Verge, L. Averous, Y. Habibi, *ACS Sustainable Chem. Eng.* **2016**, 4, 5212.
- [101] H. Nimz, *Angew. Chem., Int. Ed. Engl.* **1974**, 13, 313.
- [102] W. G. Glasser, C. A. Barnett, T. G. Rials, V. P. Saraf, *J. Appl. Polym. Sci.* **1984**, 29, 1815.
- [103] S. Sen, S. Patil, D. S. Argyropoulos, *Green Chem.* **2015**, 17, 1077.
- [104] S. Laurichesse, L. Avérous, *Polymer* **2013**, 54, 3882.
- [105] M. J. Chen, J. J. Meister, D. W. Gunnells, D. J. Gardner, *Adv. Polym. Technol.* **1995**, 14, 97.
- [106] J. J. Meister, M. J. Chen, *Macromolecules* **1991**, 24, 6843.
- [107] A. Ayoub, R. A. Venditti, H. Jameel, H. M. Chang, *J. Appl. Polym. Sci.* **2014**, 131, 39743.
- [108] H. Chung, A. Al-Khouja, N. R. Washburn, in *Green Polymer Chemistry: Biocatalysis and Materials II* (Eds: H. N. Cheng, R. A. Gross, P. B. Smith), American Chemical Society, WA **2013**.
- [109] S. L. Hilburg, A. N. Elder, H. Chung, R. L. Ferebee, M. R. Bockstaller, N. R. Washburn, *Polymer* **2014**, 55, 995.
- [110] M.-J. Chen, D. W. Gunnells, D. J. Gardner, O. Milstein, R. Gersonde, H. J. Feine, A. Hüttermann, R. Frund, H. D. Lüdemann, J. J. Meister, *Macromolecules* **1996**, 29, 1389.
- [111] R. Liu, L. Dai, L.-Q. Hu, W.-Q. Zhou, C.-L. Si, *Mater. Sci. Eng., C* **2017**, 80, 397.
- [112] M. Wennerblom, A. D. Frovi, A.-M. Olsson, L. Salmen, *Nord. Pulp Pap. Res. J.* **1996**, 11, 279.
- [113] S. Isao, S. Ryoichi, *J. Appl. Polym. Sci.* **1975**, 19, 2799.
- [114] D. Feldman, D. Banu, J. Campanelli, H. Zhu, *J. Appl. Polym. Sci.* **2001**, 81, 861.
- [115] D. Banu, A. El-Aghoury, D. Feldman, *J. Appl. Polym. Sci.* **2006**, 101, 2732.
- [116] D. W. Park, A. N. Neogi, J. Ludwig Furtner (Weyerhaeuser NR Co), *US8383784B2* **2013**.
- [117] J. F. Kadla, S. Kubo, *Composites, Part A* **2004**, 35, 395.
- [118] P. Mousavioun, P. J. Halley, W. O. S. Doherty, *Ind. Crops Prod.* **2013**, 50, 270.
- [119] Y. Teramoto, S.-H. Lee, T. Endo, *J. Appl. Polym. Sci.* **2012**, 125, 2063.
- [120] Y. Teramoto, S.-H. Lee, T. Endo, *Polym. J.* **2009**, 41, 219.
- [121] S. Kim, S. Oh, J. Lee, N. Ahn, H. Roh, J. Cho, B. Chun, J. Park, *Fibers Polym.* **2014**, 15, 2458.
- [122] Y. Li, S. Sarkanen, *Macromolecules* **2005**, 38, 2296.
- [123] J. G. Lynam, N. Kumar, M. J. Wong, *Bioresour. Technol.* **2017**, 238, 684.
- [124] T. Akiba, A. Tsurumaki, H. Ohno, *Green Chem.* **2017**, 19, 2260.
- [125] A. George, K. Tran, T. J. Morgan, P. I. Benke, C. Berruoco, E. Lorente, B. C. Wu, J. D. Keasling, B. A. Simmons, B. M. Holmes, *Green Chem.* **2011**, 13, 3375.
- [126] C. S. Miranda, M. S. Ferreira, M. T. Magalhães, W. J. Santos, J. C. Oliveira, J. B. A. Silva, N. M. José, *Mater. Today: Proc.* **2015**, 2, 63.
- [127] A. Kalliola, T. Vehmas, T. Liitiä, T. Tamminen, *Ind. Crops Prod.* **2015**, 74, 150.
- [128] A. Kalliola, T. Vehmas, T. Liitiä, *Presented at 8th Nordic Wood Biorefinery Conference, Helsinki, Finland, October 2018*.
- [129] X. Lin, M. Zhou, S. Wang, H. Lou, D. Yang, X. Qiu, *ACS Sustainable Chem. Eng.* **2014**, 2, 1902.
- [130] P. Mousavioun, W. O. S. Doherty, G. George, *Ind. Crops Prod.* **2010**, 32, 656.
- [131] S. Kubo, J. F. Kadla, *Biomacromolecules* **2003**, 4, 561.
- [132] M. Julinová, R. Slavík, M. Vyoralová, A. Kalendová, P. Alexy, *J. Polym. Environ.* **2018**, 26, 1459.
- [133] H. Li, N. Legros, M. T. Ton-That, A. Rakotoveloa, *Plast. Eng.* **2013**, 69, 60.
- [134] R. S. Kumar, S. N. Maiti, A. K. Ghosh, *Polym.-Plast. Technol. Eng.* **2016**, 55, 475.
- [135] L. Jianchun, H. Yong, I. Yoshio, *Polym. Int.* **2003**, 52, 949.
- [136] Y.-L. Chung, J. V. Olsson, R. J. Li, C. W. Frank, R. M. Waymouth, S. L. Billington, E. S. Sattely, *ACS Sustainable Chem. Eng.* **2013**, 1, 1231.
- [137] E. Zong, X. Liu, L. Liu, J. Wang, P. Song, Z. Ma, J. Ding, S. Fu, *ACS Sustainable Chem. Eng.* **2018**, 6, 337.
- [138] W. G. Glasser, J. S. Knudsen, C.-S. Chang, *J. Wood Chem. Technol.* **1988**, 8, 221.
- [139] J. Dörrstein, R. Scholz, D. Schwarz, D. Schieder, V. Sieber, F. Walther, C. Zollfrank, *Compos. Struct.* **2018**, 189, 349.
- [140] M. Alekhina, J. Erdmann, A. Ebert, A. M. Stepan, H. Sixta, *J. Mater. Sci.* **2015**, 50, 6395.
- [141] I. Blanco, G. Cicala, A. Latteri, G. Saccullo, A. M. M. El-Sabbagh, G. Ziegmann, *J. Therm. Anal. Calorim.* **2017**, 127, 147.
- [142] G. Kim, I. K. Park, S. H. Kim, Y. Kim, H. W. Seo, J. H. Yun, S. H. Kim, D. K. Kim, J. D. Nam, *Polymer (Korea)* **2016**, 40, 313.
- [143] N. Yan, X. Chen, *Nature* **2015**, 524, 155.
- [144] M.-K. Jang, B.-G. Kong, Y.-I. Jeong, C. H. Lee, J.-W. Nah, *J. Polym. Sci., Part A: Polym. Chem.* **2004**, 42, 3423.
- [145] M. Rinaudo, *Prog. Polym. Sci.* **2006**, 31, 603.
- [146] E. S. Abdou, K. S. A. Nagy, M. Z. Elsabee, *Bioresour. Technol.* **2008**, 99, 1359.
- [147] N. H. Marei, E. A. El-Samie, T. Salah, G. R. Saad, A. H. M. Elwahy, *Int. J. Biol. Macromol.* **2016**, 82, 871.
- [148] H. Ehrlich, V. V. Bazhenov, C. Debitus, N. de Voogd, R. Galli, M. V. Tsurkan, M. Wysokowski, H. Meissner, E. Bulut, M. Kaya, T. Jesionowski, *Int. J. Biol. Macromol.* **2017**, 104, 1706.
- [149] B. A. Juárez-de la Rosa, P. Quintana, P.-L. Ardisson, J. M. Yáñez-Limón, J. J. Alvarado-Gil, *J. Mater. Sci.* **2012**, 47, 990.
- [150] S. Erdogan, M. Kaya, I. Akata, *AIP Conf. Proc.* **2017**, 1809, 020012.
- [151] S. P. O. Alvarez, D. A. R. Cadavid, D. M. E. Sierra, C. P. O. Orozco, D. F. R. Vahos, P. Z. Ocampo, L. Atehortua, *Biomed. Res. Int.* **2014**, 2014, 1.
- [152] S. Ifuku, R. Nomura, M. Morimoto, H. Saimoto, *Materials* **2011**, 4, 1417.
- [153] T. Wu, S. Zivanovic, F. A. Draughon, C. E. Sams, *J. Agric. Food Chem.* **2004**, 52, 7905.
- [154] S. Liu, J. Sun, L. Yu, C. Zhang, J. Bi, F. Zhu, M. Qu, C. Jiang, Q. Yang, *Molecules* **2012**, 17, 4604.
- [155] J. Majtán, K. Biličková, O. Markovič, J. Gróf, G. Kogan, J. Šimúth, *Int. J. Biol. Macromol.* **2007**, 40, 237.
- [156] M. Kaya, T. Baran, *Int. J. Biol. Macromol.* **2015**, 75, 7.
- [157] M. Kaya, V. Baublys, I. Šatkauskienė, B. Akyuz, E. Bulut, V. Tubelytė, *Int. J. Biol. Macromol.* **2015**, 79, 126.
- [158] A. Sjaifullah, A. B. Santoso, *Procedia Chem.* **2016**, 18, 49.
- [159] Y. Qin, X. Lu, N. Sun, R. D. Rogers, *Green Chem.* **2010**, 12, 968.
- [160] C. Zhu, R. M. Richardson, Y. Song, S. S. Rahatekar, in *Polysaccharide-Based Fibers and Composites* (Eds: L. Lucia, A. Ayoub), Springer, Cham, Switzerland **2018**.
- [161] Y. Wu, T. Sasaki, S. Irie, K. Sakurai, *Polymer* **2008**, 49, 2321.
- [162] M. Jaworska Malgorzata, T. Kozlecki, A. Gorak, *J. Polym. Eng.* **2012**, 32, 67.
- [163] S. S. Silva, J. F. Mano, R. L. Reis, *Green Chem.* **2017**, 19, 1208.



- [164] M. Shimo, M. Abe, H. Ohno, *ACS Sustainable Chem. Eng.* **2016**, *4*, 3722.
- [165] G. Santos-López, W. Argüelles-Monal, E. Carvajal-Millan, Y. López-Franco, M. Recillas-Mota, J. Lizardi-Mendoza, *Polymers* **2017**, *9*, 722.
- [166] G. L. Zhao, X. F. Lang, F. L. Wang, J. R. Li, X. F. Li, *Biochem. Eng. J.* **2017**, *126*, 24.
- [167] W.-T. Wang, J. Zhu, X.-L. Wang, Y. Huang, Y.-Z. Wang, *J. Macromol. Sci., Part B* **2010**, *49*, 528.
- [168] F. Sun, M. Xu, K. Li, S. Zhang, P. Liu, *Prog. Chem.* **2013**, *25*, 832.
- [169] E. Jin, M. Li, S. Zhou, *J. Mater. Cycles Waste Manag.* **2017**, *20*, 496.
- [170] F. H. Li, Y. Sun, S. X. Li, S. J. Ma, *App. Mech. Mater.* **2012**, 166–169, 1433.
- [171] K. Kurita, S. Mori, Y. Nishiyama, M. Harata, *Polym. Bull.* **2002**, *48*, 159.
- [172] H. Sashiwa, Y. Shigemasa, R. Roy, *Chem. Lett.* **2000**, *29*, 862.
- [173] F. S. Pereira, D. L. da Silva Agostini, A. E. Job, E. R. P. González, *J. Therm. Anal. Calorim.* **2013**, *114*, 321.
- [174] Y. Kurita, A. Isogai, *Int. J. Biol. Macromol.* **2012**, *50*, 741.
- [175] L. Li, X. Cao, X. Shen, S. Yu, F. Su, S. Liu, F. Liu, C. Xie, *J. Biomed. Mater. Res., Part A* **2017**, *105*, 3034.
- [176] Y. Omura, E. Renbutsu, M. Morimoto, H. Saimoto, Y. Shigemasa, *Polym. Adv. Technol.* **2003**, *14*, 35.
- [177] C. Yu, X. Kecen, Q. Xiaosai, in *Biopolymer Grafting–Synthesis and Properties* (Ed: V. K. Thakur), Elsevier, Amsterdam, Netherlands **2018**.
- [178] Z. Zhang, F. Jin, Z. Wu, J. Jin, F. Li, Y. Wang, Z. Wang, S. Tang, C. Wu, Y. Wang, *Carbohydr. Polym.* **2017**, *177*, 203.
- [179] E. M. d.A. Braz, S. C. C. e. Silva, D. A. da Silva, F. A. d. A. Carvalho, H. M. Barreto, L. d. S. Santos Júnior, E. C. da Silva Filho, *Int. J. Biol. Macromol.* **2018**, *117*, 640.
- [180] T. A. Akopova, L. V. Vladimirov, V. A. Zhorin, A. N. Zelenetskii, *Polym. Sci., Ser. B* **2009**, *51*, 124.
- [181] H. Sashiwa, Y. Shigemasa, *Carbohydr. Polym.* **1999**, *39*, 127.
- [182] S. Khattak, F. Wahid, L.-P. Liu, S.-R. Jia, L.-Q. Chu, Y.-Y. Xie, Z.-X. Li, C. Zhong, *Appl. Microbiol. Biotechnol.* **2019**.
- [183] A. D. Li, Z. Z. Sun, M. Zhou, X. X. Xu, J. Y. Ma, W. Zheng, H. M. Zhou, L. Li, Y. F. Zheng, *Colloids Surf., B* **2013**, *102*, 674.
- [184] T. Setoguchi, K. Yamamoto, J.-I. Kadokawa, *Polymer* **2012**, *53*, 4977.
- [185] F. Liangdong, Z. Ziyang, D. Alain, H. Jin, W. Ming, A. Lijia, *J. Appl. Polym. Sci.* **2009**, *112*, 2830.
- [186] A. Abu Naim, A. Umar, M. M. Sanagi, N. Basaruddin, *Carbohydr. Polym.* **2013**, *98*, 1618.
- [187] K. Yamamoto, S. Yoshida, S. Mine, J.-I. Kadokawa, *Polym. Chem.* **2013**, *4*, 3384.
- [188] L. Cano, E. Pollet, L. Avérous, A. Tercjak, *Composites, Part A* **2017**, *93*, 33.
- [189] M. Matet, M.-C. Heuzey, E. Pollet, A. Ajji, L. Avérous, *Carbohydr. Polym.* **2013**, *95*, 241.
- [190] L. Avérous, E. Pollet, *AIP Conf. Proc.* **2015**, 1713, 140009.
- [191] V. Epure, M. Griffon, E. Pollet, L. Avérous, *Carbohydr. Polym.* **2011**, *83*, 947.
- [192] S. Hein, P. Imgrund (Fraunhofer-Gesellschaft zur Förderung der angewandten Forschung e.V.), *DE 102010021085 A1* **2011**.
- [193] H. R. Fischer, S. Fischer (Nederlandse Organisatie Voor Toegepast-Natuurwetenschappelijk Onderzoek Tno), *US 6811599 B2* **2004**.
- [194] I. Kelnar, J. Kovářová, G. Tishchenko, L. Kaprálková, E. Pavlová, F. Carezzi, P. Morganti, *J. Polym. Res.* **2015**, *22*, 5.
- [195] D. B. Lima, R. D. Almeida, M. Pasquali, S. P. Borges, M. L. Fook, H. M. Lisboa, *Carbohydr. Polym.* **2018**, *189*, 238.
- [196] A. Giannakas, A. Patsaoura, N. M. Barkoula, A. Ladavos, *Carbohydr. Polym.* **2017**, *157*, 550.
- [197] M. Vlacha, A. Giannakas, P. Katapodis, H. Stamatis, A. Ladavos, N.-M. Barkoula, *Food Hydrocolloids* **2016**, *57*, 10.
- [198] M. P. Sokolova, M. A. Smirnov, A. A. Samarov, N. V. Bobrova, V. K. Vorobiov, E. N. Popova, E. Filippova, P. Geydt, E. Lahderanta, A. M. Toikka, *Carbohydr. Polym.* **2018**, *197*, 548.
- [199] A. C. Galvis-Sánchez, M. C. R. Castro, K. Biernacki, M. P. Gonçalves, H. K. S. Souza, *Food Hydrocolloids* **2018**, *82*, 478.
- [200] M. Sabbah, P. Di Piero, M. Cammarota, E. Dell'Olmo, A. Arciello, R. Porta, *Food Hydrocolloids* **2019**, *87*, 245.
- [201] J. Zhang, Q. Zhou, W. Li, O. Petrov, C. Mattea, S. Stapf, *Carbohydr. Polym.* **2018**, *189*, 15.
- [202] M. Benítez, J.-E. Diosa, R. A. Vargas, *Ionics* **2018**, *24*, 2029.
- [203] R. Grande, L. A. Pessan, A. J. F. Carvalho, *Carbohydr. Polym.* **2018**, *191*, 44.
- [204] J. F. Mendes, R. T. Paschoalin, V. B. Carmona, A. R. Sena Neto, A. C. P. Marques, J. M. Marconcini, L. H. C. Mattoso, E. S. Medeiros, J. E. Oliveira, *Carbohydr. Polym.* **2016**, *137*, 452.
- [205] M. Sugimoto, M. Kawahara, Y. Teramoto, Y. Nishio, *Carbohydr. Polym.* **2010**, *79*, 948.
- [206] M. Hasan, R. F. I. Rahmayani, Munandar, *IOP Conf. Ser.: Mater. Sci. Eng.* **2018**, *333*, 012087.
- [207] A. Kausar, *J. Plast. Film Sheeting* **2017**, *33*, 384.
- [208] O. Lopez, M. A. Garcia, M. A. Villar, A. Gentili, M. S. Rodriguez, L. Albertengo, *LWT–Food Sci. Technol.* **2014**, *57*, 106.
- [209] R. C. R. Souza Rosa, C. T. Andrade, *J. Appl. Polym. Sci.* **2004**, *92*, 2706.
- [210] H. Hashiwaki, Y. Teramoto, Y. Nishio, *Carbohydr. Polym.* **2014**, *114*, 330.
- [211] S. Moriyuki, K. Tomohiro, K. Yasuko, I. Isamu, K. Yasuo, *J. Appl. Polym. Sci.* **2004**, *93*, 1616.
- [212] K. Jantanasakulwong, N. Leksawasdi, P. Seesuriyachan, S. Wongsuriyasak, C. Techapun, T. Ougizawa, *Carbohydr. Polym.* **2016**, *153*, 89.
- [213] M. Yousfi, S. Livi, J. Duchet-Rumeau, *Chem. Eng. J.* **2014**, *255*, 513.

4 Ionic liquid aided solution-precipitation method to prepare polymer blends from cellulose with polyesters or polyamide

by Kerstin Müller and Cordt Zollfrank¹¹⁰

Eur. Polym. J. **2020**, *133*, 109743. <https://doi.org/10.1016/j.eurpolymj.2020.109743>

Cellulose is commonly considered unsuitable for melt blending. To investigate the properties of blends from synthetic polymers and cellulose, an ionic liquid based solution-precipitation process is presented. Based on expected favorable interactions with the hydroxyl groups of the cellulose, polyesters, namely poly(ϵ -caprolactone), poly(butylene succinate), poly(lactic acid), poly(hydroxyl alcanoate) and polyamide 6 were chosen as blend partners. Cellulose was dissolved in 1-ethyl-3-methylimidazolium acetate and dimethyl sulfoxide, while the latter was also used for dissolution of the synthetic polymers. After precipitation in an anti-solvent, the materials were dried and thermomechanically formed into platelets, investigating their thermoplastic behavior. Blends were mixed and precipitated in different weight ratios, namely 7:3, 1:1 and 3:7. For comparison, pure cellulose and polymers were also dissolved and precipitated.

For poly(ϵ -caprolactone)/cellulose blends, phase separation was already macroscopically visible after precipitation, while all other combinations and compositions showed macroscopic homogenous mixtures. Compatibility of the pressed platelets was further evaluated by polymer-polymer interactions. Hydrogen bonding was studied by infrared spectroscopy. Results showed strong interactions between poly(lactic acid) and cellulose, mainly indicated from systematic shifts of the carbonyl band assigned to poly(lactic acid). Although a semi-crystalline poly(lactic acid) grade was used, no melting enthalpies could be measured after blending with cellulose, assuming that the cellulose chains prevented crystallization of the poly(lactic acid) based on favorable interactions and therewith interference of the initial supramolecular structure. For the other combinations of cellulose and polyesters, no specific interactions were detected. Regarding poly(butylene succinate), even immiscibility with cellulose at tested ratios is assumed based on the spectra and morphological analysis. The combination of cellulose and polyamide 6 resulted in coherent and transparent pressed films at all prepared ratios. However, crystalline polyamide domains were still detectable during thermal analysis, indicating rather a hybrid structure of both polyamide and cellulose domains with favorable interactions at the interfaces. Additionally, melting point depression of the polyamide with increasing cellulose contents indicate interactions between the polymers.

Author contributions: Kerstin Müller developed the design of experiments, the concept for the manuscript and wrote the manuscript. Cordt Zollfrank revised the manuscript.



Contents lists available at ScienceDirect

European Polymer Journal

journal homepage: www.elsevier.com/locate/europolj



Ionic liquid aided solution-precipitation method to prepare polymer blends from cellulose with polyesters or polyamide



Kerstin Müller^{a,b,*}, Cordt Zollfrank^a

^a Biogenic Polymers, TUM Campus Straubing for Biotechnology and Sustainability, Technical University of Munich, Schulgasse 16, 94315 Straubing, Germany

^b Fraunhofer Institute for Process Engineering and Packaging IVV, Gießenhauser Str. 35, 85354 Freising, Germany

ARTICLE INFO

Keywords:

Cellulose
Solution Blending
Ionic Liquid
Polymer Blends
Biopolymers

ABSTRACT

Cellulose is commonly regarded unsuitable for melt blending. Therefore, direct use of cellulose in thermoplastic applications is still a challenge without further modification, and limited compatibility may result in poor mechanical performance of melt compounded polymer/cellulose composites. In this study, blends of various synthetic polymers and cellulose with thermoplastic properties were successfully produced using an ionic-liquid based solution-precipitation process and subsequent hot-pressing. Dimethyl sulfoxide was used in the presence of 1-ethyl-3-methylimidazolium acetate as an appropriate co-solvent for cellulose dissolution and as the sole solvent for poly(ϵ -caprolactone), poly(butylene succinate), poly(lactic acid), poly(hydroxyl alkananoate) and polyamide 6 prior to solution blending. Both blended solutions as well as single polymer solutions were precipitated with an anti-solvent. A slight decrease in molecular weight was detected for poly(butylene succinate) as well as the cellulose regenerates. Precipitated and dried materials were thermomechanically formed into platelets, investigating their thermoplastic behavior. Depending on their polymeric nature and the ability to interact with the polymer chains, different compatibility behavior of the regenerated blends was observed during precipitation as well as thermomechanical forming. Promising interactions were detected for polyamide 6 and poly(lactic acid), expressed via melting point depression (polyamide 6), hydrogen bonding (poly(lactic acid)) and homogeneous morphology of the transparent blend films.

1. Introduction

Cellulose is one of the most abundant natural polymers and is also used in thermoplastic processing. Beside chemical modification inducing thermoplasticity as an intrinsic property, existing studies using compounding for polymer mixing are focussing on interphase compatibility of the thermoplastic polymer matrix and cellulose as a filler. Since cellulose does not melt and always stays solid in those processes, multiphase composites are obtained instead of homogeneous blends. Another well-known processing method to solve this problem is solution blending. Unfortunately, only few solvents are capable to dissolve cellulose, and most of them are derivatizing the cellulose chains to modify the solubility. Due to this, miscibility behavior of blends with thermoplastic polymers from solution is rarely studied. The basic issue of such blend preparation is to find a suitable solvent system that is capable of dissolving both polysaccharide and second component without major decomposition [1]. Solvents may differ in their dissolution performance. Two basic, consecutive steps are distinguished when dissolving polymers, namely solvent diffusion and chain

entanglement [2]. Both steps depend on the ability of the solvent molecules to interact with the polymer, and especially chain entanglement is important when different polymers are aimed to be well mixed in a solution, as in this study. Research on ionic liquids as solvents for cellulose [3] offers new approaches to study polymer interactions in such native cellulose-based blends. The ionic liquid 1-ethyl-3-methylimidazolium acetate (EmimAc) has been referred to as a good or even as a theta solvent for cellulose at certain temperatures and concentrations [4–6]. The co-solvent dimethyl sulfoxide (DMSO) not only does significantly reduce the solution viscosity, but may also promote a decreased dissolution temperature and time with the appropriate composition, and hence possibly prevent polymer degradation [7]. DMSO is an important aprotic solvent, able to dissolve a variety of polymers with polar functional groups. Therefore, homogeneous mixtures of cellulose solutions in EmimAc/DMSO and synthetic polymer solutions in DMSO provide a valuable platform to study the miscibility behavior in regenerated cellulose/synthetic polymer blends. Polymer blends have special properties which differ from those of the individual blend components. Properties such as morphology, thermal properties or

* Corresponding author.

E-mail address: kerstin.mueller@ivv.fraunhofer.de (K. Müller).

<https://doi.org/10.1016/j.eurpolymj.2020.109743>

Received 17 March 2020; Received in revised form 29 April 2020; Accepted 3 May 2020

Available online 11 May 2020

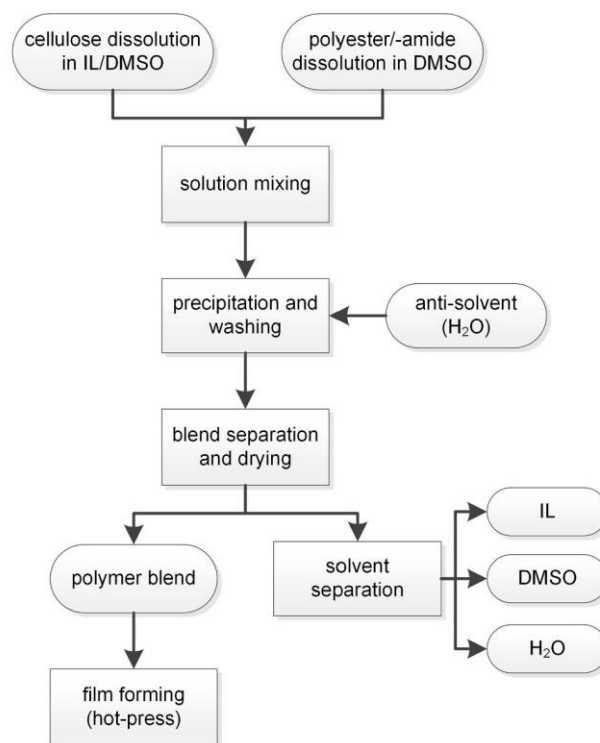
0014-3057/ © 2020 Elsevier Ltd. All rights reserved.

mechanical properties depend on interactions between the different polymer components and the processing method. When different polymers are physically blended, the miscibility of the components is a crucial question. Miscibility is a thermodynamic term most commonly defined in the literature by Flory and Huggins [8,9] and was originally used to predict polymer–solvent miscibility. It is assumed that miscible polymer blends behave similarly to a single-phase system, whereas immiscible polymer blends have two or more phases. Nevertheless, a single-phase system cannot be a general state or property, but is always related to a certain scale [10,11]. Furthermore, blend composition and environmental conditions such as temperature or pressure influence the phase stability of a blend and can also lead to phase separation, based on a change in the free energy of mixing [11,12]. This can also be the case if a polymer blend is precipitated from solution by adding a “poor” solvent or non-solvent. The term compatibility is rather a technical term that refers to interphase interactions favorable for final material properties such as processing and mechanical properties for a certain application [13,14]. Both for miscibility on a molecular level or compatibility at the interphases of a multi-phased blend, strong intermolecular interactions are necessary. As immiscible and mainly incompatible blends usually depict a coarse structure, which is reflected in poor mechanical performance, favorable interactions between the components are desired in the development of new blend materials [15]. In the case of cellulose, intermolecular interactions between the polysaccharide chains are dominated by hydrogen bonding. Therefore, the ability to strongly interact with the hydroxyl group of the cellulose and form hydrogen bonds is a main requirement when searching for compatible synthetic polymers. In this study, different polyesters as well as polyamide 6 are investigated for their ability to form thermoplastic, compatible or possibly miscible blends with cellulose.

2. Material and methods

McAirlaid's Vliesstoffe (Frankfurt, Germany) provided Cotton fibers (COT). Microcrystalline cellulose (MCC) Parmcel 101 was purchased from Gustav Parmentier (Steinfurt, Germany). Both the degree of polymerization (DP) and molecular weight (M_w) of the two celluloses and their regenerates rCOT and rMCC were calculated on the basis of intrinsic viscosities determined according to ISO 5351 and the relation of intrinsic viscosity and DP or M_w given by Kes and Christensen [16]. Cellulose regenerates used for DP determination were ground and additionally extracted with ethanol using a Soxhlet apparatus for 12 h to eliminate any residual ionic liquid. The used thermoplastic polymers were poly(caprolactone) (PCL) Capa™ 6500 provided by Perstop Holding (Malmö, Sweden); poly(butylene succinate) BioPBS™ FD92PM (PBS) from PTT MCC Biochem (Bangkok, Thailand); poly(lactic acid) Ingeo™ 3251D (PLA) from NatureWorks (Minnetonka, MN, USA), poly(hydroxyl alkanoate) PHI002 (PHA) from NaturePlast (Iffs, France) and polyamide Ultramid® B40L (PA6) purchased from BASF (Ludwigshafen, Germany). M_w of polymer granulates and regenerates from DMSO were determined via size exclusion chromatography (SEC). SEC was performed with a Dionex System using 1,1,1,3,3,3-hexafluoro-2-isopropanol (HFIP) with 0.02 mol L⁻¹ trifluoroacetic acid as solvent. A DIONEX Ultimate 3000 injector was used, and the flow rate was fixed to 1 mL min⁻¹ (HPLC gradient pump Gynkotek M480). Detection was performed with a refractive index detector Gynkotek SE-61. PSS-PFG columns, tempered to 40 °C, were used (PSS, Mainz, Germany: 7 µm, 300 × 8 mm). Samples were solved in HFIP with a concentration of 5000 µg/mL and filtered with a 0.20 µm PTFE membrane. An amount of 100 µL was injected (DIONEX Ultimate 3000). A narrow molecular weight distribution PMMA standard (PSS Mainz, Germany) was used as calibration. The curves were examined with the WinGPC®UniChrom (Version 8.1) Software (PSS, Mainz, Germany).

EmimAc (97%) and DMSO (99%) were received from proionic (Raaba-Grambach, Austria) and Merck (Darmstadt, Germany). All polymers were dried at 60 °C for at least 12 h prior to processing.



Scheme 1. Flow diagram of applied solution-precipitation process for polymer blend formation.

Cellulose samples were dissolved in a mixture of EmimAc and DMSO (1:1 by weight) with a total concentration of 2.5 wt% at 60 °C and 150 rpm for at least two hours using a magnetic stirrer. Dissolution was visually assessed by clarity of the solutions. All thermoplastic polymers were dissolved in DMSO with a concentration of 2.5 wt%. PCL, PBS and PLA were dissolved at 60 °C and 150 rpm, PHA at 120 °C and PA6 at 150 °C. The polymer solutions were mixed in their respective weight ratios (70:30, 50:50, 30:70) at 90 °C and 150 rpm for one hour and subsequently cast on a glass Petri dish. Gel films were cooled to room temperature and precipitated with an excess of deionized water (five times the amount of water in terms of weight). Films were then washed with the same amounts of water in 3–4 washing steps to remove residual DMSO and EmimAc. Additionally, regenerates of pure polymers were obtained by aqueous precipitation from DMSO solutions. Films were dried using a vacuum drying cabinet at 90 °C and 20 mbar for five hours and stored in a desiccator at 23 °C before further characterization. Scheme 1 gives an overview of the applied processing steps. The solvent separation step, which can be performed via solvent evaporation, is shown as an optional step for solvent recovery and is not further described within this study.

Differential scanning calorimetry (DSC) was performed on a DSC 821e instrument and the corresponding software STAR^e Version 15.00 of Mettler-Toledo (Gießen, Germany). Two heating runs from 0 to 200 °C (PA6: 250 °C) were performed with a heating/cooling rate of 15 K min⁻¹ with 5–10 mg of each sample.

Fourier transform infrared (FTIR) spectroscopy was performed using a Frontier™ FTIR spectrometer L1280034 with the software PerkinElmer Spectrum IR, Version 10.6.1, both supplied by Perkin Elmer (Shelton, CT, USA). Measurements were performed at ambient temperature and pressure. The ATR (attenuated total reflectance, Perkin Elmer, Shelton, CT, USA) device, named golden gate with a germanium crystal, was utilized. A constant contact pressure was realized by tightening the securing screw with a ratchet, which is limited to a torque of 30 cNm. 16 scans were recorded within a wavenumber

range from 4000 to 600 cm^{-1} with a resolution of 4 cm^{-1} . All spectra were baseline corrected.

To prepare thermomechanically formed platelets of approximately 100–150 μm thickness, films were hot-pressed with a load of 2.5 t held for 3 min. Temperatures were adapted to the polymer melting points. Microtome sections of 20 μm thickness from the hot-pressed films were prepared with an Autocut 2055 of Leica Microsystems (Wetzlar, Germany). Phase compositions were examined in transmission mode using a Leica Microsystems Dioplan optical microscope with a polarizing filter. Due to macroscopic phase separation of the regenerate, no films were pressed from the PCL blends. For the hot-pressed polyamide blends, cross-sections were prepared using a JEOL IB-19530CP Cross Section Polisher with an Argon beam and examined with a JEOL 7200F scanning electron microscope with a backscatter electron detector (Jeol, Freising, Germany). Images were taken at a working distance of 10 mm and an accelerating voltage of 5.0 kV.

3. Results and discussion

Molecular weight determination. Generally, processes including energy input such as mechanical or thermal energy can cause chain degradation. Thermal or thermo-oxidative degradation of polymers in general [17] and the used polyesters [18–21] and polyamide [22] used here in particular may occur during processing or storage, depending on the environment to which the polymers are subjected. Regarding cellulose dissolution in general, solvents applied can be non-derivatizing or derivatizing [23], of which the latter might not only alter the cellulose chemical structure but also diminish the polymer chain length. To maintain initial polymer properties, it is therefore preferred that only minor changes in polymer molecular weights occur. Molecular weight determination was performed to check if and to what extent the solution-precipitation process influences the molecular weight of the used polymers. Since all polymers underwent thermal stress during dissolution and drying, we expected little chain degradation for all polymers. Table 1 shows the determined molecular weights for all polyesters and polyamide as well as their regenerates. The corresponding distribution curves can be found in the [supporting information](#).

As these are relative measurements, however, the observed fluctuations are to be rated as very small, since an accuracy < 5% is common for M_w [24]. Therefore, only PBS showed slight chain degradation when dissolved, precipitated and dried. The applied processing temperatures therefore still seem to be adequate to maintain initial polymer molecular weights on a high level.

For the cellulose samples, molecular weight was determined with a viscosimetric method in CED. Viscosity data and the calculated DP and M_w are shown in Table 2. Detailed data for the determination of the intrinsic viscosities can be found in the [supplementary information](#).

The DP of cellulose is a key parameter to evaluate solution-precipitation processes, especially since duration and temperature of the cellulose dissolution process highly influence DP loss in regenerates. Quite remarkably, DP decreases of cellulose regenerates, compared to pure cellulose samples, were already detected for other ionic liquids [25,26] also in the IL combination used here [7,27]. The DP loss is

Table 1

Molecular weights of the polyesters and polyamide ($M_{w,0}$), their regenerates precipitated from DMSO solutions ($M_{w,reg}$) and the corresponding percentage deviation (Dev. M_w).

polymer	$M_{w,0}[\text{g mol}^{-1}]$	$M_{w,reg}[\text{g mol}^{-1}]$	Dev. M_w [%]
PA6	84,642	80,692	-4.66
PLA	80,945	81,083	+0.17
PBS	116,620	103,437	-11.30
PCL	117,242	117,971	+0.62
PHBV	315,377	311,858	-1.12

Table 2

Intrinsic viscosities and therefrom-calculated degree of polymerization and molecular weight for COT, MCC and their regenerates.

type of cellulose	$[\eta][\text{g (100 mL)}^{-1}]$	$DP_w[-]$	$M_w[\text{g mol}^{-1}]$
COT	599	2,989	471,013
rCOT	454	2,009	316,601
MCC	129	334	52,627
rMCC	97	221	34,765

mainly attributed to partial cleavage of the β -glycosidic bonds as well as possible chemical modifications caused by the solvent and energy input [27] that may influence measured intrinsic viscosity and thus affect the calculated DP value. In our case, both cellulose samples showed minor DPs after regeneration. The measured DPs decreased by approximately 30%. Cellulose degradation in ionic liquids is especially observed for long time dissolution (≥ 24 h) or high temperature dissolution (≥ 130 °C) processes [28]. Although mild conditions (2 h @ 60 °C, 1 h @ 90 °C) were applied, still relatively high DP deviations were observed in EmimAc/DMSO. However, comparable results for cotton linters (DP decrease from 920 to 649) were reported by Cheng et al. using the same IL/DMSO combination with a similar cellulose concentration [7] as well as for other cellulose types using only EmimAc [27]. Although cellulose regenerates used for DP determination were Soxhlet-extracted, residual EmimAc molecules may still be contained and could possibly alter the CED solution viscosities. By acting as a plasticizer, solution viscosities are lowered and resulting DP values decrease.

Morphology. For a polymer blend, morphology decides upon important properties, such as mechanical performance. When using solution blending, a crucial step is the removal of solvent from the mixture, either by evaporation or precipitation with a non-solvent. If the blend partners are immiscible, phase separation occurs during solvent removal, which depends strongly on the rate of evaporation or precipitation [29]. Phase morphologies of immiscible blends, such as co-continuous, laminar or dispersed structures may alter not only on the basis of composition, but also during solvent removal [30]. Depending on the velocity of the solvent removal, metastable blend morphologies are also possible [31]. In our study, rapid precipitation was performed by adding an excess of non-solvent to the blend solutions. For better comparability, all samples were treated equally at this point. It should be noted that for some pairings the choice of precipitant and precipitation temperatures could certainly be adjusted to reduce possible phase segregation. For example, severe loss of material occurred during precipitation and washing of the PHA/COT sample containing 70 wt% PHA, preventing further processing and material characterization. Immediate, macroscopically visible phase separation was observed for all PCL/cellulose samples. Other combinations showed no such phase separation.

Further thermal processing such as annealing may additionally affect the phase morphology [29]. We tested our samples for their thermomechanical formability by hot pressing. All polymer combinations showed different behavior during testing. For the PHA, PLA and PBS samples, films were hardly coherent after pressing. The high brittleness was also evident in the preparation of microtome sections, where material breakage occurred. Therefore, microtome cuts were only taken where possible (for additional photos, see [supporting information](#)), and cuts are shown exemplarily for the 50% cellulose blends (Fig. 1).

We obtained transparent press films for all PA6/cellulose blends (for additional microtome cuts, see [supporting information](#)). Optical microscopy of cross-sections showed uniform appearance with few defects. Compared to all other samples, few or no artefacts resulting from the sample cutting with the blade were detected. PLA blends were transparent at coherent areas and less brittle compared to the other polyesters. Here, we detected many flaws and material inclusions and

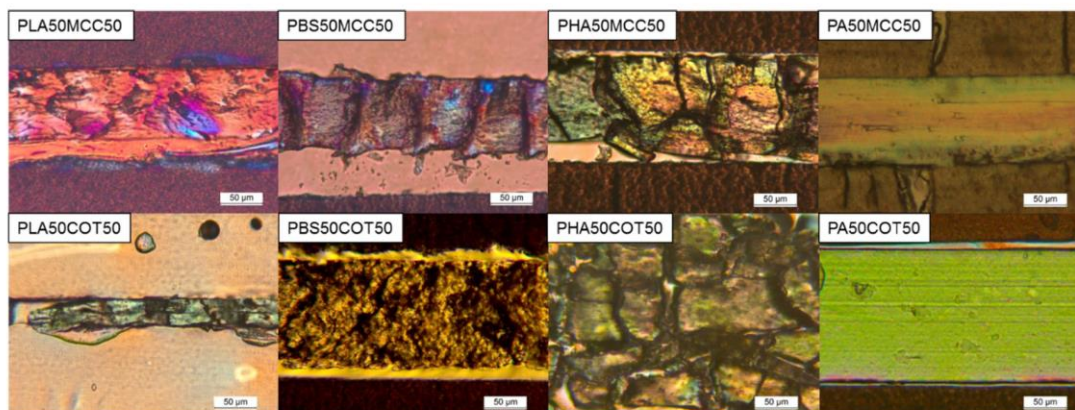


Fig. 1. Optical microscopy of microtome sections (20 μm thickness) of hot pressed films from synthetic polymer/cellulose blends (weight ratio: 50–50).

the platelets were fractured during pressing or cut preparation. PHA/cellulose regenerates were extremely brittle and non-coherent, resulting in fractured press films at all blend ratios. PBS/cellulose films were translucent at coherent areas, but still depicted brittleness visible as fractions and an irregular surface. Although PLA tends to precipitate as a powder from water precipitation, regenerates were coherent and press films showed only few fractions. Still flaws and marks from the microtome blade are visible, indicating the blend material to be less flexible than the PA6 samples. It has to be noted that the quality of the microtome sections depends strongly on the handling during pressing and the cutting technique. Even if an attempt has been made to treat all specimens in the same way, individual deviations may occur. This visual assessment should therefore only serve as a support for the analytical material characterization.

To further investigate the morphology of the PA6/cellulose blends, cross sections were analyzed via SEM. Since cryo-fractured images showed no morphological differences apart from common topographical evidence from the fraction (images see [supporting information](#)), cross sections were polished with an Argon beam. The images taken showed morphological differences for both cellulose samples, shown exemplarily for the 50:50 blend ratio (Fig. 2). Inclusions in the small micron scale showing oblong agglomerates can be attributed to the MCC (Fig. 2d). For the COT, inclusions rather indicate accumulated spherical aggregates and are proportionally large in size (Fig. 2b). In both cases, inclusions could be attributed to predominantly crystalline parts of the cellulose and might have occurred during blend

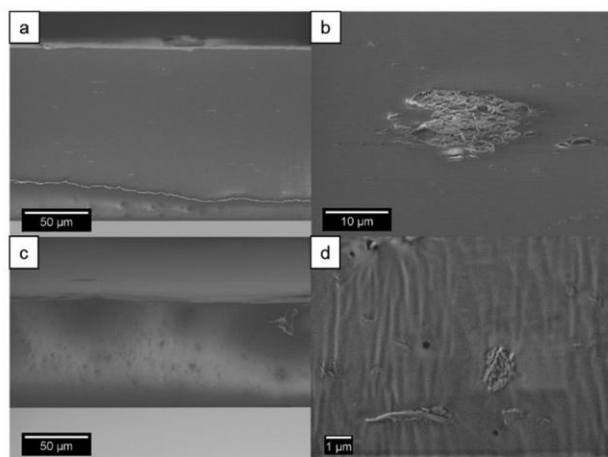


Fig. 2. SEM of cross section polished hot pressed and subsequently films from PA6/cellulose blends (weight ratio: 50–50): PA6/COT (a, b) and PA6/MCC (c, d) at different levels of magnification.

precipitation by partial demixing and recrystallization, or represent previously undissolved cellulose. In general, cellulose aggregates represent only small areas that are not representative of the original cellulose content. This may indicate partial miscibility in terms of a predominantly single-phase structure in the scale studied. However, both polymers are quite similar in chemical composition, and the morphological differences shown with this technique are, apart from topography, due to differences in density rather than chemical composition.

From the SEM images shown, we presume a hybrid structure independent from the cellulose type for the investigated samples. A homogeneous mixed phase, probably within the amorphous regions of PA6 and cellulose, as well as crystalline areas for both polymers is proposed. However, only on the basis of the SEM images shown, a binary phase distribution in the apparently homogeneous phase, e.g. at the nanoscale, cannot be excluded.

Calorimetric analysis. The thermal behavior of a blended sample can give some information on polymer compatibility or miscibility. For semi-crystalline polymers, typical transitions such as melting of the crystalline areas or the glass transition of the amorphous regions can be enlarged or reduced in intensity and shifts of the respective temperatures can indicate interactions between different polymer chains or interactions with plasticizer/solvent molecules. With regard to miscibility evaluation of polymer blends, the presence of a single, concentration dependent T_g is the most popular indicator for polymer miscibility. In this study, however, we did not use an indicator for several reasons. In the case of cellulose, a glass transition can hardly be determined due to degradation processes in the relevant temperature ranges as well as the high sensitivity to water[32–33]. Therefore, a single measured glass transition temperature of cellulose-polymer blends is not necessarily a decisive criterion to evaluate blend miscibility. In addition, it was shown that the DSC method is not particularly appropriate for measuring the T_g , especially for compositions with high cellulose contents[15]. Furthermore, an opposite influence on the T_g by possible residual IL is to be expected in our case. Residual ionic liquid can act as a plasticizer for cellulose[34]; and in our case is also expected to plasticize the used polyesters and polyamides. Although the washing steps were performed in a way that no IL can be detected via FTIR in the regenerates, residues of approximately 1 wt% or lower cannot be excluded. The dry matter of the loaded washing water from last washing step ranged between approximately 0.05–0.9 wt%. Since the named different influences on the blend's glass transition cannot be separated from each other based on a single measured value, changes in the melting area or shifts of the melting points could be more meaningful in our study.

During the solution-precipitation process, possibly contained additives of the neat thermoplastic polymers may be depleted and the

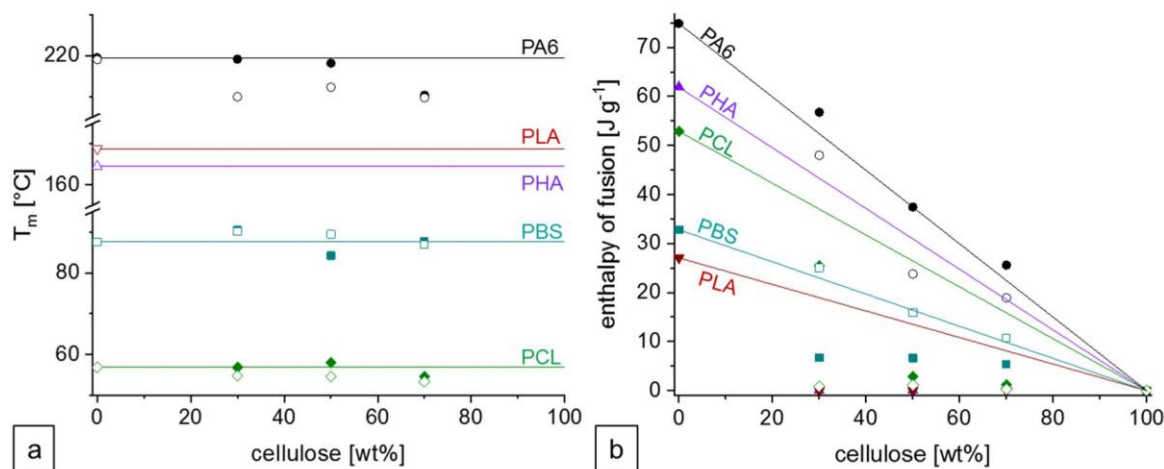


Fig. 3. Melting temperatures (a) and enthalpy of fusion per total weight of sample (b) of synthetic polymers versus cellulose content for synthetic polymer/cellulose blends. Blends with MCC are marked with solid symbols; blends with COT with open symbols. Lines indicate the melting temperature of the pure synthetic polymer (a) and the theoretical curve for the enthalpy of fusion of the synthetic polymers in blended samples; naturally decreasing along with the synthetic polymer ratio (b). All data shown refer to the 2nd heating run.

polymer properties, such as their thermal behavior, might change. Therefore, values for pure polymer samples are referring to precipitated samples from DMSO.

Fig. 3 shows the results from the calorimetric analysis, separated in melting point and enthalpy of melting for all polyesters and polyamide depending on the cellulose concentration. Phase separation was macroscopically visible in the regenerated PCL/cellulose blends. Infrared spectroscopy showed an almost pure PCL phase and a cellulose-rich mixed phase (supporting information) for all samples, indicating partial compatibility for cellulose rich blends, which contradicts former findings suggesting small amounts of cellulose being partially miscible in PCL-rich blends[35]. For DSC measurements, we chose the cellulose-rich mixed phase; therefore, the x-axis displays only the initial cellulose content of the samples during solution mixing. This also explains the much lower enthalpy of melting for the PCL/cellulose blend samples, since the measured value is normalized to the sample weight and initial polymer content.

Except for PHA and PLA, synthetic polymers were crystalline at every tested composition; however, occasionally there was some degree of disproportional reduced crystallinity with an increase of cellulose content, especially for the PA6/COT and PBS/MCC blends. In a polymer blend where at least one component is crystalline, the melting behavior can potentially be associated with the extent of intermolecular interactions between the polymers and give information about compatibility. A depression of the melting point of the crystallizable polymer component could therefore indicate intermolecular interaction between the two blend components[36]. For the PA6 sample, melting point depression with both cellulose types ($\Delta T_m \sim 10$ °C at 70 wt% cellulose) was detected, suggesting interactions between the cellulose and polyamide chains. This is contrary to a former study using lithium chloride/N,N-dimethylacetamide as solvent, stating PA6 and cellulose to be immiscible[35,37]. A similar approach utilized a solvent mixture of N-methylmorpholine-N-oxide and phenol to blend cellulose with PA66. However, crystallization of the polyamide already occurred when both solutions were mixed, resulting in a two phase morphology[38]. The choice of solvent therefore seems to be decisive concerning polymer-polymer interactions in solution blended materials.

For all other polymers, no comparable melting point depression was detected. PBS samples showed similar melting points independent from the type of cellulose. For PCL, slightly lower melting points were measured for blends with COT ($\Delta T_m \sim 3.5$ °C at 70 wt% cellulose). Unlike the pure PLA and PHA regenerates, blends showed no crystallization or melting during the DSC non-isothermal heating and cooling

runs. Even in the first heating run (data not shown) no evaluable melting range could be detected. Although PLA and PHA both show slow crystallization rates[39–40] and the applied heating/cooling rate is relatively fast, the absence of melting or crystallization areas in all blend compositions is quite noticeable. With regard to the cellulose blends, this could, however, enable improved mixing within the amorphous polymer regions.

Infrared spectroscopy. FTIR is used to detect structural differences that occur within the samples caused by the applied solution-precipitation process. The removal of EmimAc could also be proven by the absence of IL-characteristic bands, such as the COO^- asymmetric stretching of the acetate anion at 1559 cm^{-1} [41]. However, it should be noted that the sensitivity of infrared spectroscopy is not particularly high in the low percentage range and residual IL concentrations of a few percent or less might not necessarily be detected.

FTIR spectra of MCC, COT and their regenerates are shown in Fig. 4. For both celluloses, crystallinity is reduced after regeneration. While the absorption band at 1428 cm^{-1} , associated with the symmetrical CH_2 bending vibration and also referred to as the crystallinity band, is decreased, the signal at 894 cm^{-1} , associated with the COC bridge extension and referred to as the amorphous absorption band, increases [42–44]. Based on this, the solution-precipitation process leads to decreased crystallinity connected with an increase of amorphous regions. This is additionally indicated by an increased absorption of the 1640 cm^{-1} band, associated with water in the amorphous regions [45–46].

Although Imidazolium-based ILs are widely considered as non-derivatizing solvents for polysaccharides such as cellulose, it was also observed that EmimAc may also react with the reducing end of the cellulose polymer or oligomer[48], based on the reaction of the aldehyde with the reactive proton of the IL at C2[49]. Although EmimAc gives many advantages compared to other imidazolium-based ILs, such as its liquid state at room temperature, high cellulose dissolution capacity, low toxicity, low corrosivity and even biodegradability [50], such proposed side reactions can be considered a major drawback. The cellulose derivatization does not only result in uncontrolled product properties after regeneration, but also limits IL recycling for the whole process.

To gain a compatible or even miscible polyester-/amid/cellulose blend, favorable polymer chain interactions are prerequisite. Comparable literature for cellulose/polymer blends from solution is rather rare, but the use of cellulose as filler in biopolymer composites, especially nanocomposites, has been a field of high interest over the

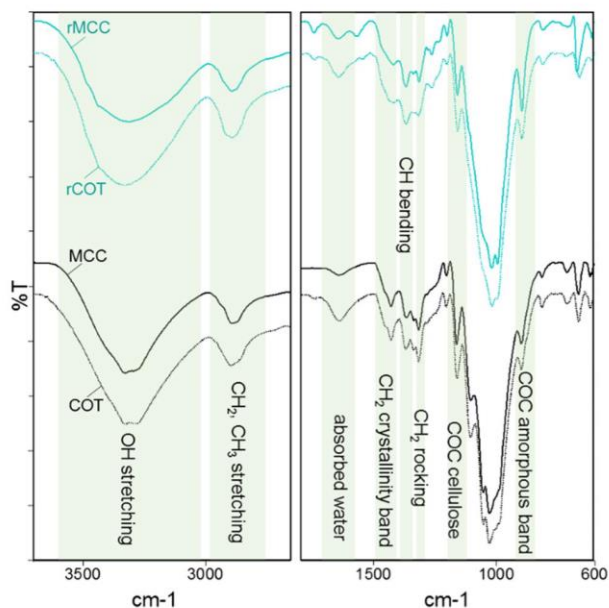


Fig. 4. FTIR Spectra and band assignments for cellulose (black) and its regenerates (cyan). COT and rCOT are shown in dotted lines, MCC and rMCC in solid lines. Band assignments are marked according to [47].

past decades[51–54]. Here, interphase interactions can also give hints about general compatibility. As mentioned before, hydrogen bonding is expected to be necessary for blend compatibility. FTIR can be used to study hydrogen bonding in polymer blends, since they affect different absorption regions in the spectrum. There are early studies which were conducted more than 30 years ago[55–57].

The FTIR spectra of all regenerated polymers as well as their blends with MCC and COT can be found in Fig. 5 and Fig. 6, respectively. Since the carbonyl oxygen is the common acceptor of hydrogen bonds for our polyester/-amide/cellulose blends, the focus of investigation for hydrogen bonding via FTIR is on the C = O absorption bands.

The spectra of the PLA/Cellulose blends show a strong shift of the carbonyl band $\nu(\text{C} = \text{O})$ at 1755 cm^{-1} [58] to 1749 cm^{-1} (30% MCC), 1742 cm^{-1} (50% MCC) and 1726 cm^{-1} (70% MCC). The $\nu_s \text{COC}$ band at 1086 cm^{-1} [58] also slightly shifts to 1083 cm^{-1} (30% MCC). The PLA/COT blends show similar results, with a shift of the $\nu(\text{C} = \text{O})$ band to 1735 cm^{-1} (70% COT). The reduced stretching frequency of the C = O bond can be ascribed to interactions between a hydrogen donor and the carbonyl acceptor group[57,59], which in our case concludes hydrogen bonding between PLA and cellulose. FTIR studies on PLA/cellulose composites showed no shift of the carbonyl band[60–61]. It can therefore be assumed that the applied blending process resulted in strongly interacting, compatible PLA/cellulose materials. Except for the spectrum of the 30% MCC blend, which can be mainly assigned to cellulose derived bands, all PBS/Cellulose samples show mixed band absorptions of PBS and cellulose in every blend composition without

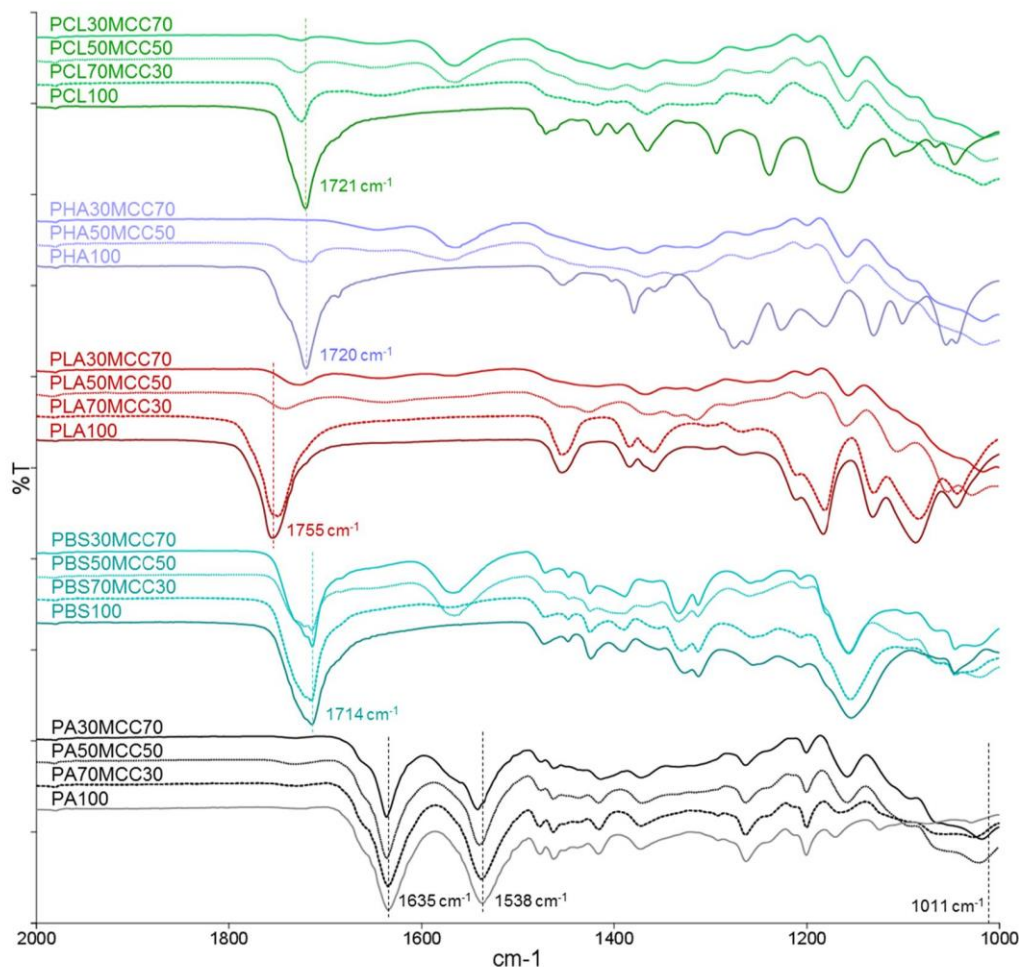


Fig. 5. FTIR spectra of polyester and polyamide regenerates and their blends with MCC. Carbonyl bands (PCL, PHA, PLA, PBS) and amid bands (PA6) for the pure polymer regenerates are marked with dashed lines. For PA6 and its blends, the additional dashed line at 1011 cm^{-1} represents the C-O stretching of MCC.

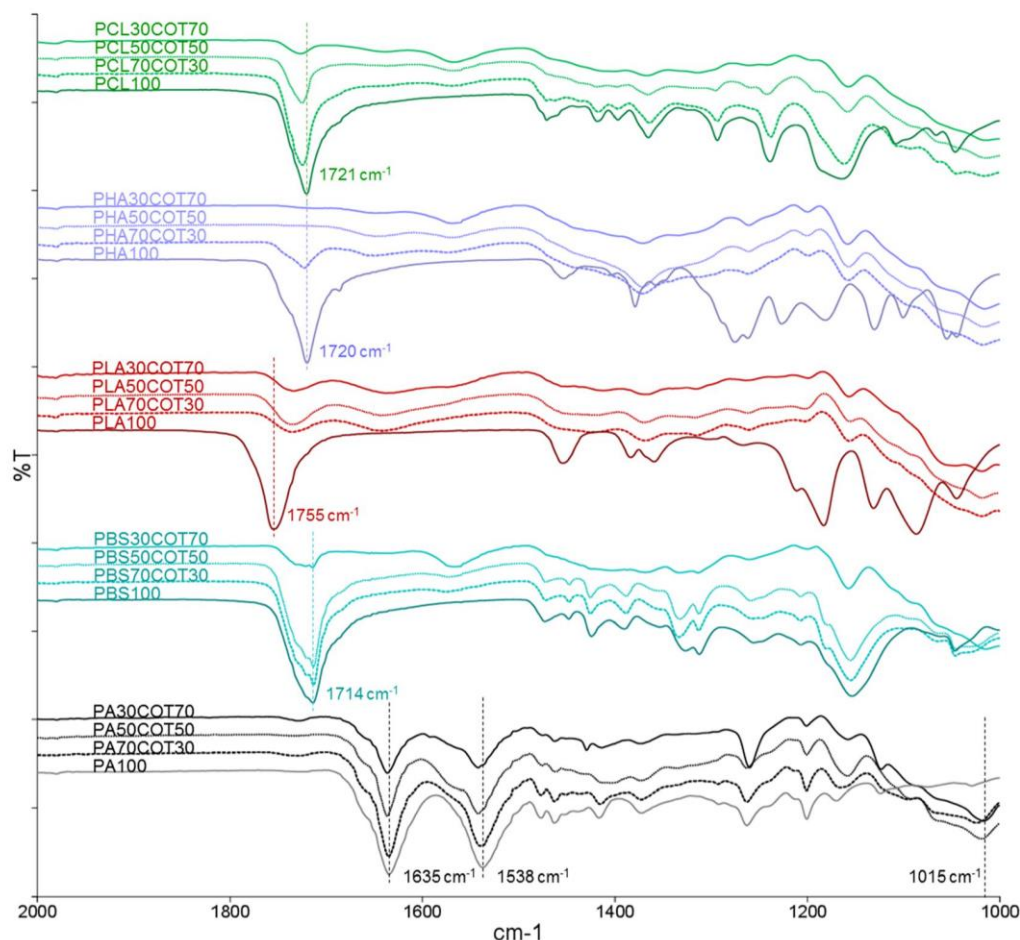


Fig. 6. FTIR spectra of polyester and polyamide regenerates and their blends with COT. Carbonyl bands (PCL, PHA, PLA, PBS) and amid bands (PA6) for the pure polymer regenerates are marked with dashed lines. For PA6 and its blends, the additional dashed line at 1015 cm^{-1} represents the C-O stretching of COT.

any detectable shifts of the carbonyl-band position. Comparable MCC/PBS composites containing 70 wt% cellulose showed similar FTIR results. Poor interactions between both components were also concluded from MCC aggregation in the composite[54]. With regard to DSC and microscopic images in this study, immiscibility and low compatibility of the components is assumed.

For the PHA/Cellulose blends, the strong absorption of the carbonyl C = O of the ester group at 1720 cm^{-1} of the polyhydroxyalkanoates [62] shows no distinct shift and is not detectable for the samples with 50% and 70% COT, indicating a depletion of polymer during washing. With MCC as a blending partner, the PHA carbonyl band can still be found in the 50% MCC blend without notable shifts, disappearing in the 70% MCC sample. All other bands assigned to groups involved in hydrogen bonding show no abnormalities for both sample sets.

PCL/Cellulose blends showed phase separation when precipitated at all applied ratios. A PCL and a cellulose-rich phase were detected via FTIR (supporting information). Comparing the cellulose-rich phases, the C = O stretching of PCL at 1721 cm^{-1} [63] slightly shifts to 1726 cm^{-1} and 1725 cm^{-1} at the 70% COT and MCC sample. When normalized to the cellulose assigned band to C-O stretching of cellulose at around 1015 cm^{-1} , the spectra show different contents of PCL regarding the transmission of the PCL carbonyl band at 1725 cm^{-1} . The signal strength matches the original concentration of the blends for both MCC and COT.

PA6 blended films gave a mixed spectrum of cellulose and the polyamide for all samples. Both the hydrogenbonded N-H stretch peak at 3295 cm^{-1} [64] as well as the amide I and amide II bands at

1635 cm^{-1} and 1538 cm^{-1} , respectively, could be found to be strong absorption bands in every composition. The amide I bands, of which the main contribution can be ascribed to the C = O stretching[65–66], depicts no noticeable shifts. The amide II band to which the NH deformation mainly contributes[65–66], slightly shifts to higher wavenumbers with increasing cellulose content. What is noticeable, however, is the shift of the band assigned to the C-O stretching of cellulose [47] from 1011 cm^{-1} (MCC100) or 1015 cm^{-1} (COT100) in the pure cellulose regenerate to 1027 cm^{-1} or 1024 cm^{-1} at the PA6 concentration of 70%, respectively. This might be a result of interactions of the NH group with the cellulose backbone.

4. Conclusions

Based on the presented solution-precipitation process, it is possible to produce a variety of new synthetic polymer/cellulose blends with good compatibility, no phase separation in dissolved state and only slight cellulose degradation. Yet, process adaptations regarding the choice of solvent or anti-solvent and precipitation parameters may be useful for the respective polymer combinations, since they directly affect the blend morphology. After regeneration, phase separation was macroscopically visible for the PCL/cellulose blends. All other tested blend compositions which were precipitated showed macroscopic homogenous mixtures of both cellulose and synthetic polymers, confirmed by FTIR analysis. However, in case of PLA and PHA, FTIR spectra indicated a depletion of polymer during precipitation and washing, especially when blended with MCC. As just mentioned above,

the applied anti-solvent has to be carefully chosen, also in order to reduce polyester losses during processing. Blend compatibility was evaluated by means of synthetic polymer/cellulose interactions. Regarding hydrogen bonding interactions, FTIR provided evidence of strong interactions between PLA and cellulose. Since all PLA/cellulose blends showed no melting areas during DSC measurement, we assume that a homogeneously mixed PLA/cellulose phase prevented PLA crystallization. For the other polyesters, no specific interaction with cellulose was detected via FTIR. Spectra for PBS/MCC composites in comparing studies and microscope images shown here are leading to the assumption of immiscibility of PBS/cellulose blends in the tested ratios.

Although hydrogen bonding interactions could not be clearly detected via FTIR for the PA6/cellulose blends, coherent and transparent films could be thermomechanically pressed from the produced blend materials with a one-phase morphology in the micrometer scale. Further investigation using SEM give reason to presume a hybrid structure composed of a homogeneous mixed phase and crystalline areas for both polymers. Also, a reduction in the PA6 melting point was observed as a function of the cellulose content, which additionally indicates interactions between the polymers.

Further tests and extended polymer ratios are necessary for investigation of miscibility behavior in synthetic polymer/cellulose blends, especially for PA6 and PLA, where first results indicate favorable interactions with cellulose in samples prepared with the applied solution-precipitation method. This opens up the field for thermo-plastic processing of cellulose for the manufacture of novel polymer/cellulose blend materials. Possible fields of application might be moulded parts for various industries or blend fibers for textiles or technical applications. The solvent system used is of particular interest with regard of commercial fiber production, as ionic liquids have already shown to be applicable for industrial applications, e.g. in the Ioncell™ process.

CRedit authorship contribution statement

Kerstin Müller: Conceptualization, Methodology, Formal analysis, Investigation, Writing - original draft, Visualization. **Cordt Zollfrank:** Writing - review & editing.

Declaration of Competing Interest

The authors declared that there is no conflict of interest.

Acknowledgements

We thank Anna Kotlyar for her help with sample preparation and characterization, Markus Schmid for discussions on the manuscript and Sigrun Brand-Müller for proofreading. This research did not receive any specific grant from funding agencies in the public, commercial, or not-for-profit sector.

Data Availability Statements.

Part of the raw/processed data required to reproduce these findings are available from the [supporting information](#), including capillary viscosity results, FTIR spectra of PCL/COT samples, molecular weight distribution curves from SEC measurements, additional microscope images of microtome sections and additional SEM images of cryo-fractured cross-sections. The raw data from DSC measurements required to reproduce these findings cannot be shared at this time due to technical limitations.

Appendix A. Supplementary material

Supplementary data to this article can be found online at <https://doi.org/10.1016/j.eurpolymj.2020.109743>.

References

- [1] S.Z. Rogovina, G.A. Vikhoreva, Polysaccharide-based polymer blends: Methods of their production, *Glycoconj. J.* 23 (7) (2006) 611.
- [2] B.A. Miller-Chou, J.L. Koenig, A review of polymer dissolution, *Prog. Polym. Sci.* 28 (8) (2003) 1223–1270.
- [3] R.P. Swatoski, S.K. Spear, J.D. Holbrey, R.D. Rogers, Dissolution of Cellulose with Ionic Liquids, *J. Am. Chem. Soc.* 124 (18) (2002) 4974–4975.
- [4] S. Napso, D.M. Rein, R. Khalfin, Y. Cohen, Semidilute solution structure of cellulose in an ionic liquid and its mixture with a polar organic co-solvent studied by small-angle X-ray scattering, *J. Polym. Sci., Part B: Polym. Phys.* 55 (11) (2017) 888–894.
- [5] Q.-L. Kuang, J.-C. Zhao, Y.-H. Niu, J. Zhang, Z.-G. Wang, Celluloses in an Ionic Liquid: the Rheological Properties of the Solutions Spanning the Dilute and Semidilute Regimes, *J. Phys. Chem. B* 112 (33) (2008) 10234–10240.
- [6] M. Gericke, K. Schluffer, T. Liebert, T. Heinze, T. Budtova, Rheological Properties of regenerated cellulose film from cotton linter using organic electrolyte solution (OES), *Cellulose* 24 (4) (2017) 1631–1639.
- [7] D. Cheng, X. An, J. Zhang, X. Tian, Z. He, Y. Wen, Y. Ni, Facile preparation of regenerated cellulose film from cotton linter using organic electrolyte solution (OES), *Cellulose* 24 (4) (2017) 1631–1639.
- [8] P.J. Flory, Thermodynamics of High Polymer Solutions, *J. Chem. Phys.* 10 (1) (1942) 51–61.
- [9] M.L. Huggins, Solutions of Long Chain Compounds, *J. Chem. Phys.* 9 (5) (1941) 440–440.
- [10] L.A. Utracki, *Polymer Blends Handbook*, Springer, 2003.
- [11] L.A. Utracki, *Polymer Alloys and Blends: Thermodynamics and Rheology*, Hanser Gardner Publications (1990).
- [12] P. Knychala, K. Timachova, M. Banaszak, N.P. Balsara, 50th Anniversary Perspective: Phase Behavior of Polymer Solutions and Blends, *Macromolecules* 50 (8) (2017) 3051–3065.
- [13] C. Koning, M. Van Duin, C. Pagnoulle, R. Jerome, Strategies for compatibilization of polymer blends, *Prog. Polym. Sci.* 23 (4) (1998) 707–757.
- [14] B. Imre, B. Pukánszky, Compatibilization in bio-based and biodegradable polymer blends, *Eur. Polym. J.* 49 (6) (2013) 1215–1233.
- [15] R.S.J. Manley, Blends of Cellulose and Synthetic Polymers. *Cellulose Derivatives*, American Chemical Society 688 (1998) 253–264.
- [16] M. Kes, B.E. Christensen, A re-investigation of the Mark–Houwink–Sakurada parameters for cellulose in Cuen: A study based on size-exclusion chromatography combined with multi-angle light scattering and viscometry, *J. Chromatogr. A* 1281 (2013) 32–37.
- [17] P. Gijmsan, Review on the thermo-oxidative degradation of polymers during processing and in service. 8 (1) (2008) 065.
- [18] A.A. Cuadri, J.E. Martín-Alfonso, Thermal, thermo-oxidative and thermo-mechanical degradation of PLA: A comparative study based on rheological, chemical and thermal properties, *Polym. Degrad. Stab.* 150 (2018) 37–45.
- [19] F. Carrasco, D. Dionisi, A. Martinelli, M. Majone, Thermal stability of polyhydroxyalkanoates, *J. Appl. Polym. Sci.* 100 (3) (2006) 2111–2121.
- [20] P. Rizzarelli, S. Carroccio, Thermo-oxidative processes in biodegradable poly(butylene succinate), *Polym. Degrad. Stab.* 94 (10) (2009) 1825–1838.
- [21] Y. Aoyagi, K. Yamashita, Y. Doi, Thermal degradation of poly[(R)-3-hydroxybutyrate], poly[ε-caprolactone], and poly[(S)-lactide], *Polym. Degrad. Stab.* 76 (1) (2002) 53–59.
- [22] W. Dong, P. Gijmsan, Influence of temperature on the thermo-oxidative degradation of polyamide 6 films, *Polym. Degrad. Stab.* 95 (6) (2010) 1054–1062.
- [23] T. Heinze, A. Koschella, Solvents applied in the field of cellulose chemistry: a mini review, *Polímeros* 15 (2005) 84–90.
- [24] F. Gores, P. Kilz, Examining accuracy and precision in GPC/SEC, *The Column* 4 (2008) 20–23.
- [25] Z. Liu, H. Wang, Z. Li, X. Lu, X. Zhang, S. Zhang, K. Zhou, Characterization of the regenerated cellulose films in ionic liquids and rheological properties of the solutions, *Mater. Chem. Phys.* 128 (1) (2011) 220–227.
- [26] H. Zhang, J. Wu, J. Zhang, J. He, 1-Allyl-3-methylimidazolium Chloride Room Temperature Ionic Liquid: A New and Powerful Nonderivatizing Solvent for Cellulose, *Macromolecules* 38 (20) (2005) 8272–8277.
- [27] J. Pang, M. Wu, Q. Zhang, X. Tan, F. Xu, X. Zhang, R. Sun, Comparison of physical properties of regenerated cellulose films fabricated with different cellulose feedstocks in ionic liquid, *Carbohydr. Polym.* 121 (2015) 71–78.
- [28] J. Yang, X. Lu, X. Yao, Y. Li, Y. Yang, Q. Zhou, S. Zhang, Inhibiting degradation of cellulose dissolved in ionic liquids via amino acids, *Green Chem.* 21 (10) (2019) 2777–2787.
- [29] K. Yang, C.D. Han, Effects of shear flow and annealing on the morphology of rapidly precipitated immiscible blends of polystyrene and polyisoprene, *Polymer* 37 (26) (1996) 5795–5805.
- [30] E.B. Nauman, S.-T. Wang, N.P. Balsara, A novel approach to polymeric micro-dispersions, *Polymer* 27 (10) (1986) 1637–1640.
- [31] S. Mawson, S. Kanakia, K.P. Johnston, Metastable polymer blends by precipitation with a compressed fluid antisolvent, *Polymer* 38 (12) (1997) 2957–2967.
- [32] L. Szczeniński, A. Rachocki, J. Tritt-Goc, Glass transition temperature and thermal decomposition of cellulose powder, *Cellulose* 15 (3) (2008) 445–451.
- [33] M. Ioelovich, Isophase Transitions of Cellulose – A Short Review, *Athens Journal of Sciences* 3 (4) (2016) 309–322.
- [34] M.A. Haq, Y. Habu, K. Yamamoto, A. Takada, J.-I. Ka-dokawa, Ionic Liquid Induces Flexibility and Thermoplasticity in Cellulose Film, *Carbohydr. Polym.* 115058 (2019).
- [35] Y. Nishio, R.S.J. Manley, Blends of cellulose with nylon 6 and poly(ε-caprolactone)

- prepared by a solution-coagulation method, *Polym. Eng. Sci.* 30 (2) (1990) 71–82.
- [36] J. Runt, P.B. Rim, S.E. Howe, Melting point elevation in compatible polymer blends, *Polym. Bull.* 11 (6) (1984) 517–521.
- [37] J.F. Masson, R.S.J. Manley, Solid-state NMR of some cellulose/synthetic polymer blends, *Macromolecules* 25 (2) (1992) 589–592.
- [38] M. Garcia-Ramirez, J.Y. Cavallé, D. Dupeyre, A. Péguy, Cellulose-polyamide 66 blends. I. Processing and characterization, *J. Polym. Sci., Part B: Polym. Phys.* 32 (8) (1994) 1437–1448.
- [39] Z. Refaa, M. Boutaous, D.A. Siginer, PLA Crystallization Kinetics and Morphology Development, *Int. Polym. Proc.* 33 (3) (2018) 336–344.
- [40] C. Zhu, C.T. Nomura, J.A. Perrotta, A.J. Stipanovic, J.P. Nakas, The effect of nucleating agents on physical properties of poly-3-hydroxybutyrate (PHB) and poly-3-hydroxybutyrate-co-3-hydroxyvalerate (PHB-co-HV) produced by *Burkholderia cepacia* ATCC 17759, *Polym. Test.* 31 (5) (2012) 579–585.
- [41] Z.-D. Ding, Z. Chi, W.-X. Gu, S.-M. Gu, H.-J. Wang, Theoretical and experimental investigation of the interactions between [emim]Ac and water molecules, *J. Mol. Struct.* 1015 (2012) 147–155.
- [42] D. Ciolacu, F. Ciolacu, V.I. Popa, Amorphous Cellulose - Structure and Characterization, *Cellul. Chem. Technol.* 45 (1–2) (2011) 13–21.
- [43] S.-Y. Oh, D.I. Yoo, Y. Shin, H.C. Kim, H.Y. Kim, Y.S. Chung, W.H. Park, J.H. Youk, Crystalline structure analysis of cellulose treated with sodium hydroxide and carbon dioxide by means of X-ray diffraction and FTIR spectroscopy, *Carbohydr. Res.* 340 (15) (2005) 2376–2391.
- [44] L.P. De Figueiredo, F.F. Ferreira, The Rietveld Method as a Tool to Quantify the Amorphous Amount of Microcrystalline Cellulose, *J. Pharm. Sci.* 103 (5) (2014) 1394–1399.
- [45] J. Yin, K. Luo, X. Chen, V.V. Khutoryanskiy, Miscibility studies of the blends of chitosan with some cellulose ethers, *Carbohydr. Polym.* 63 (2) (2006) 238–244.
- [46] J.-H. Pang, X. Liu, M. Wu, Y.-Y. Wu, X.-M. Zhang, R.-C. Sun, Fabrication and Characterization of Regenerated Cellulose Films Using Different Ionic Liquids, *Journal of Spectroscopy* 2014 (2014) 8.
- [47] M. Poletto, V. Pistor, A.J. Zattera, Structural characteristics and thermal properties of native cellulose, in: T.G.M. Van De Ven (Ed.), *Cellulose - Fundamental Aspects*, IntechOpen, 2013.
- [48] T. Heinze, S. Dorn, M. Schöbitz, T. Liebert, S. Köhler, F. Meister, Interactions of Ionic Liquids with Polysaccharides - 2: Cellulose, *Macromolecular Symposia* 262 (1) (2008) 8–22.
- [49] V.K. Aggarwal, I. Emme, A. Mereu, Unexpected side reactions of imidazolium-based ionic liquids in the base-catalysed Baylis-Hillman reaction, *Chem. Commun.* 15 (2002) 1612–1613.
- [50] Heinze, T., *Cellulose: Structure and Properties. In Cellulose Chemistry and Properties: Fibers, Nanocelluloses and Advanced Materials*, Rojas, O. J., Ed. Springer International Publishing: Basel, Switzerland, 2016.
- [51] C.T. Mokhena, S.J. Sefadi, R.E. Sadiku, J.M. John, J.M. Mochane, A. Mtibe, Thermoplastic Processing of PLA/Cellulose Nanomaterials Composites, *Polymers* 10 (2018) (12).
- [52] H.-Y. Mi, X. Jing, J. Peng, M.R. Salick, X.-F. Peng, L.-S. Turng, Poly(ϵ -caprolactone) (PCL)/cellulose nano-crystal (CNC) nanocomposites and foams, *Cellulose* 21 (4) (2014) 2727–2741.
- [53] K.C.C. de Carvalho, S.R. Montoro, M.O.H. Cioffi, H.J.C. Voorwald, Polyhydroxyalkanoates and Their Nanobiocomposites With Cellulose Nanocrystals, in: S. Thomas, R. Shanks, S. Chandrasekharakurup (Eds.), *Design and Applications of Nanostructured Polymer Blends and Nanocomposite Systems*, William Andrew Publishing, Boston, 2016, pp. 261–285.
- [54] O. Platnieks, S. Gaidukovs, A. Barkane, G. Gaidukova, L. Grase, K.V. Thakur, I. Filipova, V. Fridrihsone, M. Skute, M. Laka, Highly Loaded Cellulose/Poly (butylene succinate) Sustainable Composites for Woody-Like Advanced Materials Application, *Molecules* 25 (2019) (1).
- [55] M.M. Coleman, D.J. Skrovanek, J. Hu, P.C. Painter, Hydrogen bonding in polymer blends. 1. FTIR studies of urethane-ether blends, *Macromolecules* 21 (1) (1988) 59–65.
- [56] P.C. Painter, Y. Park, M.M. Coleman, Hydrogen bonding in polymer blends. 2. Theory, *Macromolecules* 21 (1) (1988) 66–72.
- [57] D. Braun, N. Eidam, D. Leif, FTIR studies of polar interactions in polymer blends, *Makromol. Chem. Macromol. Symp.* 52 (1) (1991) 105–111.
- [58] Goncalves, C. M. B.; Coutinho, J. A. P.; Marrucho, I. M., *Optical Properties. In Poly (lactic acid): Synthesis, Structures, Properties, Processing, and Applications*, Auras, R. A.; Lim, L. T.; Selke, S. E. M.; Tsuji, H., Eds. Wiley: Hoboken, New Jersey, 2011.
- [59] L. Paoloni, A. Patti, F. Mangano, The hydrogen bond with carbonyl groups: theoretical study of the correlation between the X-H stretching frequency shift and the C=O group properties, *J. Mol. Struct.* 27 (1) (1975) 123–137.
- [60] S. Sousa, A. Costa, A. Silva, R. Simões, Poly(lactic acid)/Cellulose Films Produced from Composite Spheres Prepared by Emulsion-Solvent Evaporation Method, *Polymers* 11 (2019) (1).
- [61] E.E. Popa, M. Rapa, O. Popa, G. Mustatea, V.I. Popa, A.C. Mitelut, M.E. Popa, Poly(lactic acid)/Cellulose Fibres Based Composites for Food Packaging Applications, *Mater. Plast.* 54 (4) (2017) 673–677.
- [62] Volova, T. G.; Zhila, N. O.; Shishatskaya, E. I.; Mironov, P. V.; Vasil'ev, A. D.; Sukovatyi, A. G.; Sinskey, A. J., The physicochemical properties of polyhydroxyalkanoates with different chemical structures. *Polymer Science Series A* 2013, 55 (7), 427-437.
- [63] M.M. Coleman, J. Zarian, Fourier-transform infrared studies of polymer blends. II. Poly(ϵ -caprolactone)-poly(vinyl chloride) system, *J. Polym. Sci.: Polymer Physics Edition* 17 (5) (1979) 837–850.
- [64] S.M. Aharoni, *N-Nylons: Their Synthesis, Structure, and Properties*, Wiley, Chichester, England, 1997.
- [65] R. Iwamoto, H. Murase, Infrared spectroscopic study of the interactions of nylon-6 with water, *J. Polym. Sci., Part B: Polym. Phys.* 41 (14) (2003) 1722–1729.
- [66] G. Socrates, *Infrared and Raman Characteristic Group Frequencies: Tables and Charts*, 3 ed., Wiley, Chichester, England, 2001.

Supporting Information

Ionic liquid aided solution-precipitation method to prepare polymer blends from cellulose with polyesters or polyamide

Kerstin Müller^{†, ‡, *}, Cordt Zollfrank[†]

[†]*Biogenic Polymers, TUM Campus Straubing for Biotechnology and Sustainability, Technical University of Munich, Schulgasse 16, 94315 Straubing, Germany*

[‡]*Fraunhofer Institute for Process Engineering and Packaging IVV, Giggenhauser Str. 35, 85354 Freising, Germany*

*Corresponding author. E-mail address: kerstin.mueller@ivv.fraunhofer.de

Capillary Viscosimetry

The degradation of cellulose in the ionic liquid-based solution-precipitation process was determined by comparison of the intrinsic viscosities and therefrom calculated molecular weights. The flow time of sample solutions were measured with a capillary viscosimeter according to the International Standard ISO 5351 with a four-fold determination of four different concentrations. The reduced viscosity (η_{red}) was calculated as follows:

$$\eta_{red} = \frac{\eta - \eta_0}{\eta_0 * c}$$

With η_0 being the viscosity of the CED solvent and c being the cellulose concentration in g (100 mL)^{-1} . The limiting viscosity number or intrinsic viscosity $[\eta]$ is defined as follows

$$[\eta] = \lim_{c \rightarrow 0} \left(\frac{\eta - \eta_0}{\eta_0 * c} \right)$$

and can therefore be determined by the extrapolation method. Figure 1 shows the reduced viscosities depending on the cellulose concentration and the calculated linear fits.

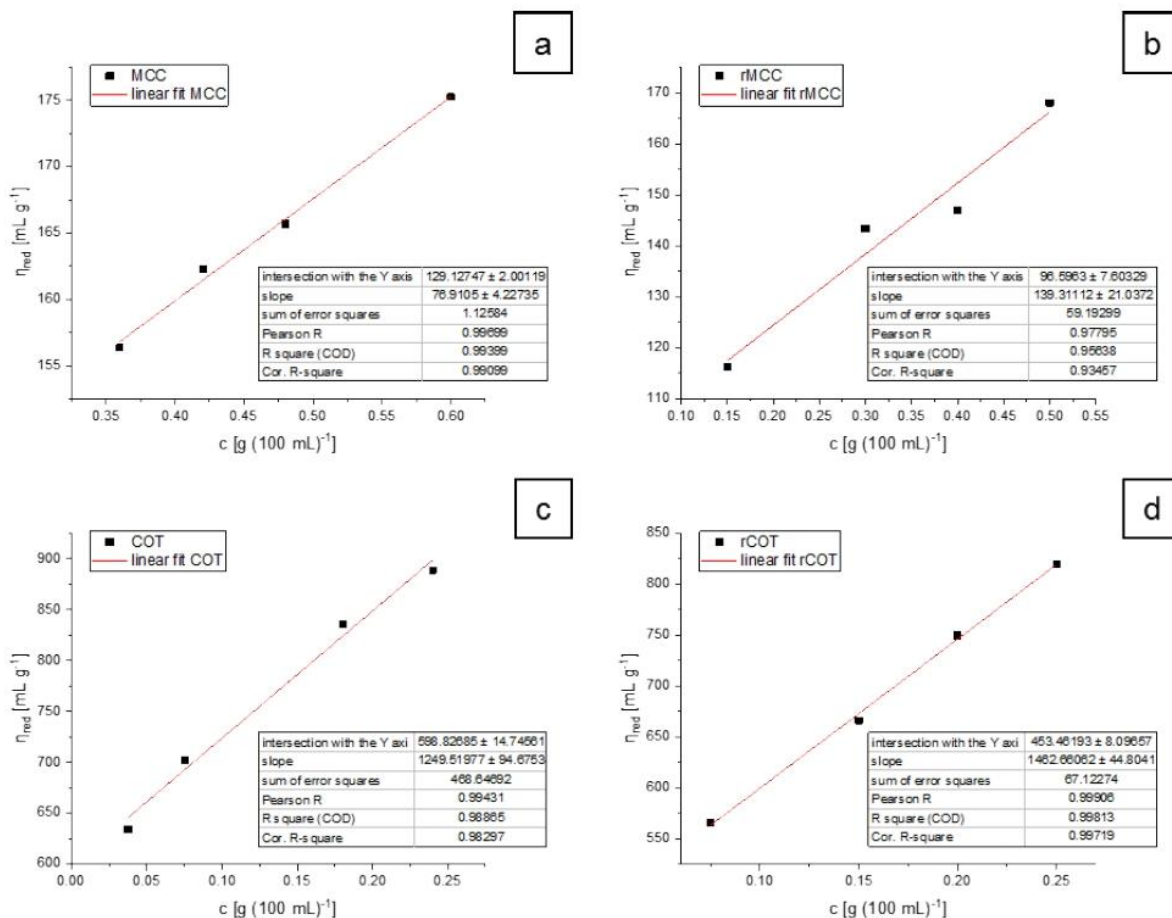


Figure 1. Reduced viscosity vs. concentration of MCC (a), rMCC (b), COT (c) and rCOT (d). Linear fits were used to determine intersections with the y-axis, giving intrinsic viscosity values.

Table 1 shows calculated intrinsic viscosities used for molecular weight determination.

Table 1. Intrinsic viscosities of both celluloses and their regenerates determined by the extrapolation method.

Cellulose sample	$[\eta]$ [mL g ⁻¹]
MCC	129.13 ± 2.00
rMCC	96.60 ± 7.60
COT	598.83 ± 14.75
rCOT	453.46 ± 8.10

Fourier-Transform Infrared Spectroscopy

For the PCL/Cellulose samples, phase separation occurred at all blend ratios when precipitated. Figure 2 shows the IR-spectra of the PCL/COT blends.

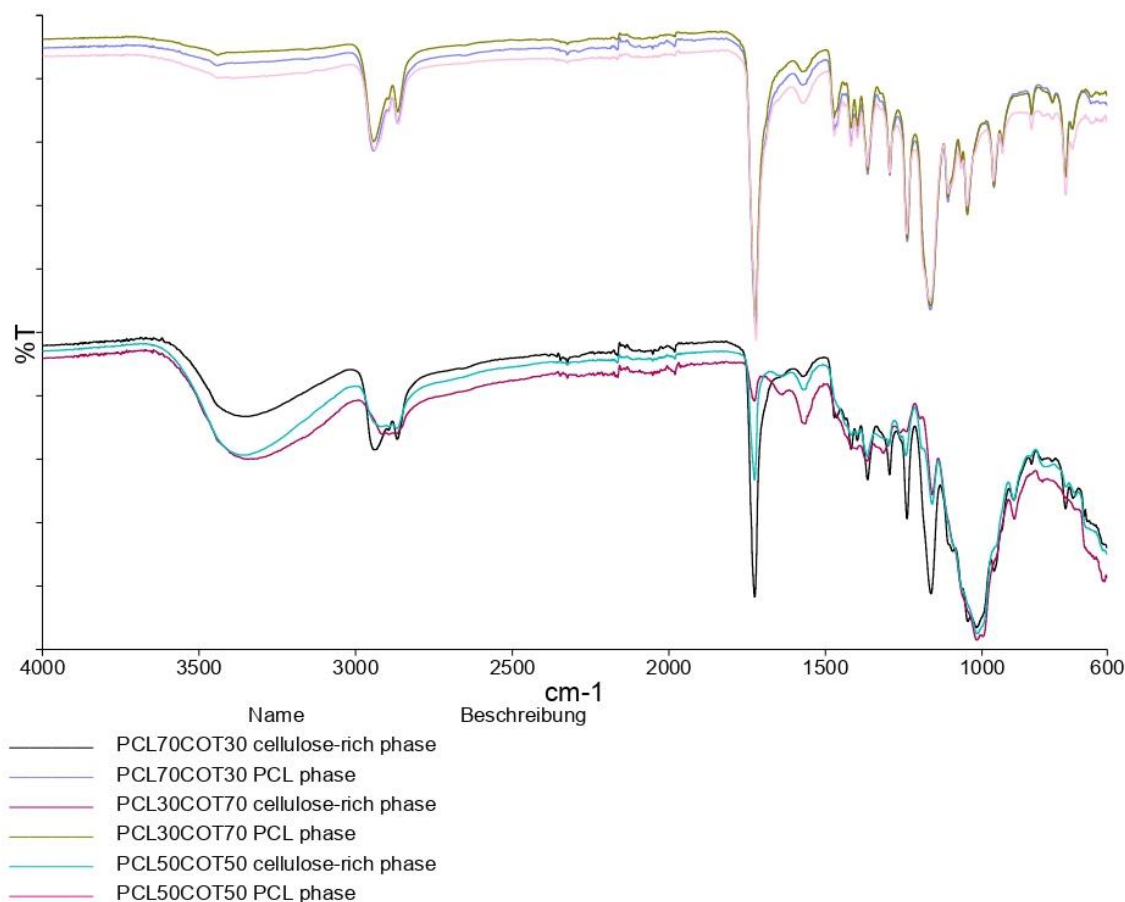


Figure 2. FTIR spectra of separable phases from the PCL/COT samples

Since phase separation occurred during precipitation, both phases were analyzed separately. The transparent phases, which was expected to be PCL, also showed a spectrum where no bands could be assigned to cellulose. Since all spectra for the PCL phase show comparable transmission for all bands, they are expected to be pure PCL. The second phase showed a mixed spectrum of PCL and cellulose, which can clearly be seen at the bands assigned to the cellulose glycosidic bonds at around 850 to 1200 cm⁻¹. When normalized to the cellulose assigned band to C-O stretching of cellulose at around 1015 cm⁻¹, the spectra show different contents of PCL regarding the transmission of the PCL carbonyl band at 1725 cm⁻¹. The signal strength matches the original concentration of the blends.

Size exclusion chromatography

Relative molecular weight measurements were performed using a narrow distributed PMMA standard. Distribution curves for as received polyesters/polyamide (virgin material) and their regenerates from DMSO solutions are shown in Figure 3.

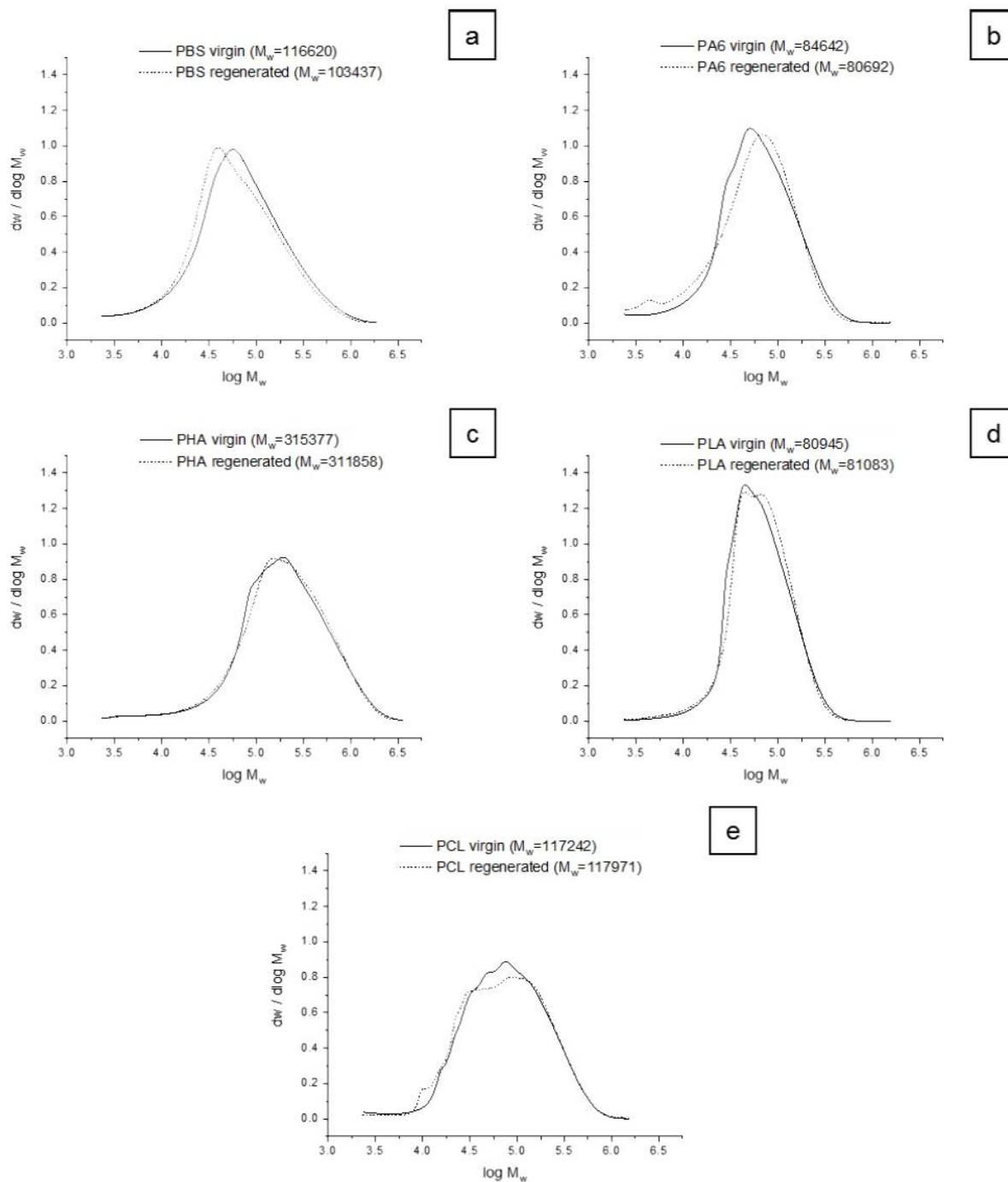


Figure 3. Molecular weight distribution curves for virgin and regenerated polymers. Poly(butylene succinate) (PBS; a), polyamide 6 (PA6; b), poly(hydroxyl alkanooate) (PHA; c), poly(lactic acid) (PLA; d) and poly(caprolactone) (PCL; e).

Microtome Sectioning

When applicable, microtome sections were cut from produced synthetic polymer/cellulose blends. Figure 4 to Figure 7 show additional microscope images. For polyamide/cellulose samples, cuts could be produced with all cellulose types at every concentration.

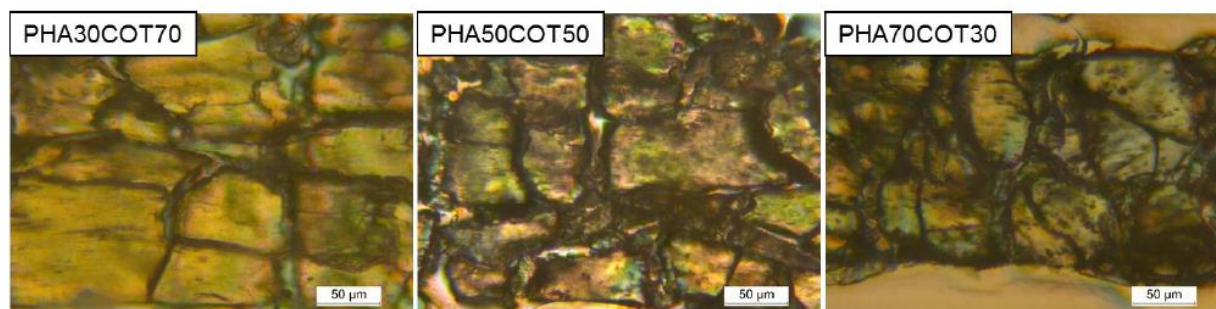


Figure 4. Microscope images of microtome sections from PHA/COT samples.



Figure 5. Microscope images of microtome sections from PLA/COT samples.

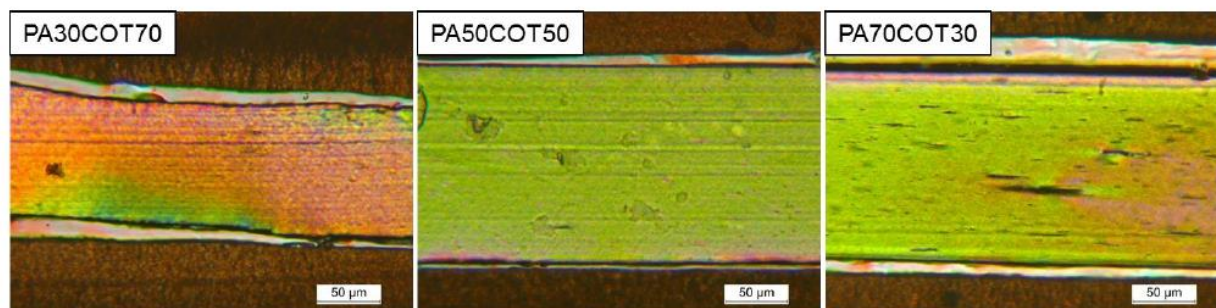


Figure 6. Microscope images of microtome sections from PA/COT samples.

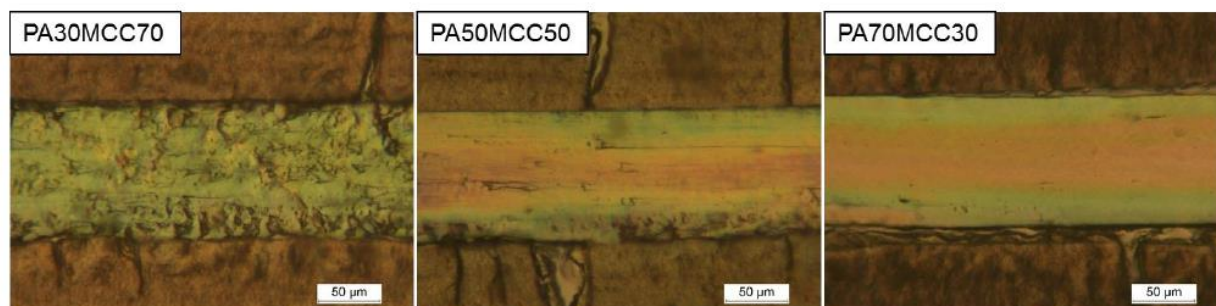


Figure 7. Microscope images of microtome sections from PA/MCC samples.

Scanning electron microscopy

For further investigation of the blend morphology, SEM images of cryo-fractured cross-sections were taken for selected PA/COT and PA/MCC samples (Figure 8).

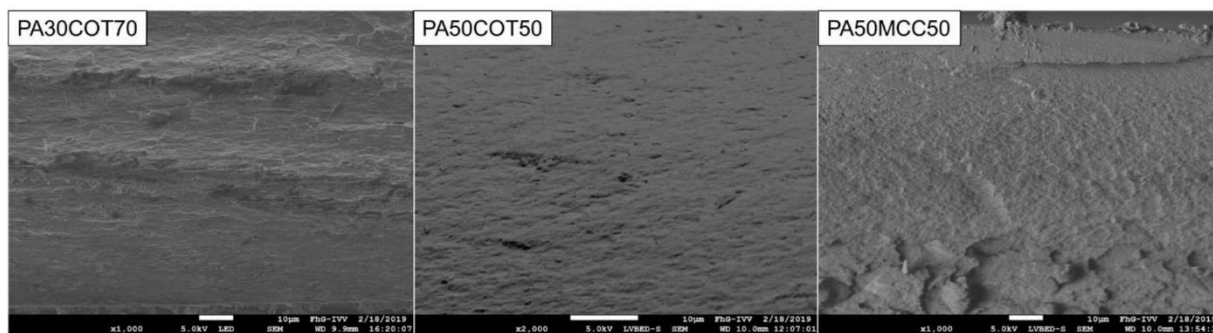


Figure 8. SEM images of cryo-fractured cross-sections of PA/COT and PA/MCC samples.

5 Cellulose blends with polylactic acid or polyamide 6 from solution blending: microstructure and polymer interactions

by Kerstin Müller, Daniel Van Opdenbosch and Cordt Zollfrank¹¹¹

Mater. Today Comm. **2022**, *30*, 103074. <https://doi.org/10.1016/j.mtcomm.2021.103074>

The previous study showed interesting compatibilities of native cellulose with polylactic acid and polyamide that are not yet fully understood. Therefore, a previously presented solvent-based rapid precipitation method was used to prepare blends of cellulose with polylactic acid or polyamide 6 in varying concentrations. The ionic liquid and co-solvent used for cellulose dissolution are removed by precipitation and repeated washing with water or ethanol. Residual ionic liquid contents acts as a plasticizer and compatibilizer in the blends, interacting with both the cellulose and the synthetic polymers. Those effects were negligible at ionic liquid concentrations below 1 wt% compared to higher contents that were connected to glass transition and melting point depression of the polyamide 6.

Binary systems of cellulose and polyamide blends exhibited a two-phase structure with both amorphous and crystalline polyamide domains concluded from thermal and crystallinity analysis. At cellulose concentrations greater than 50%, the melting point depression of the polyamide and the systematic shifts in the infrared spectra suggest polymer interactions between polyamide and cellulose. This is accompanied by a homogeneous phase distribution of small polyamide domains that are not fully oriented and crystallized, in contrast to mixtures with higher polyamide fractions. This morphology is exactly the opposite of conventionally produced composites, where cellulose is always the dispersed phase.

Blends of cellulose and polylactic acid showed a homogeneously mixed phase at all blend ratios. The blend partners interact strongly via hydrogen bonds. Although both cellulose and polylactic acid are in an amorphous state after precipitation of the blend, no glass transition of the polylactic acid can be detected. Furthermore, no unique domains were identified for either blend partner, suggesting that efficient mixing down to the molecular level is possible even if the polymers are probably immiscible from a thermodynamic point of view (compare chapter 2.3.1).

All blends were thermomechanically formable into platelets. To fully investigate the potential to be used in thermoplastic processing, however, blends need to be prepared in a larger scale and possibly with lower solvent levels.

Author contributions: Kerstin Müller developed the design of experiments, the concept for the manuscript and wrote the manuscript. Daniel Van Opdenbosch analyzed and visualized the data from X-ray diffraction experiments and wrote the respective sections of the manuscript. Cordt Zollfrank revised the manuscript.



Contents lists available at ScienceDirect

Materials Today Communications

journal homepage: www.elsevier.com/locate/mtcomm

Cellulose blends with polylactic acid or polyamide 6 from solution blending: Microstructure and polymer interactions

Kerstin Müller^{a,b,*}, Daniel Van Opdenbosch^a, Cordt Zollfrank^a^a Chair for Biogenic Polymers, Technical University of Munich, Campus Straubing for Biotechnology and Sustainability, Schulgasse 16, 94315 Straubing, Germany^b Process Development for Polymer Recycling, Fraunhofer Institute for Process Engineering and Packaging IVV, Giggenhauser Str. 35, 85354 Freising, Germany

ARTICLE INFO

Keywords:

Polymer blends
Cellulose
Polylactic acid
Polyamide 6
Solution blending

ABSTRACT

The use of cellulose in polymer blends is limited due to missing thermoplasticity and incompatibility with most synthetic polymers. In this work, a solvent-based rapid precipitation method was used to overcome these limitations. Blends of cellulose with polylactic acid or polyamide 6 were prepared using a previously presented ionic liquid-based solution-precipitation method. The structural properties of the blends and the specific intermolecular interactions were studied by FTIR, DSC, XRD and SEM. With polylactic acid, cellulose formed single-phase amorphous blends with intense intermolecular hydrogen bonding detected by FTIR. Less pronounced interactions were concluded for polyamide 6 and cellulose from FTIR, DSC and XRD, resulting in a two-phase morphological structure with continuous cellulose and dispersed polyamide 6 domains. Homogeneous blend formation between polylactic acid and cellulose could be promising for further material developments.

1. Introduction

The use of cellulose in technical applications is an ongoing topic in the field of polymer materials science. Material-related properties of native cellulose such as strength, water insolubility at higher degrees of polymerization (DP), biodegradability and availability qualify it as an interesting polymer for a large number of applications [1–4]. To process cellulose without altering its chemical structure, solvent-based processes for films and fibers have been developed and established. Desired solvent-free or dry processes often require thermoplastic behavior of a material, which is not given for cellulose.

This study investigates the incorporation of polymeric spacers between the rigid cellulose chains to induce flexibility and thus facilitate thermomechanical forming processes. To address this issue, favorable polymer chain interactions are a prerequisite. Although there are numerous studies on cellulose dissolution in ionic liquids (IL) [5–10], studies describing the breaking of intermolecular hydrogen bonding within cellulose and other synthetic polymers, followed by blending to form new intermolecular interactions, are rare. Major studies of blending cellulose with synthetic polymers in solution were performed by Manley more than 20 years ago [11]. To the authors' knowledge, comparable approaches using ionic liquids as a solvent can be found by

Xu et al. [12], who mainly address biocompatibility and biodegradability of such blend materials, and by Hameed et al. [13] who were targeting a thermoset material. Therefore, knowledge on comparable materials has been limited to composites and nanocomposites where various forms of cellulose were used as an insoluble filler reinforcement material [14–18]. With regard to the synthesis of materials combining cellulose blends, parallels can be found, especially in nanocomposites. Many synthesis routes are available, with melt compounding, in-situ polymerization and solution/dispersion blending being the most common [19–21]. In the latter, low-viscosity polymer solutions and nanoparticles or nanoparticle dispersions are combined and either precipitated by adding an antisolvent or generated by solvent evaporation [20]. While the difference in the synthesis of the blends presented here is only the combination of two solutions, the final material properties may differ, as both blend partners can interact in solution down to the molecular level.

As mentioned earlier, polylactic acid (PLA) and polyamide 6 (PA) could be promising partners that can interact with cellulose and form homogeneous blend materials [22]. The method used allows combining a PLA or PA solution with a cellulose solution while avoiding material precipitation during mixing. High mixing efficiency can be achieved when blending polymer solutions, especially if the solvents used favor

* Corresponding author at: Process Development for Polymer Recycling, Fraunhofer Institute for Process Engineering and Packaging IVV, Giggenhauser Str. 35, 85354 Freising, Germany.

E-mail address: kerstin.mueller@ivv.fraunhofer.de (K. Müller).

<https://doi.org/10.1016/j.mtcomm.2021.103074>

Received 4 November 2021; Received in revised form 7 December 2021; Accepted 10 December 2021

Available online 14 December 2021

2352-4928/© 2021 Elsevier Ltd. All rights reserved.

the chain entanglement of the polymers.

Due to their morphology, homogeneous blends exhibit a different property profile than conventional matrix-filler composites, which makes their preparation technologically interesting. Although most polymers are thermodynamically immiscible, the use of compatibilizers or rapid precipitation can assist to produce homogeneous blends. As shown in the example of polymer blend precipitation from supercritical fluids, rapid removal of a solvent may lead to homogeneous blend morphologies that are not present for precipitation with lower velocity [23]. If the time scale for precipitation is significantly shorter than the time scale for phase separation to occur by polymer diffusion, precipitation of a single-phase solution could lead to a single-phase mixture of solid polymers. Another possibility to obtain homogeneous blends is metastable micromorphologies in the solid blend. Hence, the microscale domains of each polymer are homogeneously distributed, even if the blend partners are immiscible [23,24].

Following the idea to produce homogeneous blends that are applicable in thermoplastic forming processes, different blend ratios were produced and tested for their compatibility by means of polymer-polymer interactions. When using imidazolium-based ionic liquids in cellulose processing, the solvent is usually removed via extraction. Any residual content in the polymer blend may have a decisive influence on the material properties. At high IL ratios, direct thermal processing of cellulose is possible [25–29]. Cellulose gels containing between 30 wt% and 60 wt% imidazolium-based IL showed glass transition temperatures from 7 °C to –17 °C [30]. Even IL contents below 5 wt% were found to influence the thermal properties of cellulose regenerates [31]. Although there are numerous publications on regenerated cellulose from ILs [32–40], the topic of minor IL residues and their influences on material properties is rarely covered [31,41].

In this work, prepared blends were prepared from cellulose and PA or PLA, which were thermomechanically formed to platelets. The structural and thermal properties were assessed by SEM, XRD, FTIR and DSC. In order to distinguish between the effects of the blend configuration itself and the residual IL, this study also examines samples with different residual IL contents.

2. Experimental section

Microcrystalline cellulose (MCC) Parmcel 101 from wood pulp was purchased from Gustav Parmentier (Steinfurt, Germany) with a DP of 310. PLA Ingeo™ 3251D was purchased from NatureWorks (Minnetonka, MN, USA) with a molecular weight of 80 kg mol⁻¹, a D-isomer percentage of 1.2 and an acid value (mmol(COOH) kg⁻¹) of 41 (manufacturer information). The PA used was Ultramid® B40L from BASF (Ludwigshafen, Germany) with a molecular weight of 80 kg mol⁻¹. 1-ethyl-3-methylimidazolium acetate (EmimAc; purity ≥98%) and dimethylsulfoxide (DMSO; purity ≥99.5%) were received from proionic (Raaba-Grambach, Austria) and Merck (Darmstadt, Germany). MCC, PLA and PA were dried at 60 °C for at least 12 h prior to processing.

MCC samples were dissolved in a mixture of EmimAc and DMSO (1:1 by weight) at 60 °C and stirring at 150 rpm for at least two hours. To have a diluted regime but also a high cellulose concentration, the concentration for these trials was set at 2.5 wt% based on critical concentration determination (~2.6 wt% MCC at 25 °C, Fig. S1). Dissolution was judged visually by the clarity of the solutions. PLA and PA were each dissolved in DMSO with a concentration of 2.5 wt% at 90 °C and 150 °C, respectively. The polymer solutions were mixed in their respective weight ratios (PLA or PA with mass fractions of cellulose from 0.1 to 0.9 in steps of 0.1) at 90 °C and 150 rpm for one hour and subsequently cast on glass Petri dishes. Gel films were immediately precipitated with an excess of deionized water at 60 °C. Due to insufficient precipitation in water by means of material recovery via solid/liquid separation, the PLA/MCC samples were precipitated and washed in ethanol (EtOH) at room temperature. Three washing steps with an amount of approximately the five-fold mass of non-solvent relative to the cast blend

solution were performed to remove residual DMSO and EmimAc. Residual ionic liquid (RIL) was determined via dry mass measurement (analytical scale, readability 0.1 mg) of the extract from the respective washing steps: The extracts were weighed, dried in a vacuum cabinet at 90 °C and 10 mbar for five hours (to ensure evaporation of water/ethanol and DMSO) and reweighed. Final films were also dried in a vacuum drying cabinet at 90 °C and 10 mbar for five hours and stored in a desiccator at 23 °C before further characterization. Zero samples (mass fractions of cellulose of 0 and 1) were prepared analogously to the blend samples. To investigate the thermomechanical deformability of the materials, plates were produced using a heatable hydraulic press (Perkin Elmer, Shelton, CT, USA) at a temperature of 190 °C for 2 min with a load of 3 tons.

Film morphology was examined by means of scanning electron microscopy (SEM). Pieces of the pressed plates were cryo-fractured to investigate the fracture surface. Cryo-fracturing creates coarse surfaces, prohibiting differentiation between the constituent phases. A complicating factor is that the blend partners are quite similar in their chemical composition and therefore no material differences can be detected on the basis of an SEM image. To determine the blend morphology in this work, one fracture side was treated with 1,1,1,3,3,3-hexafluoro-2-propanol (HFIP) to etch its surface by partially dissolution of PLA and PA. Samples from both sides were air-dried for a minimum of 48 h to evaporate residual HFIP and sputtered with gold. Prepared samples were examined with a JEOL 7200 F scanning electron microscope with a lower electron detector (JEOL, Freising, Germany). Images were taken at an accelerating voltage of 1.0 kV.

Differential scanning calorimetry (DSC) was used to determine thermal properties by means of specific enthalpy of melting h_{fus} , glass transition temperature T_g and melting temperature T_m . The T_g was set at half height of the transition. The peak area (linear baseline) assigned to polymer melting was used to calculate h_{fus} by division through the total sample weight; T_m was set by the peak maximum. DSC was performed on a TA Instruments DSC Q2000 (New Castle, DE, USA) and the corresponding evaluation software TA Universal Analysis 2000 Version 4.3 A. Two heating runs were performed from –80–200 °C (PA: 260 °C) with a heating/cooling rate of 15 K min⁻¹ on 10–15 mg of each sample. The second heating run was used to determine h_{fus} , T_g and T_m .

Fourier transform infrared (FTIR) spectroscopy can be used to study intermolecular interactions and especially hydrogen bonding in polymer blends [42]. The formation of a hydrogen bond may lead to a red shift of the X–H stretching vibrations of the proton donor [43,44]. Assuming the classical electrostatic model of hydrogen bonding, the electron density of the proton acceptor has an attractive force on the proton, and the donor-acceptor approach should always extend the X–H bond of the donor [45]. Taking into account that in the following, a significant transfer of charge from the proton acceptor to the proton donor takes place, the X–H bond should also be weakened and simultaneously lengthened during the formation of the hydrogen bond [46]. This stretching of the X–H bond leads to a decrease in the frequency of the X–H stretching oscillation. Hydrogen bonding involved bands were therefore investigated for shifts with respect to blend composition. Spectra were recorded with a Frontier™ FTIR spectrometer L1280034, using the software Spectrum IR, Version 10.6.1, both supplied by Perkin Elmer (Shelton, CT, USA). Measurements were performed at ambient temperature and pressure. An attenuated total reflectance device with a germanium crystal was utilized (Perkin Elmer, Shelton, CT, USA). A constant contact pressure was achieved by tightening the securing screw with a ratchet, which is limited to a torque of 30 cNm. 16 scans were recorded within a wavenumber range from 4000 to 600 cm⁻¹ with a resolution of 4 cm⁻¹.

X-ray diffraction (XRD) was performed on a Rigaku (Tokyo, Japan) MiniFlex 600 diffractometer with Cu-K α radiation. Diffractograms were refined by BGMN [47], using the Profex interface. The machine line function was verified by prior refinement of NIST standards 640e and 660c (silicon and lanthanum hexaboride for peak shapes and positions).

The scattering angle range $5^\circ < 2\theta < 55^\circ$ was considered, and the sample offset from the goniometer axis refined. The background was modeled as the sum of a polynomial with 10 coefficients and two amorphous peaks to account for the scattering from paracrystalline ('smectic') domains (for more details, see supporting information) [48,49]. The applied crystal structures of cellulose I α (for the raw materials, in the following referred to as 'cellulose I') and II polymorphs were taken from French [50], of PA α from Holmes et. al [51], and of PLA α from Wasanasuk et. al. [52]. The lattice parameters were refined within limits of 1% for the cellulose polymorphs, 2% for PLA and 3% for PA. The averaged crystallite sizes L were refined anisotropically for cellulose I and PLA, and isotropically for cellulose II and PA. For all phases, microstrain was refined isotropically. Preferred orientation was allowed for cellulose I α via the spherical harmonic function Y20 (unidirectional, in BGMN: SPHAR2) and for PA and PLA via the function Y40 (bidirectional, SPHAR4) [53,54], yielding directional weighting factors ϕ . The fractions of crystallinity (f_c) of the respective blending partners were determined from the measured and refined phase data by the method of Ruland and Vonk, using the Rietveld-refined Bragg-peak intensities [55, 56]. A measurement-dependent floating lower scattering vector boundary s_p was applied, according to the recommendation that in the curve-fitting procedure, a lower limit must be set to s_p^2 which is preferably taken higher than the s^2 value corresponding to the second crystalline peak in the diagram [56]. The method also returns the overall disorder parameter k , which accounts for the attenuation of intensities from the Bragg reflexes into the background due to the thermal vibrational disorder, as well as the structural disorder of the first and second kinds [55–57]. Its accuracy was confirmed by the value determined for the cellulose I phase in the MCC educt of $k = 6.10 \pm 0.06 \text{ \AA}^2$ [57]. However, refining its structural disorder components, also leading to angular reflex broadening $\beta(2\theta)$, was not feasible: While reflexes were visible up to $2\theta = 50^\circ$, and sufficiently intense for determining their position (as noted in the following), $\beta(2\theta)$ could not be consistently determined. Fig. S6 shows the unfolding of diffractograms in the example of processed PA, MCC and their blend.

3. Results

3.1. DSC. PA/MCC

Thermal properties h_{fus} , T_m , T_g and RIL for PA/MCC blends at different washing steps over the fractions of cellulose f_{cell} are given in Fig. 1.

The residual solvent changes the thermal properties of the PA/MCC blends. At high PA concentrations, PA melting enthalpies as well as T_g decrease with increasing residual solvent. Also, the T_m of the initial PA polymer decreases a lot with increasing IL content, while for the second and third washing step (RIL approx. ≤ 1.5 wt%), only slight differences are detected. For the samples after the third washing step, thermal properties of the PA (T_g , T_m , H_{fus}) hardly changed. Starting from $f_{\text{cell}} = 0.5$, a systematic melting point depression with increasing f_{cell} was observed, also present in the samples from WS2 with RIL < 1 wt%. The calculated h_{fus} for the blends are slightly lower than the theoretical specific enthalpies (Fig. 1, h_{fus} , dashed line) with processed PA ($f_{\text{cell}} = 0$) as reference. However, the absolute values are significantly lower than expected from the actual f_c of the educt. The measurement of the PA's glass transition remains difficult via DSC, especially for low PA contents. Besides the plasticizing effect, which can be attributed to RIL ≥ 1 wt% and is accompanied by a lowering of the T_g , no influence in dependence of f_{cell} on the T_g could be detected (DSC thermograms see Fig. S2a–c).

PLA/MCC. Although for the pure PLA sample ($f_{\text{cell}} = 0$) the T_g was clearly visible, no transition could be detected for all PLA/MCC blend samples. Fig. 2 summarizes the thermal properties as well as the respective RIL for the PLA/MCC blend series.

Only few blend ratios with higher PLA contents showed melting or crystallization. Comparing the specific enthalpies of melting, PLA

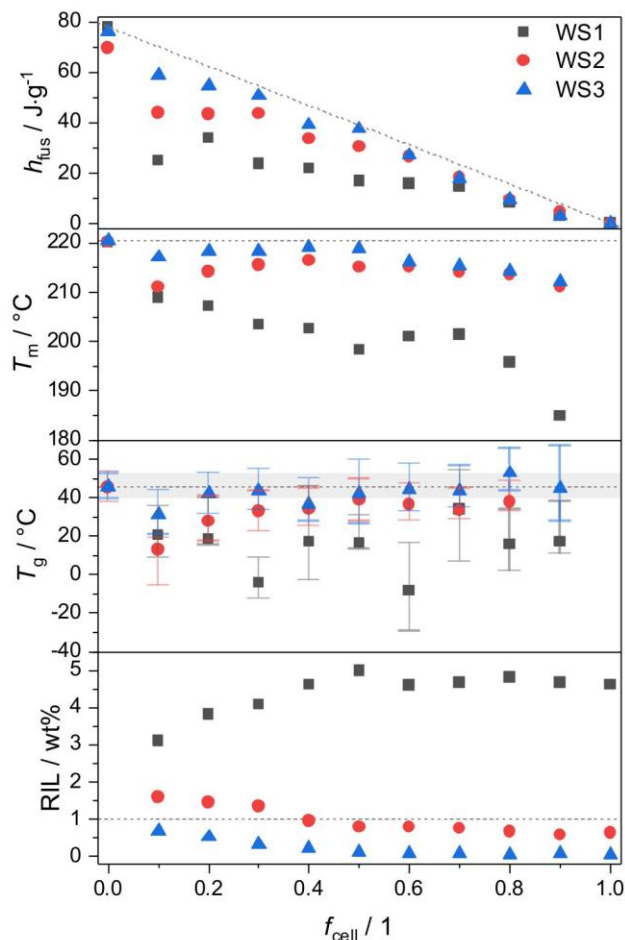


Fig. 1. h_{fus} , T_m , T_g and residual ionic liquid content for PA/MCC blends at different washing steps WS1, WS2 and WS3. T_g bars represent the transition range from onset to endset. Reference lines show theoretical specific enthalpy of melting proportionally decreasing with increasing f_{cell} ; T_m and T_g of the pure PA component ($f_{\text{cell}} = 0$) and a RIL of 1 wt%.

crystallinity was drastically reduced already at $f_{\text{cell}} = 0.1$. For all samples that showed crystalline phases, cold crystallization occurred in the 2nd heating run. When comparing the different washing steps (relating to different amounts of residual IL), the number of samples revealing crystalline PLA phases differed. At WS2, melting enthalpies were significantly detectable for all samples with $f_{\text{cell}} \leq 0.2$, for WS3 at $f_{\text{cell}} \leq 0.4$ (for the DSC thermograms, see Fig. S2d–e). Melting points that could be measured at high PLA ratios clearly decreased with increasing f_{cell} , even at RIL ≤ 1 wt%.

3.2. FTIR. PA/MCC

In the PA polymer, several groups are involved in hydrogen bonding that cause characteristic infrared absorption spectra. These include the amide I and amide II bands with main absorption at 1635 cm^{-1} and 1538 cm^{-1} , respectively, as well as hydrogen bonded N–H stretching at 3295 cm^{-1} [58]. A small but consistent blue shift of the amide I band, ascribed to C=O stretching [59,60], was observed for all blend samples. Comparing the different washing steps, the blue shift is more intense for samples with the higher RIL. For the sample set containing the lowest RIL (WS3), only a slight blue shift occurred for samples with $f_{\text{cell}} \geq 0.5$ (Fig. S4(b)). A similar behavior was observed for the amide II band (main contribution: C–N stretch + C(O)–N–H bend [59,60], see Fig. S4 (c)) for the sample set with the lowest RIL. A slight blue shift for

K. Müller et al.

Materials Today Communications 30 (2022) 103074

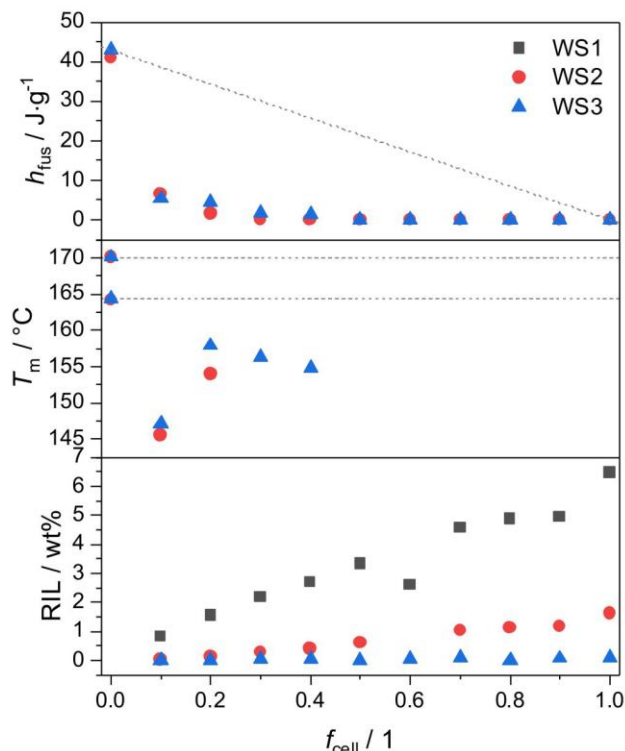


Fig. 2. h_{fus} , T_m , and residual ionic liquid content for PLA/MCC blends at different washing steps WS1, WS2 and WS3. Reference lines show theoretical specific enthalpy of melting proportionally decreasing with increasing f_{cell} and T_m of the pure PLA component ($f_{\text{cell}}=0$, double peak).

$f_{\text{cell}} \geq 0.5$ was observed. An f_{cell} of only 0.1 already caused a blue shift of 5 cm^{-1} . N—H stretching bands showed slight differences between the sample sets regarding RIL. The NH-stretching band shifts associated with

the washing steps are not systematically correlated to f_{cell} (Fig. S4(a)). For additional visualization, the second derivative spectra of the PA/MCC blends after the third washing step are presented in Fig. S5.

3.3. PLA/MCC

The carbonyl group is one of the main functional groups involved in hydrogen bonding regarding the PLA polymer. The band assigned to C=O stretching occurs at 1756 cm^{-1} for pure PLA [61]. The band shifts systematically to lower wavenumbers with cellulose concentration, Fig. 3(b). At $f_{\text{cell}} = 0.8$, the carbonyl signal appeared at 1735 cm^{-1} . The OH-stretching of the cellulose hydroxyl groups show a slight blue shift for $f_{\text{cell}} \leq 0.4$, Fig. 3(a). Spectra over the whole wavelength range can be found in Fig. S3.

The so-called amorphous band of the cellulose (ascribed to $\nu(\text{C-O-C})$ [62,63]) can also be involved in hydrogen bonding. The band fluctuates around 897 cm^{-1} and started to shift to higher wavenumbers systematically with a PLA concentration starting at $f_{\text{cell}} \leq 0.6$ (shift to 902 cm^{-1} at $f_{\text{cell}} = 0.1$, Fig. S6). This behavior was similar for both WS3 and WS2.

3.4. XRD

Diffraction patterns for the blend materials were recorded from the hot-pressed films for all samples from the third washing step. The original MCC powder showed a cellulose I type structure. After regeneration, the crystallinity decreased and only the cellulose II polymorphs were found. While polymer blends of PA/MCC showed mixed diffraction patterns with reflexes from both blend partners, Fig. 4(a), PLA/MCC blends, showed mainly one or two broad amorphous reflexes, Fig. 4(b).

3.5. PA/MCC

In Fig. 5, f_c are plotted over the fractions of cellulose f_{cell} by mass. The values for the unprocessed educts are plotted outside the compositional range $0 \leq f_{\text{cell}} \leq 1$. The unprocessed PA granulates had $f_c = 0.45 \pm 0.04$. These agreed with some values reported in the literature [64,65], but higher than others [66], the reported values themselves varying with

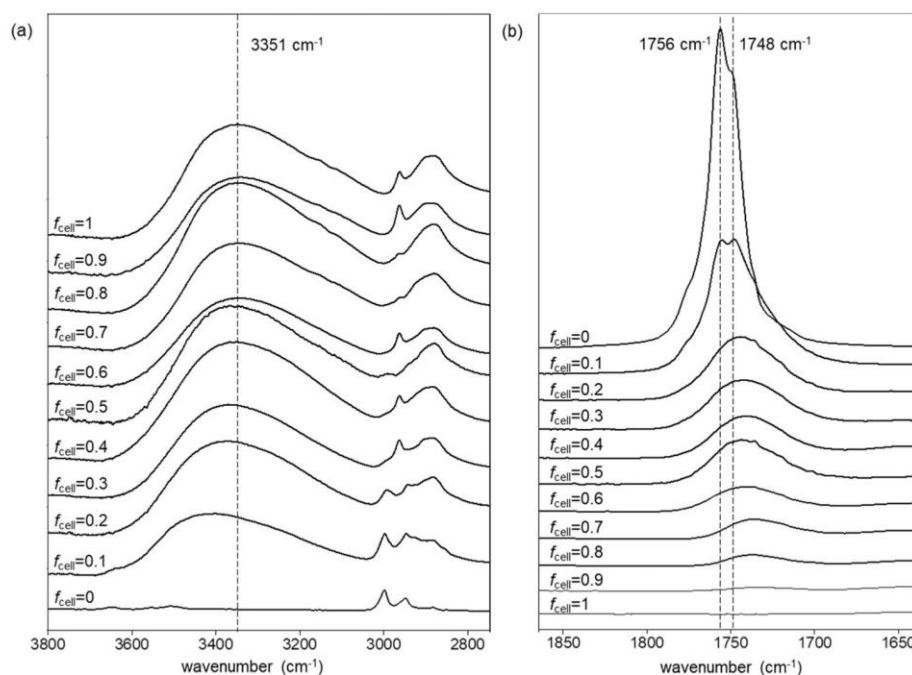


Fig. 3. FTIR spectra of PLA/MCC blend samples as well as precipitated MCC ($f_{\text{cell}}=1$) and PLA ($f_{\text{cell}}=0$) from the third washing step. Wavenumber regions for (a) OH-stretching and (b) carbonyl bands are shown.

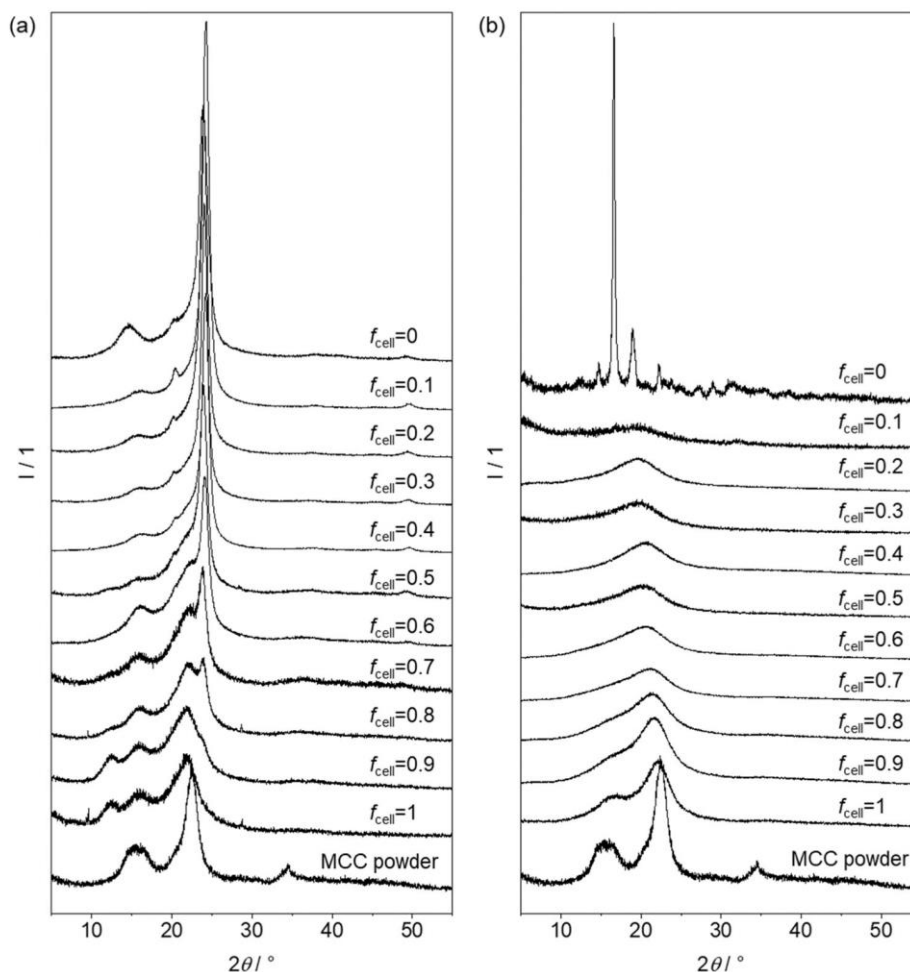


Fig. 4. Diffraction patterns of MCC powder and (a) PA/MCC blends and (b) PLA/MCC blends from WS3.

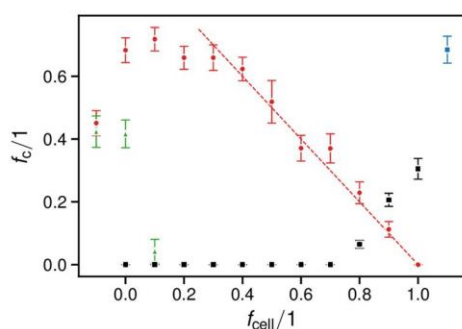


Fig. 5. Fractions of crystalline phases for the PA/MCC blends: PA α (red circles) and cellulose II (black squares), and for the PLA/MCC blends: PLA α (green upward triangles) and cellulose II (none at all) as a function of cellulose content by mass. The data points outside of the interval $0 \leq f_{\text{cell}} \leq 1$ signify the PA, PLA and cellulose I (blue squares) crystallinities of the educt granulates and MCC powder. The red dashed line marks a section of the function $f_c = 1 - f_{\text{cell}}$.

annealing time. Similarly, the crystallinities of PLA reported in the literature depend on their respective thermal histories [67,68]. The value $f_c = 0.42 \pm 0.05$ determined for the unprocessed PLA granulate in this work is within the range reported for non-annealed materials. In case of the MCC powder, values determined by the method of Hermans et al. [69] were similar, yet lower by up to 5% than the value of f_c

$= 0.68 \pm 0.04$ determined in this work. Since this method does not extrapolate over the disorder-attenuated intensities, it is likely to underestimate crystallinities.

Within the range $0 \leq f_{\text{cell}} \leq 1$ for the processed PA/MCC blends, the fractions of PA α started from $f_c = 0.68 \pm 0.04$ at $f_{\text{cell}} = 0$, which gradually decreased to 0 for $f_{\text{cell}} = 1$. Notably, above $f_{\text{cell}} = 0.3$, the fractions of PA α conform to the function $f_c = 1 - f_{\text{cell}}$, indicating a complete crystallization of the contained PA, since $f_{\text{PA}} = 1 - f_{\text{cell}}$. On the other hand, the fractions of cellulose II remained low, compared to the crystallinity determined for the MCC powder educt, with a final value of $f_c = 0.31 \pm 0.03$ for the pure MCC regenerate.

The averaged crystallite sizes L for the PA α phase in blends with cellulose contents $0 \leq f_{\text{cell}} \leq 0.5$ remained steady around 13 nm, similar to the value determined for the granulate educt, Fig. 6. Intriguingly, for the processed pure PA, considerably smaller $L = 7.4 \pm 0.2$ nm were found. Above $f_{\text{cell}} = 0.5$, the L decreased linearly to a final value of 5.1 ± 0.3 nm at $f_{\text{cell}} = 0.9$.

In PA α , the disorder parameters assumed values of $5.5 \text{ \AA}^2 \lesssim k \lesssim 8.4 \text{ \AA}^2$ for the granulate educts and for $0.5 \leq f_{\text{cell}} \leq 0.9$, Fig. 6. They were noticeably reduced to $2.4 \text{ \AA}^2 \lesssim k \lesssim 3.8 \text{ \AA}^2$ in processed blends with $f_{\text{cell}} < 0.5$, and to $k = 0.85 \pm 0.03 \text{ \AA}^2$ for $f_{\text{cell}} = 0.9$.

The PA/MCC blends were strongly textured, as exemplified by the high-intensity (202) reflex at $2\theta = 24^\circ$, Fig. 4(a, b). In Holmes et al.'s model of Nylon 6, the chains run along the direction [010], normal to the planes (010) [51]. Hence, large intensities from planes $\{h0l\}$ indicates a preferred orientation of the chains within the sample plane.

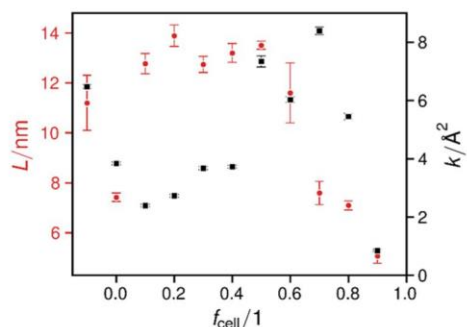


Fig. 6. Average crystallite sizes and disorder parameters (black squares) for PA α (red circles) as a function of cellulose content by mass. The data below 0 signifies the PA educt granulates.

The directional weighting parameters ϕ , as obtained from the spherical harmonic correction function [53,54], were normalized to a sum of 1.

Fig. 7 differentiates between the crystallographic directions parallel and perpendicular to the molecular chains. Here, $\phi = 0$ indicates an orientation exclusively within the sample plane and $\phi = 1$ exclusively out of plane. Values of $\phi = 0.33$ for the parallel direction, together with $\phi = 0.67$ for the sum of the two perpendicular directions, indicate no preferred orientation. The large error bars for the perpendicular directions and $0.5 < f_{\text{cell}}$ are carried over from the two individual directions and reflect the uncertainty of the assignment of weights to either $\{h00\}$ or $\{00l\}$. With the exception of $f_{\text{cell}} = 0$, the values for texture are indicative of randomized orientations for $f_{\text{cell}} < 0.5$. For $0.5 \leq f_{\text{cell}}$, however, the molecular long axes are uniformly oriented within the plane of the processed material sheets.

It was found that the densities ρ_c of the PA α phase showed a remarkably clear progression with f_{cell} , Fig. 8. Since the considered diffraction angles included the sufficiently intense (404) and {414} reflexes at $49^\circ < \theta < 50^\circ$, the values of ρ_c are considered reliable. They are further supported by the agreement of the value for the educt granulate with that for the 'regular lamellae model' by Li et al. of $\rho_c = 1.18 \pm 0.02 \text{ g cm}^{-3}$ [70].

3.6. PLA/MCC

For the processed PLA/MCC blends, no cellulose II was determined. Hence, all black markers in Fig. 5 refer to the contents in the PA/MCC blends. The contents of PLA α rapidly decreased to 0 from a starting value of $f_c = 0.42 \pm 0.04$. This is a remarkably different behavior than the one observed in the PA/MCC blends.

In case of the PLA α phase in the respective blends, the crystallite sizes could be determined anisotropically, Fig. 9. Here, as expected from polymers forming chain-fold crystallites, their sizes along the chain

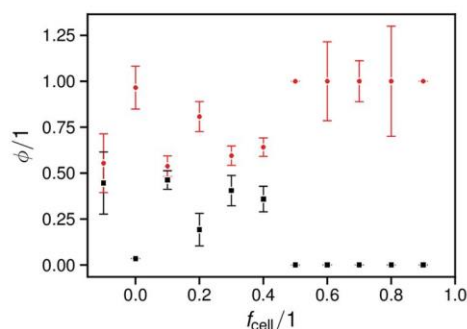


Fig. 7. Crystallographic in-plane texture for PA in directions parallel (black squares) and perpendicular (red circles) to the chain directions as a function of cellulose content by mass. The data below 0 signifies the PA educt granulates.

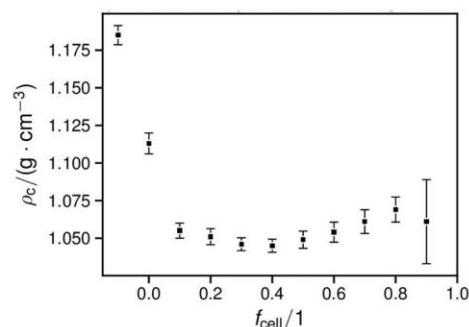


Fig. 8. Density of crystalline PA as a function of cellulose content by mass. The data below 0 signifies the PA educt granulates.

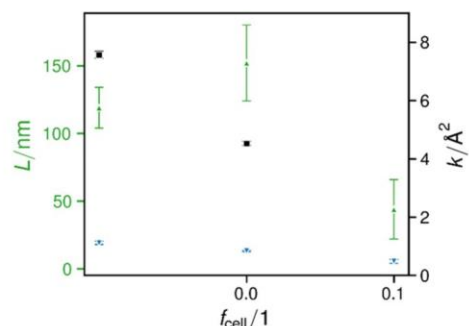


Fig. 9. Average crystallite sizes and disorder parameters (black squares) for PLA α (green upward triangles) as a function of cellulose content by mass. The crystallite sizes along the chain directions, i.e. between folds, are marked by blue downward triangles. The data below 0 signifies the PLA educt granulates.

directions are limited to the characteristic inter-fold distance. This distance was determined to be, on average, $L = 19.2 \pm 1.2$ for the educt granules, $L = 13.2 \pm 0.5$ for the processed pure PLA and $L = 5.5 \pm 1.5$ for the blend with $f_{\text{cell}} = 0.1$. The former correspond roughly to values from the literature [71], while the latter is considered unreliable, due to the small amount of refineable Bragg-diffracted intensities. The green markers in Fig. 9 show the crystallite sizes perpendicular to the chain directions. They are notably larger than the average sizes of PA α , supporting the formation of extended chain-fold crystallites.

The disorder parameters determined for PLA α declined from $k = 7.57 \pm 0.12 \text{ \AA}^2$ for the educt granulates over $k = 4.53 \pm 0.07 \text{ \AA}^2$ for the processed pure PLA. For the composition with $f_{\text{cell}} = 0.1$, the value could not be determined.

3.7. SEM

In general, cryo-fractioning of the PA/MCC blends resulted in a more uniform, coarse structure than the PLA/MCC blends, Fig. 10. With the latter, the fracture surface appears much rougher and more uneven. PA and their blends are much stiffer and also had a higher film thickness, which facilitated sample preparation. During HFIP treatment, the PA/MCC film swelled and turned from transparent to opaque, while the PLA/MCC blend remained its original transparency.

Large PA domains of the structure were removed by etching, leaving either voids from the before dispersed PA domains or layered structures of the non-dissolvable cellulose phase (Fig. 10a–c, Fig. S8). While at higher PA phase ratios ($f_{\text{cell}} = 0.3$, Fig. S8), large oblong PA domains, oriented in press direction, were removed by etching, lower ratios ($f_{\text{cell}} = 0.7$, Fig. S8) revealed finely dispersed spherical PA domains with diameters ranging from a few micrometers to approximately 100 nm. At both $f_{\text{cell}} = 0.7$ and $f_{\text{cell}} = 0.5$ blends, the cellulose formed a continuous

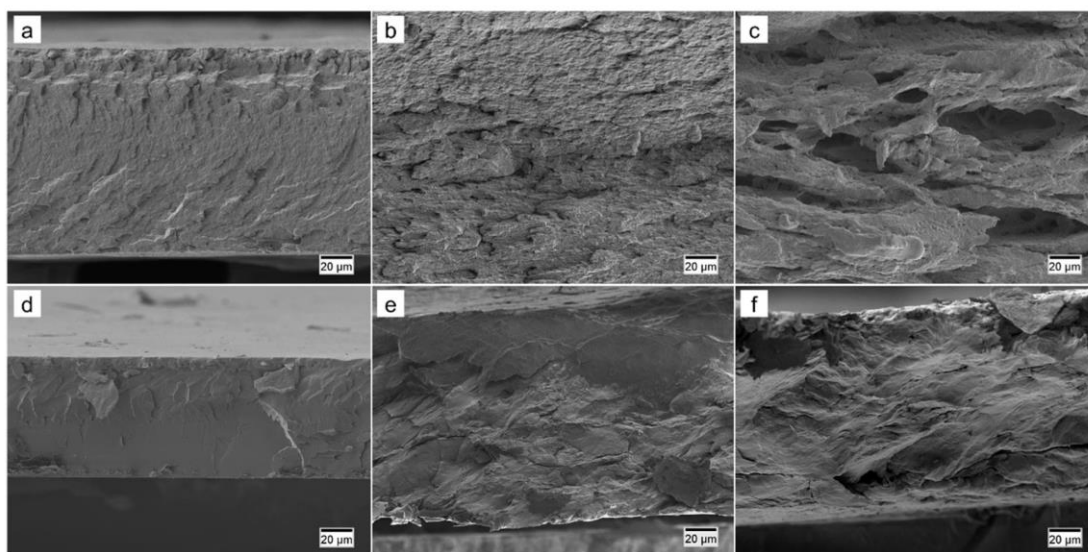


Fig. 10. SEM images of cryo-fractured cross sections of PA press film (a), PA/MCC blend ($f_{\text{cell}}=0.5$) press film (b), etched PA/MCC blend ($f_{\text{cell}}=0.5$) press film (c), PLA press film (d), PLA/MCC blend ($f_{\text{cell}}=0.5$) press film (e) and etched PLA/MCC blend ($f_{\text{cell}}=0.5$) press film (f).

phase, while PA domains were homogeneously dispersed, albeit with different domain sizes. At $f_{\text{cell}} = 0.3$, a more lamellar structure was developed.

Etched PLA/MCC blends showed little difference from the morphology of the untreated blends (Fig. 10c–f, Fig. S9). No separate domains are visible. The etched surface, however, appears smoother for all samples.

4. Discussion

4.1. Precipitation and residual ionic liquid

Although in earlier studies PLA/MCC blend samples of distinct f_{cell} were produced using water as precipitant [22], complete precipitation in water was not achieved over the whole composition range in this study. Especially for samples with $f_{\text{cell}} < 0.5$, no solid/liquid separation of the precipitant was possible in quantities that would have enabled further processing and analytics. Ethanol, which is also widely applied as an anti-solvent for cellulose – IL solutions, was found to be a more suitable precipitant for the investigated PLA/MCC samples.

Generally, the choice of anti-solvent can be crucial not only for successful precipitation itself, but also for altering the final material properties. This was also visible when comparing the pure MCC samples from two sample sets, which were regenerated in water (PA/MCC series) and ethanol (PLA/MCC series). While in water, the cellulose domains rearranged into crystalline cellulose II; in ethanol, the sample showed only amorphous reflexes not attributable to cellulose II (see: Comments on background function; Supporting information). This applies not only to $f_{\text{cell}} = 1$, but to the whole composition range (Fig. 4, Fig. 5). In general, the addition of water results in a faster regeneration of the cellulose [40]. During precipitation, both anti-solvents compete with the cellulose hydroxyl groups for the acetate anion [72], while selectivity is based on the scale of acidity and basicity of the solvents. For cellulose solutions in EmimAc/DMSO, half as much ethanol as water on a molar basis is required to induce coagulation [73]. Faster precipitation in water is accompanied by preferred intramolecular hydrogen bonding of the cellulose. Rearrangements in crystalline structures are therefore more likely in water-precipitated samples and explain the absence of cellulose II in samples precipitated with ethanol.

Due to the chemical composition of the IL EmimAc used, direct determination of residual solvent is challenging. Many studies reveal the

absence of IL in washed samples via FTIR (no IL assigned bands visible), although in the authors' experience the absence of FTIR signals can still be associated with IL levels as high as 3 wt%. Also, extraction methods can never reach a zero level based on an equilibrium distribution of the IL between sample and extract according to Nernst's distribution law. In this study, residual solvent was checked by means of the dry matter of the washing water, based on the fact that the IL does not evaporate, but anti- and co-solvents do. This method assumes a partition coefficient of 1 for both ethanol and water. Based on previous trials, three successive washing steps were performed targeting a residual solvent content (RIL) below 1 wt%. Naturally, a higher cellulose content implies a higher IL content, therefore, the RIL varies within the sample sets (Table S1).

4.2. Influence on thermal and structural properties by RIL

To investigate the thermal properties of the PA/MCC blends, only the second heating cycles of the DSC were considered for better comparability between the sample sets and to clearly determine the glass transition without overlapping with moisture evaporation in the first heating cycle. It should be noted that some decomposition of the IL may have already occurred after the first heating (onset of decomposition at 221 °C [74]), affecting the actual RIL content during the second heating. Nevertheless, clear trends were observed regarding a decrease of h_{fus} , T_{m} and T_{g} with increasing RIL. This implies that the IL molecules not only interact with the PA in amorphous phase, thereby increasing chain mobility, but also prevent crystal growth. Similar interactions were examined at ionic liquid/polyamide 6.10 blends, where it was found that chain segment mobility is enhanced and that structural defects increase with increasing ionic liquid content in the blends [75]. Tian et al. made comparable observations when mixing 1-butyl-3-methylimidazolium chloride with PA powder prior to extrusion. At higher IL loadings, the dilution effect as well as the plasticizing effect are more prominent. Similar results were found by Zheng et al. [76] While only slight changes in the melting point and crystallization enthalpy were observed up to 1 wt% 1-vinyl-3-butyl imidazole chloride in PA, a drastic decrease of both thermodynamic parameters for the samples containing 2–8 wt% IL was present [76]. It is suggested that the IL disrupts the hydrogen bonds between the PA molecules, forming new hydrogen bonds between the IL anion and the N–H group [77]. Interactions between RIL and the polymers were also detected via FTIR. Regarding the amide bands assigned to the PA, blue shifts were more intense with

higher RIL contents. This would underline the theory of hydrogen bond formation between the IL anion and the N-H groups, as this simultaneously weakens the interactions between the C=O and N-H groups of the PA, resulting in a shortening of the C=O bond accompanied by a shift to higher wavenumbers. However, especially at high RIL contents, three components are present, all of which may be involved in hydrogen bonding. Therefore, the interactions cannot be clearly attributed to binary systems. Similar interaction between IL and PLA apply for the PLA/MCC blends, where crystallization was decreased or even prevented at $f_{\text{cell}} \leq 0.4$. Possible polymer chain segment alignment during precipitation is therefore interrupted by RIL. Unfortunately, FTIR signals in the hydrogen bonding assigned regions of the polymers overlap with RIL signals especially at high contents (WS1), which does not allow further evaluation of hydrogen bond interactions.

4.3. Phase morphology, microstructure and polymer interactions

Based on negligible effects by RIL at WS3, only samples from this washing step are considered to discuss blend properties and polymer interactions between the blend partners.

4.4. PA/MCC

SEM investigations of the fractured and etched blend surfaces of PA/MCC blends showed a two-phased morphology for all samples, with MCC presenting the continuous and PA presenting the dispersed phase. The differences in size of the etched PA domains in relation to the PA contents are in line with the crystallite sizes, which were also reduced at $f_{\text{cell}} = 0.7$ compared to $f_{\text{cell}} = 0.3$.

After thermomechanic processing, the crystallinity of PA was increased compared to the values derived from the measured melting enthalpies. For PA, the h_{fus} , determined during the second heating cycle correspond qualitatively, but not quantitatively, to the PA α enthalpies of fusion of 230 J g^{-1} [78] multiplied by the f_c of the respective compositions. Notably, the f_c of the processed materials are significantly larger than those reported for annealed PA in the literature, typically in the range of $0.2 < f_c < 0.5$ [64–66]. During processing, the material is heated, increasing the crystal growth rate $G(T)$, as expressed by the theory of Lauritzen and Hoffman [79,80]. This, however, does not account for the attained crystallinities in excess of the reported values for annealed materials. Considering that the educt granulates possess a typical crystallinity, the increased f_c must have been caused by the 'mechanical' aspect of the applied thermomechanic processing.

Processing by a heatable hydraulic press also resulted in stress-induced orientation of PA α crystallites, Fig. 7. The resulting values for the complete orientation of the polymer chain long axes within the plane perpendicular to the direction of the pressing force coincide with the crystallization of the entire contained PA, Fig. 5. Hence, the material is sheared within this plane, which is proposed to lead to the phenomenon of shear-induced crystallization [81,82]. This assumption is also supported by results from a prior study (Fig. 1, panel PA50MCC50 in Müller and Zollfrank [22]), where polarization light micrographs of press film cross-sections showed uniform interference colors within the planes of the material.

This explains the observed values of f_c and ϕ , but not directly the development of ρ_c . An intriguing observation was that the crystal phase densities of processed materials were lower compared to the educt granulates, Fig. 8. In general, the isotropic L and the low ρ_c of PA α indicate the formation of bundle-like crystallites, as opposed to regular lamellae proposed for the educt granulates [70]. The progression of L and k indicates that low values of ρ_c in the processed materials correlate with large crystallites and low amounts of disorder, Fig. 9(a). Although thermal vibrational and structural disorder could not be separated, it appears reasonable that the thermal vibrational disorder remains similar for all assessed materials: at room temperature, mechanical motions in polymers are dominated by optic modes, i.e. the rotational and

vibrational contributions, which depend on the covalent bond strengths [83,84]. Hence, changes to k indicate changes to the structural component of disorder. A possible interpretation is therefore as follows: For $f_{\text{cell}} < 0.5$, the PA phase constitutes a considerable portion of the material, which provides space for relaxation and rearrangement during processing, increasing L and lowering k . Consequently, as also indicated by the values of ϕ , the PA phase is not fully aligned and stretched. For $0.5 < f_{\text{cell}}$, all PA is mechanically engaged by the surrounding cellulose matrix, leading to the opposite effects on L , k and ϕ . The observable increase in density may be attributed to the forced crystallization by drawing, by similarity to the density increase during annealing-induced crystallization [85]. Similarly, the formation of cellulose II in blends with PA occurs only when cellulose domains that are sufficiently large for crystals to form are present. The observed separate phases including crystalline domains of PA and cellulose already indicate immiscibility between PA and cellulose. In addition, the presence of only one T_g assigned to PA counteracts the miscibility theory, which implies that a miscible polymer blends shows only one T_g , which lies between those of the blend partners. Although PA and cellulose do not mix at the molecular level, the observed blend transparency and macroscopic and microscopic homogeneity [22] of the blends indicate at least some compatibility. Intermolecular interactions can be concluded from the melting point depression (Fig. 1) and a blue shift of the amide I and amide II bands at $f_{\text{cell}} \geq 0.5$. Therefore, hydrogen bonding with cellulose as the proton acceptor for the C(O)-N-H proton is therefore assumed.

4.5. PLA/MCC

Even after HFIP treatment, no separate phases were visible in the PLA/MCC blends for all observed compositions ($f_{\text{cell}} = 0.3$ and 0.7 , Fig. S9 and $f_{\text{cell}} = 0.5$, Fig. 10(e, f)). Homogeneous and dense structures without phase separation have been previously observed when studying the fracture surface of PLA/MCC blends at various ratios using SEM [12, 22]. However, compared to this study, no further treatment for polymer removal was performed. Based on the observed morphologies of the PLA/MCC blends, efficient mixing and chain entanglement prevented the formation of phase domains in the observed scale, certainly facilitated by the absence of crystalline self-association of either of the polymers.

In contrast to PA, the crystallite sizes in PLA could be directionally resolved. Here, the expected crystalline lamellae with high aspect ratios were formed [71]. The similar L for the educt granulates and the processed material, and the reduced k in the latter, can be traced to the fact that the processed materials were cooled from the melt after mechanical stressing. Both PA and PLA are similar non-branched and non-rigid folding polymers. However, PLA does not appear to be influenced by temperature or mechanical stress in the same way, since the h_{fus} (Fig. 2) corresponds quantitatively to the f_c (Fig. 5) at $0 \leq f_{\text{cell}} \leq 0.1$ using the reported enthalpy of fusion [86,87]: $(0.42 \pm 0.04) \cdot 93 \text{ J} \cdot \text{g}^{-1} = 39 \pm 4 \text{ J} \cdot \text{g}^{-1}$ and $(0.04 \pm 0.04) \cdot 93 \text{ J} \cdot \text{g}^{-1} = 4 \pm 4 \text{ J} \cdot \text{g}^{-1}$. Unlike the PA blends, the PLA was in its molten state during thermomechanical pressing, accounting for the similar f_c of the educt granulates and the processed material.

However, this does not account for the effective suppression of crystal growth in all materials containing cellulose. As indicated by the observation that PLA/MCC films remained transparent during treatment with HFIP, the progression of f_c points to a close chemical association between PLA and cellulose. This is intuitive, considering that PLA possesses 1.6 times the number of carbonyl groups per mass and more than twice the number per chain segment length than PA, these being attachment points for hydrogen bonds with cellulose hydroxyl groups.

Actual hydrogen bonding between PLA and cellulose can be concluded from FTIR. The intense red shift of the carbonyl band (Fig. 3 (b)) that can be ascribed to interactions between the carbonyl acceptor group and a hydrogen donor [88,89], which would be a hydroxyl group from the cellulose polymer chain. The formation of new hydrogen bonds

at $f_{\text{cell}} \leq 0.6$ is also indicated by a shifted OH-stretching signal of the cellulose hydroxyl groups (Fig. 3(a)). Similar blue shifts depending on the PLA concentration were recently observed by Xu et al. [12]. Assuming that the formation of hydrogen bonds between the C=O group and cellulose takes place, hydrogen bonds between the hydroxyl groups within the cellulose are weakened or broken, shortening the OH bond. Consequently, a blue shift of the OH stretching mode is visible [12,90]. The prerequisite breakage of cellulose intramolecular hydrogen bonding resulted in a shortening of the C-O-C bonds that can be correlated with an increase in the C-O-C stretching oscillation. Although miscibility is unlikely for the observed polymers, the absence of a T_g in almost all PLA/MCC blends is a new and interesting finding. For those samples, no crystalline domains were detected via DSC or XRD, so only amorphous structures are present. From SEM analysis, it is proposed that the size of the amorphous PLA domains is far below the micrometer scale based on the observed single-phase morphology after etching (Fig. 10(e, f)). In general, a low degree of miscibility leads to two separate glass transitions, while true miscibility is indicated by the presence of one distinct transition that lies between the T_g values of the pure polymers corresponding to their concentration and described by the Fox equation [91]. While neither theory can be applied to here shown results, it has also been shown that very low degrees of phase separation result in a very broad T_g value between those of the pure components [92]. Although there are different approaches to explain the merging of two T_g values into a broad transition [93,94], both suggest that in regions whose size corresponds to the radius of gyration of the polymers, the T_g value is broadened because these regions consist of only one interphase layer [92]. It is therefore possible that cellulose and PLA phase domains extend into the nanoscale and below, resulting in a very broad T_g that cannot be clearly determined by DSC measurements.

5. Conclusions

In this study, different blend systems with cellulose and two synthetic polymers, PLA and PA, are investigated for their thermal and structural properties. Intermolecular interactions with cellulose can be concluded for both systems. PA/MCC blends exhibited a two-phase structure with crystalline PA domains. Although transparent blends are produced, PA and cellulose appear immiscible based on their morphology and the fact that amorphous as well as crystalline PA domains are visible from thermal and crystallinity analysis. At $f_{\text{cell}} \geq 0.5$, polymer interactions, especially promoted hydrogen bonding between PA and cellulose, can be concluded from the melting point depression of the PA and systematic shifts in the IR spectra. This is accompanied by a homogeneous phase distribution of small PA domains that are not fully oriented and crystallized, in contrast to blends with higher PA fractions. This morphology is exactly opposite to conventionally produced composites, where cellulose always presents the dispersed phase. However, since cellulose is present as a continuous phase, further thermoplastic forming processes based on extrusion will not be possible. The combination of PA and cellulose precipitated from solution, though, could be used in fiber spinning. In PLA/MCC blends, a homogeneously mixed phase was present at all blend ratios. The blend partners interact strongly via hydrogen bonding. Although both cellulose and PLA are present in an amorphous state after blend precipitation, no glass transition of the PLA can be determined via DSC. Furthermore, no distinct domains for either blend partner can be identified in SEM, suggesting that efficient mixing down to the molecular level is possible even if polymers are expected to be immiscible.

In both blend systems, the residual solvent acted as a plasticizer. Since the used IL shows interchain interactions with both polymers, it also acts as a compatibilizer in the blend. The effects were negligible at RIL concentrations below 1 wt%, however. Although with regard to thermoplastic processing of the blend materials, which is one overarching goal of this work, and RIL can be favorable to induce flexibility, the extraction and recovering of the ILs should be favored for ecological

and economic reasons. The thermoplastic and mechanical performance of the PLA/MCC blends have to be tested on a larger scale and possibly with reduced amounts of solvent. The general possibility to use native cellulose in thermoplastic materials with new properties, however, opens a field for biomass valorization and is a huge step towards a bio-based economy.

Funding

This research did not receive any specific grant from funding agencies in the public, commercial, or not-for-profit sectors.

CRedit authorship contribution statement

Kerstin Müller: Conceptualization, Methodology, Validation, Investigation, Writing – original draft, Visualization. **Daniel Van Opdenbosch:** Formal analysis (XRD), Visualization (XRD), Writing – original draft (XRD), Writing – review & editing. **Cordt Zollfrank:** Writing – review & editing.

Declaration of Competing Interest

The authors declare the following financial interests/personal relationships which may be considered as potential competing interests: Kerstin Müller is employed by the Fraunhofer-Gesellschaft zur Förderung der angewandten Forschung e.V., which has filed a patent application (publication number WO 2021/170863 A1) partly based on these results.

Acknowledgements

The authors thank Anna Tichy and Tina Friedenauer for their help with sample preparation and analysis. We also thank Moritz Klotz for his assistance with the XRD measurements and Michael Schott and Dominik Fiedler for their assistance with SEM analysis. We acknowledge Siegfried Fürtauer for his comments on the manuscript.

Appendix A. Supporting information

Supplementary data associated with this article can be found in the online version at [doi:10.1016/j.mtcomm.2021.103074](https://doi.org/10.1016/j.mtcomm.2021.103074).

References

- [1] B. Baghaei, M. Skrifvars, All-cellulose composites: a review of recent studies on structure, properties and applications, *Molecules* 25 (12) (2020) 2836.
- [2] Y.-Y. Li, B. Wang, M.-G. Ma, B. Wang, Review of recent development on preparation, properties, and applications of cellulose-based functional materials, *Int. J. Polym. Sci.* 2018 (2018), 8973643.
- [3] D. Klemm, B. Heublein, H.-P. Fink, A. Bohn, Cellulose: fascinating biopolymer and sustainable raw material, *Angew. Chem. Int. Ed.* 44 (22) (2005) 3358–3393.
- [4] S. Kalia, B.S. Kaith, I. Kaur, Cellulose Fibers: Bio- and Nano-Polymer Composites: Green Chemistry and Technology, Springer Berlin Heidelberg, 2011.
- [5] R.P. Swatloski, S.K. Spear, J.D. Holbrey, R.D. Rogers, Dissolution of cellulose with ionic liquids, *J. Am. Chem. Soc.* 124 (18) (2002) 4974–4975.
- [6] H. Wang, G. Gurau, R.D. Rogers, Ionic liquid processing of cellulose, *Chem. Soc. Rev.* 41 (4) (2012) 1519–1537.
- [7] F. Hermanutz, M.P. Vocht, N. Panzier, M.R. Buchmeiser, Processing of cellulose using ionic liquids, *Macromol. Mater. Eng.* 2019 (2019), 1800450.
- [8] S. Zhu, Y. Wu, Q. Chen, Z. Yu, C. Wang, S. Jin, Y. Ding, G. Wu, Dissolution of cellulose with ionic liquids and its application: a mini-review, *Green. Chem.* 8 (4) (2006) 325–327.
- [9] Y. Li, J. Wang, X. Liu, S. Zhang, Towards a molecular understanding of cellulose dissolution in ionic liquids: anion/cation effect, synergistic mechanism and physicochemical aspects, *Chem. Sci.* 9 (17) (2018) 4027–4043.
- [10] C. Verma, A. Mishra, S. Chauthan, P. Verma, V. Srivastava, M.A. Quraishi, E. E. Eibenso, Dissolution of cellulose in ionic liquids and their mixed cosolvents: a review, *Sustain. Chem. Pharm.* 13 (2019), 100162.
- [11] R.S.J. Manley, Blends of Cellulose and Synthetic Polymers. Cellulose Derivatives, American Chemical Society, 1998, pp. 253–264.

- [12] A. Xu, Y. Wang, J. Gao, J. Wang, Facile fabrication of a homogeneous cellulose/polylactic acid composite film with improved biocompatibility, biodegradability and mechanical properties, *Green Chem.* 21 (16) (2019) 4449–4456.
- [13] N. Hameed, J. Bavishi, J. Parameswaranpillai, N.V. Salim, J. Joseph, G. Madras, B. L. Fox, Thermally flexible epoxy/cellulose blends mediated by an ionic liquid, *RSC Adv.* 5 (65) (2015) 52832–52836.
- [14] F.G. Torres, O.P. Troncoso, C. Torres, C.J. Grande, Cellulose based blends, composites and nanocomposites, in: S. Thomas, P.M. Visakh, A.P. Mathew (Eds.), *Advances in Natural Polymers: Composites and Nanocomposites*, eds. ..., Springer Berlin Heidelberg, Berlin, Heidelberg, 2013, pp. 21–54.
- [15] M.M. Khattab, N.A. Abdel-Hady, Y. Dahman, Cellulose nanocomposites: opportunities, challenges, and applications, in: M. Jawaid, S. Boufi, H.P.S. A. K. (Eds.), *Cellulose-Reinforced Nanofibre Composites*, Woodhead Publishing, 2017, pp. 483–516.
- [16] S. Rogovina, K. Aleksanyan, E. Prut, A. Gorenberg, Biodegradable blends of cellulose with synthetic polymers and some other polysaccharides, *Eur. Polym. J.* 49 (1) (2013) 194–202.
- [17] S.Z. Rogovina, G.A. Vikhoreva, Polysaccharide-based polymer blends: methods of their production, *Glycoconj. J.* 23 (7) (2006) 611.
- [18] A. Dufresne, Cellulose nanomaterial reinforced polymer nanocomposites, *Curr. Opin. Colloid Interface Sci.* 29 (2017) 1–8.
- [19] K. Ravichandran, P.K. Praseetha, T. Arum, S. Gobalakrishnan, Chapter 6 - synthesis of nanocomposites, in: S. Mohan Bhagyaraj, O.S. Oluwafemi, N. Kalarikkal, S. Thomas (Eds.), *Synthesis of Inorganic Nanomaterials*, Woodhead Publishing, 2018, pp. 141–168.
- [20] K. Müller, E. Bugnicourt, M. Latorre, M. Jorda, Y. Echegoyen Sanz, J. Lagaron, O. Miesbauer, A. Bianchin, S. Hankin, U. Bölz, G. Pérez, M. Jesdinski, M. Lindner, Z. Scheuerer, S. Castelló, M. Schmid, Review on the processing and properties of polymer nanocomposites and nano-coatings and their applications in the packaging, automotive and solar energy fields, *Nanomaterials* 7 (4) (2017) 74.
- [21] J. Fawaz, V. Mittal, Synthesis of polymer nanocomposites: review of various techniques, *Synth. Tech. Polym. Nanocompos.* (2014) 1–30.
- [22] K. Müller, C. Zollfrank, Ionic liquid aided solution-precipitation method to prepare polymer blends from cellulose with polyesters or polyamide, *Eur. Polym. J.* 133 (2020), 109743.
- [23] A.K. Lele, A.D. Shine, Effect of RESS dynamics on polymer morphology, *Ind. Eng. Chem. Res.* 33 (6) (1994) 1476–1485.
- [24] S. Mawson, S. Kanakia, K.P. Johnston, Metastable polymer blends by precipitation with a compressed fluid antisolvent, *Polymer* 38 (12) (1997) 2957–2967.
- [25] B. Adak, S. Mukhopadhyay, All-cellulose composite laminates with low moisture and water sensitivity, *Polymer* 141 (2018) 79–85.
- [26] L. Li, Y. Zhang, Y. Sun, S. Sun, G. Shen, P. Zhao, J. Cui, H. Qiao, Y. Wang, H. Zhou, Manufacturing pure cellulose films by recycling ionic liquids as plasticizers, *Green Chem.* 22 (12) (2020) 3835–3841.
- [27] M. Shibata, N. Teramoto, T. Nakamura, Y. Saitoh, All-cellulose and all-wood composites by partial dissolution of cotton fabric and wood in ionic liquid, *Carbohydr. Polym.* 98 (2) (2013) 1532–1539.
- [28] J.M. Spörl, F. Batti, M.-P. Vocht, R. Raab, A. Müller, F. Hermanutz, M. R. Buchmeiser, Ionic liquid approach toward manufacture and full recycling of all-cellulose composites, *Macromol. Mater. Eng.* 303 (1) (2018), 1700335.
- [29] J. Wu, J. Bai, Z. Xue, Y. Liao, X. Zhou, X. Xie, Insight into glass transition of cellulose based on direct thermal processing after plasticization by ionic liquid, *Cellulose* 22 (1) (2015) 89–99.
- [30] M.A. Haq, Y. Habu, K. Yamamoto, A. Takada, J.-i. Ka-dokawa, Ionic liquid induces flexibility and thermoplasticity in cellulose film, *Carbohydr. Polym.* (2019), 115058.
- [31] S.K. Mahadeva, J. Kim, Influence of residual ionic liquid on the thermal stability and electromechanical behavior of cellulose regenerated from 1-ethyl-3-methylimidazolium acetate, *Fibers Polym.* 13 (3) (2012) 289–294.
- [32] J. Pang, M. Wu, Q. Zhang, X. Tan, F. Xu, X. Zhang, R. Sun, Comparison of physical properties of regenerated cellulose films fabricated with different cellulose feedstocks in ionic liquid, *Carbohydr. Polym.* 121 (2015) 71–78.
- [33] L. Sun, J.Y. Chen, W. Jiang, V. Lynch, Crystalline characteristics of cellulose fiber and film regenerated from ionic liquid solution, *Carbohydr. Polym.* 118 (2015) 150–155.
- [34] J.-H. Pang, X. Liu, M. Wu, Y.-Y. Wu, X.-M. Zhang, R.-C. Sun, Fabrication and characterization of regenerated cellulose films using different ionic liquids, *J. Spectrosc.* 2014 (2014) 8.
- [35] D. Cheng, X. An, J. Zhang, X. Tian, Z. He, Y. Wen, Y. Ni, Facile preparation of regenerated cellulose film from cotton linter using organic electrolyte solution (OES), *Cellulose* 24 (4) (2017) 1631–1639.
- [36] X. Zheng, F. Huang, L. Chen, L. Huang, S. Cao, X. Ma, Preparation of transparent film via cellulose regeneration: Correlations between ionic liquid and film properties, *Carbohydr. Polym.* 203 (2019) 214–218.
- [37] N. Taheri, A. Abdolmaleki, H. Fashandi, Impact of non-solvent on regeneration of cellulose dissolved in 1-(carboxymethyl)pyridinium chloride ionic liquid, *Polym. Int.* 68 (12) (2019) 1945–1951.
- [38] L.K.J. Hauri, M. Hummel, A.W.T. King, I. Kilpeläinen, H. Sixta, Role of solvent parameters in the regeneration of cellulose from ionic liquid solutions, *Biomacromolecules* 13 (9) (2012) 2896–2905.
- [39] Z.-D. Ding, Z. Chi, W.-X. Gu, S.-M. Gu, J.-H. Liu, H.-J. Wang, Theoretical and experimental investigation on dissolution and regeneration of cellulose in ionic liquid, *Carbohydr. Polym.* 89 (1) (2012) 7–16.
- [40] K.M. Gupta, Z. Hu, J. Jiang, Cellulose regeneration from a cellulose/ionic liquid mixture: the role of anti-solvents, *RSC Adv.* 3 (31) (2013) 12794–12801.
- [41] S.K. Mahadeva, K.-S. Kang, J. Kim, S.H. Ha, Y.-M. Koo, The effect of residual ionic liquid for cellulose based electro-active paper actuator, *Soft Mater.* 8 (3) (2010) 254–262.
- [42] U. Riaz, S.M. Ashraf, Characterization of polymer blends with FTIR spectroscopy, in: S. Thomas, Y. Grohens, P. Jyotishkumar (Eds.), *Characterization of Polymer Blends*, Wiley VCH, Weinheim, Germany, 2014, pp. 625–678.
- [43] P. Schuster, *Hydrogen Bonds*, Springer-Verlag, Heidelberg, Germany, 1984.
- [44] X. Li, L. Liu, H.B. Schlegel, On the physical origin of blue-shifted hydrogen bonds, *J. Am. Chem. Soc.* 124 (32) (2002) 9639–9647.
- [45] R.F.W. Bader, A model for the hydrogen bond and proton transfer reactions, *Can. J. Chem.* 42 (8) (1964) 1822–1834.
- [46] H. Ratajczak, Charge-transfer properties of the hydrogen bond. II. Charge-transfer theory and the relation between the enhancement of dipole moment and the ionization potential of hydrogen-bonded systems, *J. Phys. Chem.* 76 (26) (1972) 3991–3992.
- [47] J. Bergmann, P. Friedel, R. Kleeberg, BGMN—a new fundamental parameters based Rietveld program for laboratory X-ray sources, its use in quantitative analysis and structure investigations, *CPD Newsl.* 20 (1998) 5.
- [48] G., Natta, P. Corradini, Structure and properties of isotactic polypropylene II, *Nuovo Cim.* 15 1 1960, pp.40–51.
- [49] R. Zannetti, G. Celotti, A. Fichera, R. Francesconi, The structural effects of annealing time and temperature on the paracrystal-crystal transition in isotactic polypropylene, *Die Makromol. Chem.* 128 (1) (1969) 137–142.
- [50] A.D. French, Idealized powder diffraction patterns for cellulose polymorphs, *Cellulose* 21 (2) (2014) 885–896.
- [51] D.R. Holmes, C.W. Bunn, D.J. Smith, The crystal structure of polycapronamide: nylon 6, *J. Polym. Sci.* 17 (84) (1955) 159–177.
- [52] K. Wasanasuk, K. Tashiro, M. Hanesaka, T. Ohhara, K. Kurihara, R. Kuroki, T. Tamada, T. Ozeki, T. Kanamoto, Crystal structure analysis of poly(L-lactic acid) α form on the basis of the 2-dimensional wide-angle synchrotron x-ray and neutron diffraction measurements, *Macromolecules* 44 (16) (2011) 6441–6452.
- [53] M. Järvinen, Texture models in powder diffraction analysis, *Mater. Sci. Forum* 278–281 (1998) 184–199.
- [54] J. Bergmann, T. Monecke, R. Kleeberg, Alternative algorithm for the correction of preferred orientation in Rietveld analysis, *J. Appl. Crystallogr.* 34 (1) (2001) 16–19.
- [55] W. Ruland, X-ray determination of crystallinity and diffuse disorder scattering, *Acta Crystallogr.* 14 (11) (1961) 1180–1185.
- [56] C. Vonk, Computerization of Ruland's X-ray method for determination of the crystallinity in polymers, *J. Appl. Crystallogr.* 6 (2) (1973) 148–152.
- [57] K.P. Sao, B.K. Samantaray, S. Bhattacharjee, Analysis of lattice distortions in ramie cellulose, *J. Appl. Polym. Sci.* 66 (10) (1997) 2045–2046.
- [58] S.M. Aharoni, *Nylons: Their Synthesis, Structure, and Properties*, Wiley, Chichester, England, 1997.
- [59] R. Iwamoto, H. Murase, Infrared spectroscopic study of the interactions of nylon-6 with water, *J. Polym. Sci. Part B Polym. Phys.* 41 (14) (2003) 1722–1729.
- [60] G. Socrates, *Infrared and Raman Characteristic Group Frequencies: Tables and Charts*, third ed., Wiley, Chichester, England, 2001.
- [61] C.M.B. Goncalves, J.A.P. Coutinho, I.M. Marrucho, Optical properties, in: R. A. Auras, L.T. Lim, S.E.M. Selke, H. Tsuji (Eds.), *Poly(lactic acid): Synthesis, Structures, Properties, Processing, and Applications*, Wiley, Hoboken, New Jersey, 2011.
- [62] D. Giolacu, F. Giolacu, V.I. Popa, Amorphous cellulose – structure and characterization, *Cellul. Chem. Technol.* 45 (1–2) (2011) 13–21.
- [63] L.P. De Figueiredo, F.F. Ferreira, The rietveld method as a tool to quantify the amorphous amount of microcrystalline cellulose, *J. Pharm. Sci.* 103 (5) (2014) 1394–1399.
- [64] G. Gurato, A. Fichera, F.Z. Grandi, R. Zannetti, P. Canal, Crystallinity and polymorphism of 6-polyamide, *Die Makromol. Chem.* 175 (3) (1974) 953–975.
- [65] T. Arakawa, F. Nagatoshi, N. Arai, Melting behavior and morphology of drawn nylon 6, *J. Polym. Sci. Part A 2 Polym. Phys.* 7 (9) (1969) 1461–1472.
- [66] W. Ruland, Crystallinity and disorder parameters in nylon 6 and nylon 7, *Polymer* 5 (1964) 89–102.
- [67] A.C. Renouf-Glauser, J. Rose, D.F. Farrar, R.E. Cameron, The effect of crystallinity on the deformation mechanism and bulk mechanical properties of PLLA, *Biomaterials* 26 (29) (2005) 5771–5782.
- [68] C. Migliarese, A. De Lollis, L. Fambri, D. Cohn, The effect of thermal history on the crystallinity of different molecular weight PLLA biodegradable polymers, *Clin. Mater.* 8 (1) (1991) 111–118.
- [69] J.J. Hermans, P.H. Hermans, D. Vermaas, A. Weidinger, Quantitative evaluation orientation in cellulose fibres from the X-ray fibre diagram. *Recueils des Travaux Chimiques des Pays-Bas*, Wiley, 1946, pp. 427–447.
- [70] Y. Li, W.A. Goddard, Nylon 6 crystal structures, folds, and lamellae from theory, *Macromolecules* 35 (22) (2002) 8440–8455.
- [71] B. Kalb, A.J. Pennings, General crystallization behaviour of poly(L-lactic acid), *Polymer* 21 (6) (1980) 607–612.
- [72] J. Bengtsson, C. Olsson, A. Hedlund, T. Köhnke, E. Bialik, Understanding the inhibiting effect of small-molecule hydrogen bond donors on the solubility of cellulose in tetrabutylammonium acetate/DMSO, *J. Phys. Chem. B* 121 (50) (2017) 11241–11248.
- [73] A. Hedlund, T. Köhnke, H. Theliander, Coagulation of EminiAc-cellulose solutions: dissolution/precipitation disparity and effects of non-solvents and cosolvent, *Nord. Pulp Pap. Res. J.* 30 (1) (2015) 32.
- [74] Y. Cao, T. Mu, Comprehensive investigation on the thermal stability of 66 ionic liquids by thermogravimetric analysis, *Ind. Eng. Chem. Res.* 53 (20) (2014) 8651–8664.

- [75] P. Xu, Q. Hao, H. Gui, S. Yang, Y. Ding, Effect of ionic liquid on chain segment motion and charge detrapping in ionic liquid/polyamide 610 blends, *Polym. Mater. Sci. Eng.* 30 (8) (2014) 54–57.
- [76] X. Zheng, Q. Lin, P. Jiang, Y. Li, J. Li, Ionic liquids incorporating polyamide 6: miscibility and physical properties, *Polymers* 10 (5) (2018) 562.
- [77] Y. Tian, H. Qin, X. Yang, C. Chi, S. Liu, Influence of ionic liquids on the structure of polyamide 6, *Mater. Lett.* 180 (2016) 200–202.
- [78] C. Millot, L.-A. Fillot, O. Lame, P. Sotta, R. Seguela, Assessment of polyamide-6 crystallinity by DSC, *J. Therm. Anal. Calorim.* 122 (1) (2015) 307–314.
- [79] J.I. Lauritzen, J.D. Hoffman, Extension of theory of growth of chain-folded polymer crystals to large undercoolings, *J. Appl. Phys.* 44 (10) (1973) 4340–4352.
- [80] J.D. Hoffman, R.L. Miller, H. Marand, D.B. Roitman, Relationship between the lateral surface free energy σ and the chain structure of melt-crystallized polymers, *Macromolecules* 25 (8) (1992) 2221–2229.
- [81] K. Kobayashi, T. Nagasawa, Crystallization of sheared polymer melts, *J. Macromol. Sci. Part B* 4 (2) (1970) 331–345.
- [82] S. Torza, Shear-induced crystallization of polymers. I. The four-roller apparatus, *J. Polym. Sci. Polym. Phys. Ed.* 13 (1) (1975) 43–57.
- [83] J.G. Curro, Calculation of Grüneisen parameters of polymers, *J. Chem. Phys.* 58 (1) (1973) 374–380.
- [84] T.G. Gibbons, Grüneisen functions of polymer polycrystals, *J. Chem. Phys.* 60 (3) (1974) 1094–1100.
- [85] P.F. Dismore, W.O. Statton, Chain folding in oriented nylon 66 fibers, *J. Polym. Sci. Part C Polym. Symp.* 13 (1) (1966) 133–148.
- [86] D. Garlotta, A literature review of poly(lactic acid), *J. Polym. Environ.* 9 (2) (2001) 63–84.
- [87] E.W. Fischer, H.J. Sterzel, G. Wegner, Investigation of the structure of solution grown crystals of lactide copolymers by means of chemical reactions, *Kolloid Z. Z. Polym.* 251 (11) (1973) 980–990.
- [88] L. Paoloni, A. Patti, F. Mangano, The hydrogen bond with carbonyl groups: theoretical study of the correlation between the X-H stretching frequency shift and the C=O group properties, *J. Mol. Struct.* 27 (1) (1975) 123–137.
- [89] D. Braun, N. Eidam, D. Leiß, FTIR studies of polar interactions in polymer blends, *Makromol. Chem. Macromol. Symp.* 52 (1) (1991) 105–111.
- [90] H. Wang, S. Liu, Y. Zhao, H. Zhang, J. Wang, Molecular origin for the difficulty in separation of 5-hydroxymethylfurfural from imidazolium based ionic liquids, *ACS Sustain. Chem. Eng.* 4 (12) (2016) 6712–6721.
- [91] T.G. Fox, Influence of diluent and of copolymer composition on the glass temperature of a polymer system, *Bull. Am. Phys. Soc.* 1 (1956) 123–132.
- [92] L.A. de Graaf, M. Möller, Glass transition temperatures of microphase-separated semi-interpenetrating polymer networks of polystyrene-inter-poly(cross-2-ethylhexyl methacrylate), *Polymer* 36 (18) (1995) 3451–3457.
- [93] L.H. Sperling, H.F. George, V. Huelck, D.A. Thomas, Viscoelastic behavior of interpenetrating polymer networks: poly(ethyl acrylate)-poly(methyl methacrylate), *J. Appl. Polym. Sci.* 14 (11) (1970) 2815–2824.
- [94] V.V. Shilov, Y.S. Lipatov, L.V. Karabanova, L.M. Sergeeva, Phase separation in the interpenetrating polymeric network on the basis of polyurethane and polyurethane acrylates, *J. Polym. Sci. Polym. Chem. Ed.* 17 (10) (1979) 3083–3093.

Supporting Information: Cellulose blends with polylactic acid or polyamide 6 from solution blending: Microstructure and polymer interactions

Kerstin Müller^{1,2}, Daniel Van Opdenbosch¹, Cordt Zollfrank¹

¹ Chair for Biogenic Polymers, Technische Universität München, Campus Straubing for Biotechnology and Sustainability, Schulgasse 16, 94315, Straubing, Germany

² Process Development for Polymer Recycling, Fraunhofer Institute for Process Engineering and Packaging IVV, Giggenhauser Str. 35, 85354 Freising, Germany

Critical cellulose concentration in EmimAc/DMSO

Measurements were performed with a rotational rheometer (MCR301, Anton Paar, Germany) with TruGap™ cone-plate geometry (1° - 25 mm, d=0.049 mm) and a peltier temperature control system at 25 °C. Flow curves of solutions with different cellulose concentrations were used to determine their steady state viscosities. The overlap concentration was determined at 0.0245 g/ml, which corresponds to 2.611 wt%.

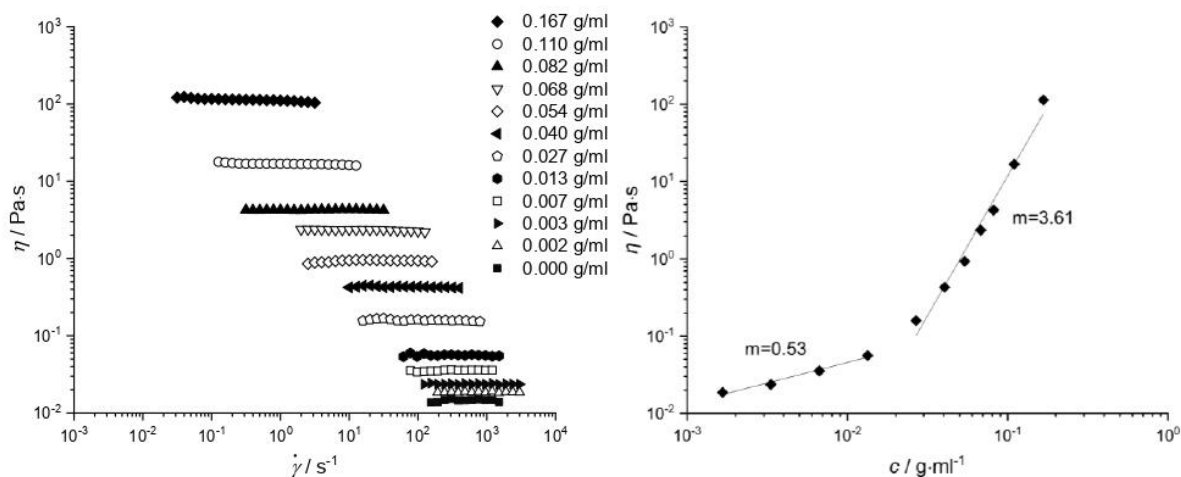


Figure S 1. Flow curves for EmimAc/DMSO and different concentrations of cellulose in EmimAc/DMSO-solutions in the Newtonian behavior areas (left) and corresponding steady state viscosities as a function of cellulose concentration, showing respective slopes for dilute ($m=0.53$) and concentrated ($m=3.61$) areas (right).

Residual ionic liquid contents

Residual ionic liquid (RIL) was determined via dry mass measurement (analytical scale, readability 0.1 mg) of the extracts from the different washing steps. The method assumes a partition coefficient of 1 for both ethanol and water.

Table S 1. Residual ionic liquid contents (RIL) of PLA/MCC blends (ethanol precipitated) and PA/MCC blends (water precipitated) at different washing steps WS1, WS2 and WS3.

$f_{\text{cell}} / 1$	RIL _{PLA/MCC} / wt%			RIL _{PA/MCC} / wt%		
	WS1	WS2	WS3	WS1	WS2	WS3
0.1	0.814	0.027	0.000	3.088	1.584	0.668
0.2	1.544	0.110	0.017	3.812	1.435	0.517
0.3	2.182	0.275	0.052	4.079	1.340	0.310
0.4	2.695	0.390	0.051	4.607	0.944	0.221
0.5	3.330	0.601	0.000	4.987	0.784	0.106
0.6	2.604	n/a	0.046	4.596	0.770	0.060
0.7	4.583	1.042	0.115	4.661	0.752	0.069
0.8	4.880	1.130	0.000	4.803	0.661	0.045
0.9	4.940	1.179	0.075	4.657	0.564	0.060
1	6.463	1.623	0.092	4.614	0.619	0.036

DSC thermograms

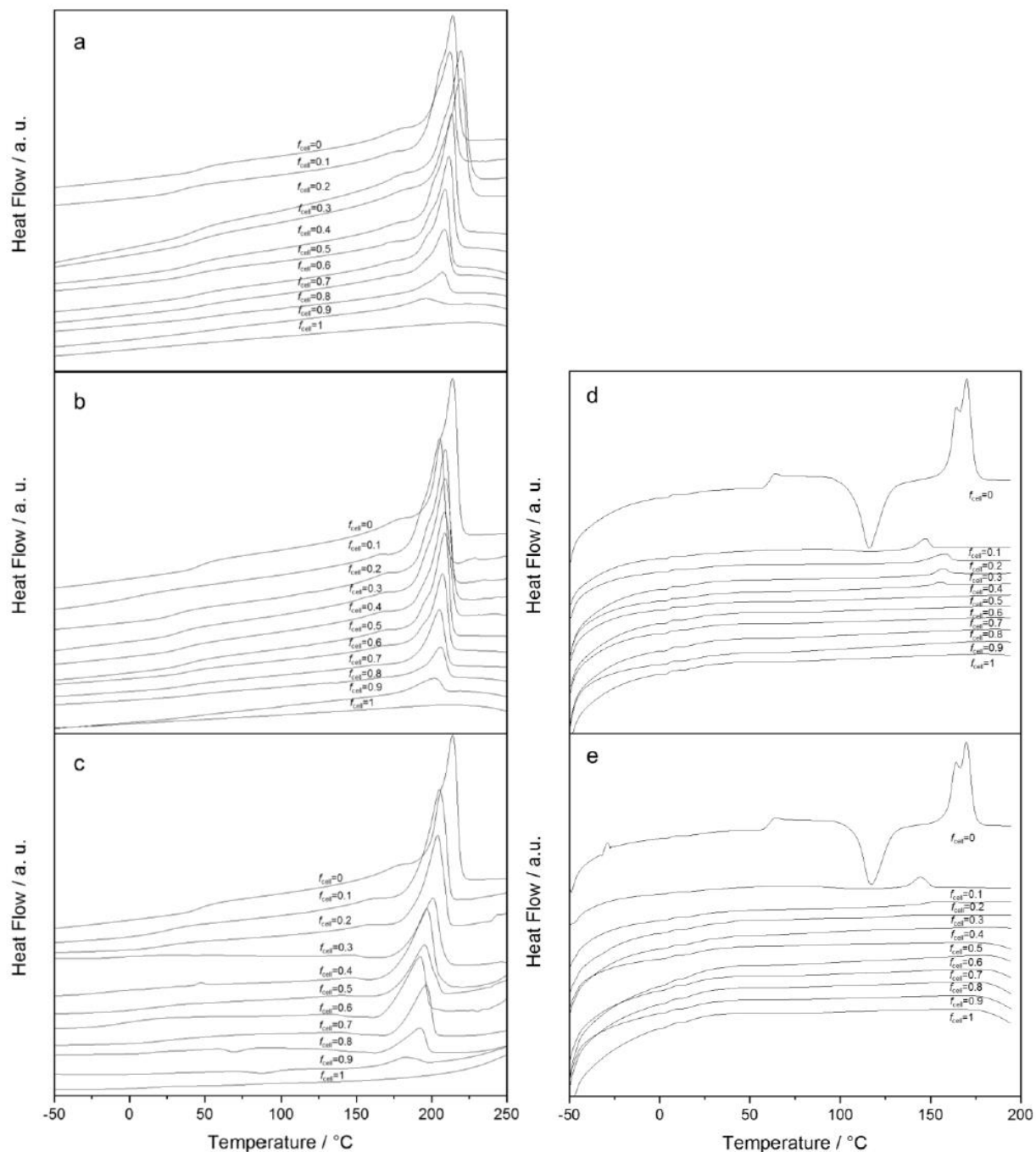


Figure S 2. DSC thermograms (2nd heating run) of PA/MCC blends after the third (a), second (b) and first (c) washing step and PLA/MCC blends after the third (d) and second (e) washing step.

FTIR supporting data

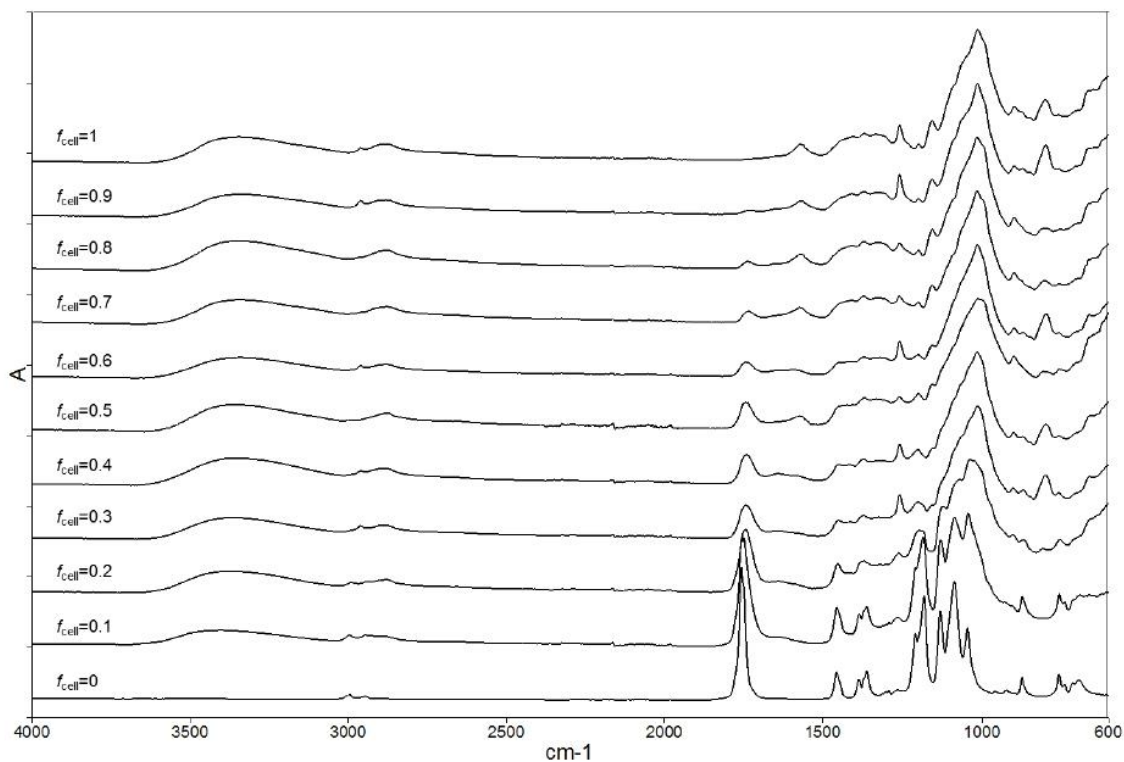


Figure S 3. FTIR spectra of PLA/MCC blend samples as well as precipitated MCC ($f_{cell}=1$) and PLA ($f_{cell}=0$) from the third washing step over the whole wavelength range.

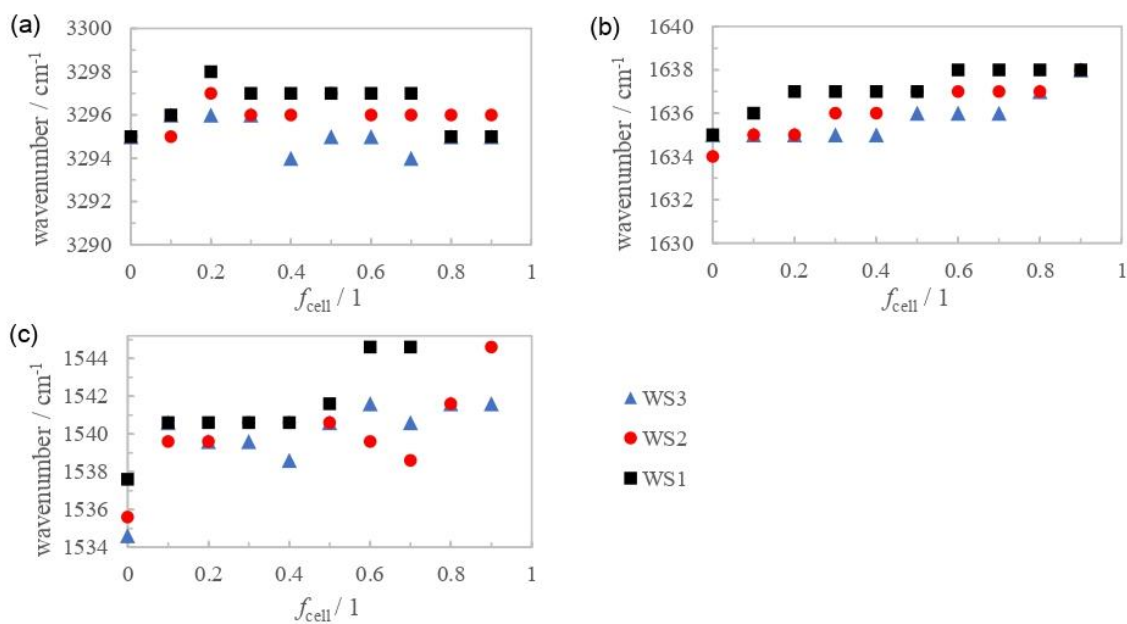


Figure S 4. FTIR peak maxima for bands assigned to NH-stretching (a), amid I (b) and amid II (c) of PA in PA/MCC blends in relation to f_{cell} for the three washing steps

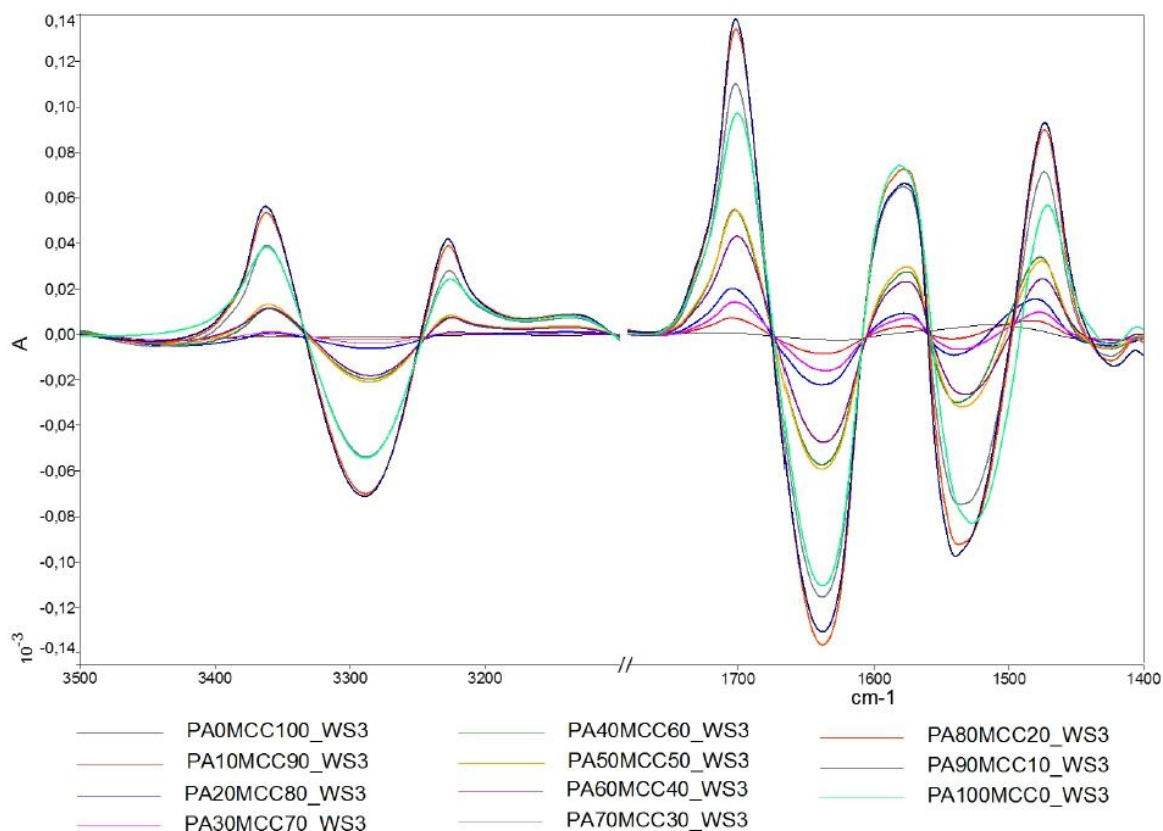


Figure S 5. 2nd derivative FTIR spectra of PA/MCC blends after the third washing steps. Wavelength regions for NH-stretching (left) and amid I and II bands (right) are shown.

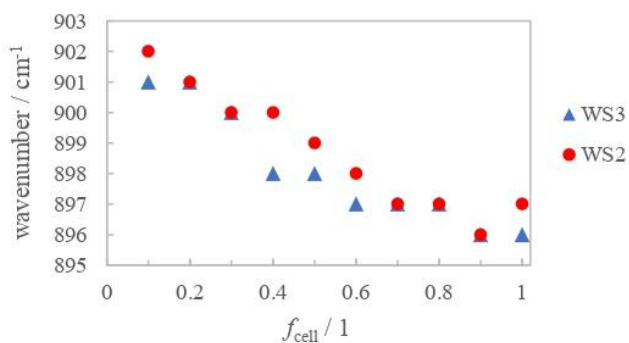


Figure S 6. FTIR peak maxima of the amorphous band (C-O-C stretching) of MCC in PLA/MCC blends in relation to f_{cell} for WS2 and WS3. Data for WS1 was not clearly detectable due to overlapping signals from ionic liquid/DMSO

XRD Refinement

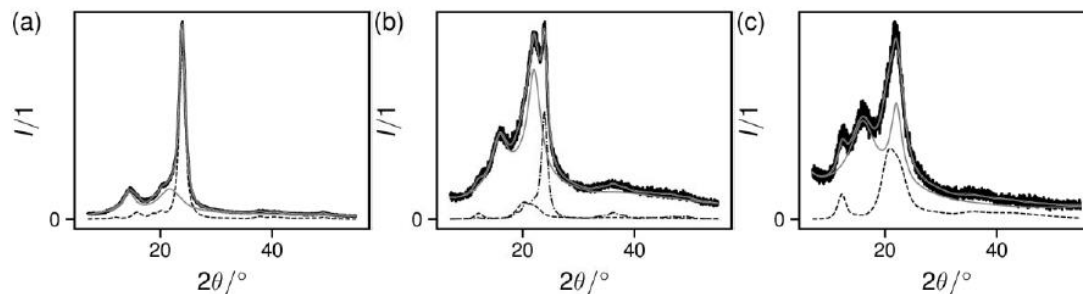


Figure S 7. Scheme of the unfolding of the diffractograms into cellulose II (dashed line) and PA (dash-dotted line) for (a) $f_{\text{cell}}=0$, (b) $f_{\text{cell}}=0.2$ and (c) $f_{\text{cell}}=1$. The background (full gray line) is composed of amorphous scattering, intensities attenuated from the crystalline phase and scattering from smectic morphologies.

Comment on background function

The background functions shown in Figure S7 exhibit the uncommon feature of two maxima, where amorphous background functions typically show only one. Presented with the diffractograms, we first systematically excluded the presence of other cellulose, PA and PLA phases, except II, and the α -forms. Having initially modeled the background function via a polynomial, a scalable reference pattern of amorphous cellulose and an additional amorphous peak to account for amorphous PA and PLA, we found that the broad peaks around $2\theta=15^\circ$ occurring in PA and PLA composites remained unaccounted for. In Figure 4, sample $f_{\text{cell}}=1$ from the PLA/MCC series exhibits this double-amorphous peak in pure form, while sample from the PA/MCC series shows additional intensities attributable to crystalline cellulose II.

Such additional 'amorphous' peaks occur in linear polymers that form smectic paracrystalline structures, see Figures 4(II),¹ 1(c),² 1(a)³ and 1(b)⁴ in the respective references. The spacing corresponding to $2\theta=15^\circ$ is 5.9 Å, exceeding the characteristic interchain- (4.4 Å) and intersheet (3.7 Å) distances of folded Nylons.⁵ Similarities in the respective peak positions further support the argument that in this work, smectic superstructures were formed.^{1, 3-4} Paracrystalline arrangements can be obtained by quenching,^{1, 3} or by stretching.² We propose that the manner of processing in this work is the cause for the formation of such structuring in our composites.

SEM images of PA/cellulose and PLA/cellulose blends

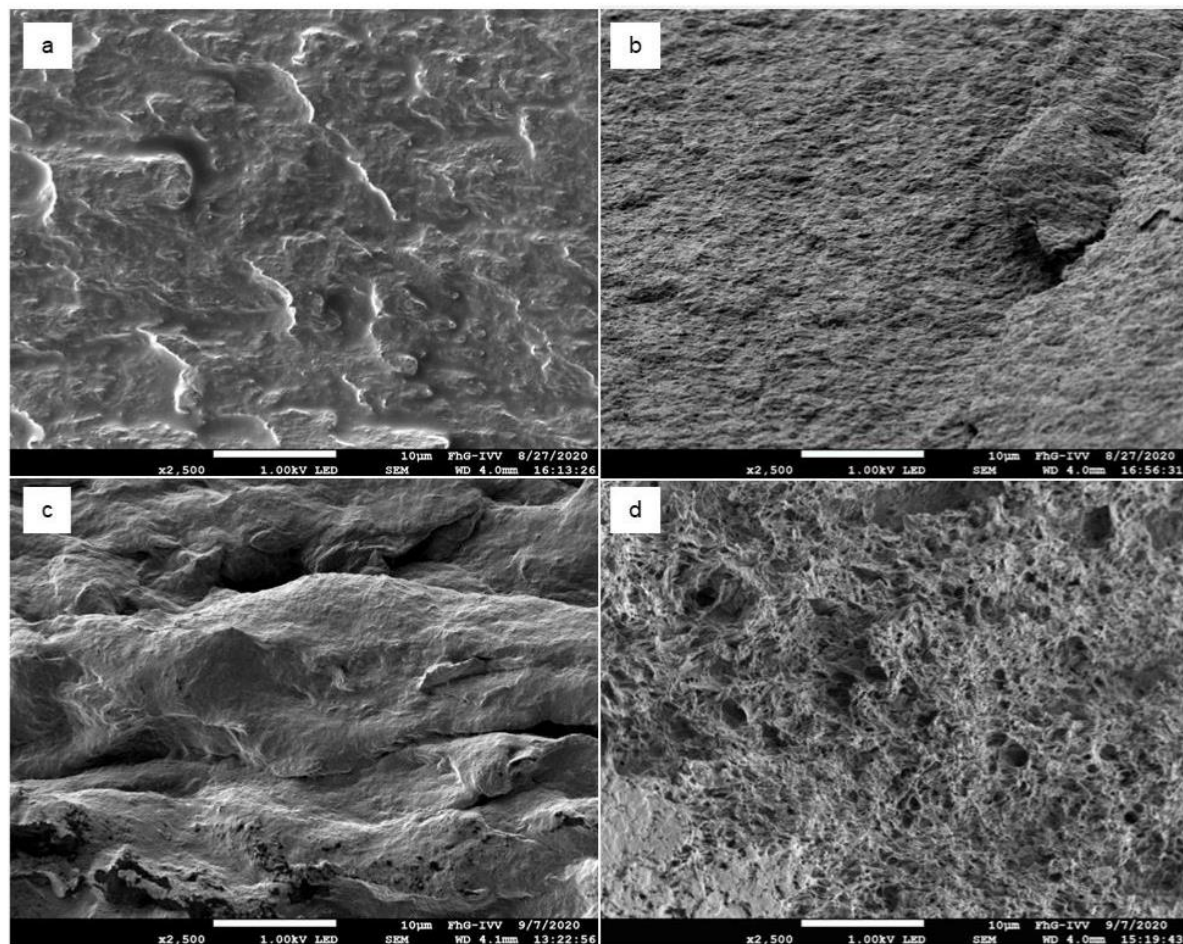


Figure S 8. SEM images of cryo-fractured cross sections of PA/MCC blend press films at $f_{cell}=0.3$ (a) and $f_{cell}=0.7$ (b) and their etched counterparts (c, $f_{cell}=0.3$) and (d, $f_{cell}=0.7$).

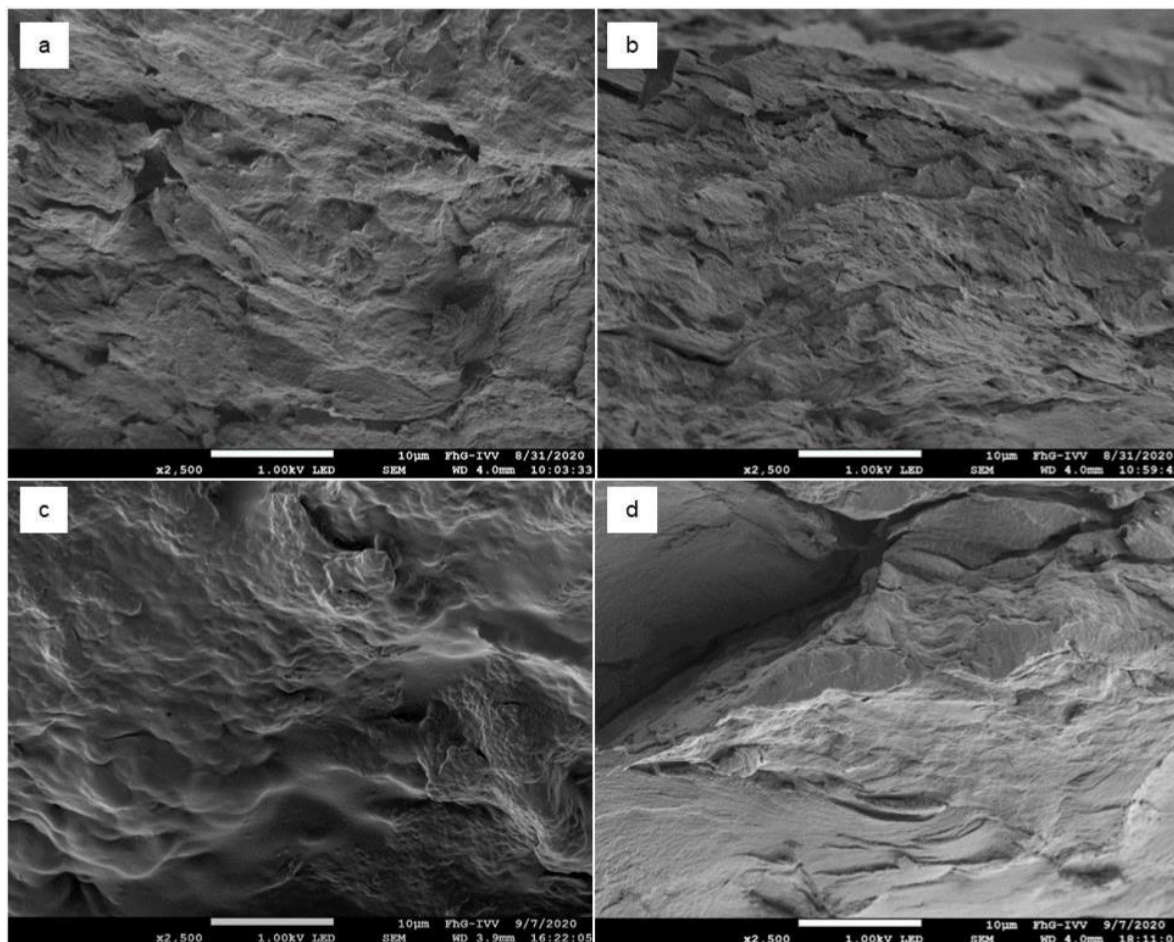


Figure S 9 SEM images of cryo-fractured cross sections of PLA/MCC blend press films at $f_{cell}=0.3$ (a) and $f_{cell}=0.7$ (b) and their etched counterparts (c, $f_{cell}=0.3$) and (d, $f_{cell}=0.7$).

References

1. Natta, G.; Corradini, P., Structure and properties of isotactic polypropylene. *Il Nuovo Cimento (1955-1965)* **1960**, *15* (1), 40-51.
2. Hosemann, R., Parakristalline Phasen. Teil I: Entstehung, Kennzeichnung und Eigenschaften. *Chemie Ingenieur Technik* **1970**, *42* (20), 1252-1258.
3. Zannetti, R.; Celotti, G.; Fichera, A.; Francesconi, R., The structural effects of annealing time and temperature on the paracrystal-crystal transition in isotactic polypropylene. *Die Makromolekulare Chemie* **1969**, *128* (1), 137-142.
4. Van Opendenbosch D.; Haslböck M.; Zollfrank C., Determining paracrystallinity in mixed-tacticity polyhydroxybutyrates. *Journal of Applied Crystallography* **2021**, *54* (1), 217-227.
5. Jones, N. A.; Atkins, E. D. T.; Hill, M. J.; Cooper, S. J.; Franco, L., Chain-Folded Lamellar Crystals of Aliphatic Polyamides. Comparisons between Nylons 4 4, 6 4, 8 4, 10 4, and 12 4. *Macromolecules* **1996**, *29* (18), 6011-6018.

6 Cellulose blends from gel extrusion and compounding with polylactic acid

by Kerstin Müller, Siegfried Fürtauer, Markus Schmid and Cordt Zollfrank¹¹²

J. Appl. Polym. Sci. **2022**, 139(37), e52794. <https://doi.org/10.1002/app.52794>

Former studies showed that homogeneous, single-phase blends of cellulose and polylactic acid (PLA) can be prepared using a solution-precipitation process with ionic liquids. Material characterization and possible applications for this material have not been investigated further based on the small lab scale applied. This study demonstrates that an efficient blending between PLA and cellulose can be achieved by a continuous extrusion process using only small amounts of solvent as an intermediate compatibilizer. First, a cellulose gel was prepared by extrusion of microcrystalline cellulose (MCC) with an IL and a co-solvent, namely 1-ethyl-3-methylimidazolium acetate and dimethyl sulfoxide. Cellulose gels with 40 wt% cellulose showed viscosities comparable to the PLA melt at applied processing temperatures, enabling efficient mixing during compounding. The resulting PLA/cellulose gel blends were thermoformable into films by compression molding. After IL and co-solvent extraction, transparent films showed a homogeneous morphology with only minor cellulose particle inclusions, and intense polymer interactions in the main phase were concluded from FTIR and DSC analysis. Those results were nearly similar to those obtained from the blends prepared from dilute solutions in earlier studies. The cellulose blend of 40 wt% gels compounded at 150 °C showed strength and elongation of 37 MPa and 1.34%, respectively, comparable to a heterophase PLA/MCC composite and pure PLA. Blends prepared from gel concentrations of 35 and 45 wt% cellulose, however, showed higher levels of cellulose inclusions and, as a result, high brittleness and poor mechanical strength. At the same time, severe polymer degradation was observed for the cellulose blends. PLA in the cellulose blend of 40 wt% gels compounded at 150 °C had a molecular weight of only 24 kg·mol⁻¹, while the composite had 53 kg·mol⁻¹. In addition, the IL degradation products led to impurities, which can further reduce the strength and elongation. Other blend samples also showed similar levels of PLA degradation, with the influence of IL concentration being more pronounced than the influence of processing temperature or Soxhlet extraction.

Author contributions: Kerstin Müller developed the design of experiments, the concept for the manuscript and wrote the manuscript. Siegfried Fürtauer helped with the evaluation of the FTIR results and contributed to the manuscript. Markus Schmid and Cordt Zollfrank revised the manuscript.



Received: 24 February 2022 | Revised: 20 June 2022 | Accepted: 25 June 2022

DOI: 10.1002/app.52794

RESEARCH ARTICLE

Applied Polymer
SCIENCE WILEY

Cellulose blends from gel extrusion and compounding with polylactic acid

Kerstin Müller^{1,2} | Siegfried Fürtauer² | Markus Schmid³ | Cordt Zollfrank¹

¹Chair for Biogenic Polymers, Technische Universität München, Campus Straubing for Biotechnology and Sustainability, Straubing, Germany

²Materials Development, Fraunhofer Institute for Process Engineering and Packaging IVV, Freising, Germany

³Faculty of Life Sciences, Albstadt-Sigmaringen University, Sustainable Packaging Institute SPI, Sigmaringen, Germany

Correspondence

Kerstin Müller, Materials Development, Fraunhofer Institute for Process Engineering and Packaging IVV, Giggenhauser Str. 35, 85354 Freising, Germany.
Email: kerstin.mueller@ivv.fraunhofer.de

Abstract

Cellulose, dissolved in ionic liquids (IL), can be used successfully in the processing of thermoplastics. To recover the ionic liquid while maintaining the thermoplastic properties, other spacers than IL might be introduced into the cellulose network. Such blend materials have been prepared before by solution blending as reported in the literature. In this study, the preparation and investigation of cellulose and polylactic acid (PLA) blends using an extrusion process with an ionic liquid and co-solvent for intermediate compatibilization is reported. The obtained transparent films show a homogeneous morphology without phase separation. Thermal analysis showed no separated glass transition for PLA, and FTIR showed hydrogen bonding between cellulose and PLA chains. Thermal stability of the blends with a degradation onset around 270°C lies between regenerated cellulose and pure PLA. The blend tensile strength and elongation of ~40 MPa and 1.3%, respectively, were comparable to a multi-phase composite containing twice the molecular weight of PLA. Generally, mechanical performance of the blends was strongly influenced by degradation reactions mainly caused by the ionic liquid used, as well as blend morphology. The study shows that transfer from solution to extrusion processing is generally possible to obtain novel cellulose blends.

KEYWORDS

biopolymers and renewable polymers, blends, cellulose and other wood products, extrusion, ionic liquids

1 | INTRODUCTION

The idea of using cellulose in thermoplastic processing has been an ever-present topic in material research for a century. The combination of cellulose and polylactic acid (PLA) in green composites is a current topic in this context and could replace fossil materials in various applications.^{1–5} Apart from using cellulose as a filler in thermoplastic matrices, only few attempts with

regard to thermoplastic processing of cellulose as a matrix have been reported so far. In addition to dry processes using high shear and pressure,^{6,7} the plastic deformation of cellulose has been studied mainly in wet processes. Cellulose hydrogels derived from solution-precipitation process were dried and subsequently hot-pressed, both changing crystallinity and structural orientation of the cellulose.⁸ Recently, pectin, a gel-forming and non-melting polysaccharide, was

This is an open access article under the terms of the [Creative Commons Attribution](https://creativecommons.org/licenses/by/4.0/) License, which permits use, distribution and reproduction in any medium, provided the original work is properly cited.

© 2022 The Authors. *Journal of Applied Polymer Science* published by Wiley Periodicals LLC.

successfully molded by thermo-compression to semi-transparent films using the natural deep eutectic solvent or its components glycerin and choline chloride as plasticizers.⁹ Regarding wet processing of cellulose, several imidazolium-based ionic liquids (IL) proved to be efficient solvents for cellulose.¹⁰ At higher cellulose concentrations, so called ionogels have shown potential in medicine, energy storage, or electrochemistry¹¹ as well as composite materials.¹² In this context, the influence of ILs has been investigated not only for cellulose, but also for other polymer composites.¹³ Recently, cellulose films via the solution-precipitation method were produced with different contents of residual IL.¹⁴ 1-Butyl-3-methylimidazolium chloride clearly acted as a plasticizer and thermomechanical processing was possible. This study also concluded that 40% residual IL was optimum to enhance mechanical properties in terms of tensile strength and elongation.¹⁴ Due to the ecological and economic disadvantages associated with IL, the use of ILs in technical applications is still limited.^{15,16} Biodegradability and ecotoxicity can be adjusted based on the combination of cation, anion and alkyl side chain moieties.¹⁵ From a technical point of view, high viscosity¹⁷ is a critical processing factor, but can be effectively reduced by the use of co-solvents.^{18,19} In addition, IL are not always innocent solvents in terms of degradation reactions, especially when combined with cellulose at elevated temperatures.²⁰ Ionic liquids are generally several times more expensive than conventional molecular solvents, which is due to the production and especially the purification costs. Therefore, this study aims to use the IL only as an intermediate solvent to enable cellulose chain availability and introduce other polymeric spacers into the cellulose network, but is extracted from the final material. Among the blends with other synthetic polymers that have been described before,^{21–23} PLA seemed to be a good blending partner for cellulose by means of compatibility. Attempts to use IL and PLA resulted in homogeneous, transparent and soil degradable blends, either by solution blending^{21,24} or via welding of cellulose nanofibers and PLA.²⁵ To the authors' knowledge, however, there have been no production trials on a technical scale to investigate potential applications to date, as most studies with IL have been conducted on a laboratory scale with a material output of a few grams. The main objective of this work was therefore to investigate whether the manufacturing process of homogeneous PLA/cellulose blends can be transferred from solution to extrusion, as this would allow easy upscaling with a material output in the kilogram range. Another question to be answered in this study is to what extent the properties of these new blends are

comparable to the properties of state-of-the-art composites using cellulose as filler.

The study presents the following process as an innovative idea for larger scale preparation: A cellulose gel is prepared by extrusion of microcrystalline cellulose (MCC) with an IL and a co-solvent, namely 1-ethyl-3-methylimidazolium acetate (EmimAc) and dimethyl sulfoxide (DMSO). In the second step, the cellulose gels are compounded with a PLA melt without further use of a solvent. The blend can be thermoplastically molded and the solvents recovered.

2 | METHODOLOGY

2.1 | Materials

MCC Parmcel 101 from wood pulp was purchased from Gustav Parmentier (Steinfurt, Germany) with a degree of polymerization (DP) of 310.²³ PLA Luminy® LX930 was purchased from Total Corbion PLA (Gorinchem, The Netherlands). This PLA grade is amorphous based on a D-isomer content of 8%. EmimAc (purity ≥98%) and DMSO (purity ≥99.5%) were received from proionic (Raaba-Grambach, Austria) and Merck (Darmstadt, Germany). Microcrystalline cellulose and PLA were dried at 60°C and 40°C, respectively, for at least 12 h prior to processing. Ethanol (purity = 99%) and hexafluoroisopropanol (HFIP; purity ≥99%) were purchased from Staub & Co.-Silbermann GmbH (Gablingen, Germany) and abcr GmbH (Karlsruhe, Germany), respectively.

2.2 | Blend preparation

Preparation of homogeneous PLA/cellulose blends was divided into three main processing steps. Figure 1 illustrates the mechanisms and interactions of the components during the preparation process.

2.2.1 | Cellulose gel extrusion

The cellulose gel formulations were extruded using a Haake Rheocord with Rheomex PTW 16 co-rotating twin screw extruder (Thermo Fisher Scientific, Karlsruhe, Germany) with a barrel diameter of 16 mm and a length-to-diameter ratio of 25. EmimAc was used as the cellulose solvent, and DMSO was added as a co-solvent to lower the viscosity, enabling stable solvent pumping and wetting of the cellulose. The ratio between EmimAc and DMSO was set to 4:1 by volume. Liquid feeding was performed with an Ecom Alpha

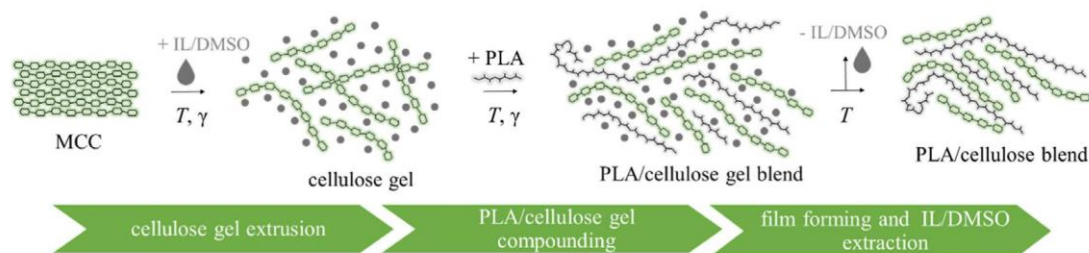


FIGURE 1 Schematic of the blend formation divided in three processing steps and the respective intermediates [Color figure can be viewed at wileyonlinelibrary.com]

50 Plus isocratic pump (Ecom spol. s r.o., Prague, Czech Republic) and took place in the second zone of the extruder. Solid feeding (MCC) took place with a gravimetric twin-screw feeder on a scale platform (K-Tron AG, Niederlenz, Switzerland) in the first zone of the extruder. Continuous cellulose gel strands were extruded at different cellulose concentrations, namely 35 wt% (EX35), 40 wt% (EX40) and 45 wt% (EX45) cellulose (relative to the EmimAc content). The screw speed was 150 rpm with a barrel temperature profile of 20–60–60–80–90 (°C). The screw configuration was divided into a conveying zone, where also the liquid feed took place, a kneading block zone and a compression zone with a reverse conveying element. The extrudates were pelletized using a CSG 171 T strand pelletizer (Dr. Collin GmbH, Ebersberg, Germany). Approximately, 500 gram pellets per gel sample were stored in a polyethylene bag at room temperature for 2 weeks before the next compounding step.

2.2.2 | PLA/cellulose gel compounding

Blends with PLA with a target concentration of PLA/cellulose = 1:1 were compounded with EX35 (compound C35), EX40 (compound C40) and EX45 (compound C45) cellulose gels at 100 rpm in a co-rotating twin screw extruder ZK 27 T × 24 D (Dr. Collin GmbH, Ebersberg, Germany) with length to diameter ratio of 24. Both cellulose gel and PLA granules were predried at 60°C and 40°C, respectively, and manually mixed with their respective weight contents. The seven heating zones varied depending on the compound, but each started at room temperature at the pellet feeder. Ambient degassing was performed in zones 4 and 5 to eliminate evaporating moisture and DMSO. Table 1 shows the applied blend concentrations and extrusion parameters. The screw configuration was composed of alternating conveying, kneading and compression elements as shown in the supporting information (Figure S2). Due to the usual variations in material dosage and ratios when mixing two different solids, as well as the relatively low throughput,

the compounding parameters fluctuate around a certain optimum. Therefore, the averaged samples were selected only within the ranges of melt temperature and die pressure given in Table 1.

The different compositions should show the influence of the cellulose concentration in the cellulose gel on the final blend. Thus, it can be evaluated how high the cellulose concentration may be to still achieve an efficient blend with PLA resulting in a single phase blend. Based on the rheological measurements of the gels and PLA, different temperatures were applied to determine if efficient mixing is possible at temperatures lower than the expected softening points of the cellulose gels due to the higher shear in the compounder.

For comparison, pure PLA LX930 and a PLA/MCC microcomposite (1:1) were also compounded at 170°C.

2.2.3 | Film forming and extraction

To investigate thermomechanical deformability of the blends, plates were prepared using a heatable hydraulic press (Perkin Elmer, Shelton, CT, USA) at a temperature of 150 °C for 2 min with a load of 2 tons. The films were cut into strips, and the EmimAc/DMSO were extracted from the film strips with ethanol in a soxhlet apparatus for at least 12 h prior to drying in a vacuum cabinet at 90 °C and 40 mbar. For comparison, pure PLA and the PLA/MCC composite were treated the same way. Final film thicknesses ranged from 130 to 170 μm depending on the sample.

2.3 | Analytics

2.3.1 | Rheological analysis

Rheological behavior of the cellulose gels and PLA were examined using a closed cavity rheometer RPA elite (TA Instruments, New Castle, DE, USA). Time sweeps ($T = 150^{\circ}\text{C}$) and strain sweeps were performed prior to temperature and frequency sweeps to ensure thermal

TABLE 1 Applied concentrations and extrusion parameters of PLA/cellulose gel blends

Sample	Mass temperature (°C)	Die pressure (bar)	Cellulose concentration in gel rel. to IL (wt%)	Cellulose gel: PLA ratio (wt/wt)	EmimAc: PLA ratio (wt/wt)	EmimAc: PLA ratio (mol/mol)	Cellulose: PLA ratio (wt/wt)
C35_130 °C	131–134	13–21	35	3.08/1 (~9/3)	~1.83/1	~0.78/1	1/1
C35_150 °C	151–155	10–16					
C40_130 °C	130–135	11–16	40	2.67/1 (~8/3)	~1.48/1	~0.63/1	1/1
C40_150 °C	147–152	10–12					
C45_150 °C	145–152	11–14	45	2.35/1 (~7/3)	~1.20/1	~0.51/1	1/1
C45_170 °C	162–171	5–10					

stability and determine the linear viscoelastic range, respectively. About 5–10 g of the gel sample was placed between two polyamide films and loaded between the two cones in the apparatus, where the sample was pressed at 150 °C. Temperature sweeps from 50 to 175 °C were performed at constant angular frequency $\omega = 1$ Hz, a strain $\gamma = 1\%$ and a heating rate of 20 K min⁻¹. Frequency sweeps from 0.1–50 Hz were performed at constant strain $\gamma = 1\%$ and temperature $T = 150$ °C.

2.3.2 | Thermal analysis

Thermal analysis of the films by means of differential scanning calorimetry was performed on a Mettler Toledo DSC3+ (Gießen, Germany) and the corresponding evaluation software STARe Version 16.20. The first heating run from 25 °C to 120 °C, followed by 10 min at 120 °C, was used to eliminate residual moisture. After cooling to 0 °C, the second heating run was performed to 450 °C with a heating/cooling rate of 15 K·min⁻¹. A Linseis STA PT 1600 (Selb, Germany) was used for simultaneous thermogravimetric analysis (TGA) and differential thermal analysis (DTA). Samples were heated from room temperature to 600 °C with a heating rate of 15 K·min⁻¹ under nitrogen atmosphere. Sample weights for thermal analysis ranged from 10 to 15 mg.

2.3.3 | Mechanical testing

Mechanical properties of the films were determined using a tensile testing machine Z005 (Allround Line) of Zwick GmbH & Co. KG (Ulm, Germany). Tests were performed with a clamping length of 25 mm at a test speed of 200 mm min⁻¹ with a load shut-off at 95%. Minimum five replicates were tested for each sample, with the exception of C45_150 °C, where only two determinations were possible due to the extreme brittleness of the sample, which led to material breakage during preparation

and measurement. OriginPro Version 2018b (Origin Lab Co., Northampton, MA, USA) was used for statistical analysis. A one-way ANOVA was performed. Homogeneity of variances was checked with Brown-Forsythe test. If the effect was significant, we compared multiple means with a post-hoc Tukey test ($p < 0.05$).

2.3.4 | Scanning electron microscopy

Film morphology was examined by scanning electron microscopy (SEM). Pieces of the pressed and extracted films were cryo-fractured to investigate the fracture surface. Cryo-fracturing creates coarse surfaces, prohibiting differentiation between the constituent phases. A complicating factor is that the blend partners are quite similar in their chemical composition and therefore no material differences can be detected on the basis of an SEM image. To determine the blend morphology in this work, one fracture side was treated with HFIP to etch its surface by partial dissolution of PLA. Etched samples were air-dried for a minimum of 48 h to evaporate residual HFIP and sputtered with gold. Prepared samples were examined with a JEOL 7200F scanning electron microscope with a lower electron detector (JEOL, Freising, Germany). Images were taken at an accelerating voltage of 3.0 kV.

2.3.5 | Infrared spectroscopy

FTIR spectra of the films were recorded on a Frontier™ FTIR spectrometer L1280034 using the Spectrum IR software, version 10.6.1, both supplied by Perkin Elmer (Shelton, CT, USA). Measurements were performed at an ambient temperature and pressure. An attenuated total reflectance device was used (Golden Gate™, Specac Ltd., Oprington, UK). A constant contact pressure was achieved by tightening the securing screw with a ratchet limited to a torque of 30 cNm. A total of 16 scans were

recorded within a wavenumber range from 4000 to 600 cm^{-1} with a resolution of 4 cm^{-1} .

2.3.6 | Molecular weight determination

Molecular mass distribution of PLA, PLA/MCC composite and the blends was determined via size exclusion chromatography (SEC) using a Dionex System with HFIP and 0.02 mol L^{-1} trifluoroacetic acid as solvent. A DIONEX Ultimate 3000 injector was used, and the flow rate was fixed to 1 ml min^{-1} (HPLC gradient pump Gynkotek M480). Detection was performed with a refractive index detector Gynkotek SE-61. PSS-PFG columns, tempered to 40 °C, were used (PSS, Mainz, Germany: 7 μm , 300 \times 8 mm). Samples were dissolved in HFIP with a concentration of 5000 $\mu\text{g ml}^{-1}$ and filtered with a 0.20 μm PTFE membrane. For the blends, samples were milled with an Ultra Centrifugal Mill ZM 200 (Retsch GmbH, Haan, Germany) and extracted in HFIP for 48 h at room temperature to be able to extract as much PLA as possible. An amount of 40 μl was injected (DIONEX ASI-100). A narrow molecular weight distribution PMMA standard (PSS Mainz, Germany) was used as calibration. The curves were examined with the WinGPC[®]UniChrom (Version 8.1) Software (PSS, Mainz, Germany).

Cellulose degradation during extrusion and storage was exemplarily determined with EX40. The gel was precipitated, soxhlet-extracted with ethanol for at least 12 h to remove EmimAc/DMSO, dried in a vacuum cabinet at 90 °C and 40 mbar and grinded with an Ultra Centrifugal Mill ZM 200 (Retsch GmbH, Haan, Germany). The DP was calculated on the basis of intrinsic viscosities following ISO 5351 as well as Kes and Christensen.²⁶

3 | RESULTS AND DISCUSSION

3.1 | Cellulose gel

3.1.1 | Cellulose gel extrusion

Cellulose gels EX35, EX40 and EX45 with high contents of MCC were produced in a continuous extrusion process with EmimAc, chosen based on its high dissolution capacity for cellulose,²⁷ and DMSO. The addition of co-solvent was necessary to lower the solvent viscosity, enabling a stable liquid feed and wetting of the MCC. Since there must be sufficient solidification when the gel strand cools, however, the concentration of the co-solvent was set at 20 vol% after preliminary tests. The gel extrusion step is crucial to increase the availability of the cellulose molecular chains prior the following mixing steps with PLA. Although for dissolution (characterized by

solvent diffusion and chain entanglement) maximum cellulose concentrations in the EmimAc/DMSO system were assumed to be around 25–27 wt%,²⁸ chain availability is also possible at higher ratios based on plasticization and swelling of the polymer.²⁹ However, this clearly depends on the transport processes of the solvent, which are in our case also determined by extrusion parameters such as shear and temperature. Based on known interactions between EmimAc and cellulose,³⁰ extrusion temperatures were kept <100 °C to avoid undesired degradation. Still, the DP of the cellulose gels after storage prior to the next compounding step was 270, which correlated to a decrease of ~13% compared to the untreated MCC powder (DP = 310).

3.1.2 | Optical properties

Extruded gels showed inclusion of gas bubbles, which are expected to originate from residual water that could not be removed during predrying or was re-adsorbed during processing. Therefore, some prepared strands still looked opaque after cooling down to room temperature, although transparency was apparent when exiting the die. Strands were coherent at 35 and 40 wt% cellulose. At 45 wt%, the extruded strand broke off at regular intervals and small Microcrystalline cellulose particles were still visible (Figure S1a–c). Therefore, at this cellulose concentration only partial cellulose dissolution or swelling was expected.

3.1.3 | Rheological properties

Cellulose gel strands were granulated and viscoelastic properties were determined using a closed cavity rheometer. Based on the following compounding step, viscosities at certain temperatures and shear rates were of certain interest, since a flow behavior close to that of the PLA was desired for efficient mixing at extrusion conditions.

Temperature sweeps for the extruded gels (Figure 2a) showed solid-like behavior ($G' > G''$) over a wide temperature range for all samples. Unfortunately, the expected cross-over or gel point lies below the resolution limit of the device used. Still, the gel point for EX35 and EX40 are expected to be around 150 °C and 170 °C, respectively. For the PLA, measurements show a glass transition around 60 °C and a flow point at 126 °C, which is in line with the manufacturer's data. All gels show a softening with increasing temperature, which can be deduced from the decreasing difference between G' and G'' .

However, only very low shear was applied for the temperature sweeps. To investigate shear dependence, a frequency sweep was performed at 150 °C (Figure 2b). This temperature was chosen as low as possible to

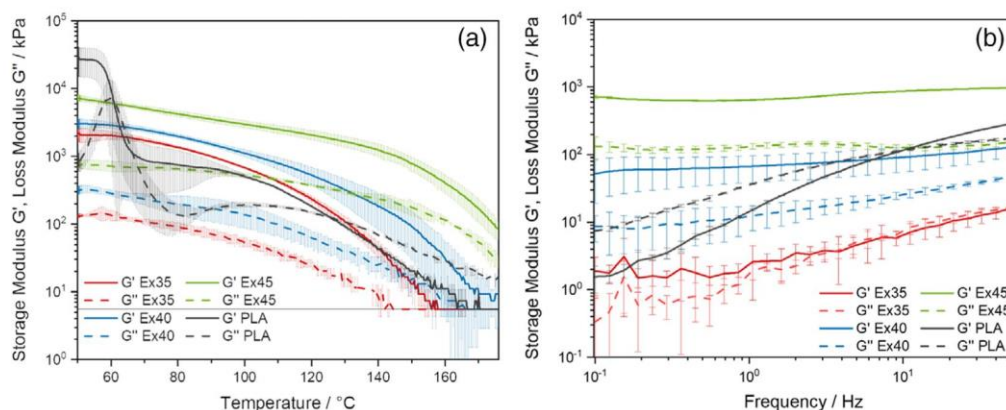


FIGURE 2 (a) Temperature sweep and (b) frequency sweep at 150 °C of the cellulose gels EX35 (red), EX40 (blue) and EX45 (green) and PLA LX930 (black) showing storage modulus G' (solid line) and loss modulus G'' (dashed line). The horizontal line depicts the resolution limit of the device during temperature sweep [Color figure can be viewed at wileyonlinelibrary.com]

prevent decomposition, but as high as necessary to allow the gels and the PLA to flow.

As already expected from the temperature sweep, EX35 has its flow point around 150 °C, leading to fluctuations between G' and G'' . For both other samples, a maximum frequency of 50 Hz equivalent to a shear rate of 3.068 s^{-1} still represents too little shear to induce flowing. We estimate the average shear rate during our extrusion process to be about 100 s^{-1} ,³¹ which makes flowing of the cellulose gels likely also below 150 °C.

To be able to estimate the flow behavior at such high shear rates, flow curves can usually be modeled based on the Cox–Merz rule,³² stating that the complex dynamic viscosity as a function of frequency is consistent with the shear viscosity as a function of shear rate in the non-Newtonian flow regime. However, this empirical rule is only applicable in the absence of energetic interactions (e.g. hydrogen bonding, dipole–dipole interactions),³³ leading to high deviations for polysaccharide gels.³⁴ Therefore, a prediction for the apparent viscosities extrusion temperature and shear rates was not possible based on the performed oscillatory tests.

Since EX40 and EX45 are not actually flowing within the linear viscoelastic range (LVE range) at the applied shear and temperature, it is also not practicable to present the viscosity curves.³⁵ However, to be able to compare all samples and to roughly estimate the flow behavior of the different materials, flow curves of all samples are shown in Figure 3. Both the temperature and frequency sweep show that the viscosity of EX35 is far below the PLA melt, which could lead to difficulties in mixing. Although not flowing, EX40 shows complex viscosities closest to the PLA around and above the 150 °C, while EX45 always displays a higher complex viscosity.

3.2 | Cellulose gel/PLA blends and film forming

Preliminary trials using different amorphous and semi-crystalline PLA grades showed that apparent viscosities of the gels and PLA melt should match within the extrusion process to enable efficient mixing (exemplary pictures see Figure S1d and e). Since both components need to flow, temperatures of minimum 130 °C (flow point of PLA) had to be applied. However, higher temperatures results in unwanted degradation reactions, therefore, temperatures were limited to 170 °C. Blend samples at two different processing temperatures were produced with each cellulose gel. Sample labelling and description can be found in Table 1 in the experimental section.

Already optically visible, higher temperatures led to higher coloring and darkening of the samples (Figure S3). For the highest applied temperatures of 170 °C, dark brown and sticky samples were obtained. Imidazole-based ILs are temperature-sensitive and tend to form high-boiling impurities like chromophores and reactive by-products,³⁶ leading to yellow-to-brown coloring²⁰ and also possible degradation of the cellulose^{37,38} as well as degradation of the PLA,³⁹ which will be discussed later. Primarily based on the solvent content, blends showed good thermoplastic behavior and were subsequently hot-pressed to films. Before further characterization, films and were soxhlet-extracted with ethanol for at least 12 h to guarantee sufficient IL and DMSO removal from the samples. This is an important step to be able to discuss the properties of binary PLA/cellulose mixtures, since otherwise the influence of the residual solvent would have to be taken into account.²⁴

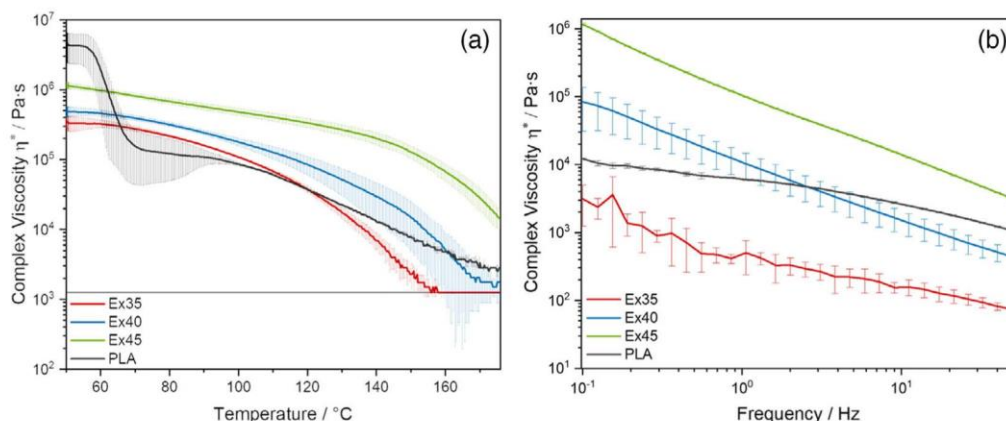


FIGURE 3 Flow curves from (a) temperature sweep and (b) frequency sweep at 150°C of the cellulose gels EX35 (red), EX40 (blue) and EX45 (green) and PLA LX930 (black). The horizontal line depicts the resolution limit of the device during temperature sweep [Color figure can be viewed at wileyonlinelibrary.com]

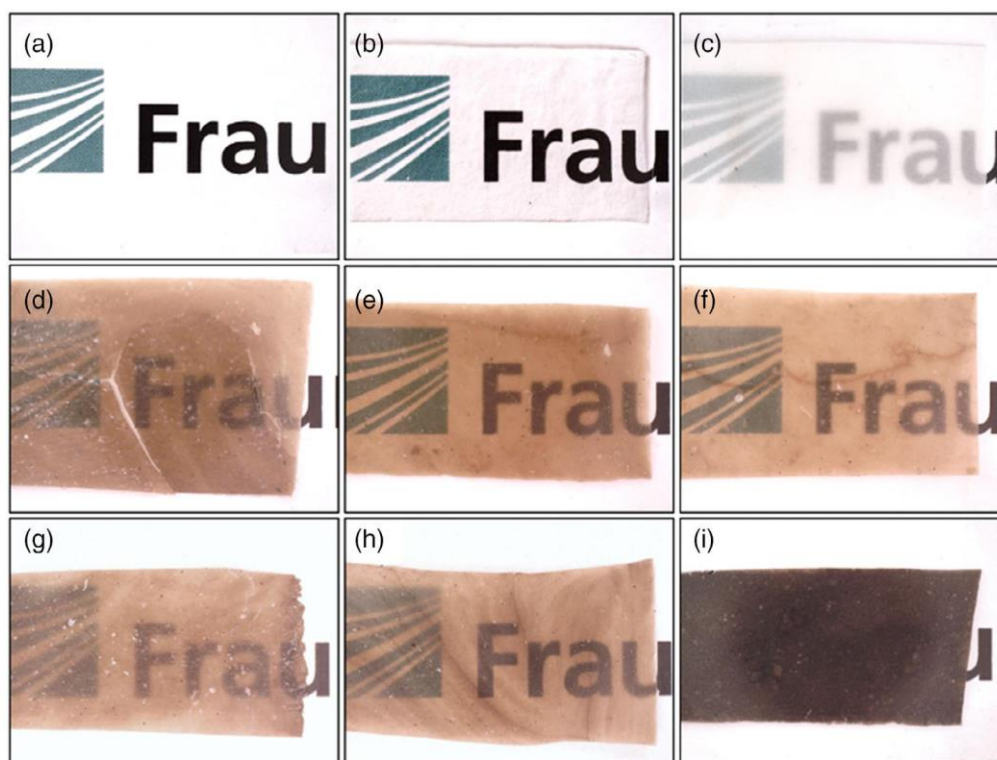


FIGURE 4 Transparency of blend films and references; (a) no film, (b) PLA, (c) PLA/MCC composite, (d) C35_130°C, (e) C40_130°C, (f) C45_150°C, (g) C35_150°C, (h) C40_150°C, and (i) C45_170°C [Color figure can be viewed at wileyonlinelibrary.com]

3.3 | Material properties of extracted blends

3.3.1 | Optical properties

Test strips were mainly transparent but showed a dark color most probably originating from degradation

products of the ionic liquid. Both the C35 and C45 samples showed macroscopically visible particle inclusions and were less flexible. The PLA/MCC microcomposite was more opaque at comparable film thicknesses around 160 μm .

The strong discoloration can be attributed to the formation of high-boiling impurities such as chromophores

in the ionic liquid during processing at higher temperatures.³⁶ Especially in EmimAc, side reactions occur at the C2-atom of imidazolium, with the formation of reactive carbenes.^{36,37} As a function of temperature, the intensity of discoloration increased with extrusion temperature, resulting in dark brown samples at extrusion temperatures of 170°C (Figure 4i).

Blend morphology was examined by SEM using cryo-fractured solvent-etched films (to remove the PLA component). Figure 5 shows the unetched and etched cross-sections of the blends, as well as a PLA/MCC microcomposite and the pure PLA for comparison.

All untreated blends contained small impurities that were most likely undissolved cellulose particles (marked with red circles). However, the size of these inclusions varied among the individual blends. Compared to the PLA/MCC microcomposite (Figure 5g) with particle sizes around 20 µm, cellulose inclusions of about 10 µm (C45, C35) or 2–4 µm (C40) were found. Etched samples showed a smoother surface, but with many cracks. The cellulosic inclusions remained after etching. It is assumed that the cracks originate from swelling of the samples during solvent treatment. When analyzed under high vacuum, the remaining solvent evaporates quickly, leaving the cracked surface.

Based on the limited solubility, high cellulose loads during gel extrusion prevented complete dissolution of the cellulose. Still, due to cellulose swelling, most of the cellulose molecular chains are easily available for further processing, as already investigated during extrusion of lignocellulosic biomass with EmimAc/DMSO.⁴⁰ As expected, crystallinity decreased with an increasing processing temperature and residence time, the latter caused by lower screw speeds.⁴⁰ In our samples, increasing processing temperature also led to a slightly better homogeneity regarding inclusions and general surface smoothness, mainly visible for the C40 samples (Figure S4).

3.3.2 | Structural and thermal properties

Former studies with two-phased composites already revealed that PLA and cellulose interact via hydrogen bonding, mainly concluded from the intensity and shifting of the carbonyl peak.^{41,42} All blends C35, C40, and C45 showed a mixed spectrum with typical bands that can be assigned to both PLA and cellulose (Figure 6). No differences were found between the processing temperatures of the respective blends.

The carbonyl group is one of the most important functional groups involved in the hydrogen bonding of PLA. The band associated with C=O stretching was

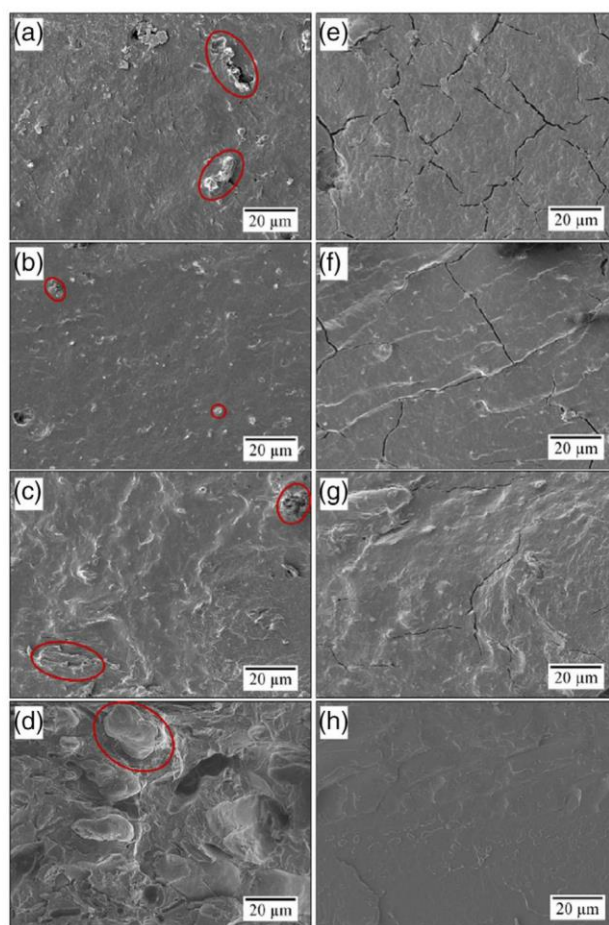


FIGURE 5 SEM images of cryo-fractured cross sections of PLA/cellulose blend films (a) C35_150°C, (b) C40_150°C and (c) C45_170°C and their etched counterparts (e) C35_150°C, (f) C40_150°C, and (g) C45_170°C; PLA/MCC microcomposite film (d) and PLA film (h) [Color figure can be viewed at wileyonlinelibrary.com]

1746 cm^{-1} for pure PLA and the composite, but shifted to $1736 \pm 1 \text{ cm}^{-1}$ for all blends (except C40_130°C). Assuming that efficient mixing allows the formation of hydrogen bonds between the C=O group and the cellulose, the results indicate that interactions between PLA and cellulose can occur down to the molecular level. However, at C40_130°C, the intermixing was not efficient enough to allow homogeneous distribution of the components. We assume that the processing temperature was too low to ensure sufficient flow of the cellulose gel EX40.

Interestingly, new absorption peaks occurred at 3692, 3619, and 796 cm^{-1} . Sharp peaks in the region between 3670 and 3550 cm^{-1} are usually assigned either to certain inorganic substances and minerals, where they are indicative of a 'free' OH-group either on the surface or within

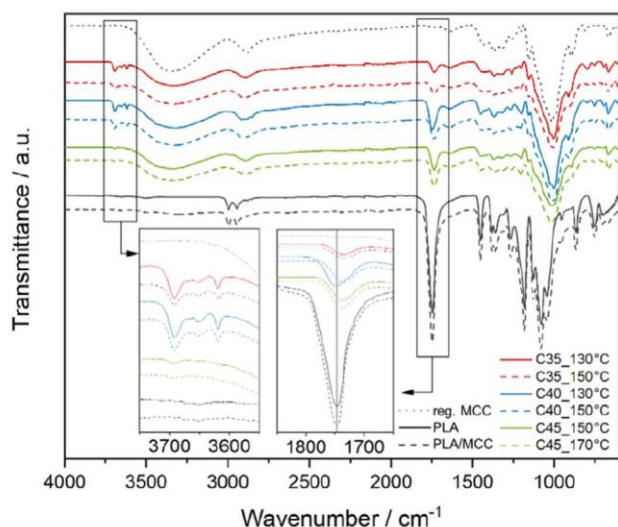


FIGURE 6 FTIR spectra of regenerated cellulose (gray pointed), C35 compounded at 130°C (red solid) and 150°C (red dashed); C40 compounded at 130°C (blue solid) and 150°C (blue dashed), C45 compounded at 150°C (green solid) and 170°C (green dashed), extruded PLA (black solid) and a PLA/MCC composite (black dashed) [Color figure can be viewed at wileyonlinelibrary.com]

a crystal lattice, or to alcohols or phenols with a sterically hindered hydroxyl group.⁴³

The latter may be explained by a higher amount of energy needed to interact with the mid-infrared radiation, since the fundamental vibrations are impeded. Possible structures that could be presented in the blends are reaction products from the cellulose itself or sugars derived from cellulose degradation reacting with the imidazolium. Comparable reactions of butylmethylimidazolium with glucopyranose and cellulose at its reducing end, respectively, have been described by Ebner et al.³⁷ The peaks were most pronounced in the C35 and C40 samples, which would support the described reaction due to their higher IL content. The other small peak at 796 cm^{-1} may be assigned to the C=O from PLA oligomers,⁴⁴ which also fits the DSC results shown later.

Degradation of the PLA was investigated using relative SEC measurements to determine the molecular weight distribution (Figure 7) and calculated molecular weight averages (Table S1). Please note that for SEC measurement of the PLA content in the blend, the entire PLA fraction must be dissolved or extracted from the blend. Since most PLA chains, which form a dense, amorphous network with the cellulose, are presumably trapped between the rigid cellulose chains, even ground samples are likely to have non-extractable PLA chains that are not accounted for in the analysis presented. Mass balancing (after grinding and extraction in HFIP for 5 d)

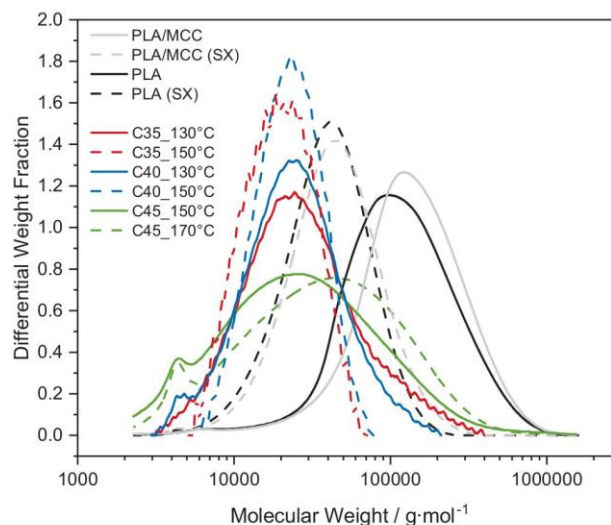


FIGURE 7 Molecular mass distribution of PLA from soxhlet extracted blends C35 compounded at 130°C (red solid) and 150°C (red dashed); C40 compounded at 130°C (blue solid) and 150°C (blue dashed), C45 compounded at 150°C (green solid) and 170°C (green dashed), extruded PLA (black solid) and a PLA/MCC composite (gray solid) and soxhlet treated PLA (black dashed) and PLA/MCC composite (gray dashed) [Color figure can be viewed at wileyonlinelibrary.com]

showed that on average only 10 wt% PLA was extracted from the blends with HFIP, while the residue showed the similar IR to the input materials (no change in carbonyl band). These results, on the one hand, make the SEC analytics of the blend unrepresentative, but on the other hand, confirm the largely homogeneous morphology of the blends. Although this means that absolute values for the blends are strongly erroneous, a comparison within the blend samples still seems reasonable.

Poly(lactic acid) as a polyester is sensitive to hydrolysis and thermal degradation.^{45,46} Two different factors are considered within our process: (a) extrusion and storage in the presence of basic IL at different temperatures and (b) soxhlet extraction with ethanol. Regarding the latter, even with small amounts of residual water, PLA hydrolytic degradation occurs in the environment of ethanol.⁴⁷ During soxhlet extraction, elevated temperatures are applied, which might lead to an intensification of the reaction. For the pure PLA and the PLA/MCC composite samples, soxhlet extraction highly decreased their M_w from approximately 160 $\text{kg}\cdot\text{mol}^{-1}$ to 50 $\text{kg}\cdot\text{mol}^{-1}$ with a slightly narrower distribution.

The gel blends and the extracted blends were measured at the same time, that is, the gels had already been stored for several weeks at ambient conditions. Comparing the gel blends to the extracted blends, it can be assumed that the entire PLA fraction is dissolved. All gel

samples showed substantial degradation of PLA down to M_w between 23 and 50 kg·mol⁻¹ (Figure S5). Therefore, it may be assumed that storage time was accompanied by further degradation (also visible with repeated measurements between 4 weeks, data not shown). For the extracted samples showing similar M_w , we suggest that the soxhlet treatment is not the main factor for PLA degradation in the blends. We suppose that rather degradation reactions caused by the IL are dominant.

Depending on temperature and exposure time, the basic imidazolium acetate can cause a strong decomposition of PLA. The increase of the PLA degradation correlates with the increase of the IL concentration. The highest degradation rate was found between 130 °C and 150 °C for 1-octyl-3-methylimidazolium acetate.³⁹ In EmimAc, PLA was found to degrade up to almost 50% at a molar ratio of 1:1 (PLA:IL) at 150 °C for 1 h.³⁹ However, less IL is present in our extruded samples (molar ratio ~ 1.3–1.9:1). Moreover, most of the IL is not freely available because of the interaction with cellulose, and the reaction time in the extruder is much shorter, about 10 min. Nevertheless, the M_w of the extracted blends ranged from 24 to 62 kg·mol⁻¹. For high EmimAc concentrations (C35, C40), higher extrusion temperatures lead to more degradation. This effect was not visible for the C45 samples. These samples showed in addition to the broad peak a small peak in the range around 4.5 kg·mol⁻¹.

DSC thermograms of the C35–45 samples showed no typical glass transition as expected for PLA (Figure 8). We previously discussed the absence of its T_g in solution-blended samples.²⁴ In a polymer blend with separate phases of the blend partners, two separate glass transitions are present. In a miscible system, only one transition can be detected, which lies between the transitions of the individual components, depending on the concentration of the polymers.⁴⁸ Very low degrees of phase separation, on the other hand, have been associated with a very broad T_g value between those of the pure components,⁴⁹ which may not be clearly determined by DSC. Based on the thermograms and our previous results, we assume an interpenetrating polymer network of PLA and cellulose with a small share of microphase-separated amorphous regions.

Interestingly, an endothermic thermal event around 108 °C occurred for the C35 (130 and 150 °C) and C40 (130 °C) samples. Since this was determined for the second heating run and this event was already visible in the cooling run, it can be attributed to melting/crystallization of a polymer structure rather than water or solvent evaporation. One possible explanation could be the crystallization of PLA oligomers. Although we used an amorphous grade with a D-isomer content of 8%, which hinders crystallization of PLLA chains, PLA degradation

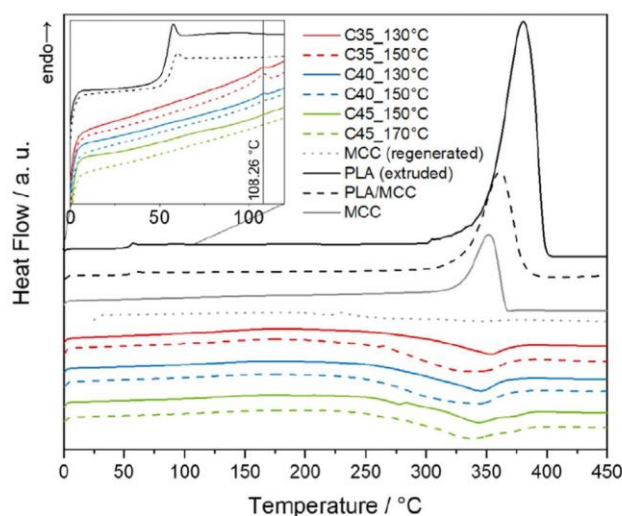


FIGURE 8 DSC thermograms of regenerated cellulose (gray pointed), microcrystalline cellulose (MCC, gray), C35 compounded at 130 °C (red solid) and 150 °C (red dashed); C40 compounded at 130 °C (blue solid) and 150 °C (blue dashed), C45 compounded at 150 °C (green solid) and 170 °C (green dashed), extruded PLA (black solid) and a PLA/MCC composite (black dashed) from the second heating run [Color figure can be viewed at wileyonlinelibrary.com]

might have resulted in oligomers with relatively few or no D-isomers. In addition, swelling of the samples during soxhlet extraction may have promoted rearrangement of the polymer chains and subsequent crystallization.^{47,50} Comparable PLA oligomers with DP < 10 showed melting points in the same temperature range around 110 °C.^{44,51}

The thermal stability of the blends and material components was investigated by means of TGA coupled with DTA (Figure 9). Usually, weight reduction occurs first due to the loss of contained moisture, followed by massive weight reduction due to thermal degradation. Cellulose, based on its chemical composition, can absorb much more water from the atmosphere than PLA,^{52–56} therefore, the moisture loss of PLA and its composite was the lowest. Both showed an onset of degradation at ~316 °C, while the degradation of MCC started around 304 °C. In general, regenerated cellulose shows lower degradation temperatures than native cellulose^{57–59} with an onset of ~218 °C, also due to its low crystallinity from ethanol precipitation.⁶⁰ For the blends, thermal stability increased compared to regenerated cellulose, while it decreased compared to MCC, PLA, and their composite.

For regenerated cellulose and blends, the degradation is clearly divided into two main steps with a plateau in between. The first step (I) is accompanied by a broad endothermic event, presumably due to breakage of long

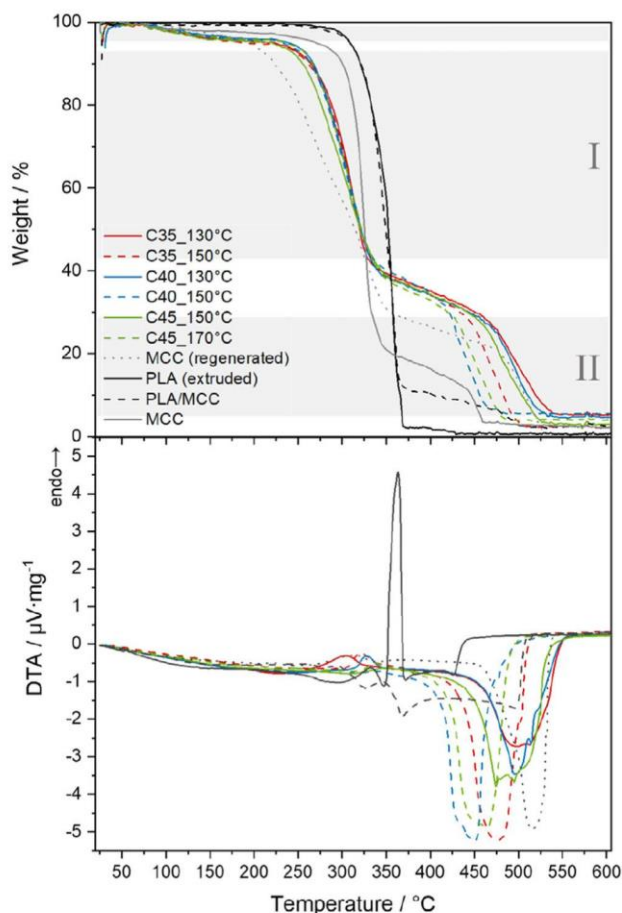


FIGURE 9 Thermogravimetric analysis and DTA thermograms of regenerated cellulose (gray pointed), MCC (gray), C35 compounded at 130°C (red solid) and 150°C (red dashed); C40 compounded at 130°C (blue solid) and 150°C (blue dashed), C45 compounded at 150°C (green solid) and 170°C (green dashed), extruded PLA (black solid) and a PLA/MCC composite (black dashed) [Color figure can be viewed at wileyonlinelibrary.com]

polysaccharide chains, as was already suggested for starch materials.⁶¹ The second degradation step (II) at temperatures of 420–540°C is caused by pyranose ring opening of the glucose units, as was previously proposed for starch and cellulose acetate, although the steps were not as pronounced as in our samples.^{61,62}

In this second step, differences between the blends become visible with regard to their processing temperatures. While lower extrusion temperatures resulted in higher stability, all blends compounded at higher temperatures (dashed lines) showed faster degradation. Since cellulose degradation already occurred during extrusion temperatures and is a function of temperature,^{30,63} the glucose concentration increases much faster, and therefore pyrolysis starts earlier. Additionally, the pyrolysis

temperature depends on the crystallinity of a substance.⁵⁹ Since the blends are expected to be completely amorphous in the mixed areas,²⁴ the second steps start way before the regenerated cellulose.

PLA and its composite shows highest thermal stability, with a degradation onset at ~316 °C, accompanied by a large endothermic peak and severe weight loss due to lactic acid evaporation. Although all blends are composed of 50 wt% PLA, no such endothermic peak was detected during DSC measurement. Therefore, the evaporation of lactic acid could be much slower than that of the PLA-only samples because the PLA chains are entrapped in the cellulose network.

3.3.3 | Mechanical properties of pressed films

Most of the extracted blends were extremely brittle. As a result, the C35 specimens could not be cut to the required dimensions, and other specimens broke during specimen preparation or specimen clamping, resulting in a reduced number of replicates (C45_150°C).

Compared to a microcomposite, a homogeneous polymer blend is expected to have higher mechanical performance in terms of tensile strength and elongation due to better load transfer between the compatible phases. In terms of modulus of elasticity, which is measured in the elastic range at very low loads, load transfer is of less importance; rather, the stiffness of the individual phases determines the stiffness of the material. Therefore, a microcomposite reinforced with crystalline cellulose is expected to have a higher modulus than the amorphous blend. Regarding the modulus, our samples showed the expected behavior (Figure 10). No significant differences were found between the blends, and both the blends and the composite exhibited higher modulus than the pure PLA (ANOVA: $F_{6,28} = 13.66$; $p = 3.36 \cdot 10^{-7}$, and $R^2 = 0.74$). Reinforced PLA with MCC exhibited higher moduli with increasing MCC content.⁶⁴ Absolute values for the Young's modulus of injection molded PLA and a PLA/MCC (1:1) microcomposite of ~2500 MPa are comparable to our data.⁶⁵ Although not significant for all blend samples, the microcomposite in this study showed slightly higher stiffness of 42 MPa⁶⁵ than our samples, probably due to their higher crystallinity the MCC and PLA type used.

For the other two mechanical key values, the measurements deviated from expectations and showed significantly lower or the same values as the composite (tensile strength: $F_{6,28} = 35.93$, $p = 6.61 \cdot 10^{-12}$, and $R^2 = 0.89$; elongation at break: $F_{6,28} = 87.66$, $p = 7.73 \cdot 10^{-17}$, and $R^2 = 0.95$). Within the blends, tensile strength and

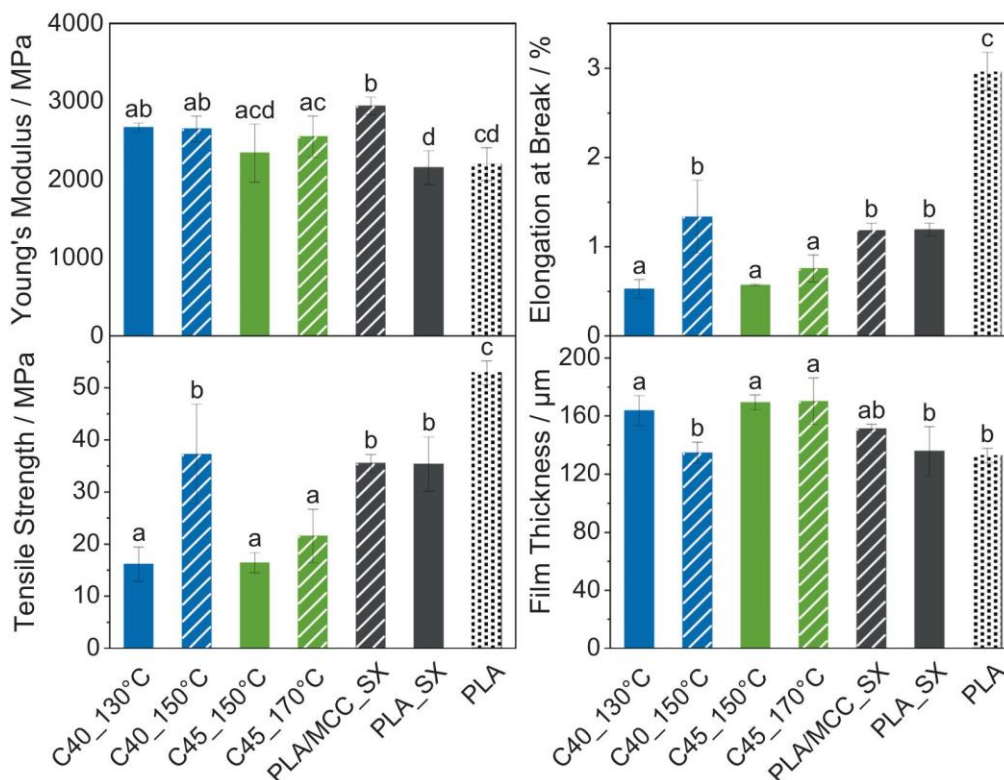


FIGURE 10 Young's modulus, tensile strength, elongation at break and film thickness of tested samples. Different letters show statistically significant ($p < 0.05$) differences between means [Color figure can be viewed at wileyonlinelibrary.com]

elongation are assumed to increase with increasing degree of mixing or homogeneity of the blend. The highest tensile strength and elongation were found for the C40 extruded at 150 °C, while all other samples had significantly lower values. It should be noted, that elongation values highly depend on the film thickness, which also differed between the samples ($F_{6,28} = 9.81$, $p = 7.70 \cdot 10^{-6}$, and $R^2 = 0.68$). As noted in the SEM analysis, higher temperatures resulted in a more homogeneous blend morphology as they allowed for more efficient mixing (Figure S4). The C40 blends were expected to have the highest compatibility in terms of the flow properties of PLA and the cellulose gel during the rheological tests, resulting in the smoothest morphology and the highest strength and elongation. Not only the comparison within our sample sets, but also with other studies preparing homogeneous PLA/cellulose blends illustrates the significant influence of the blend morphology. Blends of the same PLA/cellulose percentage, prepared via solution-precipitation process with 1-butyl-3-methylimidazolium acetate, showed a tensile strength of only 15 MPa.²¹ Being comparable to blends with lower mixing degrees from our study (C40_130°C, C45_150°C), we assume that no sufficient mixing was achieved by the other

group. This is also evident from DSC data showing crystallization of PLA in the blends.²¹

As mentioned earlier, the homogeneous, nearly single-phase morphology in some of our blends suggests higher mechanical strength but lower stiffness than heterophasic composites of PLA and cellulose. The absence of such significant effects compared to the composite and the original PLA therefore requires an explanation. The absence of such significant effects compared to the composite and the original PLA therefore requires an explanation. The first factor resulting from the molecular weight distribution of PLA is that not only processing with IL but also soxhlet extraction led to degradation reactions of PLA. Especially in elongation and tensile strength, the molecular weight of the polymer has a great influence on the performance, for example, due to the entanglement of the PLA chains, which allows higher elongation. Considering the molecular weight, the strength values of the soxhlet-extracted PLA are comparable to injection-molded samples with M_w of $\sim 50 \text{ kg} \cdot \text{mol}^{-1}$, showing values of $\sim 40 \text{ MPa}$.⁶⁶ On the positive side, the C40 blend has a comparable tensile strength and elongation despite its lower molar mass than the composite. A second factor affecting tensile strength and elongation of the blends

could be the higher levels of impurities. As discussed earlier, processing of imidazolium-based ILs at temperatures above 120°C is associated with degradation processes and the formation of chromophores, which apparently remained in the samples after extraction (Figure 4). Although there is little comparable literature, regenerated cellulosic fibers also showed decreased mechanical properties at higher impurity levels,⁶⁷ such as lower tenacity and elongation at break after repeated dissolution/regeneration cycles with the same ionic liquid.⁶⁸

4 | CONCLUSION AND OUTLOOK

We demonstrated that an efficient blending between PLA and cellulose can be achieved by a continuous extrusion process using only small amounts of solvent as intermediate compatibilizer. Cellulose gels with 40 wt% cellulose showed viscosities comparable to the PLA melt at applied processing temperatures, enabling efficient mixing during compounding. Resulting PLA/cellulose gel blends were thermoformable into films by compression molding. After IL and co-solvent extraction, transparent films showed a homogeneous morphology with only low cellulose particle inclusions, and intense polymer interactions in the main phase were concluded from FTIR and DSC analysis. The cellulose blend from 40 wt% gels compounded at 150 °C showed strength and elongation with 37 MPa and 1.34% comparable to a PLA/MCC composite and pure PLA. Based on the blend morphology, however, facilitated load transfer should result in a material with higher strength compared to the multiphase composite. Reasons are found with polymer degradation: the PLA in the blend had a molecular weight of only 24 kg·mol⁻¹, while the composite showed 53 kg·mol⁻¹. Additionally, IL degradation products led to impurities that further decreased strength and elongation. For the PLA degradation, the influence of IL concentration was more obvious than the influence of processing temperature or Soxhlet extraction. Therefore, extrusion temperatures should be as low as possible but as high as needed to ensure flow. Although side reactions can be reduced, for example, by using processing temperatures below 120°C or increasing the initial acidity, they cannot be fully prevented.²⁰ For further investigations, the authors recommend different strategies to prevent severe degradation: (1) change of the IL by choosing a less basic anion and/or changing the cation,^{20,69} (2) inhibition of cellulose degradation in IL, for example, by adding glycerol⁶⁹ or amino acids⁷⁰ (3) reduction in melt viscosity of the PLA with additives such as

plasticizers to reduce the processing temperatures.^{71–73} The importance of reducing such degradation becomes even greater when considering the economics of the process. Ensuring reasonable material costs requires a functioning ionic liquid cycle, including solvent recovery and purification. Although this study focused on the material preparation process itself, the future studies must also address IL recycling, particularly in the context of larger scale processing. Larger batches of material would also help to reduce variations in the extrusion process by aiming for higher throughput and longer process times to stabilize the process parameters. As for the final blend properties, interesting features such as transparency and biodegradability should be further investigated in the future to understand these phenomena fundamentally.

AUTHOR CONTRIBUTIONS

Kerstin Müller: Conceptualization (lead); formal analysis (lead); investigation (lead); methodology (lead); visualization (lead); writing – original draft (lead); writing – review and editing (equal). **Siegfried Fürtauer:** Writing – review and editing (equal). **Markus Schmid:** Writing – review and editing (equal). **Cordt Zollfrank:** Writing – review and editing (equal).

ACKNOWLEDGMENTS

The authors thank their colleagues Weixuan Wang (TUM), Norbert Rodler and Michael Stenger (both IVV) for their support with TGA and extrusion/compounding of the materials. We further thank Andreas Mäurer for his valuable comments on the article. Open Access funding enabled and organized by Projekt DEAL.

DATA AVAILABILITY STATEMENT

The data that support the findings of this study are available in the supplementary material of this article. Any further data are available from the corresponding author upon reasonable request.

SUPPORTING INFORMATION

Supporting Information is available from the Wiley Online Library.

ORCID

Kerstin Müller  <https://orcid.org/0000-0002-7737-4911>

REFERENCES

- [1] A. Xu, F. Wang, L. Zhang, X. Xu, Z. Xiao, R. Liu, *J. Appl. Polym. Sci.* **2021**, *138*, 50320.
- [2] Mayilswamy, N.; Kandasubramanian, B., *Emergent Materials* **2022**. <https://doi.org/10.1007/s42247-022-00354-2>

- [3] S. Chueter, P. Tantayotai, K. Cheenkachorn, Y.-S. Cheng, A. Tawai, M. Sriariyanun, in *Biodegradable Polymers, Blends and Composites* (Eds: S. Mavinkere Rangappa, J. Parameswaranpillai, S. Siengchin, M. Ramesh), Woodhead Publishing, Duxford **2022**.
- [4] M. S. Andrade, O. H. Ishikawa, R. S. Costa, M. V. S. Seixas, R. C. L. B. Rodrigues, E. A. B. Moura, *Food Packag Shelf Life* **2022**, *31*, 100807.
- [5] X. Wu, Y. Liu, H. Wu, Y. Duan, J. Zhang, *Compos. Sci. Technol.* **2022**, *218*, 109135.
- [6] X. Zhang, X. Wu, D. Gao, K. Xia, *Carbohydr. Polym.* **2012**, *87*, 2470.
- [7] J. Schroeter, F. Felix, *Cellulose* **2005**, *12*, 159.
- [8] Q. Wang, J. Cai, L. Zhang, M. Xu, H. Cheng, C. C. Han, S. Kuga, J. Xiao, R. Xiao, *J. Mater. Chem. A* **2013**, *1*, 6678.
- [9] T. I. A. Gouveia, K. Biernacki, M. C. R. Castro, M. P. Gonçalves, H. K. S. Souza, *Food Hydrocolloids* **2019**, *97*, 105175.
- [10] R. P. Swatloski, S. K. Spear, J. D. Holbrey, R. D. Rogers, *J. Am. Chem. Soc.* **2002**, *124*, 4974.
- [11] C. Hopson, M. M. Villar-Chavero, J. C. Domínguez, M. V. Alonso, M. Olet, F. Rodriguez, *Carbohydr. Polym.* **2021**, *274*, 118663.
- [12] A. Takada, J.-I. Kadokawa, *Cellulose* **2021**, *29*, 2745.
- [13] A. A. Shamsuri, S. N. A. Md. Jamil, K. Abdan, *Polymers* **2021**, *13*, 2597.
- [14] M. A. Haq, Y. Habu, K. Yamamoto, A. Takada, J.-I. Kadokawa, *Carbohydr. Polym.* **2019**, *223*, 115058.
- [15] S. P. F. Costa, A. M. O. Azevedo, P. C. A. G. Pinto, M. L. M. F. S. Saraiva, *ChemSusChem* **2017**, *10*, 2321.
- [16] H. Baaqel, I. Díaz, V. Tulus, B. Chachuat, G. Guillén-Gosálbez, J. P. Hallett, *Green Chem.* **2020**, *22*, 3132.
- [17] F. Philippi, D. Rauber, K. L. Eliassen, N. Bouscharain, K. Niss, C. W. M. Kay, T. Welton, *Chem. Sci.* **2022**, *13*, 2735.
- [18] N. D. Khupse, A. Kumar, *J. Solution Chem.* **2009**, *38*, 589.
- [19] F. Yang, P. Feng, *Appl. Sci.* **2020**, *10*, 8342.
- [20] M. T. Clough, K. Geyer, P. A. Hunt, S. Son, U. Vagt, T. Welton, *Green Chem.* **2015**, *17*, 231.
- [21] A. Xu, Y. Wang, J. Gao, J. Wang, *Green Chem.* **2019**, *21*, 4449.
- [22] R. S. J. Manley, in *Cellulose Derivatives*, American Chemical Society, Washington, DC **1998**, Ch. 18.
- [23] K. Müller, C. Zollfrank, *Eur. Polym. J.* **2020**, *133*, 109743.
- [24] K. Müller, D. Van Opdenbosch, C. Zollfrank, *Mater. Today Commun.* **2022**, *30*, 103074.
- [25] X. Niu, S. Huan, H. Li, H. Pan, O. J. Rojas, *J. Hazard. Mater.* **2021**, *402*, 124073.
- [26] M. Kes, B. E. Christensen, *J. Chromatogr. A* **2013**, *1281*, 32.
- [27] Y.-R. Liu, K. Thomsen, Y. Nie, S.-J. Zhang, A. S. Meyer, *Green Chem.* **2016**, *18*, 6246.
- [28] K. A. Le, C. Rudaz, T. Budtova, *Carbohydr. Polym.* **2014**, *105*, 237.
- [29] B. A. Miller-Chou, J. L. Koenig, *Prog. Polym. Sci.* **2003**, *28*, 1223.
- [30] S. Dorn, F. Wendler, F. Meister, T. Heinze, *Macromol. Mater. Eng.* **2008**, *293*, 907.
- [31] B. Vergnes, *Polymer* **2021**, *13*, 304.
- [32] W. P. Cox, E. H. Merz, *J. Polym. Sci.* **1958**, *28*, 619.
- [33] W. M. Kulicke, R. S. Porter, *Rheol. Acta* **1980**, *19*, 601.
- [34] C. Seidel, W.-M. Kulicke, C. Heß, B. Hartmann, M. D. Lechner, W. Lazik, *Starch-Stärke* **2001**, *53*, 305.
- [35] Mezger, T. G., *The Rheology Handbook*; Vincentz Network, **2012**.
- [36] M. Watts, B. Kosan, J. Hammerschmidt, S. Dorn, F. Meister, S. Scholl, *Chem. Ing. Tech.* **2017**, *89*, 1661.
- [37] G. Ebner, S. Schiehsler, A. Potthast, T. Rosenau, *Tetrahedron Lett.* **2008**, *49*, 7322.
- [38] E. Ohno, H. Miyafuji, *J. Wood Sci.* **2014**, *60*, 428.
- [39] X.-Y. Li, Q. Zhou, K.-K. Yang, Y.-Z. Wang, *Chem. Pap.* **2014**, *68*, 1375.
- [40] S. Y. Han, C. W. Park, T. Endo, F. Febrianto, N.-H. Kim, S.-H. LEE, *Wood Sci Technol.* **2020**, *54*, 599.
- [41] W. H. Wan Ishak, N. A. Rosli, I. Ahmad, *Sci. Rep.* **2020**, *10*, 11342.
- [42] N. A. Rosli, I. Ahmad, F. H. Anuar, I. Abdullah, *Cellulose* **2019**, *26*, 3205.
- [43] J. Coates, in *Encyclopedia of Analytical Chemistry* (Eds: R. A. Meyers, M. L. McKelvy), John Wiley & Sons, Ltd, New Jersey **2006**.
- [44] J. Ambrosio-Martín, M. J. Fabra, A. Lopez-Rubio, J. M. Lagaron, *J. Mater. Sci.* **2014**, *49*, 2975.
- [45] A. A. Cuadri, J. E. Martín-Alfonso, *Polym. Degrad. Stab.* **2018**, *150*, 37.
- [46] V. Speranza, A. De Meo, R. Pantani, *Polym. Degrad. Stab.* **2014**, *100*, 37.
- [47] F. Iñiguez-Franco, R. Auras, G. Burgess, D. Holmes, X. Fang, M. Rubino, H. Soto-Valdez, *Polymer* **2016**, *99*, 315.
- [48] T. G. Fox, *Bullet. Am. Phys. Soc.* **1956**, *1*, 123.
- [49] L. A. de Graaf, M. Möller, *Polymer* **1995**, *36*, 3451.
- [50] S. Sato, D. Gondo, T. Wada, S. Kanehashi, K. Nagai, *J. Appl. Polym. Sci.* **2013**, *129*, 1607.
- [51] M. R. ten Breteler, J. Feijen, P. J. Dijkstra, F. Signori, *React. Funct. Polym.* **2013**, *73*, 30.
- [52] R. A. Cairncross, S. Ramaswamy, R. O'Connor, *Int. Polym. Process.* **2007**, *22*, 33.
- [53] M. Garg, V. Apostolopoulou-Kalkavoura, M. Linares, T. Kaldéus, E. Malmström, L. Bergström, I. Zozoulenko, *Cellulose* **2021**, *28*, 9007.
- [54] K. Kachrimanis, M. F. Noisternig, U. J. Griesser, S. Malamataris, *Eur. J. Pharm. Biopharm.* **2006**, *64*, 307.
- [55] D. Koo, A. Du, G. R. Palmese, R. A. Cairncross, *Polymer* **2012**, *53*, 1115.
- [56] J. Trifol, D. Plackett, P. Szabo, A. E. Daugaard, M. Giacinti Baschetti, *ACS Omega* **2020**, *5*, 15362.
- [57] N. Muhammad, Z. Man, M. Azmi Bustam Khalil, I. M. Tan, S. Maitra, *Waste Biomass Valoriz.* **2010**, *1*, 315.
- [58] A. Shakeri, M. P. Staiger, *BioResources* **2010**, *5*, 979.
- [59] H. Satani, M. Kuwata, A. Shimizu, *Carbohydr. Res.* **2020**, *494*, 108054.
- [60] X. Tan, L. Chen, X. Li, F. Xie, *Int. J. Biol. Macromol.* **2019**, *124*, 314.
- [61] X. Liu, L. Yu, H. Liu, L. Chen, L. Li, *Cereal Chem.* **2009**, *86*, 383.
- [62] M. Da, C. C. Lucena, A. E. De-Alencar, S. E. Mazzeto, E. S. De, *Polym. Degrad. Stab.* **2003**, *80*, 149.
- [63] J. L. Thomason, J. L. Rudeiros-Fernández, *Polym. Degrad. Stab.* **2021**, *188*, 109594.

- [64] A. P. Mathew, K. Oksman, M. Sain, *J. Appl. Polym. Sci.* **2005**, *97*, 2014.
- [65] U. C. Paul, D. Fragouli, I. S. Bayer, A. Zych, A. Athanassiou, *ACS Appl. Polym. Mater.* **2021**, *3*, 3071.
- [66] G. Perego, G. D. Cella, C. Bastioli, *J. Appl. Polym. Sci.* **1996**, *59*, 37.
- [67] Watts, M., PhD Thesis, Technical University Braunschweig **2019**.
- [68] S. Elsayed, S. Hellsten, C. Guizani, J. Witos, M. Rissanen, A. H. Rantamäki, P. Varis, S. K. Wiedmer, H. Sixta, *ACS Sustainable Chem. Eng.* **2020**, *8*, 14217.
- [69] M. T. Clough, J. A. Griffith, O. Kuzmina, T. Welton, *Green Chem.* **2016**, *18*, 3758.
- [70] J. Yang, X. Lu, X. Yao, Y. Li, Y. Yang, Q. Zhou, S. Zhang, *Green Chem.* **2019**, *21*, 2777.
- [71] H. Ge, F. Yang, Y. Hao, G. Wu, H. Zhang, L. Dong, *J. Appl. Polym. Sci.* **2013**, *127*, 2832.
- [72] D. Xie, Y. Zhao, Y. Li, A. M. LaChance, J. Lai, L. Sun, J. Chen, *Materials* **2019**, *12*, 3519.
- [73] R. N. Darie-Niță, C. Vasile, A. Irimia, R. Lipșa, M. Răpă, *J. Appl. Polym. Sci.* **2015**, *133*, 1332016.

SUPPORTING INFORMATION

Additional supporting information can be found online in the Supporting Information section at the end of this article.

How to cite this article: K. Müller, S. Fürtauer, M. Schmid, C. Zollfrank, *J. Appl. Polym. Sci.* **2022**, e52794. <https://doi.org/10.1002/app.52794>

WILEY-VCH

Supporting Information

Cellulose blends from gel extrusion and compounding with polylactic acid

Kerstin Müller^{1,2*}, Siegfried Fürtauer², Markus Schmid³ and Cordt Zollfrank¹

¹Chair for Biogenic Polymers, Technische Universität München, Campus Straubing for Biotechnology and Sustainability, Schulgasse 16, 94315, Straubing, Germany

²Fraunhofer Institute for Process Engineering and Packaging IVV, Giggenhauser Str. 35, 85354 Freising, Germany

³Faculty of Life Sciences, Sustainable Packaging Institute SPI, Albstadt-Sigmaringen University, Anton-Günther-Str. 51, 72488 Sigmaringen, Germany

*corresponding author, e-mail: kerstin.mueller@ivv.fraunhofer.de

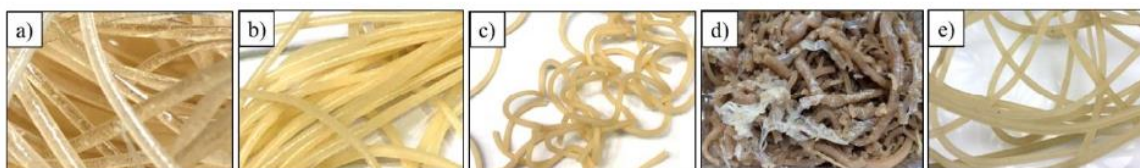


Figure S1. Cellulose gel strands at different cellulose concentrations relative to ionic liquid: 35 wt% (a), 40 wt% (b) and 45 wt% (c); Cellulose gel/PLA compounds without (d) and with (e) viscosity matching

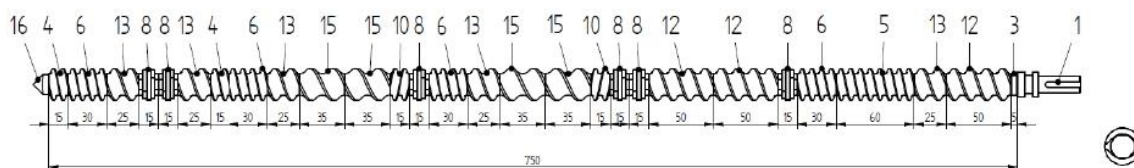


Figure S2. Screw configuration of the Collin compounder (©COLLIN Lab & Pilot Solutions GmbH)

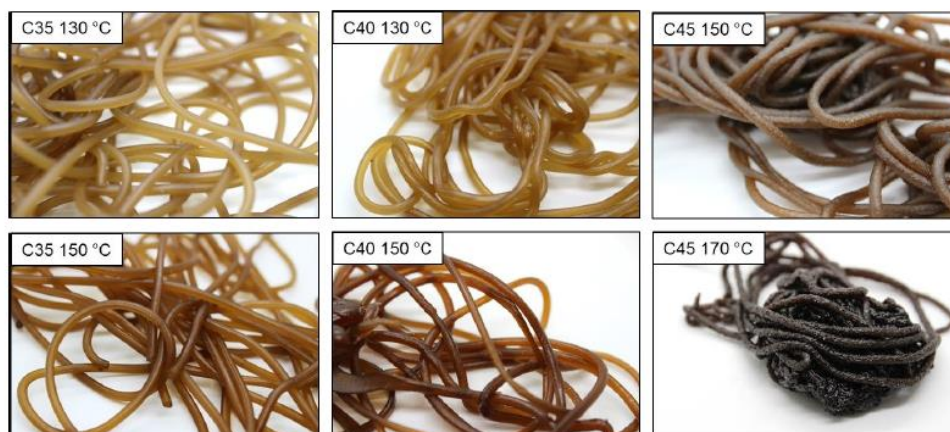


Figure S3. Cellulose gel/PLA compounds at different concentrations and extrusion temperatures

WILEY-VCH

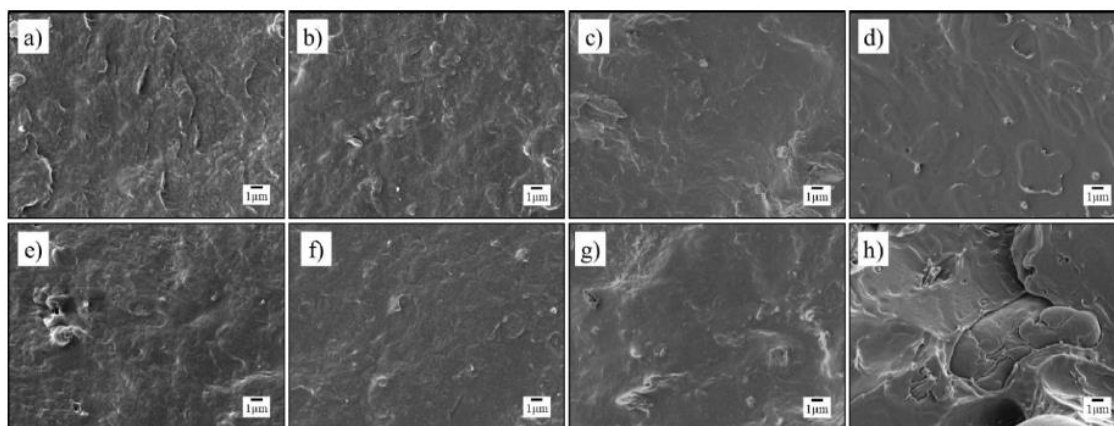


Figure S4. SEM images of cryo-fractured cross sections of cellulose/PLA blend films a) C35_130 °C, e) C35_150 °C, b) C40_130 °C, f) C40_150 °C, c) C45_150 °C and g) C45_170 °C; d) PLA film (d) and PLA/MCC microcomposite film (h).

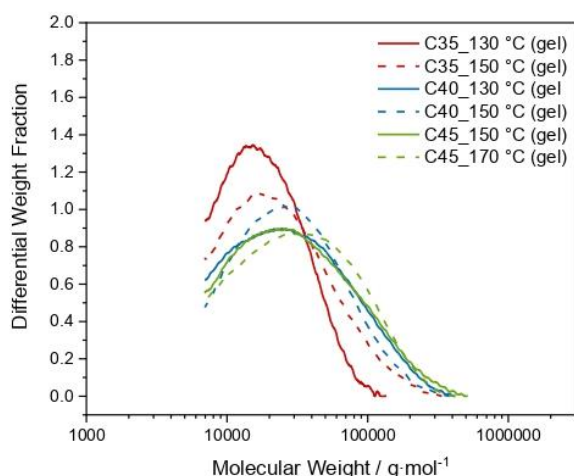


Figure S5. Molecular weight distribution of the cellulose gel/PLA compounds.

Table S1. Molecular weight averages of PLA from relative SEC measurement. M_w =weight average molecular weight; M_n =number average molecular weight; M_p =molecular weight of the highest peak; PD=polydispersity index.

Sample	M_p (g·mol ⁻¹)	M_n (g·mol ⁻¹)	M_w (g·mol ⁻¹)	PD
C35_130_gel	15357	15936	22687	1.4236
C35_150_gel	17243	18541	33760	1.8208
C40_130_gel	24838	21230	44676	2.1044
C40_150_gel	31188	21119	39807	1.8849
C45_150_gel	26367	21918	48518	2.2136
C45_165_gel	38643	23349	49093	2.1026
C35_130_SX	24394	18976	38828	2.0462
C35_150_SX	19465	19286	25641	1.3295
C40_130_SX	25321	17525	29933	1.708
C40_150_SX	22765	18860	23759	1.2598
C45_150_SX	27600	14092	50447	3.5798
C45_170_SX	47442	17580	61752	3.5126
PLA	97302	72049	153003	2.1236
PLA_SX	41883	30136	45926	1.524
PLA/MCC1	121370	81490	176251	2.1629
PLA/MCC1_SX	44769	32056	52984	1.6529

7 Discussion, conclusion and outlook

To extend the technical use of native cellulose, the possibility of inserting polymeric spacers between the cellulose chains was investigated to develop a material that can potentially be processed in thermoplastic molding processes. Cellulose was chosen because it can be obtained from lignocellulosic biomass and does not compete with food or feed. In addition, cellulose's polymer structure makes it an interesting candidate for thermoplastic processing, as it is a linear homopolymer with a broad and sufficiently high molecular weight range. The problem to be solved is how to impart thermoplasticity to a natural polymer that is not thermoplastic. The difficulty lies in the tendency to self-associate based on intense hydrogen bonding, which leads to the degradation of the polymer before it softens or melts. Therefore, the goal of the modification is clearly to mask the hydroxyl groups to limit intermolecular hydrogen bonding. Previous experiments have focused mainly on chemical modification (see chapter 3.3, heading 3.1). However, the structural modification is accompanied by a loss of the original properties such as biodegradability. If the natural structure is to be preserved, a physical modification will remain the only alternative. External plasticizers are low molecular weight molecules that have low persistence and a tendency to migrate, resulting in the material not being stable and losing thermoplasticity over time (further information on external plasticizers see chapter 3.3, headings 2 and 3.1.2). A simple way to prevent migration is to use higher molecular weight structures. When blending other polymers with native cellulose, miscibility or compatibility are the main factors that determine stable, single-phase mixed structures or heterogeneous, multiphase systems. With the goal of masking the hydroxyl groups of cellulose, only single-phase mixing would correlate with the introduction of polymeric spacers at the molecular level. Figure 11 shows the schematic approach to incorporate a polymeric spacer between native cellulose polymer chains.

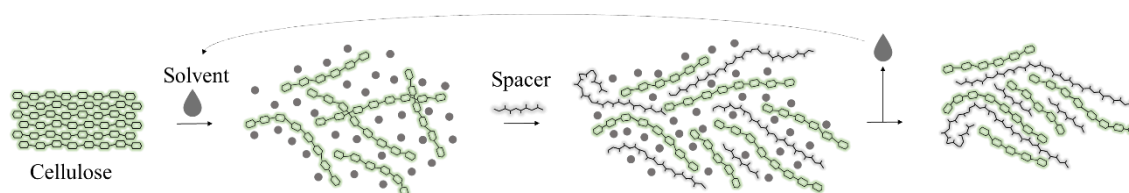


Figure 11. Schematic approach to the physical modification of cellulose with polymeric spacers. Adapted from Müller et al.¹¹²

In this context, the scientific questions proposed in chapter 1.2 will be discussed and answered in the following.

7.1 Compatibility of synthetic polymers with cellulose

Basically, from a thermodynamic point of view, there are hardly any polymers that are miscible (also see chapter 2.3.1).⁷¹ From a technical point of view, a blend system can be described as miscible when separate phases are no longer detectable. The prerequisite for this is interactions between the polymer chains down to the molecular level. Cellulose, a polysaccharide with a high density of hydroxyl groups, tends to self-associate rather than interact with other substances. This is already evident in the difficult solubility of cellulose compared to other natural polymers and, depending on polymer concentration, molecular weight, and temperature, in little interaction of polysaccharides with a second component, leading in most cases to precipitation or phase separation.^{94, 113-115} The fundamental problem in preparing cellulose blends for compatibility evaluation is to find a suitable solvent system that can dissolve both the polysaccharide and the second component without derivatization or decomposition¹¹³, is thermally stable, and at best is non-toxic and environmentally friendly. This further narrows the already limited choice of solvents for cellulose with regard to the second component. As a result, only a few synthetic polymers have been studied for their compatibility with cellulose, with only a fraction of those showing good compatibility at all (chapter 2.3.4). In this work, polymers were selected based on their possible interactions with cellulose via hydrogen bonding (polyesters and polyamide 6) as well as their processability in the selected solvent system (ionic liquid and co-solvent) without phase separation in solution. Additionally, bio-based polyesters such as poly(3-hydroxybutyrate-*co*-3-hydroxyvalerate), polybutylene succinate and PLA have not been investigated so far and were added to the compatibility studies.

Research question 1: Which synthetic polymers can be used as spacers based on compatibility with cellulose?

When comparing different biopolyesters, the results in chapter 1, heading 3 show that PLA is a suitable partner for cellulose, which can interact with the polysaccharide chains down to the molecular level. A single-phase blend is formed almost independently from the polymer ratio, showing that PLA can be used as a spacer due to its compatibility with cellulose. Although polyamide 6 interacts with cellulose via hydrogen bonds in the amorphous regions, no influence on crystalline polyamide 6 domains was detected (chapter 5, headings 3.1 and 3.5), concluding that compatibility may not be sufficient to act as a polymeric spacer. It should be noted here, however, that the crystallinity of the polyamide 6 can be influenced by varying the precipitation parameters (e.g. precipitant, temperature, shear, solvent-polymer-precipitant ratio), which this work did not investigate in detail. None of the other biopolyesters, namely poly(3-hydroxybutyrate-*co*-3-hydroxyvalerate), polybutylene succinate, and polycaprolactone are suitable spacers

based on the phase-separated morphologies of the blends (chapter 1, heading 3: Morphology).

7.2 Influence of formulation and process parameters on blend structure and properties

As discussed in chapter 5, heading 4.5, PLA crystal growth is effectively suppressed in cellulose/PLA blends in all materials containing cellulose. The progression of crystallization indicates a close chemical link between cellulose and PLA, independent of composition. This is intuitive given that PLA has 1.6 times the number of carbonyl groups per mass compared to PA 6, providing points of attachment for hydrogen bonds with the hydroxyl groups of cellulose.

Research question 2: How does the polymer ratio influence the blend structure of a compatible system?

The crystalline structure and intermolecular interactions of cellulose blends were investigated and discussed in chapter 5, headings 3 and 4.2-4.5. Strong interactions were visible for cellulose/PLA blends over a wide range of compositions. Only at high PLA contents (≥ 90 wt%), crystalline domains of PLA could be detected, meaning that separate phases of PLA that were not interrupted by cellulose chains were present. At high cellulose contents (≥ 80 wt%) few crystal cellulose domains were apparent. It seems inappropriate to use the term "phase separation" here, since individual PLA or cellulose phases can also occur at those concentrations which, in terms of polymer volumes, cannot be disturbed by PLA or cellulose chains.

No phase separation during temperature treatment up to 190 °C (hot press) was detected, indicating that the LCST has to be at a higher temperature and is unlikely to reach before the degradation processes of the material will start.

Research question 4: How do process parameters influence blend properties?

Attempts to combine PLA and cellulose with the help of ionic liquids resulted in homogeneous, transparent blends (chapters 4-6). Soil degradability even faster than cellulose itself is a further interesting property that was assessed in studies from another⁹⁷ and the own research group^{116, 117}. When using solution blending for the preparation of such polymer blends, the selection of solvents is important. The dissolution of a polymer can be separated into two basic steps, solvent diffusion and chain entanglement (chapter 2.2). For efficient mixing of the polymers, both steps have to be reached sufficiently. It is important to choose a good solvent that enables the polymers to be present as extended coils. Based on available literature on thermodynamics in cellulose solutions, the ionic liquid used in this work is a good solvent for cellulose. It even seems to be a theta solvent¹¹⁸, which allows balanced interactions between polymer and solvent with

unperturbed chains and is therefore appropriate for solution blending. Being a thermodynamic issue, however, the dissolution ability and quality of a polymer solution are always linked to temperature. The system EmimAc/DMSO allowed polymer dissolution and homogeneous mixing over a wide temperature range, therewith also enabling combinations with polyamide 6 or poly(3-hydroxybutyrate-*co*-3-hydroxyvalerate).

Not only the selection of the solvent system or dissolution and mixing temperatures, but also the precipitation process influences the final blend morphology (chapter 2.3.1 and chapter 5, headings 1 and 4.1). Rapid precipitation can contribute to the production of homogeneous blend morphologies that are not present when precipitating at a lower velocity.⁷² So even if blend partners are immiscible and no compatibilizers are used, the precipitation process can be used to produce metastable micromorphologies in the solid blend, where microscale domains are homogeneously distributed.^{72, 73} This was especially apparent for the cellulose/polyamide 6 blends prepared in this work, which were found to be immiscible,^{88, 94} but occurred as macroscopically homogeneous films when rapidly precipitated from solution in chapters 4 and 5.

The selection of an anti-solvent was shown to be a crucial parameter for cellulose blends, too. For the precipitation of cellulose/PLA blends in IL-solution, ethanol has to be chosen over water. No complete precipitation is possible in water, particularly not at lower cellulose concentrations, as discussed in chapter 5, heading 4.1. Although water can precipitate both PLA from a DMSO solution and cellulose from an IL/DMSO solution, the addition of water to a combination of those solutions results in a stable colloidal dispersion.

Additionally, cellulose crystallinity differed with anti-solvent (chapter 5, headings 3.5, 3.6). While the water precipitation rearranged the cellulose domains to crystalline cellulose II, the ethanol-precipitated sample showed only amorphous reflexes not attributable to cellulose II.

Being a good choice for the dissolution of cellulose, EmimAc showed major drawbacks concerning the processing of PLA. Severe PLA degradation can occur in the IL depending on concentrations, temperature, and time combinations.¹¹⁹ In cellulose/PLA blends prepared via extrusion in chapter 6, heading 3.3.2, high IL loadings and processing temperatures led to PLA degradation of an M_w from approx. $160 \text{ kg}\cdot\text{mol}^{-1}$ to $23\text{-}50 \text{ kg}\cdot\text{mol}^{-1}$. In solution blended samples in chapter 4, heading 3, no such degradation was detected. However, a different PLA grade was used, and repeated washing with water was performed rather than Soxhlet extraction with ethanol. Also, the contact time of PLA with the IL was much longer for the extruded blends, since the molding process of the blend gels had a significant time lag (several days) for preparation, while the blends from

solution were directly precipitated. Therefore, the design of both studies unfortunately does not allow a reasonable comparison.

In terms of cellulose, imidazolium-based ILs can also cause polymer degradation. When in solution, cellulose is prone to undergo hydrolysis in presence of an acid, especially at temperatures above 100 °C¹²⁰⁻¹²², which limits the processing temperature window for cellulose blends. Celluloses regenerated from dissolution in chapter 4 and gel extrusion in chapter 6 both showed degradation up to 30% and ~13%, respectively. Since both processes were performed at temperatures below or around 100 °C, higher degradation of cellulose in dilute solutions can be attributed to the much higher IL concentration.

Additionally, the IL used showed degradation reactions at higher processing temperatures during extrusion, which also lead to non-extractable reaction products in the final blends that influenced their optical and structural properties (chapter 6, headings 3.3.1 and 3.3.2). An influence of the degradation products on the mechanical properties is also to be expected.

Regarding the results from tensile testing of extruded cellulose blends in chapter 6, heading 3.3.3, however, the correlation between tensile strength and molecular weight became particularly apparent. Absolute tensile strength and elongation values of extruded cellulose/PLA blends (1:1) were ~40 MPa and 1.3%, respectively. These were comparable to a multiphase composite of the same composition containing twice the molecular weight of PLA.

The last factor investigated that influences final blend properties is the amount of residual IL after solvent extraction. Existing literature on cellulose regenerated containing residual IL are rare,^{123, 124} since most studies just assume that the IL has been completely removed. In cellulose blends with PLA and polyamide 6 prepared in chapter 5, residual IL acts as a plasticizer and compatibilizer in the blends. Thermal properties showed prevented crystallization and decreased glass transition of the synthetic polymers as a result of the plasticizing effect in both crystalline as well as amorphous regions. Plasticizing effects in terms of decreased glass transition (polyamide 6) increased with the amount of IL (chapter 5, heading 3.1). Plasticizing effects on cellulose were already discussed in the literature, where high IL ratios even enabled direct thermal processing.^{58, 125-128} As discussed in chapter 5, headings 4.1 and 4.2, plasticizing effects in cellulose blends become negligible in a technical context at residual ionic liquid contents below 1 wt%. The same is expected for cellulose regenerates.

7.3 Blend preparation: solution and extrusion blending with ionic liquids

In the last section of this work, the possibility to prepare cellulose blends with minimum use of solvent was investigated.

Research question 3: Can the manufacturing process of such blends be transferred from solution to extrusion?

The transfer from solution blending to extrusion blending of cellulose blends includes several sub-tasks and questions linked to them. When the solvent is reduced, the system changes from a dilute to a concentrated solution. Following polymer solution theory, concentrations above a critical concentration are accompanied by chain entanglement that would consequently limit efficient mixing with a second polymer when added. However, such entanglements or gel networks are highly sensitive to shear and can therefore be overcome with sufficient input of mechanical energy. Although maximum cellulose concentrations in the EmimAc/DMSO system have been reported to be about 25-27 wt%,¹²⁹ the influence of shear and temperature showed that extruded gels with cellulose contents up to 45 wt% are feasible. However, based on the shorter dissolution time and limited wetting of the cellulose powder during extrusion, undissolved cellulose remains, especially at concentrations higher than 40 wt%.

The step for a process transfer from solution to extrusion blending would be successful blending with PLA by means of a single-phase morphology of the final material. Although this single-phase morphology could be re-attained for the main parts of the blends, results showed that high cellulose loads in gels and little time for dissolution left cellulose parts only in a swollen state within the boundary layer that could not be mixed with PLA on a molecular level. This again shows that the availability of the cellulose chains is a crucial factor for preparing cellulose blends with incorporated polymeric spacers. For the main phase, no differences in mixing in dilute or concentrated solutions were found, however, under the condition of sufficient shear and temperature during the mixing of concentrated solutions with a polymer melt. This additional input of energy may cause degradation reactions of both the ionic liquid and the polymers, especially since temperatures above 100 °C are necessary for the PLA to flow. Final blend properties such as mechanical and thermal properties are easily influenced by altered molecular weights of the polymers. Degradation processes therefore slightly changed the material properties compared to blends from solution blending. Therefore, the main question has to be answered as follows: the preparation process of cellulose blends can be transferred by technical means, however, parameters have to be chosen wisely to prevent polymer degradation and maintain blend properties apparent in solution-blended materials.

7.4 Conclusion

This work aimed to investigate how and to what extent physical modifications influence the structure-property relationships of moldable blends based on native cellulose. Using an ionic liquid as an intermediate, polymeric spacers can be inserted between cellulose chains as a physical modification approach. As a result, intermolecular interactions between the cellulose chains are disrupted and single-phase blends are formed when using PLA as a spacer. These blends can be formed under thermomechanical energy input.

To be used as a substitute material in thermoplastic processing, however, the thermoplastic behavior must ensure a certain flow or melt viscosity for further processing. After extraction of the ionic liquid, the cellulose blends appeared stiff and rigid. Due to the glycosidic bond and the stabilization by internal hydrogen bonding, the cellulose backbone is rigid and, unlike most other macromolecules, has limited mobility within the polymer chains. Even though physical modifications can affect the interactions between the different cellulose chains, the mobility of the cellulose backbone remains the same. This means that, on the one hand, the incorporation of a polymeric spacer can mask the intramolecular hydroxyl groups of the cellulose and thus achieve a certain thermomechanical formability, but on the other hand, the thermoplastic formability of these compounds might still be too low for further processing such as extrusion or injection molding. However, it is clear that further plasticization with low molecular weight components, as shown for the ionic residual liquid, is an effective means to ensure the thermoplastic processing of native cellulose blends. This is already evident for thermoplastic starches or cellulose derivatives.

Combinations of native cellulose and PLA show a homogeneous, single-phase morphology. Although not expected to be miscible by thermodynamic theory, precipitation provides the ability to freeze the structure compatibilized by the IL/co-solvent combination. This enables the investigation of many more combinations of natural and synthetic polymers in the future, especially those that are assumed to be immiscible or incompatible. The morphology found in prepared cellulose/PLA blends shows major differences compared to state-of-the-art composites using cellulose as filler. Based on the amorphicity and the absence of phase boundaries in the micrometer scale, the blends are transparent. They are also readily biodegradable in soil, which is a clear advantage over most industrial bio-based polymers that can only be composted in industrial facilities. Although first mechanical results were strongly influenced by polymer degradation, strength and elongation were still comparable to pure PLA or a composite containing twice the molecular weight. Based on the results, it can still be assumed that the homogeneous structure facilitated the transfer of load within the blend as expected. Still, the degradation of polymers and solvent have a negative effect on mechanical performance and should be prevented by changing the process parameters.

Cellulose blends contribute to the expansion of the technical use of cellulose through thermomechanical processing methods. It is true that solvent-based processes must always be evaluated in terms of their environmental impact. In the process presented here, however, it should be noted that the possibility of production via extrusion can be implemented with a greatly reduced solvent consumption. Experiments showed, however, that when using high cellulose loads in ILs, the use of co-solvents is advantageous since they facilitate dissolution by wetting cellulose and therewith prevent the formation of undissolved agglomerates. Still, the reduced amounts of solvents needed in extrusion processing mean that the manufacturing process is comparatively favorable compared to other solvent-based cellulose processes in the fiber sector (e.g. Ioncell[®], Lyocell). This advantage in the preparation of new cellulose blends should be seen in particular in the context of a bioeconomy, which on the one hand aims to reduce dependence on fossil raw materials for material synthesis and at the same time minimizes environmental impacts. In this context, solvent recovery and reuse remain an important issue. Extraction methods used in this work resulted in residual solvent contents far below 1 wt%. The minimum residual ionic liquid content to remain in the blend is not only an ecological but also an economic issue that is yet to be investigated for cellulose blends.

7.5 Outlook

Cellulose blends prepared in this work show promising properties to replace fossil-based plastics with bio-based and biodegradable materials. Accessing the native structure of cellulose for further technical use, e.g. for thermoplastic processing, could form an important basis for the development of bio-based materials.

Although the use of ionic liquids in this process has some drawbacks, this class of solvents is quite young and research is ongoing. There are various possible combinations regarding anion and cation offering flexibility which has certainly not been fully exploited. However, economic and environmental concerns must be further considered in future developments. The trend is clearly toward bio-based ionic liquids, which would also live up to the designation "green solvent." Nevertheless, examples of the use of ionic liquids on a larger scale are already available today: fiber fabrication processes such as HighPerCell[™] developed at the German Institute of Textile and Fiber Research Denkendorf in Germany¹³⁰, Ioncell[®] developed at Aalto University in Finland¹³¹ or Metsä Spring¹³² are entering pilot or even demo scale. The companies Worn Again Technologies or Re:newcell use an ionic liquid-based process for textile recycling, being suitable to recover mixed textiles from synthetics and cellulose.¹³³

In this work, disadvantages were found in the use of imidazolium-based ionic liquids, especially with regard to polymer degradation. To prevent degradation, in addition to changing the composition of the ionic liquid, other additives such as plasticizers can be

used to allow processing at lower temperatures. Another advantage here is also seen in the improved thermoformability of the compounds even after solvent removal.

The importance of miscible systems such as the blends presented is expected to increase with the need for recyclable materials and the possibility of reusing recycled polymers in blends. Cellulose, for example, could come from biomass side streams or worn textiles, while PLA could also originate from post-consumer packaging waste.

Transparency and biodegradability are further advantages of the developed blends. Applications that potentially remain in the environment after use and therefore require increased biodegradability are conceivable. Examples can especially be found in the agricultural and forestry sector, such as mulching films or tree covers.

Bibliography

1. Philp, J., Balancing the bioeconomy: supporting biofuels and bio-based materials in public policy. *Energy & Environmental Science* **2015**, 8 (11), 3063-3068.
2. United Nations, Transforming our world: the 2030 Agenda for Sustainable Development. In *UN General Assembly*, United Nations: 2015; Vol. A/RES/70/1.
3. Directorate-General for Research and Innovation (European Commission), *How the bioeconomy contributes to the European Green Deal*. Publications Office: 2020, doi/10.2777/67636
4. Philp, J. C.; Ritchie, R. J.; Guy, K., Biobased plastics in a bioeconomy. *Trends in Biotechnology* **2013**, 31 (2), 65-67.
5. Hillmyer, M. A., The promise of plastics from plants. *Science* **2017**, 358 (6365), 868-870.
6. Tiseo, I., Annual production of plastics worldwide from 1950 to 2020. Statista: 2022.
7. Geyer, R.; Jambeck, J. R.; Law, K. L., Production, use, and fate of all plastics ever made. *Science Advances* **2017**, 3 (7), e1700782.
8. Garcia, J. M.; Robertson, M. L., The future of plastics recycling. *Science* **2017**, 358 (6365), 870-872.
9. Albertsson, A.-C.; Hakkarainen, M., Designed to degrade. *Science* **2017**, 358 (6365), 872-873.
10. Mohanty, A. K.; Vivekanandhan, S.; Pin, J.-M.; Misra, M., Composites from renewable and sustainable resources: Challenges and innovations. *Science* **2018**, 362 (6414), 536-542.
11. Bonten, C., *Kunststofftechnik: Einführung und Grundlagen*. Carl Hanser Verlag GmbH & Company KG: München 2014; Vol. 1.
12. Gruenwald, G., *Plastics: How Structure Determines Properties*. Hanser Publishers: Munich 1993.
13. Laloui, L.; Rotta Loria, A. F., Chapter 4 - Deformation in the context of energy geostructures. In *Analysis and Design of Energy Geostructures*, edited by Laloui, L.; Rotta Loria, A. F., Academic Press: New York 2020; pp 137-205.
14. Prager, W., Recent Developments in the Mathematical Theory of Plasticity. *Journal of Applied Physics* **1949**, 20 (3), 235-241.
15. Prager, W., Non-isothermal plastic deformation. *Koninklijke Nederlandse Akademie van Wetenschappen* **1958**, 61 (3), 176-182.
16. Jancar, J., Structure-Property Relationships in Thermoplastic Matrices. In *Mineral Fillers in Thermoplastics I: Raw Materials and Processing*, edited by Jancar, J.; Fekete, E.; Hornsby, P. R.; Pukánszky, B.; Rethon, R. N., Springer Berlin Heidelberg: 1999; pp 1-65.
17. Wischniewski, A.; Richter, D., Polymer Dynamics in Melts. In *Soft Matter, Volume I: Polymer Melts and Mixtures*, edited by Gompper, G.; Schick, M., Wiley-VCH: Weinheim, 2006; Vol. 1.

18. Keith, H. D., Morphology of polymers. In *Encyclopedia of Materials Science and Engineering*, edited by Bever, M. B.; Cahn, R. W., Pergamon Press: New York, 1986.
19. Wunderlich, B., Macromolecular Physics - Volume 2: Crystal Nucleation, Growth, Annealing. Academic Press: New York 1976.
20. Crawford, R. J.; Throne, J. L., 2 - Rotational Molding Polymers. In *Rotational Molding Technology*, edited by Crawford, R. J.; Throne, J. L., William Andrew Publishing: Norwich, NY, 2002; pp 19-68.
21. Shrivastava, A., 1 - Introduction to Plastics Engineering. In *Introduction to Plastics Engineering*, edited by Shrivastava, A., William Andrew Publishing: Norwich, NY 2018; pp 1-16.
22. Lin, Y.; Bilotti, E.; Bastiaansen, C. W. M.; Peijs, T., Transparent semi-crystalline polymeric materials and their nanocomposites: A review. *Polymer Engineering & Science* **2020**, *60* (10), 2351-2376.
23. Miller-Chou, B. A.; Koenig, J. L., A review of polymer dissolution. *Progress in Polymer Science* **2003**, *28* (8), 1223-1270.
24. Triebert, D.; Hanel, H.; Bundt, M.; Wohnig, K., Solvent-Based Recycling. In *Circular Economy of Polymers: Topics in Recycling Technologies*, American Chemical Society: 2021; Vol. 1391, pp 33-59.
25. Zhao, Y.-B.; Lv, X.-D.; Ni, H.-G., Solvent-based separation and recycling of waste plastics: A review. *Chemosphere* **2018**, *209*, 707-720.
26. Langer, R.; Vacanti, J. P., Artificial organs. *Scientific American* **1995**, *273* (3), 130-133.
27. Peppas, N. A.; Langer, R., New Challenges in Biomaterials. *Science* **1994**, *263* (5154), 1715-1720.
28. Hauru, L. K. J.; Hummel, M.; Nieminen, K.; Michud, A.; Sixta, H., Cellulose regeneration and spinnability from ionic liquids. *Soft Matter* **2016**, *12* (5), 1487-1495.
29. Shabbir, M.; Mohammad, F., 7 - Sustainable production of regenerated cellulosic fibres. In *Sustainable Fibres and Textiles*, edited by Muthu, S. S., Woodhead Publishing: Cambridge 2017; pp 171-189.
30. Tokura, S.; Nishi, N.; Noguchi, J., Studies on Chitin. III. Preparation of Chitin Fibers. *Polymer Journal* **1979**, *11* (10), 781-786.
31. Trabbic, K. A.; Yager, P., Comparative Structural Characterization of Naturally- and Synthetically-Spun Fibers of Bombyx mori Fibroin. *Macromolecules* **1998**, *31* (2), 462-471.
32. Pekcan, Ö.; Uğur, Ş., Molecular weight effect on polymer dissolution: a steady state fluorescence study. *Polymer* **2002**, *43* (6), 1937-1941.
33. Ueberreiter, K.; Asmussen, F., Velocity of dissolution of polymers. Part I. *Journal of Polymer Science* **1962**, *57* (165), 187-198.
34. Cooper, W. J.; Krasicky, P. D.; Rodriguez, F., Effects of molecular weight and plasticization on dissolution rates of thin polymer films. *Polymer* **1985**, *26* (7), 1069-1072.
35. Papanu, J. S.; Hess, D. W.; Soane, D. S.; Bell, A. T., Dissolution of Thin Poly(methyl methacrylate) Films in Ketones, Binary Ketone/Alcohol Mixtures, and Hydroxy Ketones. *Journal of The Electrochemical Society* **1989**, *136* (10), 3077-3083.

36. Parsonage, E. E.; Peppas, N. A.; Lee, P. I., Properties of positive resists. II. Dissolution characteristics of irradiated poly(methyl methacrylate) and poly(methyl methacrylate-co-maleic anhydride). *Journal of Vacuum Science & Technology B: Microelectronics Processing and Phenomena* **1987**, *5* (2), 538-545.
37. Flory, P. J., Thermodynamics of High Polymer Solutions. *The Journal of Chemical Physics* **1942**, *10* (1), 51-61.
38. Huggins, M. L., Solutions of Long Chain Compounds. *The Journal of Chemical Physics* **1941**, *9* (5), 440-440.
39. van Dijk, M. A.; Wakker, A., *Concepts in Polymer Thermodynamics*. Taylor & Francis: London 1998.
40. Koningsveld, R.; Koningsveld, R.; Stockmayer, W. H.; Nies, E., *Polymer Phase Diagrams: A Textbook*. Oxford University Press: Oxford 2001.
41. Knychala, P.; Timachova, K.; Banaszak, M.; Balsara, N. P., 50th Anniversary Perspective: Phase Behavior of Polymer Solutions and Blends. *Macromolecules* **2017**, *50* (8), 3051-3065.
42. Huang, J.-C., Multiparameter solution model and evaluation of polymer-polymer miscibility using inverse gas chromatography data. *Journal of Applied Polymer Science* **2009**, *113* (6), 4085-4091.
43. Thomas, S.; Grohens, Y.; Jyotishkumar, P., *Characterization of Polymer Blends: Miscibility, Morphology and Interfaces*. Wiley: Weinheim 2015.
44. Abbott, S., *Solubility Science: Principles and Practice*. Steven Abbott: Ipswich/Leeds 2017.
45. Jamieson, A. M.; Simha, R., Newtonian Viscosity of Dilute, Semidilute, and Concentrated Polymer Solutions. In *Polymer Physics: From Suspensions to Nanocomposites and beyond*, edited by Utracki, L.A.; Jamieson, A.M., Wiley: Weinheim 2010; pp 15-87.
46. Mezger, T. G., *The Rheology Handbook*. 4th Edition, Vincentz Network: Hannover 2012.
47. Huang, C.-C.; Winkler, R. G.; Sutmann, G.; Gompper, G., Semidilute Polymer Solutions at Equilibrium and under Shear Flow. *Macromolecules* **2010**, *43* (23), 10107-10116.
48. Glasser, W. G., Cellulose and Associated Heteropolysaccharides. In *Glycoscience: Chemistry and Chemical Biology*, edited by Fraser-Reid, B. O.; Tatsuta, K.; Thiem, J., Springer Berlin Heidelberg: 2008; pp 1473-1512.
49. Medronho, B.; Lindman, B., Brief overview on cellulose dissolution/regeneration interactions and mechanisms. *Advances in Colloid and Interface Science* **2015**, *222*, 502-508.
50. Heinze, T.; Koschella, A., Solvents applied in the field of cellulose chemistry: a mini review. *Polímeros* **2005**, *15*, 84-90.
51. Swatloski, R. P.; Spear, S. K.; Holbrey, J. D.; Rogers, R. D., Dissolution of Cellulose with Ionic Liquids. *Journal of the American Chemical Society* **2002**, *124* (18), 4974-4975.
52. Chen, Y.-L.; Zhang, X.; You, T.-T.; Xu, F., Deep eutectic solvents (DESs) for cellulose dissolution: a mini-review. *Cellulose* **2019**, *26* (1), 205-213.

53. Heinze, T.; Dorn, S.; Schöbitz, M.; Liebert, T.; Köhler, S.; Meister, F., Interactions of Ionic Liquids with Polysaccharides – 2: Cellulose. *Macromolecular Symposia* **2008**, 262 (1), 8-22.
54. Gericke, M.; Liebert, T.; Seoud, O. A. E.; Heinze, T., Tailored Media for Homogeneous Cellulose Chemistry: Ionic Liquid/Co-Solvent Mixtures. *Macromolecular Materials and Engineering* **2011**, 296 (6), 483-493.
55. Verma, C.; Mishra, A.; Chauhan, S.; Verma, P.; Srivastava, V.; Quraishi, M. A.; Ebenso, E. E., Dissolution of cellulose in ionic liquids and their mixed cosolvents: A review. *Sustainable Chemistry and Pharmacy* **2019**, 13, 100162.
56. Minnick, D. L.; Flores, R. A.; DeStefano, M. R.; Scurto, A. M., Cellulose Solubility in Ionic Liquid Mixtures: Temperature, Cosolvent, and Antisolvent Effects. *The Journal of Physical Chemistry B* **2016**, 120 (32), 7906-7919.
57. Mohan, M.; Banerjee, T.; Goud, V. V., Effect of Protic and Aprotic Solvents on the Mechanism of Cellulose Dissolution in Ionic Liquids: A Combined Molecular Dynamics and Experimental Insight. *ChemistrySelect* **2016**, 1 (15), 4823-4832.
58. Li, L.; Zhang, Y.; Sun, Y.; Sun, S.; Shen, G.; Zhao, P.; Cui, J.; Qiao, H.; Wang, Y.; Zhou, H., Manufacturing pure cellulose films by recycling ionic liquids as plasticizers. *Green Chemistry* **2020**, 22 (12), 3835-3841.
59. Pinkert, A.; Marsh, K. N.; Pang, S.; Staiger, M. P., Ionic Liquids and Their Interaction with Cellulose. *Chemical Reviews* **2009**, 109 (12), 6712-6728.
60. Clough, M. T.; Geyer, K.; Hunt, P. A.; Son, S.; Vagt, U.; Welton, T., Ionic liquids: not always innocent solvents for cellulose. *Green Chemistry* **2015**, 17 (1), 231-243.
61. Ebner, G.; Schiehser, S.; Potthast, A.; Rosenau, T., Side reaction of cellulose with common 1-alkyl-3-methylimidazolium-based ionic liquids. *Tetrahedron Letters* **2008**, 49 (51), 7322-7324.
62. Costa, S. P. F.; Azevedo, A. M. O.; Pinto, P. C. A. G.; Saraiva, M. L. M. F. S., Environmental Impact of Ionic Liquids: Recent Advances in (Eco)toxicology and (Bio)degradability. *ChemSusChem* **2017**, 10 (11), 2321-2347.
63. Thuy Pham, T. P.; Cho, C.-W.; Yun, Y.-S., Environmental fate and toxicity of ionic liquids: A review. *Water Research* **2010**, 44 (2), 352-372.
64. Zavrel, M.; Bross, D.; Funke, M.; Büchs, J.; Spiess, A. C., High-throughput screening for ionic liquids dissolving (ligno-)cellulose. *Bioresource Technology* **2009**, 100 (9), 2580-2587.
65. Mazza, M.; Catana, D.-A.; Vaca-Garcia, C.; Cecutti, C., Influence of water on the dissolution of cellulose in selected ionic liquids. *Cellulose* **2009**, 16 (2), 207-215.
66. Chawla, K. K., *Composite Materials: Science and Engineering*. 3rd Edition; Springer: New York, 2013.
67. Boyd, R.; Smith, G., *Polymer Dynamics and Relaxation*. Cambridge University Press: Cambridge 2007.
68. Utracki, L. A., *Polymer Alloys and Blends: Thermodynamics and Rheology*. Hanser Publishers: Munich 1990.
69. Utracki, L. A., *Polymer Blends Handbook*. Springer Netherlands: Dordrecht 2003.
70. Robeson, L. M., *Polymer Blends: A Comprehensive Review*. Hanser Publishers: Munich 2007.

71. Utracki, L. A., Polymer blends: fundamentals. In *Polypropylene: An A-Z reference*, edited by Karger-Kocsis, J., Springer Netherlands: Dordrecht, 1999; pp 601-605.
72. Lele, A. K.; Shine, A. D., Effect of RESS dynamics on polymer morphology. *Industrial & Engineering Chemistry Research* **1994**, *33* (6), 1476-1485.
73. Mawson, S.; Kanakia, S.; Johnston, K. P., Metastable polymer blends by precipitation with a compressed fluid antisolvent. *Polymer* **1997**, *38* (12), 2957-2967.
74. Harrats, C.; Thomas, S.; Groeninckx, G., Micro- and Nanostructured Multiphase Polymer Blend Systems: Phase Morphology and Interfaces. CRC Press: Boca Raton 2005.
75. Sperling, L. H., Phase Structure and Continuity in Polymer Blends and Composites. *Polym Eng Sci* **1976**, *16* (2), 87-92.
76. Macosko, C. W., Morphology development and control in immiscible polymer blends. *Macromolecular Symposia* **2000**, *149* (1), 171-184.
77. Chen, C. C.; White, J. L., Compatibilizing agents in polymer blends: Interfacial tension, phase morphology, and mechanical properties. *Polymer Engineering & Science* **1993**, *33* (14), 923-930.
78. Fox, T. G., Influence of diluent and of copolymer composition on the glass temperature of a polymer system. *The Bulletin of the American Physical Society* **1956**, *1*, 123-132.
79. Gordon, M.; Taylor, J. S., Ideal copolymers and the second-order transitions of synthetic rubbers. i. non-crystalline copolymers. *Journal of Applied Chemistry* **1952**, *2* (9), 493-500.
80. Couchman, P. R.; Karasz, F. E., A Classical Thermodynamic Discussion of the Effect of Composition on Glass-Transition Temperatures. *Macromolecules* **1978**, *11* (1), 117-119.
81. Kwei, T. K., The effect of hydrogen bonding on the glass transition temperatures of polymer mixtures. *Journal of Polymer Science: Polymer Letters Edition* **1984**, *22* (6), 307-313.
82. Coleman, M. M.; Skrovanek, D. J.; Hu, J.; Painter, P. C., Hydrogen bonding in polymer blends. 1. FTIR studies of urethane-ether blends. *Macromolecules* **1988**, *21* (1), 59-65.
83. Coleman, M. M.; Zarian, J., Fourier-transform infrared studies of polymer blends. II. Poly(ϵ -caprolactone)-poly(vinyl chloride) system. *Journal of Polymer Science: Polymer Physics Edition* **1979**, *17* (5), 837-850.
84. Painter, P. C.; Park, Y.; Coleman, M. M., Hydrogen bonding in polymer blends. 2. Theory. *Macromolecules* **1988**, *21* (1), 66-72.
85. Riaz, U.; Ashraf, S. M., Characterization of Polymer Blends with FTIR Spectroscopy. In *Characterization of Polymer Blends*, edited by Thomas, S.; Grohens, Y.; Jyotishkumar, P., Wiley VCH: Weinheim 2014; pp 625-678.
86. Ougizawa, T.; Inoue, T., Morphology of Polymer Blends. In *Polymer Blends Handbook*, edited by Utracki, L. A.; Wilkie, C. A., Springer Netherlands: Dordrecht 2014; pp 875-918.
87. Manley, R. S. J., Blends of Cellulose and Synthetic Polymers. In *Cellulose Derivatives*, American Chemical Society: 1998; Vol. 688, pp 253-264.

88. Nishio, Y.; Manley, R. S. J., Blends of cellulose with nylon 6 and poly(ϵ -caprolactone) prepared by a solution-coagulation method. *Polymer Engineering & Science* **1990**, *30* (2), 71-82.
89. Nishio, Y.; Manley, R. S. J., Cellulose-poly(vinyl alcohol) blends prepared from solutions in N,N-dimethylacetamide-lithium chloride. *Macromolecules* **1988**, *21* (5), 1270-1277.
90. Nishio, Y.; Roy, S. K.; Manley, R. S. J., Blends of cellulose with polyacrylonitrile prepared from N,N-dimethylacetamide-lithium chloride solutions. *Polymer* **1987**, *28* (8), 1385-1390.
91. Masson, J. F.; Manley, R. S. J., Miscible blends of cellulose and poly(vinylpyrrolidone). *Macromolecules* **1991**, *24* (25), 6670-6679.
92. Masson, J. F.; Manley, R. S. J., Cellulose/poly(4-vinylpyridine) blends. *Macromolecules* **1991**, *24* (22), 5914-5921.
93. Cogliano, V.; Grosse, Y.; Baan, R.; Straif, K.; Secretan, B.; Ghissassi, F. E., Advice on formaldehyde and glycol ethers. *The Lancet Oncology* **2004**, *5* (9), 528.
94. Ingildeev, D.; Hermanutz, F.; Bredereck, K.; Effenberger, F., Novel Cellulose/Polymer Blend Fibers Obtained Using Ionic Liquids. *Macromolecular Materials and Engineering* **2012**, *297* (6), 585-594.
95. Hameed, N.; Bavishi, J.; Parameswaranpillai, J.; Salim, N. V.; Joseph, J.; Madras, G.; Fox, B. L., Thermally flexible epoxy/cellulose blends mediated by an ionic liquid. *RSC Advances* **2015**, *5* (65), 52832-52836.
96. Niu, X.; Huan, S.; Li, H.; Pan, H.; Rojas, O. J., Transparent films by ionic liquid welding of cellulose nanofibers and polylactide: Enhanced biodegradability in marine environments. *Journal of Hazardous Materials* **2021**, *402*, 124073.
97. Xu, A.; Wang, Y.; Gao, J.; Wang, J., Facile fabrication of a homogeneous cellulose/polylactic acid composite film with improved biocompatibility, biodegradability and mechanical properties. *Green Chemistry* **2019**, *21* (16), 4449-4456.
98. Kakadellis, S.; Harris, Z. M., Don't scrap the waste: The need for broader system boundaries in bioplastic food packaging life-cycle assessment – A critical review. *Journal of Cleaner Production* **2020**, *274*, 122831.
99. Kakadellis, S.; Rosetto, G., Achieving a circular bioeconomy for plastics. *Science* **2021**, *373* (6550), 49-50.
100. Kumaran, S. K.; Chopra, M.; Oh, E.; Choi, H.-J., Chapter 11 - Biopolymers and natural polymers. In *Polymer Science and Nanotechnology*, edited by Narain, R., Elsevier: Amsterdam 2020; pp 245-256.
101. Ercan, N.; Durmus, A.; Kaşgöz, A., Comparing of melt blending and solution mixing methods on the physical properties of thermoplastic polyurethane/organoclay nanocomposite films. *Journal of Thermoplastic Composite Materials* **2017**, *30* (7), 950-970.
102. Welton, T., Solvents and sustainable chemistry. *Proc Math Phys Eng Sci* **2015**, *471* (2183), 20150502-20150502.
103. Shenoy, A. V.; Saini, D. R., *Thermoplastic Melt Rheology and Processing*. CRC Press: Boca Raton 1996.

104. Kohlgrüber, K., *Co-Rotating Twin-Screw Extruders: Fundamentals*. Carl Hanser Verlag GmbH & Company KG: München 2019.
105. Kohlgrüber, K.; Bierdel, M., *Der gleichläufige Doppelschneckenextruder: Grundlagen, Technologie, Anwendungen*. Carl Hanser Verlag GmbH & Company KG: München 2007.
106. Domininghaus, H.; Eyerer, P.; Elsner, P.; Hirth, T., *Kunststoffe: Eigenschaften und Anwendungen ; mit 240 Tabellen*. Springer Berlin Heidelberg: 2008.
107. BASF, *Kunststoff-Verarbeitung im Gespräch, 2 Extrusion*. BASF Aktiengesellschaft: Ludwigshafen 1982.
108. Limper, A., *Verfahrenstechnik der Thermoplastextrusion*. Carl Hanser Verlag GmbH & Company KG: München 2012.
109. Müller, K.; Zollfrank, C.; Schmid, M., Natural Polymers from Biomass Resources as Feedstocks for Thermoplastic Materials. *Macromolecular Materials and Engineering* **2019**, *304* (5), 1800760.
110. Müller, K.; Zollfrank, C., Ionic liquid aided solution-precipitation method to prepare polymer blends from cellulose with polyesters or polyamide. *European Polymer Journal* **2020**, *133*, 109743.
111. Müller, K.; Van Opdenbosch, D.; Zollfrank, C., Cellulose blends with polylactic acid or polyamide 6 from solution blending: Microstructure and polymer interactions. *Materials Today Communications* **2022**, *30*, 103074.
112. Müller, K.; Fürtaufer, S.; Schmid, M.; Zollfrank, C., Cellulose blends from gel extrusion and compounding with polylactic acid. *Journal of Applied Polymer Science* **2022**, *139* (37), e52794.
113. Rogovina, S. Z.; Vikhoreva, G. A., Polysaccharide-based polymer blends: Methods of their production. *Glycoconjugate Journal* **2006**, *23* (7), 611.
114. Albrecht, W.; Makschin, W.; Klug, P.; Weigel, T.; Gröbe, V., Besonderheiten der Strukturbildung bei der Koagulation von Polymermischungs-lösungen. 1. Mitt.: Voraussetzungen und Mechanismus des Entstehens hochporöser Strukturen. *Acta Polymerica* **1989**, *40* (2), 98-105.
115. Albrecht, W.; Makschin, W.; Weigel, T.; Klug, P.; Gröbe, V., Besonderheiten der Strukturbildung bei der Koagulation von Polymermischungs-lösungen. 2. Mitt.: Einfluß der Konzentration, Art und Menge an Zusatzpolymeren auf die Porosität. *Acta Polymerica* **1989**, *40* (5), 314-320.
116. Jerwann, K. Bio-based plasticizers for cellulose/poly(lactic acid) blends. Master Thesis, Albert-Ludwigs-Universität Freiburg, not published, 2021.
117. Müller, K., PLA in current Research Projects: Material Development - Packaging Applications – Recycling [Conference Presentation] *7th PLA World Congress*, Munich/online, May 24-25, 2022.
118. Gericke, M.; Schlufte, K.; Liebert, T.; Heinze, T.; Budtova, T., Rheological Properties of Cellulose/Ionic Liquid Solutions: From Dilute to Concentrated States. *Biomacromolecules* **2009**, *10* (5), 1188-1194.
119. Li, X.-Y.; Zhou, Q.; Yang, K.-K.; Wang, Y.-Z., Degradation of polylactide using basic ionic liquid imidazolium acetates. *Chemical Papers* **2014**, *68* (10), 1375-1380.

120. Li, C.; Zhao, Z. K., Efficient Acid-Catalyzed Hydrolysis of Cellulose in Ionic Liquid. *Advanced Synthesis & Catalysis* **2007**, *349* (11-12), 1847-1850.
121. Rinaldi, R.; Palkovits, R.; Schüth, F., Depolymerization of Cellulose Using Solid Catalysts in Ionic Liquids. *Angewandte Chemie International Edition* **2008**, *47* (42), 8047-8050.
122. Dorn, S.; Wendler, F.; Meister, F.; Heinze, T., Interactions of Ionic Liquids with Polysaccharides – 7: Thermal Stability of Cellulose in Ionic Liquids and N-Methylmorpholine-N-oxide. *Macromolecular Materials and Engineering* **2008**, *293* (11), 907-913.
123. Mahadeva, S. K.; Kim, J., Influence of residual ionic liquid on the thermal stability and electromechanical behavior of cellulose regenerated from 1-ethyl-3-methylimidazolium acetate. *Fibers and Polymers* **2012**, *13* (3), 289-294.
124. Mahadeva, S. K.; Kang, K.-S.; Kim, J.; Ha, S. H.; Koo, Y.-M., The Effect of Residual Ionic Liquid for Cellulose Based Electro-Active Paper Actuator. *Soft Materials* **2010**, *8* (3), 254-262.
125. Adak, B.; Mukhopadhyay, S., All-cellulose composite laminates with low moisture and water sensitivity. *Polymer* **2018**, *141*, 79-85.
126. Shibata, M.; Teramoto, N.; Nakamura, T.; Saitoh, Y., All-cellulose and all-wood composites by partial dissolution of cotton fabric and wood in ionic liquid. *Carbohydrate Polymers* **2013**, *98* (2), 1532-1539.
127. Spörl, J. M.; Batti, F.; Vocht, M.-P.; Raab, R.; Müller, A.; Hermanutz, F.; Buchmeiser, M. R., Ionic Liquid Approach Toward Manufacture and Full Recycling of All-Cellulose Composites. *Macromolecular Materials and Engineering* **2018**, *303* (1), 1700335.
128. Wu, J.; Bai, J.; Xue, Z.; Liao, Y.; Zhou, X.; Xie, X., Insight into glass transition of cellulose based on direct thermal processing after plasticization by ionic liquid. *Cellulose* **2015**, *22* (1), 89-99.
129. Le, K. A.; Rudaz, C.; Budtova, T., Phase diagram, solubility limit and hydrodynamic properties of cellulose in binary solvents with ionic liquid. *Carbohydrate Polymers* **2014**, *105*, 237-243.
130. Ota, A., Cellulose and cellulose-blend fibers derived by HighPerCell technology. *International Fiber Journal*: August 12, 2021.
131. Sixta, H.; Rissanen, M.; Laine, J., Pilot production line for Ioncell launched — a top made with the stronger-than-cotton ecofibre gets its colour from Finnish fields. Press Release by Aalto University: December 13, 2021.
132. Weymarn, N. v., Metsä Spring - From lab to demo phase and onwards [Conference presentation] *2nd International Conference on Cellulose Fibers*, Cologne/online, February 2-3, 2021
133. Lane, M., Closing the apparel loop: myth versus reality. *Apparel insider*: January 22, 2018.